CONTENTS

Honorary Patronage

Marshal of the Mazowieckie Voivodeship
Adam Struzik

Supported by

Ministry of Science and Higher Education
Republic of Poland

Ministry of Science
and Higher Education
of the Republic of Poland

EAgLE
European Action towards Leading Centre for Innovative Materials

EAgLE – European Action towards
Leading Centre
for Innovative Materials

Organized by

ISSRNS 2014 is organized by the Polish Synchrotron Radiation Society together with two research centers: the Institute of Physics, Polish Academy of Sciences in Warsaw and the National Centre for Nuclear Research in Świerk.

PTPS
Polskie Towarzystwo Promieniowania Synchrotronowego

Polish Synchrotron
Radiation Society

Institute of Physics
Polish Academy of Sciences

National Centre
for Nuclear Research

12th International School and Symposium on Synchrotron Radiation in Natural Science (ISSRNS 2014)

June 15 - 20, 2014

Warsaw, Poland

Organized by Polish Synchrotron Radiation Society in cooperation with Institute of Physics PAS and National Centre for Nuclear Physics

PROGRAMME

Sunday, 15 June			
Arrival			
16^{00}-17^{30}	Registration and Reception		
17^{30}-18^{00}	Opening Address		
18^{00}-18^{40}	L-01	M. Kiskinova	**Addressing Properties of Morphology Complex Materails and Individual Nanostructures using Synchrotron-based Spectromicroscopy and Imaging**
18^{40}-19^{00}	IO-01	A. Wolska	**XAFS study of the Ni complexes with hydantoin derivatives**
19^{00}-20^{10}	Get-Together Dinner		
Monday, 16 June			
8^{00}-9^{00}	Breakfast		
9^{00}-9^{40}	L-02	M.-E. Couprie	**New Generation of Light Sources: Present and Future**
9^{40}-10^{20}	L-03	J. Krzywiński	**X-ray Free Electron Lasers (XFELs) and properties of XFEL radiation**
10^{20}-11^{00}	L-04	C. Masciovecchio	**FERMI seeded FEL**
11^{00}-11^{30}	Coffee Break		
11^{30}-11^{50}	O-01	M. Di Fraia	**Photolonization and Velocity Map Imaging spectroscopy of Atoms, Molecules and Clusters with Synchrotron and Free Electron Laser Radiation at ELETTRA**
	O-03	T. Wasiewicz	**Eu-XFEL upgrade**
11^{50}-12^{10}	IO-02	A. Czajka	**A XAS study of low phonon glass-ceramics**
	IO-06	A. J. Wojeński	**GEM-2D detector based reconfigurable measurement system for hot plasma diagnostics**
12^{10}-12^{30}	IO-03	A. Rudkowski	**X-ray absorption near-edge structure spectroscopy of bornite, Cu_5FeS_4**
	IO-07	K. Stachnik	**High resolution ptychography using off-axis illuminated zone plates**
12^{30}-12^{50}	IO-04	M. Wydra	**Electronic properties of Ti-Al-C based MAX phases**
	O-04	W. A. Sławiński	**X-Ray diffraction study of stacking faults in silicoaluminophosphate SAPO-18/34**
12^{50}-13^{10}	O-02	W. Szczerba	**X-ray absorption fine structure study on electrochromic metallo-supramolecular polyelectrolytes**
	O-05	D. T. Dul	**Attenuation and indirect excitation effects in x-ray fluorescence holography**
13^{10}-13^{30}	IO-05	M. T. Klepka	**XAFS technique used to obtain structural information for complexes of coumarin derivatives with Cu**
	O-06	O. Adiguzel	**Crystallographic Studies on Phase Transition in Copper Based Shape Memory Alloys**
13^{30}-15^{00}	Lunch		
15^{00}-15^{40}	L-05	T. Shintake	**SACLA Hard X-ray Free Electron Laser Based on Normal Conducting Accelerator Technology**
15^{40}-16^{20}	L-06	A. Madsen	**Structural Dynamics Investigated by Coherent X-ray Scattering**
16^{20}-17^{00}	L-07	I. Vartaniants	**X-ray scattering methods for the study of disordered systems. New opportunities and challenges**
17^{00}-17^{30}	Coffee Break		
17^{30}-18^{10}	L-08	J. Keckes	**X-ray Nanodiffraction Characterization of Strains and Microstructure in Nanostructured Thin Films**
18^{10}-18^{30}	O-07	M. Szklarczyk	**Advances in surface chemical state imaging and depth profiling using XPS**

18^{30}-18^{50}	O-08	G. A. Appleby	**Science Link: Cooperation between science and industry in the Baltic Sea Region**
18^{50}-19^{10}	O-09	K. Jabłońska,	**X-ray absorption spectroscopy for industry: examples from Science Link project**
19^{10}-21^{30}	Dinner		
Tuesday, 16 June			
8^{00}-9^{00}	Breakfast		
9^{00}-13^{30}	Excursion to Świerk / Warsaw		
13^{30}-15^{00}	Lunch		
15^{00}-15^{45}	L-09	A. Barty	**Serial Crystallography with X-ray Free Electron Lasers**
15^{45}-16^{30}	L-10	W. Rypniewski	**Crystallography of CNG repeats – RNA molecules relevant to human health**
16^{30}-17^{00}	Coffee Break		
17^{00}-17^{40}	L-11	M. Eriksson	**MAX IV, The World's Brightest Synchrotron Radiation Source**
17^{40}-18^{20}	L-12	P. Raimondi	**ESRF Upgrade Phase II**
18^{20}-19^{00}	L-13	F. Fauth	**Powder diffraction and X-ray absorption spectroscopy in material science at the 3rd generation ALBA synchrotron source**
19^{00}-19^{50}	Dinner		
20^{00}-22^{00}	Poster Session		
Wednesday, 17 June			
8^{00}-9^{00}	Breakfast		
9^{00}-9^{40}	L-14		to be announced
9^{40}-10^{20}	L-15	E. Bräuer-Krisch	**Microbeam radiation therapy and other therapies with synchrotron X-rays**
10^{20}-11^{00}	L-16	A. Meents	**High-resolution x-ray phase contrast microscopy with tender X-rays**
11^{00}-11^{30}	Coffee Break		
11^{30}-12^{10}	L-17	P. W. Wachulak	**Extreme ultraviolet and soft X-ray imaging with compact, table top laser plasma EUV and SXR sources**
12^{10}-12^{50}	L-18	A. Rogalev	**X-ray Magnetic Circular Dichroism under High Magnetic Field**
12^{50}-13^{30}	L-19	M. Sikora	**RIXS-MCD as a sensitive probe of 3d magnetism with hard x-rays**
13^{30}-15^{00}	Lunch		
15^{00}-15^{20}	O-10	L.A. Dadinova	**Complex formation of pyrophosphatase with protein-partners investigated by small-angle X-ray scattering in solution**
	IO-10	A. Wawro	**Relations between structural and magnetic properties in metallic ultrathin multilayers**
15^{20}-15^{40}	IO-08	E. Lipiec	**SR-FTIR microspectroscopy coupled with multivariate data analysis in study of interaction between radiation and living matter**
	O-14	I.Sveklo	**Modification of magnetic properties of Pt/Co/Pt trilayer under nanosecond EUV irradiation**
15^{40}-16^{00}	IO-09	J. Czapla-Masztafiak	**The chemical forms of sulfur in prostate cancer tissue analyzed by means of XAS**
	O-15	D.Schmeißer	**Spin state and satellite structures in Co and Fe based absorber materials and catalyst**
16^{00}-16^{20}	O-11	C. Rivard	**Speciation and distribution of phosphorus in environmental samples using the ID21 beamline, at the ESRF**
	O-16	J. Kowalska	**Spectroscopic Insights into Nitrogenase Structure**
16^{20}-16^{40}	O-12	D. Adjei	**Laboratory laser-produced plasma source of soft X-rays for radiobiology studies**
	IO-11	W. Szmyt	**XANES study of the $(H_3O)[Ni(cyclam)][Fe(CN)_6]\cdot 5H_2O$ dehydration process**

16^{40}-17^{00}	O-13		to be announced
	O-17	C. Pettenkofer	**Energy Converting Interfaces Studied by Synchrotron Radiation**
17^{00}-17^{30}	Coffee Break		
17^{30}-18^{10}	L-20	A. Locatelli	**LEEM and XPEEM to watch graphen at different substrates**
18^{10}-18^{50}	L-21	Ł. Pluciński	**The electronic structure of spintronic materials as seen by spin- and angle-resolved photoemission**
18^{50}-19^{30}	L-22	C. S. Fadley	**New directions in hard and soft x-ray photoemission with synchrotron radiation**
19^{30}-20^{00}	Free Time before Conference Dinner		
20^{00}-22^{30}	Conference Dinner		
Thursday, 19 June			
8^{00}-9^{00}	Breakfast		
9^{00}-14^{00}	Excursion to Warsaw / Żelazowa Wola		
14^{00}-15^{30}	Lunch		
15^{30}-16^{15}	L-23	M. Mezouar	**Synchrotron radiation: an advanced tool for science under extreme conditions of pressure and temperature**
16^{15}-17^{00}	L-24	M. M. Nielsen	**Time-resolved x-ray scattering in molecular liquids**
17^{00}-17^{30}	Coffee Break		
17^{30}-18^{10}	L-25	W. Gawelda	**Watching chemical reaction dynamics with ultrashort X-ray pulses**
18^{10}-18^{30}	IO-12	J. Szlachetko	**Ultrafast pump-probe X-ray spectroscopy at SwissFEL**
18^{30}-18^{50}	IO-13	T. Kubacka	**Large amplitude spin dynamics driven by a THz pulse in resonance with an electromagnon**
18^{50}-19^{10}	IO-14	W. Kaszub	**Mainstream and alternative routes to photoinduced phase transitions**
19^{10}-20^{00}	Dinner		
20^{00}-22^{00}	PTPS Meeting		
Friday, 20 June			
8^{00}-9^{00}	Breakfast		
9^{00}-9^{40}	L-26	M.J. Stankiewicz	**Present status and future development of SOLARIS project**
9^{40}-10^{00}	O-18	M. Zając	**First bending magnet beamline at Solaris**
10^{00}-10^{20}	O-19	R. Nietubyć	**Single yoke double bend achromat of the MAX IV 1.5 GeV and Solaris storage rings**
10^{20}-10^{40}	O-20	M. Ślęzak	**Prospects of X-ray Photoemission Electron Microscopy at the first beamline of Polish synchrotron SOLARIS**
10^{40}-11^{10}	Coffee Break		
11^{10}-11^{30}	O-21	T. Szymocha	**Synchrogrid: IT services for polish Synchrotron operators and users**
11^{30}-13^{00}	Discussion Panel		
13^{00}-13^{15}	Closing Remarks		
13^{15}-14^{30}	Lunch		
14^{30}	Departure		

Welcome to the 12th ISSRNS

On behalf of the Programme Committee of the 12th International School and Symposium on Synchrotron Radiation in Natural Science (ISSRNS-2014) we are pleased to welcome you to this School and Symposium.

The ISSRNS is a series of biennial conference meetings organized in Poland since 1992, traditionally devoted to recent advances and new techniques employing synchrotron radiation (SR) in physics, chemistry, materials science, crystallography, biology and medicine as well as in the fields of archeometry, environmental protection, geology, quality control, etc. The aim of this interdisciplinary meeting is also to bring together scientists working with synchrotron radiation and those who would like to learn more about the sources and specific experimental techniques. The ISSRNS has a format of advanced workshop covering recent developments of synchrotrons and short-wavelength free electron lasers and providing a forum for reporting the most recent achievements in fundamental and applied research. ISSRNS meetings owe their success mainly to the lecturers from various synchrotron and scientific centers in the world.

The 12th ISSRNS is organized by Polish Synchrotron Radiation Society (PTPS) in cooperation with two Polish institutions, the Institute of Physics of the Polish Academy of Sciences in Warsaw and the National Centre for Nuclear Physics in Otwock-Świerk and under Honorary Patronage by Marshal of the Mazowieckie Voivodeship Adam Struzik.

As the year 2014 has been proclaimed by the United Nations as the International Year of Crystallography, the programme of the 12th ISSRNS provides, on this occasion, a special session on recent milestone advances in the discipline, whose progress is strictly related to the development of modern SR sources - synchrotrons and short-wavelength FELs. In Poland, construction of the first national synchrotron SOLARIS in Krakow will soon be completed. A concept of the Polish free electron laser proposed to be constructed at National Center for Nuclear Research in Otwock/Świerk also reaches its maturity. These facts pronouncedly influence the program of the current meeting beyond its traditional topics to promote integration of the SR community of users, designers and constructors of the advanced synchrotron sources.

The Capital City of Poland, Warsaw (Polish: Warszawa [var'ʂava]) is located on the Vistula River, in the central stretch of its reaches, in the flat region only about 100 m above sea level, in the central-eastern part of Poland. The historic center of Warsaw, together with the Royal Castle, is situated on the picturesque high escarpment on the left bank of the Vistula River. The old town, with a vast majority of historical houses, palaces and churches with their interiors, had to be painstakingly rebuilt after the extensive damage it suffered in World War II, during which 85% of its buildings were destroyed. Currently, besides its leading role as a political and business center of Poland, Warsaw is now a city of culture and science, with numerous theatres, cinemas, museums, galleries, music centers and cabarets. It is also the major center of education in Poland. More than twenty university or academy-level institutions educate 300,000 students. . . .

The conference venue is in a comfortable hotel BOSS, situated on the right bank of the Vistula river, near the administrative city limit of Warsaw, 20-25 km off the city center, on the edge of the Mazovian Landscape Park, a large (c.a. 160 sq. km), natural remnant of much greater ancient forest. This picturesque region, with forest grown on sandy Mazovian soil has for years attracted visitors from the Warsaw agglomeration who relax and get in some fresh air.

We hope you will find 12th ISSRNS as a very successful and remarkable event that could combine scientific purpose with possible rest.

Jerzy B. Pełka
(Chairman)

Ryszard Sobierajski
(Scientific Secretary)

L-01 **Sun. 15. 06., 18^{00}-18^{40}**

Addressing properties of morphology complex materails and individual nanostructures using synchrotron-based spectromicroscopy and imaging

Maya Kiskinova

Elettra-Sincrotrone Trieste, Area Science Park, Trieste 34149, Italy

Exploiting the structure and composition of technologically relevant complex materials at their natural length scales and working environment is important prerequisite for understanding dimensionality dependent phenomena. In this respect processes occurring at surfaces and interfaces control the properties of many materials where issues of complexity at microscopic length scales should be faced and understood. The complementary capabilities of synchrotron-based photoelectron microscopes in terms of imaging, spectroscopy, spatial and time resolution have opened unique opportunities to explore the surface composition of micro- and nano-structured materials as a function of their size, morphology and exposure to different ambient and temperature [1]. The most recent achievements in this respect will be illustrated by selected results with special emphasize on studies of to individual supported and free-standing nanostructures [2-5] and electrochemical devices [6].

[1] A. Barinov *et al*., *Nucl. Instr. Meth. Phys. Res.* **A 601** (2009) 195–202.
[2] A. Kolmakov *et al*., *ACS Nano* **2** (2008) 1993.
[3] V. Sysoev *et al.*, *ACS Nano* **4** (2010) 4487.
[4] A. Barinov *et al.*, *Adv. Mater*. **21** (2009) 1916.
[5] F. Jabeen *et al.*, *Nano Res.* **3** (2010) 706.
[6] B. Bozzini *et al*., *Chem. Eur. Journal* **18** (2012) 101.

L-02 **Mon. 16. 06., 9^{00}-9^{40}**

New generation of light sources: present and future

M. E. Couprie*

Synchrotron SOLEIL, L'Orme des Merisiers, Saint-Aubin, BP 48, F 91 192 Gif sur Yvette, France

Keywords: synchrotron radiation, free-electron laser

*e-mail: couprie@synchrotron-soleil.fr

More than 50 years after the lasers discovery and more than 30 years after the first Free Electron Laser (FEL), VUV-X light sources are actively developed around the word. Besides X-ray laser and High order Harmonic Generation in Gas (HHG) or on solid targets, synchrotron radiation from third and fourth generation light sources rely on synchrotron radiation generated from charged particles in bending magnets or undulators, creating a periodic permanent magnetic field. In FELs, the longitudinal coherence is achieved by setting in phase the electrons, thanks to an energy exchange between the electrons and a light wave resulting in bunching and gain for light wave amplification. FELs offer femtosecond intense tuneable light. Presently, several facilities are open for users in the world : LCLS and SACLA in the 1-0.1 nm spectral range, and in the VUV soft X-ray region FLASH and FERMI, first seeded FEL open for users.

In the quest to the fifth generation of acceleration based light sources, paths towards advanced and compact FELs are open. In order to approach diffraction and Fourier limits in a wide spectral range and with versatile properties, one considers FEL oscillator in the X-ray range, advanced seeding, multiple simultaneous operation, high repetition rate. In order to search for compactness, one considers investigating further the seeding schemes for the FEL line and replacing the conventional linear accelerator by a compact alternative one, such as dielectric accelerator, inverse FEL and Laser WakeField Accelerator (LWFA). Indeed, the rapidly developing LWFA are already able to generate synchrotron radiation. With an electron divergence of typically 1 mrad and an energy spread of the order of 1 %, an adequate beam manipulation through the transport to the undulator is needed for FEL amplification.

Several directions are explored within the LUNEX5 (free electron Laser Using a New accelerator for the Exploitation of X-ray radiation of 5th generation) project, aiming at investigating the production of short, intense, and coherent pulses in the soft X-ray region with 400 MeV electron beam (both from a superconducting linear accelerator for high repetition rate multiple user operation and a LWFA, a single FEL line with HHG and Echo Enable Harmonic Generation seeding). A test experiment for the demonstration of FEL amplification with a LWFA is under preparation in the frame of the COXINEL ERC contract.

Acknowledgments: This work is supported by the COXINEL ERC Grant.

L-03 **Mon. 16. 06., 9^{40}-10^{20}**

X-ray Free Electron Lasers (XFELs) and properties of XFEL radiation

J. Krzywinski*

SLAC National Accelerator Laboratory, 2575 Sand Hill Road MS 29, Menlo Park, CA 94025, USA

Keywords: synchrotron radiation, free-electron laser

*e-mail: krzywins@slac.stanford .edu

The Free Electron Laser (FEL) was invented by J.M.J Madey [1] in 1971 at Stanford University. The FEL radiation was produced by a relativistic electron beam moving through a magnetic wiggler that was also conceived at Stanford by H.Motz in 1951 [2]. The Original Madey's theoretical treatment was based on QED. It turned out however, that for most practical applications the classical treatment of radiation is sufficient. As a matter of fact, one of the most important XFEL parameters – the Pierce parameter – was introduced by J.P. Pierce in 1947 to describe the amplification process in Traveling Wave Tubes [3].

The first FEL operated at far infrared wavelength as an oscilator or an amplifier. Such schemes of operation limited the radiation wavelength to the UV range. This limitation was overcomed by the invention of Self Amplified Spontaneous Emission FEL (SASE FEL) theory by A.M. Kondratienko, E. Saldin, R. Bonifaccio and C. Pelegrini in the early 1980s [3,4]. This theory predicted that SASE FEL could produce a laser-like photon beam in the hard X-ray regime without the use of optical elements or a seeded beam. The SASE FEL principle was first demonstrated experimentally in the VUV regime at FLASH at Deutsches Elektronen – Synchrotron DESY in Hamburg in 2000 and in the hard X-ray regime at Linear Coherent Light Source (LCLS) at SLAC National Accelerator Laboratory in 2009. At its birth the LCLS was the brightest X-ray source on Earth in the photon energy range 800 eV – 9000 eV. Soon after, in 2011, the SPring-8 Angstrom Compact Free Electron laser SACLA in Japan produced ultra-bright X-ray beam at 0.8 Angstroms. There are three other XFEL projects under construction in Germany (European XFEL), Korea (PAL-XFEL) and Switzerland (SwissFEL).

X-ray SASE FELs typically generate 10^{12} – 10^{13} photons in femtosecond pulses in the relative bandwidth of a fraction of a percent. Recently, seeded FEL schemes have been implemented at Electra FEL in Trieste in the XUV regime, and at the LCLS in the Soft and Hard X-ray regime. Seeded X-ray FELs have a potential of generating Terawatt X-ray pulses in a relative bandwidth that is better than 10^{-4}.

In my talk I will present principles of operation of SASE and seeded XFELs. I will describe basic characteristics of XFEL radiation such as pulse energy, radiation spectrum, and temporal and spatial properties which also include coherence. I will compare the theoretical predictions with the experimental results. I will also refer to recent developments at the LCLS that allow generation of two pulses, multicolor SASE and seeded X-ray beams with a tunable delay time between the pulses. I will end my talk with a brief description of the LCLS II project.

[1] J. M. J. Madey, *J. Appl. Phys.* **42** (1971) 1906
[2] H. Motz, *J. Appl. Phys.* **22** (1951) 527.
[3] J. P. Pierce, *Proc. IRE* **35** (1947) 108.
[4] A. M. Kondratenko, E.L. Saldin, *Part. Accel.* **10** (1980) 207.
[5] R. Bonifacio, C. Pellegrini, L. M. Narducci, *Opt. Comm.* **50** (1984) 373.

L-04 **Mon. 16. 06., 10^{20}-11^{00}**

FERMI seeded FEL

C. Masciovecchio*

Elettra – Sincrotrone Trieste, S.S. 14 km 163,5 in Area Science Park – 34149 Basovizza, Trieste Italy

Keywords: free-electron laser, extreme conditions

*e-mail: claudio.masciovecchio@elettra.eu

The free-electron laser (FEL) FERMI has recently been opened, as experimental facility, to the scientific community [1]. The electron bunch acceleration scheme makes FERMI unique among the present FEL's operating worldwide. The peculiarity of FERMI to deliver transform limited photon pulses opens up the way to investigations of fundamental properties of matter with unprecedented capabilities. We will discuss the expected impact of FERMI in studies of fast phenomena in solids, liquids and gases, combining scattering and spectroscopic approaches [2].

Moreover FERMI is the proof of principle that table-top laser experiments can now be carried out at much shorter wavelengths making possible to probe dynamical processes occurring in molecular and nanostructured materials with an unprecedented time-space (femtosecond-nanometer) resolution. Indeed, the use of high energy photons allows stimulating and probing electronic transitions from core levels thus providing chemical selectivity. This will advance our knowledge to the very essence of materials science, chemistry, and biology, thus opening the way to future technologies that cannot even be foreseen today [3].

[1] E. Allaria et al., *New J. of Phys.* **14** (2012) 113009.
[2] E. Allaria et al., *Nat. Comm.* **4** (2013) 2476.
[3] F. Bencivenga et al., *New J. of Phys.* **15** (2013) 123023.

L-05 **Mon. 16. 06., 15^{00}-15^{40}**

SACLA Hard X-ray free electron laser based on normal conducting accelerator technology

T. Shintake*

OIST: Okinawa Institute of Science and Technology Graduate University
1919-1, Tancha, Onna-son, Okinawa 904-0495 Japan

Keywords: free-electron laser, SACLA

*e-mail: shintake@oist.jp

SACLA X-ray Free Electron Laser started operation in 2011 June, since then it has been providing intense X-ray ultra-short pulses to users from various filed. SACLA generates hard X-ray at 1 Å wavelength by means of short-period in-vacuum undulator driven by 8 GeV electron beams, provided by the linear accelerator based on high-gradient normal-conducting C-band 5712 MHz rf technology developed in Japan [1, 2, 3]. Thanks to these technologies, the total length of SACLA facility fits within 700 meter available at SPring-8 site.

Special care was taken to ensure high uptime machine reliability and superior electron beam energy stability. The achieved energy stability is as low as 100 ppm for long-period of operation, and 20 ppm jitter in pulse-to-pulse mode. Corresponding wavelength variation in pulse-to-pulse jitter is $<10^{-4}$ on 1 Å X-ray pulses, which enables stable operation of FEL.

Typical X-ray parameter is 1~0.6 Å, peak power 10 GW, pulse length 200~30 fsec, pulse energy 0.1~0.5 mJ.

Figure 1. SACLA constructed at SPring-8 site.

Acknowledgments: Thanks to all SACLA construction team.

[1] T. Shintake *et al.*, *Nature Photonics*, **2** (2008).
[2] T. Ishikawa *et al.*, Nature Photonics **6** (2012) 540-544.
[3] T. Shintake *et al.*, "C-band Linac RF System for e+e- Linear Collider", Proc. 16th Biennial Particle Accelerator Conference: PAC '95, Dallas, TX, USA, 1 - 5 May 1995 - IEEE, New York, 1995. pp. 1099-1101.

L-06 **Mon. 16. 06., 15^{40}-16^{20}**

Structural dynamics investigated by coherent X-ray scattering

A. Madsen

European X-Ray Free-Electron Laser Facility
Albert-Einstein-Ring 19, D-22761 Hamburg, Germany

In the talk I introduce the concept of X-ray coherence with respect to scattering experiments. A high flux of coherent X-rays is available since the mid 90ies at modern synchrotron sources with low emittance and high brightness, or more recently at free-electron laser sources. Coherent scattering has advantages over "regular" scattering experiments when it comes to studies of structure and dynamics. In the talk the coherent scattering technique X-ray Photon Correlation Spectroscopy (XPCS) is introduced [1,2]. XPCS allows studies of structural dynamics in a wide range of systems and in different scattering geometries. Examples of recent applications are given as well as an outlook to the bright future.

[1] G. Grübel, A. Madsen, and A. Robert, X-Ray Photon Correlation Spectroscopy (XPCS) in Soft Matter Characterization, Borsali & Pecora (Eds.), Springer (2008) 953-995; http://link.springer.com/referenceworkentry/10.1007%2F978-1-4020-4465-6_18

[2] A. Madsen, R. L. Leheny, H. Guo, M. Sprung and O. Czakkel, *New Journal of Physics* **12** (2010) 055001.

L-07 **Mon. 16. 06., 16^{20}-17^{00}**

X-ray scattering methods for the study of disordered systems. New opportunities and challenges

I. Vartaniants

L-08 **Mon. 16. 06., 17^{30}-18^{10}**

X-ray nanodiffraction characterization of strains and microstructure in nanostructured thin films

J. Keckes*

Department of Materials Physics, Montanuniversität Leoben and Erich Schmid Institute for Materials Science, Austrian Academy of Sciences, Jahnstrrasse 12, A-8700 Austria

Keywords: synchrotron nanodiffraction, thin film, stress, microstructure

*e-mail: jozef.keckes@gmail.com

Nanocrystalline thin films exhibit typically inhomogeneous depth gradients of microstructure, strain and physical properties varying at the nanoscale. Currently it is not trivial to reveal how those gradients relate to the macroscopic film functional properties. One of the main reasons is the lack of experimental techniques which can provide thin film thickness-dependent data with sub-micron resolution.

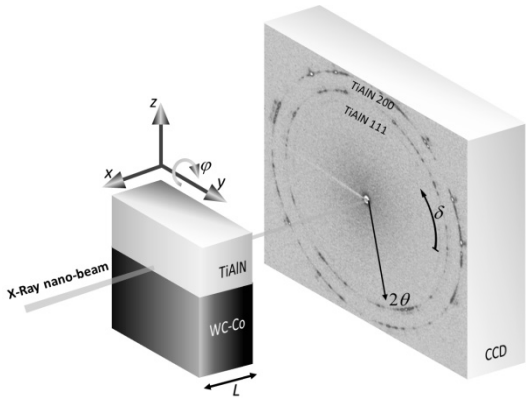

Figure 1. A schematic setup of the cross-sectional X-ray nanodiffraction experiment carried out using a monochromatic X-ray beam. The thin film on the substrate (with the thickness L=50 μm in the beam direction) was moved along the y axis with a step of 100 nm and the diffraction data were collected using a CCD detector.

In order to reveal gradients of phases, crystallographic texture, crystallite size and strains in thin films, we have developed a cross-sectional synchrotron X-ray nanodiffraction technique (Fig. 1) which operates with the X-ray beam diameters down to 50 nm [1-3]. The aim of this contribution is to discuss the methodological aspects of the new approach and its applications at the beamlines ID13 at ESRF in Grenoble and at P03 at Petra III in Hamburg. On the examples of hard nitride and metallic thin films (Fig. 2), it will be demonstrated that the new approach can serve as an effective tool to characterize the inhomogeneous thin film properties with 50nm resolution. In this way it is possible to correlate the gradient properties of thin films with the deposition conditions and functional behavior.

Additionally, results from in-situ X-ray nanodiffraction coupled with indentation will be presented. The new in-situ design is suitable to reveal microstructural changes and stress behavior under the indenter in nanomaterials. In this way, it is possible to study deformation behavior in materials with size effects.

Additionally, results from mechanical tests obtained from bending experiments on micro-cantilevers performed in scanning and transmission electron microscopes will be presented to illustrate variability and anisotropy of mechanical properties in graded nanostructured films. The results will be correlated with the X-ray nanodiffraction data. Finally, it will be demonstrated that both complementary approaches can serve as an effective tool to analyze depth gradients of structure-property relationship in nanocrystalline thin films.

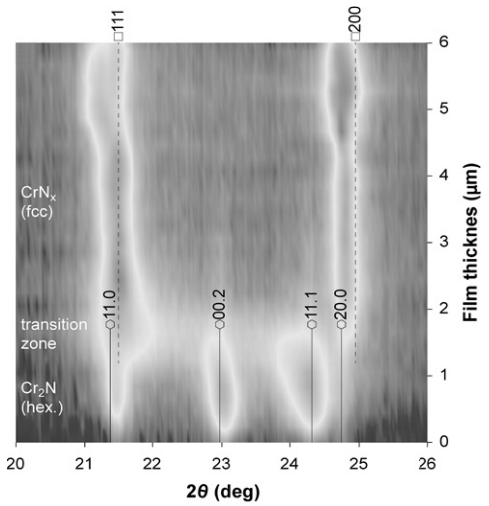

Figure 2. A result from the cross-sectional X-ray nanodiffraction experiment on a graded CrN_x 6μm thin film indicates the distribution of phases as a function of the depth.

[1] J. Keckes, M. Bartosik, R. Daniel, C. Mitterer, G. Maier, W. Ecker, J. Vila-Comamala, C. David, S. Schoeder, M. Burghammer, *Scripta Mater.* **67** (2012) 748.
[2] M. Stefenelli, J. Todt, A. Riedl, W. Ecker, T. Müller, R. Daniel, M. Burghammer, and J. Keckes, *Journal of Applied Crystallography*, **46** (2013) 1378–1385.
[3] M. Bartosik, R. Daniel, C. Mitterer, I. Matko, M. Burghammer, P.H. Mayrhofer, J. Keckes, *Thin Solid Films* **542** (2013) 1-4.

L-09 **Tue. 17. 06., 15^{00}-15^{45}**

Serial crystallography with X-ray Free Electron Lasers

A. Barty*

Center for Free Electron Laser Science, DESY, Hamburg, Germany

*e-mail: anton.barty@desy.de

The extremely intense, femtosecond duration X-ray pulses provided by X-ray free electron laser sources enable the measurement of diffraction patterns from sub-micron sized crystals before each crystal is vaporised. This has enabled a new approach to collecting X-ray diffraction data from many hundreds of thousands of microcrystals flowing across a pulsed X-ray beam. Although each crystal is destroyed in a single pulse, the X-ray pulse duration is so short that the measured diffraction data is apparently free of signs of radiation damage, while the flowing suspension provides a continual source of fresh crystals for the next pulse. Referred to as serial crystallography, this technique permits room temperature measurement of radiation sensitive microcrystals too small for study at synchrotron sources, including microcrystals grown *in vivo* [1,2] and membrane proteins embedded in lipidic phase growth medium [3]. Serial femtosecond crystallography is particularly suited to the study of time-resolved biochemistry, including the study of non-reversible or non-cyclic processes [4]. Serial crystallography requires an intense X-ray beam, a fast detector system, and the computational infrastructure to process large data volumes. Indeed, recent experiments demonstrate that serial crystallography can be performed at synchrotron sources [5].

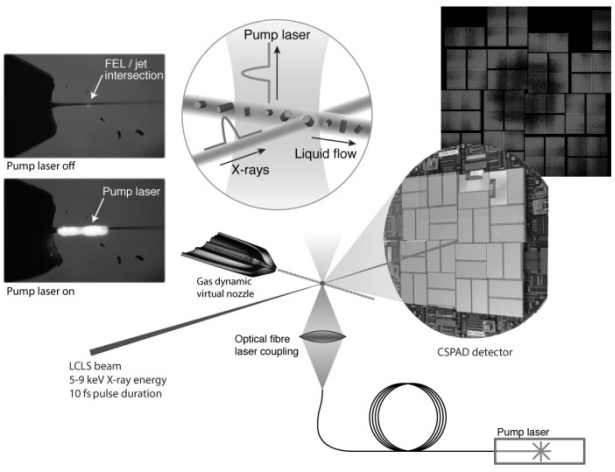

[1] R. Koopmann *et al.*, *Nature Methods* **9** (2012) 259–262.
[2] L. Redecke *et al., Science* **339** (2013) 227–230.
[3] W. Liu, *et al. Science* **342** (2013) 1521–1524 (2013).
[4] A. Aquila *et al. Opt Express* **20** (2012) 2706–2716.
[5] C. Gati, C. *et al.* research papers. *IUCrJ* **1** (2014) 87-94.

L-10 **Tue. 17. 06., 15^{45}-16^{30}**

Crystallography of CNG repeats – RNA molecules relevant to human health

W. Rypniewski*, A. Kiliszek

Institute of Bioorganic Chemistry, Polish Academy of Sciences, Noskowskiego 12/14/61-704 Poznań

Keywords: synchrotron radiation, CNG repeats, TREDs

*e-mail: wojtekr@ibch.poznan.pl

CNG repeats (N denotes one of the four natural nucleotides) are abundant in the human genome. Their abnormal expansion is the cause of twenty deurodegenerative disorders, such as Huntington's diesease, myotonic dystrophy, spinocerebellar ataxias and fragile X syndrome, together known as TREDs (Trinucleotide Repeat Disorders). The toxic factor can be protein expressed from the abnormal gene or it can be mRNA containing the extended CNG tracts, which tend to fold into long hairpin structures and precipitate in the cell nucleus.

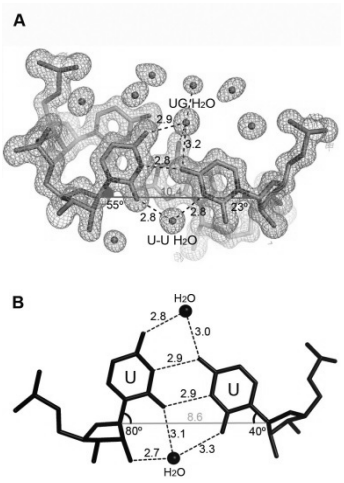

Figure 1. Non-canonical pairing of uridine residues in CUG repeats (A) and in other RNA molecules (B)

We have characterised by X-ray crystallography all four types of CNG repeats [1, 2, 3, 4] with the aim to build their detailed structural profiles to be used in structure-based drug design

Acknowledgments: This work was supported by National Science Centre [Poland, UMO-2011/01/B/NZ1/04429]

[1] A. Kiliszek, R. Kierzek, W. Krzyżosiak, W. Rypniewski, *Nucleic Acids Res.* **40** (2012) 8155.
[2] A. Kiliszek, R. Kierzek, W. Krzyżosiak, W. Rypniewski, *Nucleic Acids Res.* **39** (2011) 7308.
[3] A. Kiliszek, R. Kierzek, W. Krzyżosiak, W. Rypniewski, *Nucleic Acids Res.* **38** (2010) 8370.
[4] A. Kiliszek, R. Kierzek, W. Krzyżosiak, W. Rypniewski, *Nucleic Acids Res.* **37** (2009) 4149.

L-11 **Tue. 17. 06., 17^{00}-17^{40}**

MAX IV, the worlds brightest synchrotron radiation source.

M. Eriksson

MAX-lab, Lund University, Sweden

The MAX IV synchrotron radiation facility is currently being built in Lund, Sweden. The facility consists of 2 storage rings and one full-energy injector linear accelerator (linac).

The two storage rings are operated at 1.5 and 3 GeV respectively. Two 1.5 GeV storage rings will be built in a cooperation between MAX-lab and the Solaris facility in Krakow so one ring will be raised in Lund and the other in Krakow.

The 3 GeV storage ring in Lund is of the Multi-Bend Acromat (MBA) type which offers an emittance of 0.2 to 0.3 nm rad depending on the Insertion Devices (ID) chosen. This ring can be regarded as a fore-runner for other MBA projects around the world.

The linear accelerator will, apart from its injection task, also be used to produce fs high intensity X-ray pulses for the Short Pulse Facility (SPF). This facility has the potential of being upgraded to a Free Electron Laser (FEL) facility operated in the soft and hard X-ray spectral regions.

This talk will cover the design philosophy of the MAX IV facility as well as some of the technical solutions chosen. Finally, an international overview of Diffraction Limited Storage Rings (DLSR) being planned or constructed will be given.

L-12 **Tue. 17. 06., 17^{40}-18^{20}**

ESRF upgrade phase II

P. Raimondi

L-13 **Tue. 17. 06., 18^{20}-19^{00}**

Powder diffraction and X-Ray absorption spectroscopy in material science at the 3rd generation ALBA synchrotron source

F. Fauth*

CELLS-ALBA,E-08290 Cerdanyola del Vallès, Barcelona, Spain

Keywords: synchrotron radiation, powder diffraction, absorption spectroscopy

*e-mail: ffauth@cells.es

The ALBA-CELLS synchrotron located in the Barcelona area is actually the latest synchrotron source in Europe. Machine and beamline commissioning started at the end of 2010 and in mid 2011. First official users started in May 2012. The facility operates seven beamlines in soft X-ray energies (Resonant Absorption Scattering, Photoemission Spectroscopy and Microscopy, X-Ray Microscopy) and hard X-Ray energies (Non Crystalline Diffraction, Absorption and Emission Spectroscopy, Macromolecular Crystallography, Powder Diffraction). Two additional beamlines are under design/construction and proposals evaluation for 4 more beamlines is underway. Herewith, the two beamlines oriented to materials science essentially are presented: the Materials Science and Powder Diffraction (MSPD) beamline and the Core Level Absorption & Emission Spectroscopies (CLÆSS) beamline.

The MSPD beamline [1], with energy ranging from 8 to 50 keV consists of two experimental stations positioned in series: a High Pressure/Microdiffraction station and a high-angular resolution/high throughput powder diffraction station. The beam on the first station can be principally focused down to 15 x 15 microns using Kirckpatrick-Baetz geometry optics within a 0.25-0.60 Å wavelength range. Together with a Rayonix SX165 CCD detector and an appropriate stack of translation stages as sample/detector tower support, the station is designed to studies of limited size powder samples as is generally the case in High Pressure studies. Two standard types (Boehler and membrane-type cells) of diamond anvil cells (DACs) are parts of the standard sample environment equipment. The station is as well used for microdiffractions studies on e.g. cultural heritage samples for which exact localization of the beam impact on the sample is a perequisite. For this purpose, an online visualisation device has been in house designed.

The Powder Diffraction station consists in a 3-circles diffractometer delivered by HUBER. On the outer circle is mounted a 13-channels analyzer/YAP scintillator/PMT tube detector system allowing data collection at high angular resolution. Either 111 or 220 silicon Bragg reflections can be selected for the analyzers [2]. The middle circle is supporting 6 Si-based solid state detector modules (MYTHEN by DECTRIS) allowing simultaneous acquisition of powder patterns in a 40º 2Theta range at ms time resolution. Finally a heavy duty Eulerian Cradle can be optionally mounted on the inner circle. The wavelength range and beam size are 0.25-1.54 Å and max. 5 x 1.5 mm, respectively. Data can presently be collected in 80-1200 K temperature range, down to 5K later.

The CLÆSS beamline is dedicated to X-ray absorption (XANES, EXAFS) and X-ray emission spectroscopy. For absorption studies, a 200-500 micron beam, stable in position and size, is achieved over the energy range 2.4 - 68 keV. XANES and/or EXAFS spectra are presently collected in fluorescence mode, using standard commercial solid state detector, or in transmission mode, using the combination of ionization chambers and ALBA designed elctrometers. The so called CLEAR spectrometer is presently under commissioning and will allow X-Ray emission spectroscopy in the energy range 2-22 keV.

In the talk, I will give an overview of the two beamlines instrumentations and the most relevant steps of the commissioning. Typical examples of measurements performed on both beamlines, either by external users our in-house, will be presented. These examples cover as various filedd as cultural heritage, electrochemistry, catalysis, pharmaceutics, solid state physics and engineering studies.

Acknowledgments: Colleague scientists and post docs of both beamlines, I. Peral, C. Popescu, O. Vallcorba (MSPD) and L. Simonelli, C. Marini, M. Avila and W. Olszewski (CLÆSS) are acknowledged for their involvement in beamline operation. Former scientists who participated in the design of MSPD (M. Knapp) and CLÆSS (K. Klementiev and G. Guilera) are not forgotten.

[1] F. Fauth, I. Peral, C. Popescu, M. Knapp, *Powder Diffraction* **V28** (2014) S360.
[2] I. Peral, J. McKinley, M. Knapp, S. Ferrer, *J. Synchrotron Rad.* **18** (2011) 1.

L-15 **Wed. 18. 06., 9^{40}-10^{20}**

Microbeam radiation therapy and other therapies with synchrotron X rays

E. Bräuer-Krisch[1], C. Nemoz[1], T. Brochard[1], M. Renier[1], H. Requardt[1], R. Serduc[2],G. LeDuc[1], A. Bravin[1], S. Bartzsch[3], P. Fournier[4, 1], I. Cornelius[4], P. Berkvens[1], J.C. Crosbie[4], M.L.F. Lerch[4], A. B. Rosenfeld[4], M. Kocsis[1], M. Donzelli[1,3], U.Oelfke[3], A. Bouchet[5], V. Djonov[5],F. Estève[2], J. F. Adam[2], H. Elleaume[2], J. Balosso[6], H. Blattmann[7], B. Kaser-Hotz[8], J. A. Laissue[9]

[1]*European Synchrotron Radiation Facility, B.P.220, F-38043 Grenoble Cedex, France*
[2]*INSERM unit 836, CHU Grenoble, Grenoble, France*
[3]*Im Neuenheimer Feld 280,69120 Heidelberg,Germany*
[4]*CMRP, Northfields Ave., Wollongong, 2500, NSW, Australia*
[5]*Universität Bern Institut für Anatomie Baltzerstrasse 2CH-3000 Bern 9*
[6] *CHU Grenoble, Grenoble, France*
[7]*Niederwiesstr. 13c 5417 Untersiggenthal, Switzerland*
[8]*Animal Oncology and Imaging Center, Rothusstr. 2, CH-6331 Huenenberg/CH*
[9]*University of Bern,Faculty of Medicine, Murtenstrasse 11, CH-3010 Bern, Switzerland*

Microbeam Radiation Therapy (MRT) uses a spatially fractionated filtered white X-ray beam from a high energy wiggler Synchrotron Source (energies 50-350keV) with extremely high dose rates (up to about 20kGy/s). The typical planar beam width in an array is 25-100µm with 100-400µm wide spaces between beams. Such beams are very well tolerated by the tissue, even the high "peak" doses delivered in the path of the microbeams, when respecting a dose prescription in the "valley' that corresponds to a dose used of conventional RT converted to a single exposure . The superior tumor control when compared to that realized by conventional RT is achieved by differential effects of MRT on the normal tissue vasculature versus the tumor vasculature.

The MRT technique has been technically set up, tested and successfully applied during the last 20 years on various tumour models. Presently, the project is mature enough to be used for the treatment of spontaneous tumours in pets. Unified efforts from several teams with very different expertise now permit Microbeam Radiation Therapy in animal patients with a high degree of safety, in pursuit of the ultimate goal of clinical applications in humans.

The MRT trials for animal pets as tumor patients required substantial work for developing, upgrading and progressively implementing instrumentation, dosimetry protocol, as well as the crucial patient safety systems. Progress on the homogenous dose measurements using ionisation chambers and Alanine dosimetry as well as the comparison of high resolution dosimeters with the dose calculations based on a novel tumor planning system will be summarized. A general overview on the different achievements will be presented as well as a vision for possible human trials.

In addition, the principle of the on-going SSRT (Stereotactic Synchrotron Radiation Therapy) clinical trials will be briefly introduced.

L-16 **Wed. 18. 06., 10^{20}-11^{00}**

High-resolution x-ray phase contrast microscopy with tender X-rays

A. Meents[1]*, M. Wamer[1], I. Vartiainen[2] and C. David[2]

[1]*Deutsches Elektronen Synchrotron, DESY-PS, Notkestr. 85, D-22607 Hamburg, Germany*
[2]*Paul Scherrer Institut, CH-5232 Villigen, Switzerland*

Keywords: X-ray microscopy, biological samples

*e-mail: alke.meents@desy.de

X-ray microscopy bridges the gap between light microscopy with a spatial resolution of about 500 nm and electron microscopy with resolutions down to 2 nm investigating biological samples. The strength of X-ray microscopy is the much higher penetration depths of X-rays compared to electrons which makes X-ray microscopy the ideal tool for 3D structure determinations in tomographic mode.

X-ray microscopy with biological samples is commonly performed with soft X-rays at energies around 500 eV in the so called water window between the K-absorption edges of carbon and oxygen. Thus it provides it very good absorption contrast. A major drawback of soft X-ray microscopy is the small depths of field which limits the isotropic resolution which can be achieved in tomographic experiments.

This limitation can be overcome by using X-rays with higher energies where samples become more transparent. Zernike phase contrast microscopy is a powerful technique for such samples which provide small absorption contrast only [1] and has been also successfully applied to X-ray microscopy [2].

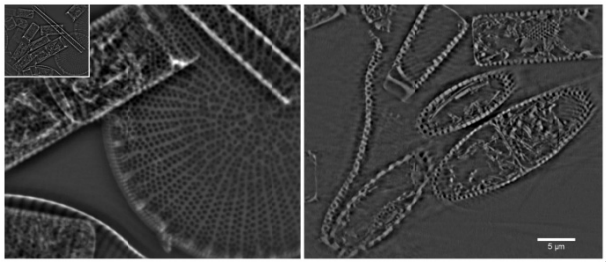

Figure 1. 2D radiography (left) and virtual slice (right) from the reconstructed tomographic volume of a fossile diatom obtained by X-ray Zernike phase contrast microscopy.

At beamline P11 at the PETRA III synchrotron in Hamburg (DESY) we have recently implemented a setup for X-ray Zernike phase contrast working with X-ray energies around 6.2 keV. We are currently working on an advanced setup which will be operated in vacuum at tender X-rays around 4 keV at a spatial resolution around 25 nm.

[1] F. Zernike, *Z. f. Techn. Physik* **11** (1935) 454.
[2] U. Neuhaeusler *et al*., *J. Phys. D* **36** (2003) A79.

L-17 **Wed. 18. 06., 11^{30}-12^{10}**

Extreme ultraviolet and soft X-ray imaging with compact, table top laser plasma EUV and SXR sources

P. W. Wachulak[1]*, A. Bartnik[1], J. Kostecki[1], A. Baranowska-Korczyc[2], D. Panek[3], P. Bruza[3], L. Wegrzynski[1], T. Fok[1], L. Pina[3], R. Jarocki[1], M. Szczurek[1], K. Fronc[2], D. Elbaum[2] , R. Hudec[4], Z. Zápražný[5], D. Korytár[5], M. Kozlova[6], J. Nejdl[6], and H. Fiedorowicz[1]

[1]*Institute of Optoelectronics, Military University of Technology, Warsaw, Poland*
[2]*Institute of Physics, Polish Academy of Sciences, Warsaw, Poland*
[3]*Czech Technical University, Czech Republic*
[4]*Astronomical Institute of the ASCR, v.v.i. , Czech Republic*
[5]*Institute of Electrical Engineering, Slovak Academy of Sciences, Bratislava, Slovakia*
[6]*Prague Asterix Laser System, Prague, Czech Republic*

Keywords: EUV/SXR imaging, EUV/SXR microscopy, EUV tomography, EUV shadowgraphy, synchrotron SOLARIS,

*e-mail: wachulak@gmail.com

Imaging with high spatial resolution is crucial in the development of nanotechnology. Manipulation of matter at the nanometer scale and the possibility of subsequent or "in situ" verification of the results of this manipulation are very important in these days, in which the direction of the development of science and technology is determined by the aspirations of the semiconductor industry, manifested in the possibility of producing ever smaller structures and more efficient devices. These aspirations of the computer industry translate well to other scientific fields such as nanotechnology, biology or materials science.

In this paper we present an overview of imaging techniques employing short wavelength extreme ultraviolet (EUV) and soft X-ray (SXR) compact, laser-plasma sources. The techniques, presented in this work, are EUV and SXR ("water-window") microscopy, EUV shadowgraphy and its direct extension to EUV tomography technique, capable of visualizing 3-D objects. EUV and SXR microscopy, employing photons with a wavelength of the order of nanometers to tens of nanometers, has a number of advantages compared to the widely used optical microscopy. It allows rendering images of objects, with spatial resolution better than 100nm, with shorter exposure times and high optical contrast in the short wavelength range, to gain additional information about the object.

At the Institute of Optoelectronics so far two experimental microscopes were developed, the first in the EUV range that is able to capture the magnified images of the objects with sizes less than 100nm [1], and the second one in the range of SXR, in the so-called "water window", which could render images of objects

with sizes of about 1 micron, but allowing to obtain a high optical contrast for the observation of biological materials and samples having a relatively thickness of 40 microns [2]. Experimental microscope systems are extremely compact. Both of them can fit on top of the optical table 1.2x1.8m^2 in size. These systems have been used for imaging different samples, demonstrating the usefulness of EUV and SXR radiation for microscopy. Through the use of optical contrast in the field of EUV and SXR is possible to obtain additional, complementary information on the same sample, not available directly from the images from the optical microscopes and SEM, with better spatial resolution than in the case of optical microscopy.

It should be emphasized that there are a few constructions of this kind in the world, and to our knowledge, these are the only experimental microscopes of this type in Poland. These devices have a high chance of future commercialization and many potential applications in nanotechnology, biology and industry. In addition EUV and SXR microscopes in the near future may be implemented in form of beamlines, or "end-station", as imaging devices for Polish synchrotron SOLARIS, Cracow, or free electron laser POLFEL in Swierk, near Warsaw.

EUV shadowgraphy or radiography is well established technique capable of obtaining projection images of semitransparent or opaque objects. We used it here to investigate and optimize the gaseous targets for applications in laser-matter interaction experiments [3, 4].

An extension of this technique to 3-D is EUV tomography at 13.5nm lithographic wavelength recently reported in [5], where a set of angularly equidistant radiograms – projections were acquired and combined to produce a 3-D representation of a multi-jet gas puff target for potential applications in high order harmonic generation.

Acknowledgments: This work was supported by The National Centre for Research and Development, LIDER programme, project no. LIDER/004/410/L-4/12/NCBR/2013, the National Centre for Science, award number DEC2011/03/D/ST2/00296, LASERLAB–EUROPE III - grant agreement 284464, COST Action MP0601 and MP1203, Research and Development Centre for Advanced X-ray Technologies, ITMS code 26220220170, Science and Technology Assistance Agency Bratislava, project No. APVV-0308-11.

[1] P. W. Wachulak, A. Bartnik, H. Fiedorowicz, J. Kostecki, *Optics Express* **19** (2011) 9541–9550.

[2] P. W. Wachulak, A. Bartnik, M. Skorupka, J. Kostecki, R. Jarocki, M. Szczurek, L. Wegrzynski, T. Fok, H. Fiedorowicz, *Applied Physics B*, accepted for publication, (2013).

[3] W. Wachulak, L. Wegrzynski, A. Bartnik, T. Fok, R. Jarocki, J. Kostecki, M. Szczurek and H. Fiedorowicz, *Laser and Particle Beams* **31** (2013) 219-227.

[4] P.W. Wachulak, A. Bartnik, R. Jarocki, H. Fiedorowicz, *Nucl. Instr. Meth.Phys. B*, **285** (2012) 102–106.

[5] P. W. Wachulak, Ł. Węgrzyński, Z. Zápražný, A. Bartnik, T. Fok, R. Jarocki, J. Kostecki, M. Szczurek, D. Korytár, H. Fiedorowicz, *Optics Letters* **39** (2014) 532-535.

L-18 **Wed. 18. 06., 12^{10}-12^{50}**

X-ray Magnetic Circular Dichroism under high magnetic field

A. Rogalev*, F. Wilhelm

European Synchrotron Radiation Facility (ESRF), 71 rue des Martyrs, 38000 Grenoble, France

Keywords: X-ray circular dichroism, magnetism

*e-mail: rogalev@esrf.fr

Discovery of X-ray Magnetic Circualr Dichroism (XMCD) ushered in a new era of magnetism research with objectives that previously would have been unattainable. Because of their inherent element and orbital specificity and ability to probe extremely small sample volumes, these spectroscopies have become an indispensable experimental method in studying the magnetism of complex materials. Moreover, derivation of magneto-optical sum rules has greatly strengthened the XMCD, offering a unique capability to deduce from the experimental spectra the orbital and spin contributions to the total magnetic moment carried by the absorbing atom.

So far, XMCD has been extensively used to investigate mainly ferro- or ferromagnetic materials, and only very few studies have been performed on paramagnetic compounds. This is partly because a sufficiently high magnetic field for magnetizing paramagnetic or antiferromagnetic materials was not available at synchrotron facilities. However, a high magnetic field could be the essential parameter to explore new phenomena in materials with important magnetic degrees of freedom. In order to achieve this goal, the external magnetic field has to be comparable with magnitude of the basic magnetic interaction energies, typically above 10 T.

In this contribution we describe recent advances in magnetism research using a high field XMCD station that has been installed at the ESRF beamline ID12 [1]. This station is based on a high vacuum ($< 10^{-7}$ mbar) 52mm cold bore solenoid producing a horizontal magnetic field of 17 Tesla. The power supply is specifically designed to ensure a fast sweep ramping of 2 Tesla/minute. The field homogeneity is better than 0.1% in a 10 mm diameter spherical volume. What is important for XMCD measurements is that for opposite directions of the field the relative difference in amplitudes is smaller than $5x10^{-5}$. The Helium continuous flow cryostat was built in-house to be ”amagnetic”. The absolute value of magnetic susceptibility of parts exposed to the magnetic field, in the zone where it is above 1 Tesla, is of the order of 10^{-5} or less. The temperature on the sample can be set in the range 2.05 K to 325 K with a stability $\Delta T/T < 10^{-3}$. All spectra are measured using total fluorescence yield detection mode using a Si photodiode mounted on a liquid nitrogen shield of the magnet.

This new high field experimental station becomes a unique experimental platform for basic research on magnetism and its performances are illustrated with few selected examples.

Spin Fluctuations of Paramagnetic Rh Clusters [2].

The magnetic moment of Rh clusters with 1.6 nm average diameter embedded in an Al_2O_3 matrix was found to vary linearly with the applied magnetic field. At 2.3 K and under 17 T, the spin magnetic moment amounts to 0.067(2) μ_B per Rh atom. The orbital moment does not exceed 2% of the spin moment. The field induced magnetization was shown to be strongly temperature dependent. This observation is in agreement with a theoretical prediction that in itinerant electron systems, close to the onset of magnetism, the renormalization of the magnetic susceptibility by electron correlations, leads to a Curie-like behavior.

Paramagnetism of Gold Nanoparticles Deposited on a Sulfolobus acidocaldarius S Layer [3].

Magnetic properties of Au nanoparticles deposited on an archaeal S layer studied with XMCD and SQUID magnetometries demonstrate that they are strongly paramagnetic, without any indication of magnetic blocking down to 16 mK. The average magnetic moment per particle is Mpart = 2.36 μ_B. This contribution originates at the particle’s Au 5d band, in which an increased number of holes with respect to the bulk value is observed. The magnetic moment per Au atom is 25 times larger than any measured in other Au nanoparticles.

Quantification of the magnetic exchange via element-selective high-field magnetometry: Co-doped ZnO films [4].

The element specific magnetization curves for 5%, 10%, and 15% Co-doped ZnO epitaxial films with high crystalline perfection have been measured using Co K-edge XMCD. The XMCD(*H*) curves do not saturate up to 17 T evidencing antiferromagnetic exchange between neighboring Co dopant atoms. Angular dependence of XMCD(*H*) in combination with theoretical calculations allow both the next-neighbor exchange *J* and the single ion anisotropy *D* to be determined quantitatively. For 5% and 10% Co doping, *J* = 15 K and *D* = 3 K, whereas for 15% Co doping, these values are reduced to 10 and 2 K, respectively.

[1] A. Rogalev *et al*. in Magnetism and Synchrotron Radiation, *Lectures Notes in Physics*, **565** (2001) 60.
[2] V.M.T.S. Barthem *et al.*, *Phys. Rev. Lett.* **109** (2012) 197204.
[3] J. Bartolomé *et al*, *Phys. Rev. Lett.* **109** (2012) 247203.
[4] A. Ney *et al.*, *Phys. Rev. B* **85** (2012) 245202.

L-19 **Wed. 18. 06., 12^{50}-13^{30}**

RIXS-MCD as a sensitive probe of 3d magnetism with hard x-rays

M. Sikora[1]*, A. Juhin[2] and P. Glatzel[3]

[1]*AGH University of Science and Technology, Academic Centre for Materials and Nanotechnology and Faculty of Physics and Appl. Comp. Sci., Al. Mickiewicza 30, 30-059 Krakow, Poland*
[2]*Institut de Minéralogie et de Physique des Milieux Condensés, CNRS and Université Pierre et Marie Curie, 4 Place Jussieu, 75252 Paris Cedex 5 France*
[3]*European Synchrotron Radiation Facility, CS 40220, 38043 Grenoble Cedex 9, France*

Keywords: magnetic moments, RIXS, RXES, XMCD

*e-mail: marcin.sikora@agh.edu.pl

The effect of magnetic dichroism was foreseen for x-ray absorption spectra (XAS) almost 25 years ago [1] and the first experimental observations of linear and circular x-ray magnetic dichroism (XMCD) spectra were subsequently reported [2]. Since then, it has turned into a common probe of element specific magnetization in para-, ferri- and ferro-magnetic systems, ranging from single atoms on surface, through molecular magnets to multilayers. At present XMCD is well understood and interpreted when measured at edges split by the spin-orbit coupling. For example, the 2*p* spin-orbit coupling gives rise to L_3 and L_2 edges providing convenient probe of 3*d* valence orbitals via the dipole-allowed $2p^6 3d^n \rightarrow 2p^5 3d^{n+1}$ transitions. XMCD at spin-orbit split edges enables simultaneous determination of spin and orbital magnetic moments upon application of the so-called "sum rules", which relate linear combinations of left and right circularly-polarized spectra to the ground state values of the magnetic moments of the absorber [3].

When applied to 3*d* transition metals and 4*f* rare earths, the main drawback of the technique is that the respective *L* and *M* absorption edges, that probe magnetic orbitals, lie in the soft x-ray range. Most soft x-ray magnetic circular dichroism (SXMCD) measurements employ total electron yield because significant self-absorption effects are observed when using total fluorescence yield detection. Thus, *L*-edge XMCD is mainly sensitive to the sample surface and, in addition, is not compatible with demanding sample environments such as high-pressure, liquid and gas cells, which limits the range of investigated materials and excludes *de facto* buried magnetic phases or multilayered samples. For these systems, the penetrating properties of hard X-rays are required, but at the *K*-edge the XMCD signal origin from the *p*-projected orbital magnetization density of unoccupied states, which is weak (~10^{-3} of the edge jump), difficult to interpret quantitatively, and do not allow for the separation of spin and orbital magnetic moments. The element specific studies of bulk magnetism and under extreme conditions have been largely limited to the very weak *K*-edge magnetic dichroism and to the Kβ emission spectroscopy [4-5]. However, the latter is sensitive to the spin and orbital kinetic moments (S and L) only, but not to the their orientation. As such, it does not provide quantitative information on the magnetic ordering and interactions.

Hence there is a need for a magnetic spectroscopic method in the hard x-ray range that can provide information on the ordering and the value of magnetic moments. We show that this goal can be achieved by coupling XMCD with 1*s*2*p* RIXS at the *K* pre-edge.

RIXS is a second-order optical process where first a core hole in a deep electron shell is created (intermediate state) that is replaced by a shallower core hole (final state). This results in sharper and often richer spectral features that origin from electron-electron and spin-orbit interactions. The 1*s*2*p* RIXS probes the evolution of $2p \rightarrow 1s$ emission (*K*α line) upon $1s \rightarrow p$ excitation (*K* absorption edge). If the incoming photon energy is in the range of *K* pre-edge, than a weak quadrupole $1s \rightarrow 3d$ excitations, possibly combined with some additional intensity due to dipole $1s \rightarrow 4p$ transitions shape the RIXS spectrum. Therefore, in 3*d* transition metals the 1*s*2*p* RIXS in the pre-edge rage probes predominantly the same final state ($2p^5 3d^{n+1}$) as the $L_{2,3}$ absorption edges, however using a hard x-ray photon in – photon out probe [6]. Combined with the idea of XMCD, i.e. using circularly polarized x-rays and external magnetic field, it becomes a promising technique to study 3*d* magnetic structure of transition metals.

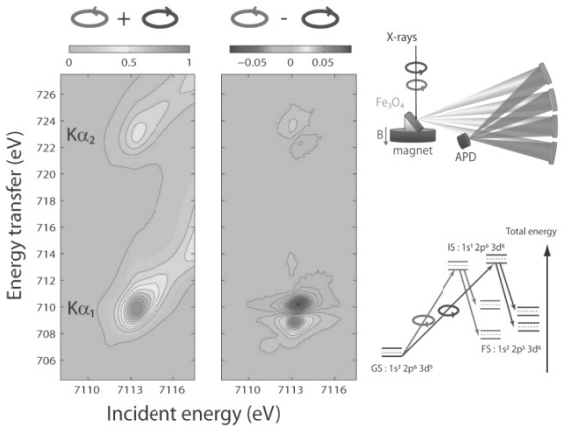

Figure 1. 1*s*2*p* RIXS (left) and RIXS-MCD (center) planes of bulk magnetite. In the right part the sketch of the experimental setup and the energy scheme of the transitions involved is shown. The energy transfer is the difference between incident and emitted photon energy (the total energy of the final state).

Figure 1 shows the experimental 1*s*2*p* RIXS-MCD plane on bulk magnetite at the Fe *K* pre-edge plotted as the difference between the spectra measured for left and right polarized light in comparison to the RIXS plane averaged over the two opposite photon helicities. It is apparent that only the resonant features give rise to the MCD effect, while the features due to non-resonant fluorescence (diagonal structures) do not show any detectable MCD. The spectra show a characteristic dispersion along incident photon energy, due to 1*s* hole lifetime broadening, and along the energy transfer, due to final state effects and 2*p* hole lifetime broadening. 1*s*2*p* RIXS-MCD reveals two groups of final states, which correspond to $K\alpha_1$ and $K\alpha_2$ emission lines, which are

composed mainly of two resonances with different spin polarization and opposite sign. The experimental data is compared with the theoretical RIXS-MCD calculated in the ligand field multiplet approach, where only the contribution of tetrahedral Fe^{III} was considered. The calculation involves an electric quadrupole excitation from $1s^2 2p^6 3d^5$ ground state to $1s^1 2p^6 3d^6$ intermediate state and electric dipole emission to $1s^2 2p^5 3d^6$ final state. It shows good agreement in terms of energy splittings and relative transition strengths of the left and right polarized channels. The only exception is the weak feature visible at 7112eV incident energy and 707eV energy transfer, that is ascribed to octahedral Fe^{II}. The theoretical model finds that the strong XMCD signal in 1*s*2*p* RIXS origin from combination of the exchange field and the 3d spin-orbit coupling in the intermediate state, that implies a different set of $1s^1 3d^6$ intermediate states to be reached from absorption of left and right handed circularly polarized x-rays. The splitting of the MCD features in horizontal and vertical direction is mainly given by the 3*d* spin-orbit coupling in the intermediate state and the 2*p*-3*d* Coulomb repulsions in the final state, respectively. The latter effect and the splitting induced by the 2*p* spin-orbit coupling act as an effective enhancer for the magnetic circular dichroism effect in 1*s*2*p*, that is at least one order of magnitude stronger than the XMCD observed in transmission. The intensity of $1s2p_{3/2}$ RIXS-MCD in bulk magnetite shows a peak-to-peak amplitude as large as 16% of the pre-edge maximum [7], that is comparable to the Fe L_3 edge XMCD [8,9].

The increase of intensity observed between *K*-edge XMCD and 1*s*2*p* RIXS-MCD is a significant advantage since it allows to measure data with better statistics. However, a strong enhancement is only expected for systems showing well defined pre-edge structures, such as oxides, molecular complexes etc… Indeed when 3*d* states are strongly hybridised with *p* states and heavily delocalised, such as in metals, it was observed experimentally that the gain in intensity is lost: for example in metallic Fe the intensity of RIXS-MCD was comparable to *K*-edge XMCD. However, it allows to separate the magnetic signal of metal sites and oxides of different formal valence states by tuning the energy transfer to the off-diagonal spectral features characteristic for a given oxidation state or site symmetry [10].

Ferro- and ferrimagnetic samples to which SXMCD would be blind (at least partially), such as buried layers, can readily be investigated using RIXS-MCD. For instance, high quality 1*s*2*p* RIXS-MCD signal was detected from a 40nm thick layer of magnetite buried under 60nm of Pt and Au. Another important observation was a significant reduction of the amplitude of the MCD signal in the thin layer to ~70% of the bulk value, which is in good agreement to the reduction of the saturation magnetization reported in literature [15]. Thus, the RIXS-MCD can be considered as a quantitative probe of net magnetization in thin layer samples. An interesting aspect of RIXS-MCD in comparison with *K*-edge XMCD is the possibility to select a region of the plane where the MCD effect is maximized for certain features of interest: for example, in the case of magnetite, the peak at 707eV energy transfer and 7112eV incident energy arises from octahedral Fe^{II}, while the double feature at 7114eV incident energy and 712eV energy transfer is dominated by the contribution from tetrahedral Fe^{III} . The RIXS plane can therefore be used to perform site-selective studies. By monitoring the changes as a function of space, pressure, temperature or time, RIXS-MCD can be adopted for element- and site-selective magnetometry and magnetic microscopy with hard x-rays. As an illustration, we show in Figure 2 the hysteresis loop measured on a thin buried layer of magnetite using a RIXS-MCD feature selectively for tetrahedral Fe^{III}, which is compared to the magnetization profile obtained with Vibrating Sample Magnetometer (VSM) .

Future studies of the dependence of RIXS-MCD on the direction of the wave-vector, the polarization vector, the magnetic field or the transfer momentum possibly combined with a polarization analysis of the scattered x-rays will enable to exploit the full potential of the technique.

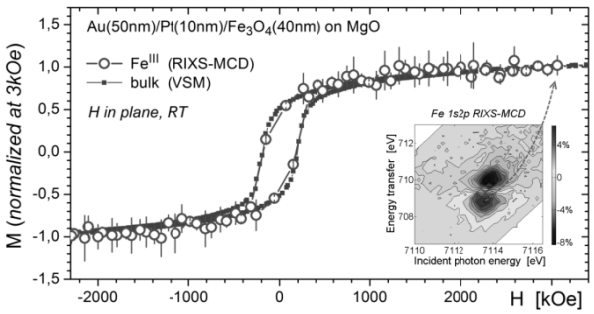

Figure 2. Element and site selective, Fe^{III} (T_d), hysteresis loop (circles) of a thin buried layer of magnetite compared to the VSM (small squares) results corrected for substrate signal.

Acknowledgments: We acknowledge ESRF for the provision of beam time. MS acknowledges support from Polish Ministry of Science and Higher Education and its grant for access to the ESRF facility.

[1] B. T. Thole *et al.*, *Phys. Rev. Lett.* **55** (1985) 2086.
[2] G. Schutz *et al.*, *Phys. Rev. Lett.* **58** (1987) 737.
[3] C. T. Chen *et al.*, *Phys. Rev. Lett.* **75** (1995) 152.
[4] J. Badro *et al.*, *Science* **300** (2003) 789.
[5] J. F. Lin *et al.*, *Nat. Geosci*. **1** (2008) 688.
[6] W. A. Caliebe *et al. Phys. Rev. B* **58** (1998) 13452.
[7] M. Sikora *et al.*, *Phys. Rev. Lett.* **105** (2010) 037202.
[8] D. J. Huang *et al.*, *Phys. Rev. Lett.* **93** (2004) 077204.
[9] C. Carvallo *et al.*, *Am. Mineral.* **93** (2008) 880.
[10] M. Sikora *et al.*, *J. Appl. Phys.* **111** (2012) 07e301.
[11] J. Orna *et al.*, *Phys. Rev. B* **81** (2010) 144420.

L-20 **Wed. 18. 06., 17^{30}-18^{10}**

Nanospectroscopy by XPEEM and LEEM: state of the art and perspectives

Andrea Locatelli*

Elettra - Sincrotrone Trieste S.C.p.A., in AREA Science Park, Basovizza, Trieste 34149, Italy

*email: andrea.locatelli@elettra.eu

During the last 20 years, synchrotron-based X-ray photoemission electron microscopy (XPEEM) has emerged as one of the most powerful methods for nanoscale characterization, with frequent use in material science, surface chemistry and nanosciences [1]. In its simplest variant, XPEEM employs secondary emission to map local differences in the oxidation state, valence, and bond orientation around the emitter. The combination with x-ray circular and linear dichroism techniques has been the most successful application of PEEM at synchrotrons, permitting to image ferromagnetic and antiferromagnetic domains. Variants of XPEEM Instruments equipped with energy filter also exist, which can implement laterally resolved versions of x-ray photoelectron spectroscopy (XPS) and angle-resolved photoelectron spectroscopy, giving access to the local chemical state and electronic structure. XPEEM instruments often combine low energy electron microscopy (LEEM), which adds structure sensitivity and capability to image dynamic processes such as growth and self-organization. Such instruments provide a unique array of advanced surface characterization tools within a single instrument, microprobe angle-resolved photoelectron spectroscopy (μ-ARPES) and low energy electron diffraction (μ-LEED) being the most frequently demanded. In my talk, I will illustrate the current state of XPEEM and report recent results from the Trieste group in fields spanning from surface science to nanomagnetism. The study of graphene on various transition metals and, in particular, on a support with non-threefold symmetry, Ir(100), will serve to demonstrate the usefulness and power of the LEEM-XPEEM multi-technique approach [2,3].

[1] A. Locatelli and E. Bauer, *J. Phys.: Condens. Matter* **20**, (2008) 093002.
[2] A. Locatelli, C. Wang, C. Africh, N. Stojic, T.O. Menteş, G. Comelli, N. Binggeli, *ACS Nano* **7** (2013) 6955–6963.
[3] A. Locatelli, G. Zamborlini and T.O. Menteş, *Carbon* **74**, (2014) 237–248.

L-21 **Wed. 18. 06., 18^{10}-18^{50}**

The electronic structure of spintronic materials as seen by spin- and angle-resolved photoemission

L. Plucinski*

Peter Grünberg Institute PGI-6, Forschungszentrum Jülich 52425 Jülich, Germany

Keywords: photoemission, electronic structure, spin-orbit coupling

*e-mail: l.plucinski@fz-juelich.de

I will introduce the basics of spin- and angle-polarized photoemission and its application to several physical systems including ferromagnetic thin films and topological insulators. Furthermore, I will review several types of modern photoemission spectrometers capable of spin analysis, discuss the key experimental challenges, and provide the outlook of the future instrumental developments.

The key quantity in spintronic devices is the spin polarization of the current flowing through the various device components, which in turn is closely determined by the components' electronic structure. Modern spin- and angle-resolved photoemission spectroscopy (spin-ARPES) can map the details of the spin-polarized electronic structure in many novel material systems – both magnetic and nonmagnetic. However, the interpretation of the experimental might be challenging in particular when the spin-orbit interaction comes into play. Furthermore, in order to separate close-lying electronic states an improvement in energy and angular resolution as well as information depth is still mandatory.

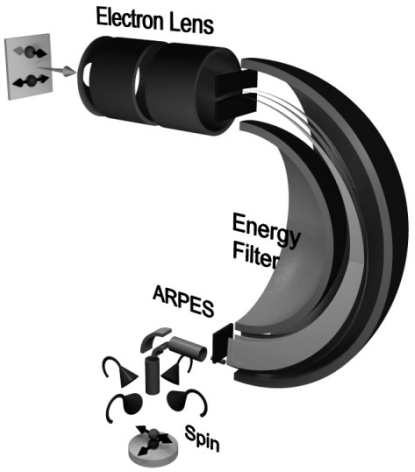

Figure 1. Schematic drawing of the state-of-the-art spin-ARPES spectrometer

[1] L. Plucinski and C. M. Schneider, *J. Electron. Spectrosc. Relat. Phenom.* **189** (2013) 137.

L-22 **Wed. 18. 06., 18^{50}-19^{30}**

New directions in hard and soft x-ray photoemission with synchrotron radiation

C.S. Fadley

Department of Physics, University of California Davis
Materials Sciences Division, Lawrence Berkeley National Laboratory

I will present some new directions in soft x-ray photoemission (XPS, SXPS) and hard x-ray photoemission (HXPS, HAXPES, HIKE) [1-18]. These involve combined SXPS and HXPS studies of buried layers and interfaces in magnetic and transition-metal oxide multilayers [5,6,8,10,12], hard x-ray photoemission studies of the bulk electronic structure of some spintronic materials [4,7,11,14]; band-offset measurements in oxide and semiconductor multilayers [12,17]; the use of standing waves from multilayer mirrors to enhance depth contrast in spectroscopy [1,5(a),6,10,15,16], as well as in angle-resolved photoemission (ARPES) [1,5(b)], photoelectron microscopy [3], and multi-Torr ambient pressure photoemission [18] ; and some first results for bulk sensitive hard x-ray ARPES (HARPES) [9,14,16] and hard x-ray photoelectron diffraction (HXPD) [2].

Acknowledgments: This work was supported by the U.S. Department of Energy under Contract No. DE-AC02-05CH11231, the Army Research Office, under MURI Grant W911-NF-09-1-0398, the Forschungszentrum Jülich, Peter Grunberg Institute-PGI-6, and the APTCOM project of Le Triangle de Physique, Paris.

---

[1] C.S. Fadley, *J. Electron Spectroscopy and Related Phenomena* **178–179** (2010) 2.

[2] A. Winkelmann, J. Garcia de Abajo and C.S. Fadley, *New J. Phys.* **10** (2008) 113002.

[3] (a) F. Kronast, R. Ovsyannikov, A. Kaiser, C. Wiemann, S.-H. Yang, D. E. Bürgler, R. Schreiber, F. Salmassi, P. Fischer, H. A. Dűrr, C. M. Schneider, W. Eberhardt, C. S. Fadley, *Appl. Phys. Lett.* **93** (2008) 243116; (b) A. X. Gray, F. Kronast, C. Papp, S.H. Yang, S. Cramm, P. Krug, F. Salmassi, E. M. Gullikson, D. L. Hilken, E. H. Anderson, P.J. Fischer, H. A. Dürr, C. M. Schneider, and C. S. Fadley, *Applied Physics Letters* **97** (2010) 062503.

[4] Z. Boekelheide, A. X. Gray, C. Papp, B. Balke, D. A. Stewart, S. Ueda, K. Kobayashi, F. Hellman, C. S. Fadley, *Phys. Rev. Letters* **105** (2010) 236404.

[5] (a) A. X. Gray, C. Papp, B. Balke, S.-H. Yang, M. Huijben, E. Rotenberg, A. Bostwick, S. Ueda, Y. Yamashita,K. Kobayashi, E. M. Gullikson, J. B. Kortright, F. M. F. de Groot, G. Rijnders, D. H. A. Blank, R. Ramesh, C. S. Fadley, *Phys. Rev. B* **82** (2010) 205116;(b) A. X. Gray, J. Minár, L. Plucinski, M. Huijben, A. Bostwick, E. Rotenberg, S.-H. Yang, J. Braun, A. Winkelmann, D. Eiteneer, A. Rattanachata, A. Greer, G. Rijnders, D. H. A. Blank, D. Doennig, R. Pentcheva, J.B. Kortright, C. M. Schneider, H. Ebert, and C. S. Fadley, *Europhysics Letters* **104** (2013) 17004.

[6] (a) S. Döring, F. Schönbohm, U. Berges, R. Schreiber, D. E. Bürgler, C. M. Schneider, M. Gorgoi, F. Schäfers, A. Papp, B. Balke, C. S. Fadley, C. Westphal, *Phys. Rev. B* **83** (2011) 165444; (b) S.H. Yang, B. Balke, C. Papp, S. Döring, U. Berges, L. Plucinski, C. Westphal, C. M. Schneider, S. S. P. Parkin, C. S. Fadley, *Phys. Rev. B* **84** (2011) 184410.

[7] A. X. Gray,J. Karel, J. Minar, C. Bordel, H. Ebert, J. Braun, S. Ueda, Y. Yamashita, L. Ouyang, D. J. Smith, K. Kobayashi, F. Hellman, C. S. Fadley, *Phys. Rev. B* **83** (2011) 195112.

[8] A. X. Gray, A. Janotti, J. Son, J. M. LeBeau, S. Ueda, Y. Yamashita, K. Kobayashi, A. M. Kaiser, R. Sutarto, H. Wadati, G. A. Sawatzky, C. G. Van de Walle, S. Stemmer, C. S. Fadley, *Phys. Rev. B* **84** (2011) 075104.

[9] (a) C. Papp, A. Gray, B. Balke, S. Ueda, K. Kobayashi, S. Sakai, H. Yoshikawa, Y. Yamashita, S. L. He, E. Yylvisaker, L. Plucinski, C. Schneider, J. Minar, J. Braun, H. Ebert , W.E. Pickett, C. S. Fadley, *Nature Materials* **10** (2011) 759; (b) D. L. Feng, *Nature Materials* **10** (2011) 729-730.

[10] A. M. Kaiser, A. X. Gray, G. Conti, J. Son, A. Greer, A. Perona, A. Rattanachata, A.Y. Saw, A. Bostwick, S. Yang, S.-H. Yang, E. M. Gullikson, J. B. Kortright, S. Stemmer, C. S. Fadley, *Phys. Rev. Letters* **107** (2011) 116402.

[11] C. Caspers, M. Müller, A. X. Gray, A. M. Kaiser, A. Gloskovskii, C. S. Fadley, W. Drube, C. M. Schneider, *Phys. Rev. B* **84** (2011) 205217.

[12] G. Conti, A. M. Kaiser, A. X. Gray, S. Nemšák, G. K. Pálsson, J. Son, P. Moetakef, A. Janotti, L. Bjaalie, C.S. Conlon D. Eiteneer, A.A. Greer, A. Keqi, A. Rattanachata, A.Y. Saw , A. Bostwick, W.C. Stolte, Gloskovskii, W. Drube, S. Ueda, M. Kobata, K. Kobayashi , C. G. Van de Walle, S. Stemmer, C. M. Schneider, C. S. Fadley, *J. Appl. Phys.* **113** (2013) 143704.

[13] C. S. Fadley, *Synchrotron Radiation News* **25** (2012) 26.

[14] A. X. Gray, J. Minar, S. Ueda, P. R. Stone, Y. Yamashita, J. Fujii, J. Braun, L. Plucinski, C. M. Schneider, G. Panaccione, H. Ebert, O. D. Dubon, K. Kobayashi, C. S. Fadley, *Nature Materials* **11** (2012) 957.

[15] C. Papp, G. Conti, B. Balke, S. Ueda, Y. Yamashita, H. Yoshikawa, S.L. He, C. Sakai, Y.S. Uritsky, K. Kobayashi, J.B. Kortright, C.S. Fadley, *J. Applied Phys.* **112** (2012) 114501.

[16] C. S. Fadley, *J. Electron Spectrosc.* **190** (2013) 165-179.

[17] M. Kapilashrami, G. Conti, I. Zegkinoglou, S. Nemšák, C. Conlon, T. Törndahl, V. Fjällström, J. Lischner, S. G. Louie, A. Riazanova, L. Belova, R. J. Hamers, L. Zhang, J. Guo, C.S Fadley, F. Himpsel, *"p-Doped Diamond Films as Donor Electrodes in Photovoltaics: An X-Ray Absorption and Hard X-Ray Photoemission Study"*, in preparation.

[18] S. Nemšák, A. Shavorskiy, O. Karslioglu, I. Zegkinoglou, A. Rattanachata, C.S. Conlon, P. K. Greene, K. Liu, F. Salmassi, E. M. Gullikson, S.-H. Yang, H. Bluhm, C. S. Fadley, *"Chemical-state resolved concentration profiles with sub-nm accuracy at solid/gas and solid/liquid interfaces using standing-wave ambient-pressure photoemission (SWAPPS)",* in preparation.

L-23 **Thu. 19. 06., 15^{30}-16^{15}**

Synchrotron radiation: an advanced tool for science under extreme conditions of pressure and temperature

M. Mezouar*, G. Garbarino, P. Parisiadis and V. Svitlyk

European Synchrotron Radiation Facility, Grenoble, France

Keywords: synchrotron radiation, X-ray diffraction, high pressure, high temperature

*e-mail: mezouar@esrf.fr

Science at extremes of pressure and temperature is a vibrant field of international research that addresses fundamental questions in domains as diverse as fundamental condensed-matter physics, Earth and planetary science, material synthesis and characterisation, and biology. Pressure strongly alters interatomic distances without changes in thermal energy or chemical environment, and is thus a better thermodynamic variable than temperature and chemical composition to explore free energy landscapes. Research at light-based large scale facilities has always been at the leading edge of extreme conditions science, and the recent advent of powerful laser sources (Omega, NIF, ELI, ...), X-ray free electron laser facilities (LCLS, European XFEL, …), and the exciting perspective of a new generation of diffraction-limited synchrotrons will allow the exploration of material properties at conditions far in excess of those currently achievable. The current third-generation synchrotron facilities have pioneered many of the major breakthroughs in extreme conditions research over the last two decades. Indeed, compared to other large-scale facilities, synchrotron radiation offers a unique diversity of state-of-the-art techniques for characterisation of matter. At the ESRF, the scope of this research field has been constantly expanding and developing such that, remarkably, the structural, dynamical, electronic and magnetic properties of materials at pressure up to 100 GPa can now be determined with the same precision as at ambient conditions. This lecture will be focus on key instrumental and scientific achievements at the high pressure XRD beamline ID27.

L-24 **Thu. 19. 06., 16^{15}-17^{00}**

Time resolved X-ray scattering of molecules in liquids

M.M. Nielsen[1]*

[1]*Molecular Movies Department of Physics, Technical University of Denmark, Fysikvej 307, DK-2800 Kgs. Lyngby, Denmark*

Keywords: Time resolution, Molecules in solution, free-x-ray electron laser

*e-mail: mmee@fysik.dtu.dk

XFELs have dramatically improved our ability to measure and understand ultrafast structural changes with X-ray scattering. Here we attempt to draw a few lines from our work at synchrotron sources to a recent series of hard X-ray pump-probe experiments conducted at the XPP end-station at LCLS and at SACLA in Japan.

X-ray scattering of molecules in solutions is sensitive to all atoms in the illuminated volume of the sample. This gives both opportunities and challenges. The opportunities include being able to study structural changes following photo excitation of the solute molecule, how the excitation leads to changes in the solvation shell around the molecule, and how the excitation energy is eventually dissipated in the surrounding solvent. This great sensitivity is also a challenge, as it can lead to ambiguities in the interpretation of the measurements, since the scattering signal contains a combination of all the above contributions as well as instrument response functions.

However, some of these ambiguities may be resolved by combining scattering experiments with element specific spectroscopic techniques. In recent experiments, we utilized concurrent detection of complementary data, namely both X-ray Diffuse Scattering and X-ray Emission Spectroscopy. Doing so significantly aids in the interpretation of the results, as information from one set of measurements can inform the analysis of the complementary set. Further, it allowed us to address simultaneously both the electronic and the structural degrees of freedom, greatly enhancing the information obtained from a single experiment.

In these experiments, we investigated the ultrafast solvent response as well as structural and electronic dynamics in $Fe(bpy)_3$ as well as in a structurally related, linked Ru-Co complex. In a second set of experiments, we studied the ultrafast structural dynamics following excited-state bond formation in $Ir_2(dimen)_4$.

The work was made in close collaboration with the groups of Christian Bressler, E-XFEL Hamburg, György Vanko, Budapest, Kelly Gaffney, Stanford, and Villy Sundström, Lund. The excellent beamline staff at XPP LCLS, SACLA, APS sectors 7 and 11, and ESRF ID09B made the experiments possible.

L-25 **Thu. 19. 06., 17^{30}-18^{10}**

Watching chemical reaction dynamics with ultrashort X-ray pulses

W. Gawelda[1]*, T. Assefa[1,2], A. Britz[1,3], A. Galler[1] and C. Bressler[1,3]

[1]*European XFEL, Albert-Einstein-Ring 19, 22761 Hamburg, Germany*
[2]*Faculty of Physics, University of Hamburg, Jungiusstrasse 9, 20355 Hamburg, Germany*
[3]*The Hamburg Centre for Ultrafast Imaging, Luruper Chaussee 149, 22761 Hamburg, Germany*

Keywords: Time-resolved X-ray spectroscopy, Synchrotron radiation, X-ray Free-electron laser

*e-mail: wojciech.gawelda@xfel.eu

Ultrafast structural dynamics is an emerging field aiming to deliver a detailed understanding of the elementary steps in reacting chemical species, which involve changes in their nuclear, electronic and spin states. Such processes are vital ingredients in chemistry and biology, but also in technological applications, including efficient charge transport in light harvesting molecules and ultrafast switchable molecular magnets.

In order to unravel this complex dynamic behavior we have implemented a suite of ultrafast X-ray spectroscopic and scattering tools to zoom into both the electronic and nuclear structures, with the goal to ultimately deliver a molecular movie of ongoing chemical processes. In view of the many potential applications in chemical and biological dynamics it is desirable to increase the sensitivity level of such experiments as well as to decrease the time resolution into the femtosecond time domain.

We present our benchmark results using a versatile setup that permits simultaneous measurements of ultrafast X-ray absorption and emission spectroscopies combined with X-ray scattering, which has been recently implemented by us at different synchrotrons [1-2] and XFELs [3]. We applied it to study different photochemical reactions, ranging from nascent radicals in solution, molecular spin transitions, ligand exchange reactions, to photocatalytic systems, with the goal to deliver a deeper understanding of the elementary steps in chemical reactivity.

Acknowledgments: This work was supported by the European XFEL GmbH and the DFG Sonderforschungsbereich 925 “Light-induced dynamics and control of correlated quantum systems” (Project A4).

[1] K. Haldrup, G. Vankó, W. Gawelda *et al.*, *J. Phys. Chem. A* **116** (2012) 9878.
[2] G. Vankó, A. Bordage, P. Glatzel *et al.*, *J. Electron. Spectrosc. Relat. Phenom.* **188** (2013) 166.
[3] H. T. Lemke, C. Bressler, L. X. Chen *et al.*, *J. Phys. Chem. A* **117** (2013) 735.

L-26 **Fri. 20. 06., 18^{30}-18^{10}**

Present status and future development of SOLARIS project

M.J. Stankiewicz[1,2]*, C. J. Bocchetta[1], R. Nietubyć[1,3], K. Szamota-Leandersson[1], A. I. Wawrzyniak[1,2] and M. Zając[1]

[1] *National Synchrotron Radiation Centre SOLARIS, Jagiellonian University, ul. Czerwone Maki 9, 30-392 Kraków, Poland*
[2]*Institute of Physics, Jagiellonian University ul. Reymonta 4, 31-059 Krakow, Poland*
[3]*Narodowe Centrum Badań Jądrowych ul. Andrzeja Sołtana, 05-400 Otwock, Świerk ,Poland*

Keywords: synchrotron radiation, free-electron laser

*e-mail: m.j.stankiewicz@uj.edu.pl

Project SOLARIS – the first Polish Synchrotron Radiation Source [1] has entered the crucial stage. The building construction with the backbone installations of cooling water and electrical systems has been completed and accepted on the 5th of May 2014. The tenders for all the major components of the machine have been resolved and hardware is ready for delivery or in production. Contracts for integration of the machine with the building installation have been awarded and the installation of the machine begins in June 2014.

The project, financed from EU Structural Funds is executed by Jagiellonian University. It is possible only due to unprecedented collaboration with MAX-lab tem in Lund, where new SR facility is being constructed, consisting of two storage rings of 1.5 and 3.0 GeV. Polish synchrotron is a replica of the smaller (96m circumference) 1.5 GeV ring. The revolutionary design of double bending achromats (DBA) forming the MAXlab storage rings [2] was made available to SOLARIS, allowing the facility to implement the technology for the first time.

The current status of the project as well as the timetable of the installation including the target milestones will be presented. The future plans of the development of the facility, including the improvement of the source and construction of the next batch of the experimental beamlines will be discussed.

Acknowledgments: The order is co-funded by the European Union from the European Regional Development Fund and state budget within the framework of the Innovative Economy Operational Programme, 2007-2013, (POIG.02.01.00-12-213/09).

[1] M.R. Bartosik *et al.*, *Radiat.Phys.Chem.*(2013), http://dx.doi.org/10.1016/j.radphyschem.2013.03.036i
[2] E.S. Reich, *Nature* **501** (2013) 148–149 doi:10.1038/501148a

IO-01 **Sun. 15. 06., 18^{40}-19^{00}**

XAFS study of the Ni complexes with hydantoin derivatives

A. Wolska[1]*, M. T. Klepka[1], A. Drzewiecka-Antonik[1], M. Puszynska-Tuszkanow[2] and M. Cieslak-Golonka[2]

[1]*Institute of Physics, Polish Academy of Sciences, Al. Lotnikow 32/46, 02-668 Warsaw, Poland*
[2] *Faculty of Chemistry, Wroclaw University of Technology, 27 Wybrzeze Wyspianskiego, 50-370 Wroclaw, Poland*

Keywords: metal-organic complexes, XANES, EXAFS, synchrotron radiation

*e-mail: Anna.Wolska@ifpan.edu.pl

Studies on parent hydantoin and its various derivatives are of fundamental and practical importance due to their physiological action as anticonvulsant, antiepileptic, anti-inflammatory and anticancer drugs [1]. Recently, the potential applications of compounds containing a hydantoin fragment for HIV-1 treatment has also been suggested [2]. Among newly synthesized transition metal complexes some exhibit activity against human cancer cell lines MCF-7 (breast adenocarcinoma) and A549 (non-small cell lung carcinoma) as well as mouse fibroblasts cell line (BALB/3T3) [3]. The cytotoxity data indicate that the antitumor activity of coordination compounds are modulated by many factors like e.g. the nature of the alkyl group substituted to the heterocyclic ligands, the hydrogen bond pattern, type of metal or/and environment around metal cation. Hydantoins are promising ligands to obtain metal-based compounds with anticancer activity due to different ways of binding to the central metal ion [4].

The metal complexation reaction usually modifies the biological activity of a ligand [5]. Since the biological properties of the compound are directly related to its structure, the study on metal-binding ability of hydantoin derivatives is necessary. The X-ray absorption fine structure spectroscopy (XAFS) technique is perfect for this task since it can provide information about local atomic neighborhood and coordination polyhedra around metal cations regardless of the state or crystallographic form of the investigated material. This is especially important for structural studies of compounds without long range order like in this case.

The Ni(II) ions with *N,O*-donor hydantoins in the novel biologically active complexes were studied. The XAFS measurements at Ni K edge were performed at I811 beamline at MAX-LAB. Both, extended X-ray absorption fine structure (EXAFS) and X-ray absorption near edge structure (XANES), regions were analysed. EXAFS analysis provided information about the average coordination number, the type of coordination atoms, their distance from the metal cation and relative structural disorder. The shape of a XANES spectrum strongly depends on the angles between the neighboring atoms, therefore, theoretical calculations based on the model proposed from EXAFS analysis allowed to determine the 3d arrangement around the absorbing atoms.

Acknowledgments: The synchrotron experiment was partially supported by the Baltic Science Link project coordinated by the Swedish Research Council, VR.

[1] S.S. Block, *Disinfection, Sterilization and Preservation*, 4th-ed., (Lea & Febiger, Philadelphia, **2003**).
[2] R. Vardanyan, H.J. Hruby, *Synthesis of Essential Drugs*, Elsevier, **2006**.
[3] M. Puszyńska-Tuszkanow, T. Grabowski, M. Daszkiewicz, J. Wietrzyk, B. Filip, G. Maciejewska, M. Cieślak-Golonka, *J. Inorg. Biochem*. **105** (2011) 17.
[4] M. Puszyńska-Tuszkanow, M. Daszkiewicz, G. Maciejewska, Z. Staszak, J. Wietrzyk, B. Filip, M. Cieślak-Golonka, *Polyhedron* **30** (2011) 2016.
[5] G. Maciejewska, W. Zierkiewicz, A. Adach, M. Kopacz, I. Zapała, I. Bulik, M. Cieślak-Golonka, T. Grabowski, J. Wietrzyk, *J. Inorg. Biochem*. **103** (2009) 1189.

IO-02 **Mon. 16. 06., 11^{50}-12^{10}**

A XAS study of low phonon glass-ceramics

A. Czajka[1]*, T. Strączek[1], K. Gąska[1], D.A. Zając[1], Cz. Kapusta[1] and M. Środa[2]

[1]*AGH University of Science and Technology, Faculty of Physics and Applied Computer Science, Department of Solid State Physics, al. A. Mickiewicza 30, 30-059 Kraków, Poland*
[2]*AGH University of Science and Technology, Faculty of Material Science and Ceramics, al. A. Mickiewicza 30, 30-059 Kraków, Poland*

Keywords: synchrotron radiation, XANES, low fonon glass-ceramic

*e-mail: Agnieszka.Czajka@fis.agh.edu.pl

Introduction

Luminescent materials are used in optical devices such as optical converters or solid state lasers. A novel class of such material consist rare earth containing oxide-fluoride glass-ceramics. They combine excellent optical properties of fluoride with the corresponding chemical and thermal parameters of the oxide phase. Rare earth ions act as optically active impurities there. To diminish the impact of phonon relaxation processes on the luminescent decay, optically active rare earth centers should be located in the structure of low-energy phonons, such as e.g. heavy metal fluorides, which reveal the lowest energies of phonons. Thereby, low phonon fluoride phase, which reduces the likelihood of non-radiative decays. This allows getting a higher luminescence efficiency and longer lifetime of excited states.

Applications of the rare earth ions in the active optical centers are linked to the specific electronic structure of lanthanides. The high refraction is related to the large number of electron shells completely filled in the lanthanide ion. This significantly increases the electron density of the medium where are lanthanides, and thereby also its polarization susceptibility.

Lanthanide ions in solids have discrete absorption and emission lines associated with the change of the resultant orbital moment and spin moment of the electron of the 4f subshell. Electronic transitions taking place on this subshell lead to the emission of radiation in the spectral range from near infrared to the near ultraviolet.

Luminescent lanthanide bands are very narrow and have almost linear character. As in the case of electronic absorption spectra, the energy shift of a band depends to a small extent on the structure of the atomic/ionic environment.

Glass-ceramics are glassy materials in which a partial crystallization was induced by means of ceramization in order to achieve particular properties. Such a material consists of a glass matrix containing crystallites of various sizes dispersed in it. The use of glass-ceramics in optoelectronics has been made possible owing to the development of thermal processing and controlled crystallization of the amorphous structure. Choosing an appropriate route of thermal treatment it is possible to obtain glass-ceramics with various degrees of transparency. In practice, the glass-ceramic materials are transparent when the size of crystallites formed is an order of magnitude smaller than the wavelengths of visible light, which correspond to the crystallite diameter less than 100 nm.

Experimental

For the study two types of oxide-fluoride glasses have been used: glass G1 doped with erbium and G2 glass doped with europium.

X-ray Absorption Spectropy (XAS) study has been carried out in the Helmholtz-Zentrum Berlin at a bending magnet beamline of the synchrotron radiation storage ring BESSY II. The spectra were recorded in the total electron yield (TEY) and partial fluorescence yield (PFY) modes at room temperature. The energy range covering the areas of O:K, F:K, Na:K, Eu:M, Gd:M, ErM, and Al:K have been scanned. The probing depth of the TEY signal varies from a few nanometers at the energy of 500 eV to tens of nanometers at energies above 1000 eV.

Results and discussion

The F:K edge TEY spectra in the XANES range are presented in Fig.1.

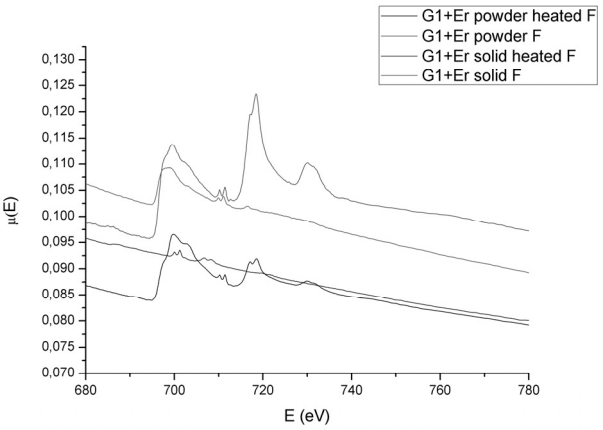

Figure 1. XAS spectra for the F:K edge of the samples studied.

This figure shows unnormalized spectra for glass G1 before and after ceramization (heat treatment). It is worth noting that the heat treated solid glass shows a much lower intensity of the fluorine spectrum than the other samples, whchich can be attributed to a sublimation of fluorine from the surface layer of a few nanometers. This does not occur for the glass powder.

Except for the main edge at about 700 eV additional peaks appear at the energies of 20 eV and 30 eV higher, which are attributed to two-electron excitations. Their intensity relatively to the main edge is the strongest for the powder glass and decreases with annealing. For the solid glass it is barely visible.

Figure 2 illustrates the spectrum of the samples G1+Er glass before and after heat treatment (ceramization), at the M_5 and M_4 edges of gadolinium.

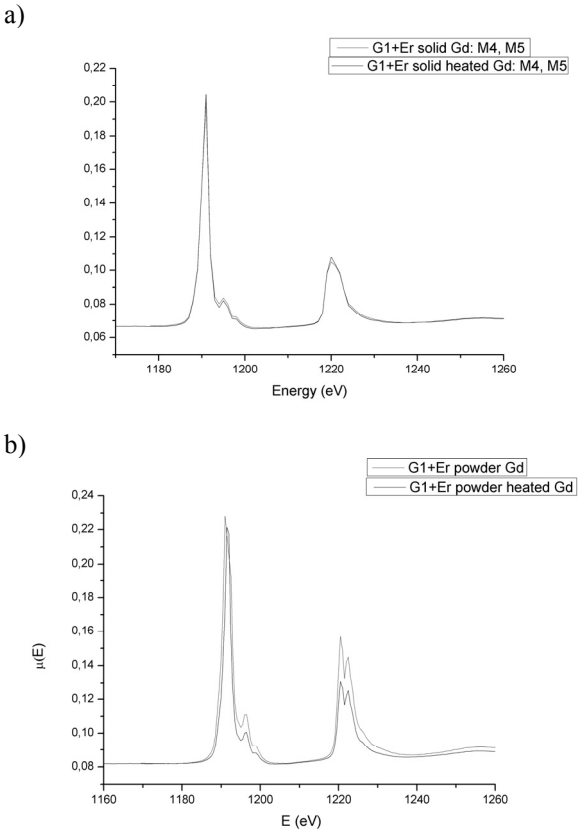

Figure 2. XAS spectra for Gd edges M_4, M_5 for a) solid glass sample, and b) the powder sample.

For solid glass samples before and after ceramization the spectra coincide. For powdered samples significant splitting of the M_4 edge white line corresponding to the final states $4f_{5/2}$ is observed. Also its intensity is considerably larger for the untreated powder. The effect can tentatively be attributed to a greater sensitivity of these states to the surface state, i.e. ceramized or untreated.

For solid glasses the thermal conductivity has been measured down to 4 K in order to check for a possible appearance of the "crystalline peak" at low temperatures after ceramization. A Thermal Transport option of the PPMS (Physical Property Measurement System) set-up was used.

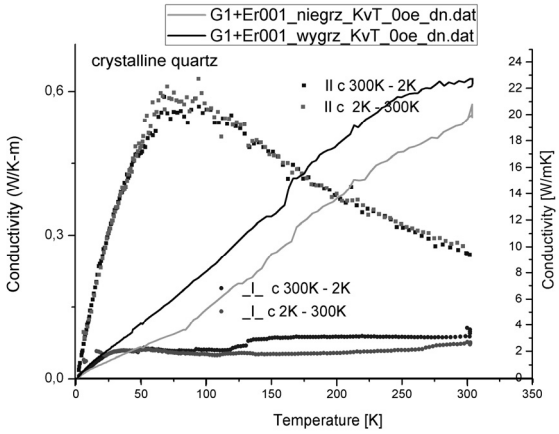

Figure 3. The temperature dependence of the thermal conductivity of the G1-Er glass "as prepared" (green line) and ceramized (black line), left side scale. The data on a quartz single crystal for the heat flux along the c-axis and perpendicular to it are also shown for a comparison, right side scale.

The thermal conductivity increases slightly after heating, but "crystalline peak" does not appear, which means that crystallization takes place to a minimal extent or at regions of nanometric size, smaller than the mean free path of phonons, which is of a few nanometers in such materials.

Conclusions

In the study we could observe the two-electron effects at the F:K edge, dependent on the type of material and its thermal treatment. Also the Gd $4f_{5/2}$ states were found to be sensitive to it. Crystallization caused by ceramization crystallization occurs at a minimal extent or at regions of nanometric size. The observed loss of fluorine from nanometric surface layer on ceramization is an important information for preparation of the optical elements using such a technological route.

[1] X. Zhang, T. Hayakawa, M. Nogami, Y. Ishikawa, *Journal of Alloys and Compounds* **509** (2011) 2076-2080.
[2] M. Nilsson, Coherent Interactions in Rare-Earth-Ion-Doped Crystals for Applications in Quantum Information Science, Thesis, Lund Institute of Technology (2004).

IO-03 **Mon. 16. 06., 12^{10}-12^{30}**

X-ray absorption near-edge structure spectroscopy of bornite, Cu_5FeS_4

A. Rudkowski[1]*, T. Strączek[1], A. Czajka[1], D.A. Zając[1], Ł. Gondek[1], J. Przewoźnik[1], D. Rybicki[1], Cz. Kapusta[1] and A. Piestrzyński[2]

[1]*AGH University of Science and Technology, Faculty of Physics and Applied Computer Science, Department of Solid State Physics, al. A. Mickiewicza 30, 30-059 Kraków, Poland*
[2]*AGH University of Science and Technology, Faculty of Geology, Geophysics and Environmental protection, al. A. Mickiewicza 30, 30-059 Kraków, Poland*

Keywords: bornite, XANES, synchrotron radiation

*e-mail: rudkowski.andrzej@gmail.com

Bornite (Cu_5FeS_4) is one of the most important copper ores. Depending on temperature, three polymorphs of it are known to exist [1, 2]. Above 535 K bornite is cubic (space group *Fm*3*m*, a = 5.50 Å) with antifluorite structure. It has six Cu and one Fe atoms and two cationic vacancies distributed randomly in the eight tetrahedral sites of a cubic close-packed S sublattice. This high-temperature form transforms on cooling to metastable structure with doubling the unit cell (a = 10.94 Å). Finally, on cooling below 473K, the low-temperature stable form is obtained. This is the only phase that occurs naturally. The transition from the metastable to the low-temperature form involves the ordering of the Cu and Fe atoms among the S atom tetrahedra. The low-temperature stable form is orthorhombic (space group *Pbca*, $a = 10.95$ Å, $b = 21.86$ Å, $c = 10.95$ Å). The unit cell contains 16 Cu_5FeS_4 units.

A complex study of bornite structure and its physical properties was carried out on a natural polycrystalline bornite from the Polkowice Mine in Poland with the composition of $Cu_{4.76}Fe_{1.24}S_4$. X-ray diffraction studies [3] on this sample showed orthorhombic structure with *Pbca* space group and unit cell parameters $a = 10.9474(9)$ Å, $b = 21.8699(13)$ Å,$c = 10.9618$ Å.

The basic building blocks (10 atoms of Cu, 2 atoms of Fe and atoms of 8 S – all symmetrically inequivalent) are presented in Fig. 1 for temperatures 15 K and 300 K respectively.

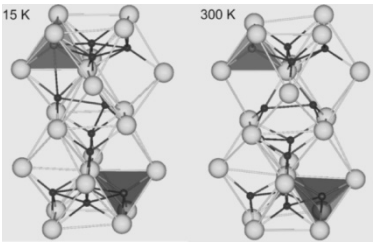

Figure 1. The basic building block of low-temperature bornite. Yellow, blue and red circles are respectively S, Cu and Fe atoms

In Fig. 2 the temperature dependence of the lattice constants is shown.

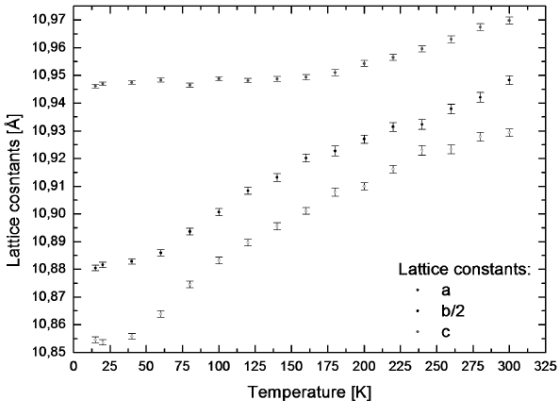

Figure 2. Temperature dependence of lattice constants of bornite.

An increase of orthorhombic distortion on decreasing temperature is pronounced.

Electrical transport measurements versus temperature indicate that bornite exhibits behaviour characteristic of semiconductor, Fig. 3.

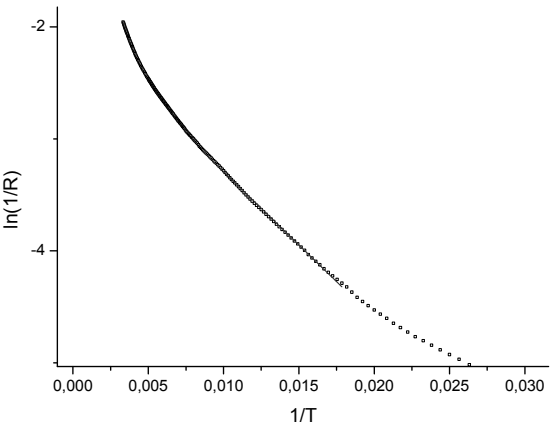

Figure 3. The dependence of logarithm of electrical conduction (reciprocal resistance) on the reciprocal temperature.

Measurements of resistance in the temperature range 2 K – 400 K were carried out, from which energy gap value was determined as equal to 0.3 eV. Significant magnetoresistance effect was also observed, corresponding to a decrease of the electrical resistance caused by the application of magnetic field.

The magnetic susceptibility measurements [3,4] indicate, that bornite undergoes antiferromagnetic-paramagnetic transition at the Neèl temperature T_N equal to 75 K. Mössbauer spectroscopy measurements [3] prove the magnetically ordered state in the compound below the T_N. They also revealed an inhomogeneous character of the transition and the occurrence of the AFM-PM phase segregation below T_N. The hyperfine field of 350 kOe, observed at 4.2 K, is higher than that for a spin Fe^{3+} in oxides (510 kOe). That effect may be attributed to Fe-S covalency and a possible copper

contribution to the effective magnetic moment of the compound. Zero field NMR measurements were also carried out. The measured NMR spectrum was very broad due to presence of several Cu lattice sites and significant quadrupole splitting. The transferred hyperfine field on Cu is in the range of 10-30 kOe. [5]

X-ray absorption near-edge structure (XANES) measurements have been carried out in the Helmholtz-Zentrum Berlin at a bending magnet beamline of the synchrotron radiation storage ring BESSY II. The Cu $L_{2,3}$- and Fe $L_{2,3}$- edge spectra were recorded in the total electron yield (TEY) and partial fluorescence yield (PFY) modes at room temperature. The spectra are presented in Figs. 3,4. The L_2 and L_3 absorption edges of Cu and Fe are associated respectively with electron transitions from the $2p_{1/2}$ and $2p_{3/2}$ core orbitals to the 3d bands.

The XANES spectra have also been preliminary computed using FEFF8.4 software package [6,7] – self-consistent real space multiple-scattering code for simultaneous calculations of x-ray absorption spectra and electronic structure. For data elaboration and analysis, Athena and Artemis [8,9] programs were used.

In Fig. 4 XANES spectra of iron L_2 and L_3 edges of bornite are presented. Electron binding energies amounts to 706.8 eV and 719.9 eV, respectively. The red solid line corresponds to experimental data recorded at the synchrotron, whereas blue dashed line corresponds to numerically calculated spectra.

The unit cell of bornite consist of two inequivalent Fe atoms. Thus, the calculations were performed for each of the two atomic sites individually and the final result was taken as a linear combination of them.

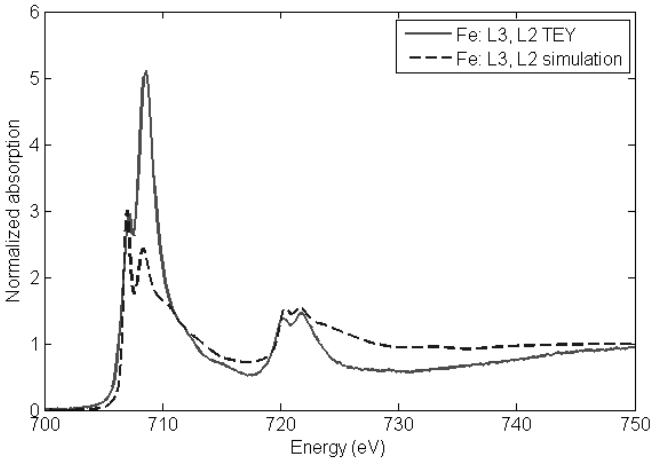

Figure 4: Experimental (red line) and preliminary calculated (blue dashed line) XANES spectra of Fe L_2 and L_3 edges in bornite.

In Fig. 5 XANES spectra of copper L_2 and L_3 edges of bornite are presented. Electron binding energies are equal to 932.7 eV and 952.3 eV respectively. As on previous picture, red line indicate values of absorption measured experimentally, while dashed blue shows calculated spectra. As the unit cell contains 10 inequivalent Cu atoms, calculations were made for each one and final result was obtained by averaging the individual results.

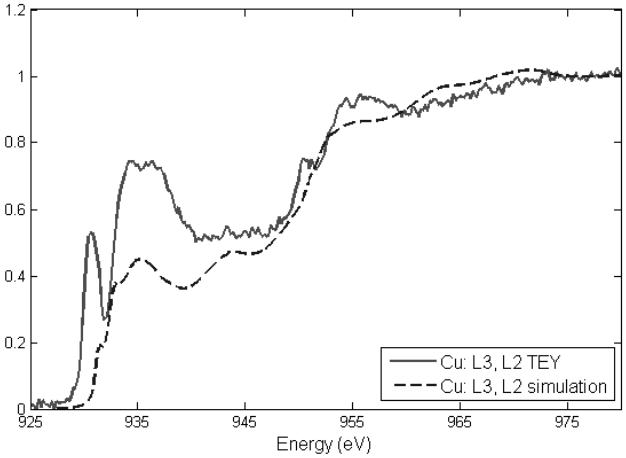

Figure 5: Experimental (red line) and preliminary calculated (blue dashed line) XANES spectra of Cu L_2 and L_3 edges in bornite.

The calculated spectra resemble well the experimental ones for iron edges. For both edges a double peak structure appearing in the experiment is reproduced in calculations. For copper the agreement is less satisfactory and a strong L_3 pre-edge peak in the experimental data corresponds to a shoulder in calculations.

The results obtained are discussed and compared to the electronic structure calculations and conclusions on modifications of band structure with variation of stoichiometry, intermixing and doping are drawn.

[1] N. Morimoto, G. Kullerud *Am. Mineral* **46** (1961) 1270.
[2] K. Koto, N. Morimoto, *Acta Crystsllogr.* **31** (1875) 2268.
[3] J. Przewoźnik, J. Żukrowski, Ł.Gondek, K.Gąska, A. Lemański, C. Kapusta, A. Piestrzyński, *Nukleonika* **58** (2013) 43.
[4] M. Brogheresi, F. Di Benedetoo, A. Caneschi, G. Pratesi, M. Romanelli, L. Sorace, *Phys Chem Minerals* **34** (2007) 609.
[5] D. Rybicki et al., unpublished
[6] A. L. Ankudinov, A. I. Nesvizhskii, J. J. Rehr, *Phys. Rev. B* **67** (2003) 115120.
[7] M.S. Moreno, K. Jorissen, J.J. Rehr, *Micron* **38** (2007) 1.
[8] B. Ravel, M. Newville, *J. Synchrotron Rad.* **12** (2005) 537.
[9] M. Newville, *J. Synchrotron Rad.* **8** (2001) 322.

IO-04 **Mon. 16. 06., 12^{30}-12^{50}**

Electronic properties of Ti-Al-C based MAX phases

M. Wydra[1]*, T. Strączek[1], Cz. Kapusta[1], L. Chlubny[2], M. Kapusta[2] and J. Lis[2]

[1]*AGH University of Science and Technology, Faculty of Physics and Applied Computer Science, Department of Solid State Physics, al. A. Mickiewicza 30, 30-059 Kraków, Poland*
[2]*AGH University of Science and Technology, Faculty of Material Science and Ceramics, al. A. Mickiewicza 30, 30-059 Kraków, Poland*

Keywords: MAX phases, electronic properties, XANES

*e-mail: martawydra91@yahoo.com

The MAX phases are the compounds comprising metals and nonmetals in a natural layered structure. They exhibit exciting physical properties which stem from a combination of covalent and metallic bonds. Their excellent mechanical properties including machineability and self-healing have already been relatively well described. However, the other basic physical properties such as the thermal and electrical conductivities, thermoelectric properties and their relation to the crystallographic order, local atomic structure, the nature and concentration of the electrical carriers, phonon properties as well as the spin and magnetic field effects are still poorly described.

Structurally, differences between the respective members of the family of MAX phases concern the number of M layers separating the A-layers: in the 211's there are two, whereas in the 321's three M-layers, Fig.1.

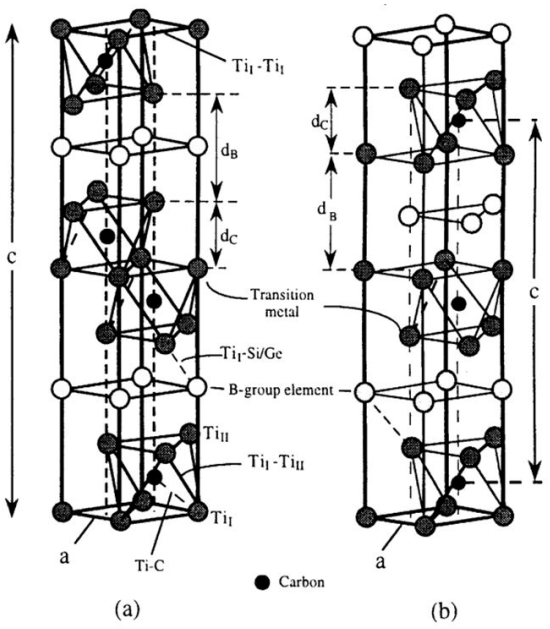

Figure 1. Structure of MAX phases compounds: a) 312 structure, b) 211 structure.

Examples of this type of structure materials are known among both naturally occurring minerals (layered silicates and aluminium silicates such as talc) and materials synthesised in technological processes, where a well-known example would be graphite or monolayered graphene form. This specific structure of MAX phases results with the features typical for structural ceramics (high bending strength and fracture toughness) combined with new set of properties, such as ductility, low hardness and, what is particularly interesting, wide spectrum of unusual properties in the field of electrical, magnetic, or heat characteristics which makes them attractive functional materials.

The aim of this work is to study the electronic properties of the Ti_2AlC and Ti_3AlC_2, type MAX phases with XANES and band structure calculations, measurements of electrical transport and thermoelectric properties, as well as with the Raman spectroscopy.

The aim of this work is to study the electronic properties of the Ti_2AlC and Ti_3AlC_2, type MAX phases with XANES and band structure calculations, measurements of electrical transport and thermoelectric properties, as well as with the Raman spectroscopy/ spectromicroscopy.

A Self-Propagating High-temperature Synthesis (SHS) was used to synthesize the precursor powders of polycrystalline nanolaminate materials of the Ti_2AlC and Ti_3AlC_2 groups. For the consolidation of powders an uniaxial hot pressing (HP) technique was used. The samples obtained were found to be of 95% purity MAX phases.

Measurements of the electrical resistivity of the sample of Ti_3AlC_2 show a small temperature coefficient and a considerable low temperature residual resistivity. This indicates a low mean free path of the electrical carriers due to scattering on structural defects. Measurements of Seebeck effect versus temperature and magnetic field show a change of its sign, which indicates that the character of dominant electrical carrier changes with temperature, Fig.2.

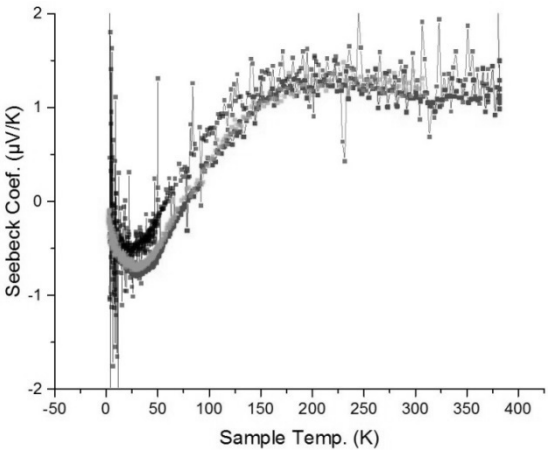

Figure 2. The temperature dependence of Seebeck coefficient of the Ti_3AlC_2 bulk sample at zero field (green symbols - cooling, red symbols - warming) and at the applied magnetic field of 8 Tesla (black symbols).

The XANES spectra have been preliminary computed using FEFF8.4 software package [6,7] – self-consistent real space multiple-scattering code for simultaneous calculations of x-ray absorption spectra and electronic structure. In Figures 3 and 4 calculated XANES spectra of carbon at the K-edge and titanium at the L_3 edge of Ti_3AlC_2 are presented. Also the spectra obtained for a vacancy in the nearest neighbor shell of the carbon and titanium are included.

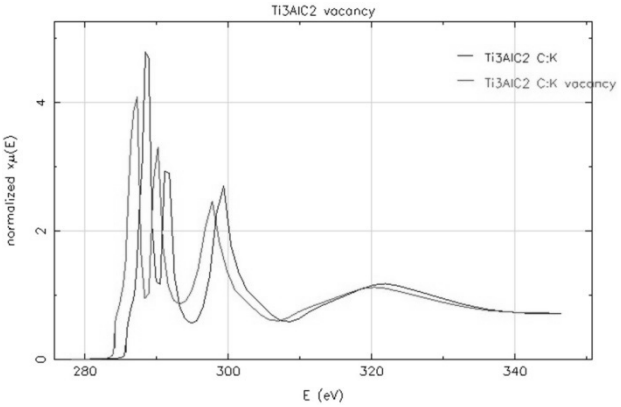

Figure 3. The calculated XANES spectra of carbon K-edge in Ti_3AlC_2 (Ti_3AlC_2 C:K) and for vacancy in the nearest neighbor shell of carbon (Ti_3AlC_2 C:K vacancy).

It is worth noting that the spectra at the carbon K-edge show a noticeable shift in the edge energy and shape with removal of one nearest neighbor to carbon from the structure. For titanium L_3 edge, L_2 edge (not shown) and also for the K edge (not shown) a minor effect is observed only.

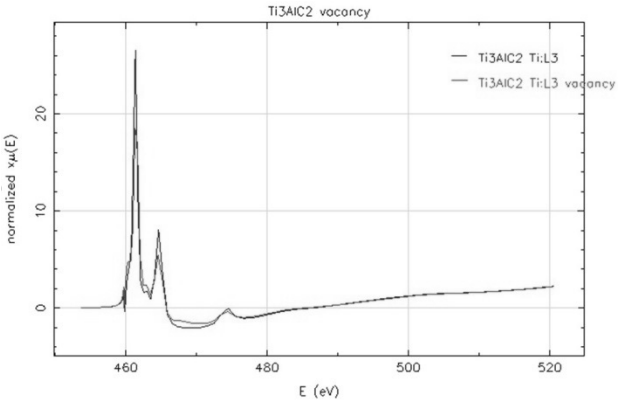

Figure 4. The calculated XANES spectra of titanium L_3-edge in Ti_3AlC_2 (Ti_3AlC_2 Ti:L3) and for vacancy in the nearest neighbor shell of titanium (Ti_3AlC_2 Ti:L_3 vacancy).

The results will be discussed and compared to the Raman spectroscopic study in order to elucidate vacancy, intermixing and possible carbon clustering effects as well as their impact on the electronic and thermal transport properties of the materials.

[1] W. Jeitschko, H. Nowotny, F.Benesovsky; *Monatsh. Chem.* **94** (1963) 672-678.
[2] H. Nowotny, *Prog. Solid State Chem.* **2** (1970) 27.
[3] M.W. Barsoum, *Solid St. Chem.* **28** (2000) 201-281.
[4] L. Chlubny, M.M. Bućko, J. Lis, *Adv. Sci. Tech*. **45** (2006) 1047-1051.
[5] J. Lis, L. Chlubny, M. Łopaciński, L. Stobierski, M. M. Bućko, *J. Eur.Ceramic Soc.*, **28** (2008) 1009-1014.
[6] J. Lis, D. Kata, L. Chlubny, M. Łopaciński, D. Zientara, *Annales de Chimie Science des Matériaux*, **28** (2003) 115-122.

IO-05 **Mon. 16. 06., 13^{10}-13^{30}**

XAFS technique used to obtain structural information for complexes of coumarin derivatives with Cu

M.T. Klepka[1]*, A. Wolska[1], A. Drzewiecka-Antonik[1], and P. Rejmak[1]

[1]*Institute of Physics, Polish academy of Sciences, Al. Lotnikow 32/46 PL-02668 Warsaw, Poland*

Keywords: XAFS, EXAFS, XANES, metalo-organic complexes

*e-mail: mklepka@ifpan.edu.pl

The coumarin and its derivatives occur naturally in plants with therapeutic effect and have been used in natural medicine as traditional remedies [1]. Moreover, natural as well as synthetic coumarin derivatives have a large spectrum of biological activity and are widely investigated. Simple coumarins vary greatly in their molecular structure and this can influence their pharmaceutical properties [2,3]. Type and strength of their biological action usually depend on the number and kind of small substituents, namely hydroxyl or methoxy group. In general, it could be noticed that coordination of metal ions to therapeutic agents improves their efficacy and accelerates their bioactivity.

Electrochemically obtained Cu complexes with hydroxy derivatives of 4-methylcoumarin were structurally investigated using X-ray absorption fine structure spectroscopy (XAFS). Measurements at Cu K edge in the transmission detection mode were performed at I811 beamline at MAX-LAB.

Analysis of the extended X-ray absorption fine structure (EXAFS) provided information about the average coordination number, the type of coordination atoms, their distance from the metal cation and the relative structural disorder. It was discovered that the first coordination sphere is formed of 4 oxygen atoms for all investigated complexes. The Cu–O bond distances were estimated to be around 1.94(1) Å.

Using structural information obtained from the EXAFS analysis, the most probable models from Cambridge Structural Database (CSD) were selected and were used as the initial models in the X-ray absorption near edge structure (XANES) analysis. The shape of a XANES spectrum, in opposition to EXAFS, strongly depends on the angles between the neighboring atoms. Therefore, by performing calculation for models with different angular arrangement of the ligands, it was possible to propose and verify coordination polyhedra of all analyzed complexes.

Acknowledgments: The research leading to these results has received funding from the Polish National Science Centre (Grant No. UMO-2012/07/D/ST5/02251). The synchrotron experiment was partially supported by the Baltic Science Link project coordinated by the Swedish Research Council, VR.

[1] L.K.A.M. Leal, A.A.G. Ferreira, G.A. Bezerra, F.J.A. Matos, G.S.B. Viana *J. Ethnopharm.* **70** (2000) 151.
[2] R.B. Arora, C.N. Mathur *Br. J. Pharmacol. Chemother.* **20** (1963) 29.
[3] I. Kostova, S. Raleva, P. Genova, R. Argirova *Bioinorg. Chem. Appl.* ***2006*** (2006) 1.

IO-06 **Mon. 16. 06., 11^{50}-12^{10}**

GEM-2D detector based reconfigurable measurement system for hot plasma diagnostics

A. J. Wojeński[1]*, G. Kasprowicz[1], K. T. Poźniak[1], A. Byszuk[1], M. Chernyshova[2], T. Czarski[2], S. Jabłoński[2], B. Juszczyk[1] and P. Zienkiewicz[1]

[1]*Institute of Electronic Systems, Warsaw University of Technology, Nowowiejska 15/19, 00-665 Warsaw, Poland*
[2]*Institute of Plasma Physics and Laser Microfusion, Hery 23, 01-497 Warsaw, Poland*

Keywords: ITER, plasma visualization, plasma diagnostics, GEM detectors, FPGA, reconfigurable measurement systems

*e-mail: A.Wojenski@elka.pw.edu.pl

In future thermofusion research reactors (tokamaks, i.e. ITER), precise determination of the level of the soft X-ray radiation of plasma with temperature above 30 keV (around 350 mln K) will be very important in plasma parameters optimization[1].

Soft X-ray radiation, emitted by plasma structures, is characterized by very high radiation emissivity, from several W/m^3 up to 20 W/m^3. Observed photon fluxes in soft X-ray energy region could generally reach values from 10^6/s·cm^2 to 10^7/s·cm^2. In case of such intensive photons streams, the measurements system requires not only adequate detectors characteristics, but also very fast electronics or data acquisition.

Conceptual works and Authors previous experience has demonstrated that multichannel proportional gas detectors are good candidates to fulfill the constraints of soft X-ray imaging of tokamaks'plasma structures and that the GEM (Gas Electron Multiplier) technique, when configured in multistep structure, can provide sufficient detection characteristics [2-3].

The paper describes modular and reconfigurable measurement system used for diagnostics of hot plasma. The system is able to measure plasma energy and position in 2D mode. The system can provide from 64 up to 512 measurement channels.

At system's input stage, GEM detector is used. Several configurations of the detector have been developed for future tests.

The system is using high-speed serial data communication interfaces, i.e. PCIe [4] and SERDES. Analog-to-digital converters have 12 bits accuracy for each channel, working at 125MSPS speed. With all input channels active, the data flow to the system reaches up to 96 Gbps (64*12bits*125MHz). The acquired data is then passed through analog front end (AFE) boards to FPGA backplane boards.

The analog part of the design allows detection of very short pulses, with very low charge (order of 100 fC). The pulses are generated by absorption of photons inside the detector sensitive volume passing through the GEM detector window. They last for about 20 ns, and intervals between pulses can be also very short. Thus, due to very narrow signals, input channels can be configured in different modes, i.e. amplifier or integrator, increasing the time resolution of photons detection.

On FPGA backplane boards, fast, online data processing is done by FPGA units. As input data flow, signals from AFE boards are connected through ADCs to FPGA units. Different algorithms can be implemented in FPGAs depending on measurement types. The processed data can be stored in DDR3 memory or internal FPGA RAM memory.

Currently developed firmware operates as a histogramming device (for plasma X-ray spectroscopy [5]) or as a multichannel digital oscilloscope. It allows detection of simulated photon pulses (test mode implemented on AFE boards). After detection, signal is registered with up to 1024 samples per one channel in FPGA internal memory. This gives up to 32MB of data per one AFE board (one event). Implemented oscilloscope algorithm can be widely configured (edge detection, delay, etc.). Once data of single photon absorption is acquired, information about this event is stored in FPGA registers. Specially designed software (FPGA/FMC Configuration Software [6]) monitors continuously the status of data acquisition and downloads data through PCI-E when it is available. Since the whole hardware of the system is built in a modular way, firmware automatic generation software can be used to speed up the development process and allow easier handling of different hardware configurations of measurement [7].

Despite of processing pure input data signal, there are also implemented in firmware components responsible for configuration of used electronics (i.e. digital interfaces, offset compensation, integrator mode, etc.).

System is highly modular, allowing interconnecting multiple FPGA backplane boards together using high speed gigabit transceivers (known as GTP links). This improves overall system performance in terms of working algorithms and provides multichannel, high-speed measurement system for different purposes.

Backplane boards can work with various number of AFE boards, depending on user needs. Due to edge connectors mounted on backplane boards, different compatible cards can be inserted in system. Advantage of using edge connectors is a high number of signals that can be connected to FPGA unit.

In order to download processed data from FPGA units, PCI-Express Gen2 interface is used. This approach provides high-speed data link for each board. Backplane boards can be connected directly to PC. Drivers and acquisition software are developed for Linux system.

Dedicated PCI-Express concentrator board was developed. It allows connecting up to 8 backplane boards to the PC unit using one PCI-E x16, Gen3 slot. Data concentrator board provides also several control signals used by backplane boards (i.e. power management, configuration interfaces).

Configuration and monitoring of AFE and backplane boards is done by FPGA mounted on the PCI-E switch. The FPGA is managed by PC computer, using USB interface.

Whole measurement system is controlled by software installed on PC. The FCS was used for this purpose. FCS provides development framework for fast development of software drivers. The main tasks performed by FCS are management, monitoring and configuration of complex electronic systems. FCS can also provide fast and easy for implementation data output of running measurement algorithms implemented on FPGA devices.

FCS is used for many other different purposes, i.e. offset regulation of AFE boards, automatic training of high-speed, serial digital interfaces (SERDES) of ADC chips. This can be easily done, thus, of modular software construction, based on different levels of data interfaces.

Data downloaded from measurement system is processed on PC computer. This can be done using FCS with adequate driver implemented (data parsing) or by direct PCI-E driver access. PC unit implements mathematical algorithms. The offline processing may be done on common PC unit, on different ways, using MATLAB or specially developed software in many languages (C, C++, Java, etc.).

Acknowledgements: This work was performed within the strategic research project "Technologies supporting the development of safe nuclear power" financed by the National Centre for Research and Development (NCBiR). Research Task "Research and development of techniques for the controlled thermonuclear fusion", Contract No. SP/J/2/143234.

[1] A. J. H. Donne et al. and the IPTA Topical Group on Diagnostics Nucl. Fusion **47** (2007) S337.

[2] K. Jakubowska et al., 35th EPS Conference on Plasma Physics, 2011.

[3] M. Chernyshova *et al*., *Development of GEM gas detectors for X-ray crystal spectrometry*, JINST, Vol. 9, C03003.

[4] A. Byszuk et al., *Implementation of PCIe-SerDes-DDR3 Communication in a Multi-FPGA Data Acquisition System*, Proc. SPIE 8903.

[5] K. T. Pozniak, et al., *FPGA based charge fast histo-gramming for GEM detector*, Proc. SPIE 8903.

[6] D. O. Tavares et al., *Development of an open-source hardware platform for SIRIUS BPM and Orbit feedback*, (ICALEPS 2013, 14th International Conference on Accelerator & Large Experimental Physics Control Systems).

[7] A. Wojenski et al, *Automatic HDL firmware generation for FPGA-based reconfigurable measurement and control systems with mezzanines in FMC standard*, Proc. SPIE 8903, 2013.

IO-07 **Mon. 16. 06., 12^{10}-12^{30}**

High resolution ptychography using off-axis illuminated zone plates

K. Stachnik[1]*, I. Mohacsi[2] and A. Meents[3]

[1]*AGH University of Science and Technology, Faculty of Physics and Applied Computer Science, Al. Mickiewicza 30, 30-059 Krakow*
[2]*Paul Scherrer Institut, 5232 Villigen PSI, Switzerland*
[3]*DESY Photon Science, Deutsches Elektronen-Synchrotron DESY, Notkestrasse 85, 22607 Hamburg, Germany*

Keywords: ptychography, X-ray phase contrast imaging, iterative phase retrieval, spatial coherence

*e-mail: karolina.stachnik@gmail.com

The recent development and increased availability of third-generation synchrotron radiation sources together with the rapid progress of novel experimental techniques have made X-ray microscopy well-known in the scientific community. Amongst its most prominent merits are high resolution and penetration depth combined with elemental or magnetic sensitivity without the need of invasive sample preparation. The development of phase contrast imaging methods have extended the use of X-ray microscopy to allow the study of even weakly absorbing biological specimens. While the coherence properties of modern synchrotron light sources increased the possible resolution considerably, accessible traditional X-ray optics were unable to confront with the demand. However, with the rapid increase of available computational power, it has become feasible to circumvent limitations of X-ray optics using lensless X-ray microscopy schemes. Lensless imaging techniques measure the diffraction pattern of the sample object and attempt to numerically solve the relationship between the sample and its measured diffraction pattern. For this, they aim at recovering the phase that was lost during the measurement using a set of constraints and boundary conditions.

Ptychography is a scanning-based high resolution coherent diffractive imaging technique. It was first proposed in 1970s for transmission electron microscopy [2,3] and has been recently demonstrated in the X-ray and optical range [3,4]. It measures multiple diffraction patterns from partially overlapping sample regions to use the overlap as a constraint to recover both the sample object and the illumination function (probe) with much higher resolution than the scanning step size. For hard X-rays, ptychography can be realized with the experimental setup shown in Figure 1 using a Fresnel zone plate as focusing optic. It is basically a form of super-resolution scanning transmission X-ray microscopy utilizing mainly coherent illumination and a two-dimensional pixel detector. The sample is scanned by a well-defined, localized, but not strongly focused illuminating probe. The step size must provide a significant overlap between subsequently illuminated regions. For each scan point, a far-field diffraction pattern is recorded which requires sufficient oversampling for the phase problem to be completely resolved.

Afterwards, the measured dataset is loaded into iterative algorithms [5-7] to reconstruct the complex object transmission function and the illuminating wave front. In ptychography there is no restriction imposed on the type or shape of the illumination, yet, rough a priori knowledge of the probe may be needed at the beginning of the reconstruction. On the contrary, the phase retrieval can start from a completely random object guess. During the refinement process, the algorithms alternate between real and reciprocal space, substituting the calculated intensity in a detector plane with the measured intensities without further artificial boundary conditions. Most modern algorithms involve the simultaneous reconstruction of both the probe and the object, yielding therefore information not only about the specimen but also about the illuminating wave front. The resolution of ptychographic reconstruction is limited by neither the size of a focal spot nor the numerical aperture of a lens any more. It is restrained only by the dose and the finite amount of measured photons in high scattering vector q values allowing sub-10-nanometer resolution in the hard X-ray regime.

The talk will provide all necessary information about ptychography as a scanning high resolution imaging technique utilizing coherent synchrotron radiation. This will be followed by its demonstration at beamline P11 at PETRA III light source [8], DESY, Hamburg. The experimental setup (see Figure 1) was designed to investigate an influence of finite spatial coherence length on the quality of ptychographic reconstruction by providing different spatial coherence conditions as reported in [9].

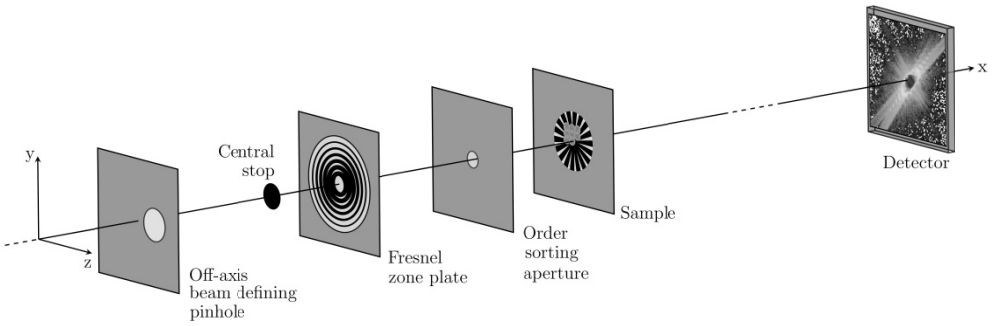

Figure 1. Schematic of the ptychography experiment using an off-axis illuminated zone plate.

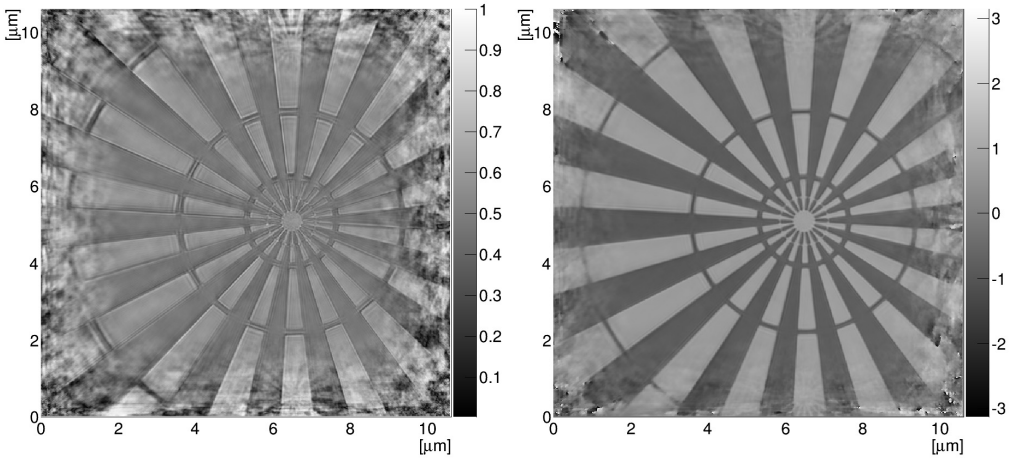

Figure 2. An example of reconstructed amplitude (left image) and phase (right image) of the Siemens star.

An evaluation of reconstructed images' resolution of a test object (Siemens star) will be discussed for those cases. Figure 2 presents reconstructed amplitude (left image) and phase (right image) of the Siemens star. Figure 3 shows a typical diffraction pattern recorded with a PILATUS 1M single photon counting detector [10] for the most coherent illumination. During the talk, ptychographic reconstructions of fossil diatoms and stained hepatoma cells will be presented as applications of the technique in biological imaging. The experimental results will be compared with simulated data. Both the simulation of the beamline and the reconstruction tools are software prepared in the C/C++ with support of the ROOT Data Analysis Framework [11].

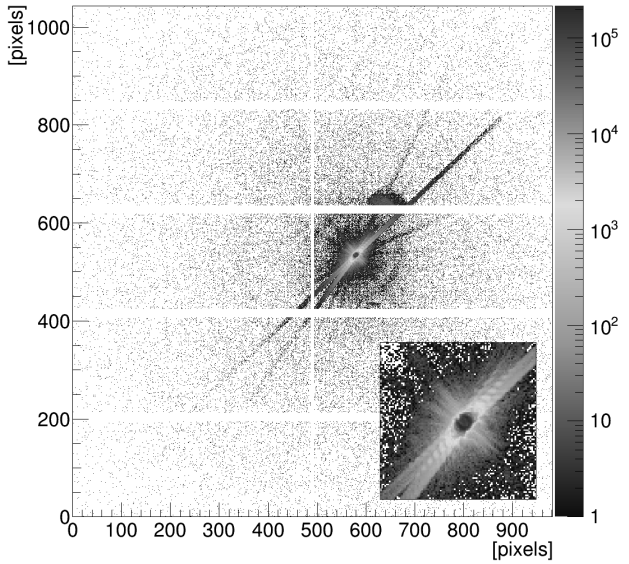

Figure 3. A typical far field diffraction pattern from the ptychographic dataset recorded with PILATUS 1M detector. Horizontal and vertical lines correspond to intermodule gaps with no readout. In the inset the central part of the diffraction pattern is presented.

[1] W. Hoppe, *Acta Cryst. A* **25** (1969) 508-514.
[2] R. Hegerl, W. Hoppe, *Ber. Bunsen-Ges.* **74** (1970) 1148-1154.
[3] J.M. Rodenburg, A.C. Hurst, A.G. Cullis, *Ultramicroscopy* **107** (2007) 227.
[4] O. Bunk, M. Dierolf, S. Kynde, I. Johnson, O. Marti, F. Pfeiffer, *Ultramicroscopy* **108(5)** (2008) 481-487.
[5] V. Elser, *J. Opt. Soc. Am. A* **20** (2003) 40-55.
[6] M. Guizar-Sicairos, J.R. Fienup, *Opt. Express* **16** (2008) 7264-78.
[7] A.M. Maiden, J.M. Rodenburg, *Ultramicroscopy* **109** (2009) 1256.
[8] PETRA III synchrotron light source at DESY, http://petra3.desy.de/index_eng.html
[9] P. Thibault, A. Menzel, *Nature* **494** (2013) 68-71.
[10] B. Henrich, A. Bergamaschi, C. Broennimann, R. Dinapoli, E.F. Eikenberry, I. Johnson, M. Kobas, P. Kraft, A. Mozzanica, B. Schmitt, *Nucl. Instrum. Meth.. A* **607** (2009) 247-49.
[11] R. Brun, F. Rademakers, *Nucl. Instrum. Meth. A* **389** (1997) 81-86 (see also http://root.cern.ch/).

IO-08 **Wed. 18. 06., 15^{20}-15^{40}**

SR-FTIR microspectroscopy coupled with multivariate data analysis in study of interaction between radiation and living matter

E. Lipiec[1]*, K. R. Bambery[2], J. Lekki[1], M. J. Tobin[2], C. Vogel[4], B. R. Wood[3] and W. M. Kwiatek[1]

[1]*The Henryk Niewodniczanski Institute of Nuclear Physics, PAN, 31-342 Kraków, Poland,*
[2]*Australian Synchrotron, 800 Blackburn Rd Clayton, Victoria 3168, Australia.*
[3]*Centre for Biospectroscopy, School of Chemistry, Monash University, 3800, Victoria, Australia.*
[4]*BAM Federal Institute for Materials Research and Testing, Division 4.4 Thermochemical Residues Treatment and Resource Recovery, Unter den Eichen 87, D-12205 Berlin, Germany*

Keywords: SR-FTIR microspectroscopy, DNA damage, bystander effect

*e-mail: Ewelina.Lipiec@ifj.edu.com

All living organisms are continually exposed to radiation through natural sources such as cosmic rays and terrestrial sources including radon thorium and uranium. Radiation has found its application in cancer treatment and diagnosis. It has direct effects on tissues and cells. The most sensitive molecule in terms of affecting cell function is DNA due to its sensitivity to damage and because the genetic information is stored here [1]. The processes at the cellular and molecular level are the basis for the macroscopic effects of ionising radiation on whole organisms. The aim of presented research is to study the effects of how radiation interacts with living cells and radio-biologically relevant molecules.

The current practice for investigating the effect of ionising radiation on cells is to use biochemical assays such as the comet assay [2], Gamma H2AX foci [3] and/or the micronuclei assay [2]. However, the assay itself may affect the biological samples leading to changes in their structure due to non–physiological chemical substances and complex preparation procedures [2-4]. Moreover, most biochemical methods are not intended to study the effect of radiation at the single cell level. Therefore, there is a need for complementary techniques to confirm cellular damage arising from radiation exposure. SR–FTIR (Synchrotron Radiation Fourier Transform Infrared) microspectroscopy has become potential analytical method in single cells studies [5] on a molecular level. A growing amount of literature data demonstrates their usefulness in studies of the conformational aspects of lipids, nucleic acids and other biomolecules. It is known also that SR-FTIR method is a sensitive tool, that can be applied to DNA damage study at chemical bond level [5]. FTIR microspectroscopy is useful as well for cellular membrane damage investigation.

In presented study the SR-FTIR microspectroscopy with subsequent multivariate analysis was applied to investigate radiation damage to nucleic acids, proteins and lipids and to monitor the cellular response to radiation exposure. Those methods were also applied successfully in study of non targeted effects such as bystander and sun-light influence.

Cellular response to proton exposure

SR-FTIR spectra of single human prostate adenocarcinoma PC3 cells, irradiated with a defined number of 2MeV protons generated by a Cracow proton microbeam along with non-irradiated control cells, were analysed using multivariate methods. A number of different Principal Component Analysis (PCA) models were tested and the spectral ranges associated with nucleic acids, proteins and lipids were analysed separately. The most important PCA results are Scores Plots and Loadings Factors. The Scores Plots represent the spectra in multidimensional space of principal components (PC-1, PC-2, PC-3….), explaining some percentage of total variance. They can be used to detect sample patterns and group them accordingly. This analysis separates the data into their principal components. Loadings Plots indicate, which variables in the data set are responsible for a clustering.

Sample results for nucleic acids spectral range (1030 cm^{-1} – 1300 cm^{-1}) are presented in Fig. 1. Score Plot (Fig. 1a) have shown two clusters of spectra collected from cells irradiated with 400 protons (open triangles) and non-irradiated ones (black points). Loadings Plot (Fig 1b) shows, which variables are responsible for the greatest degree of separation.

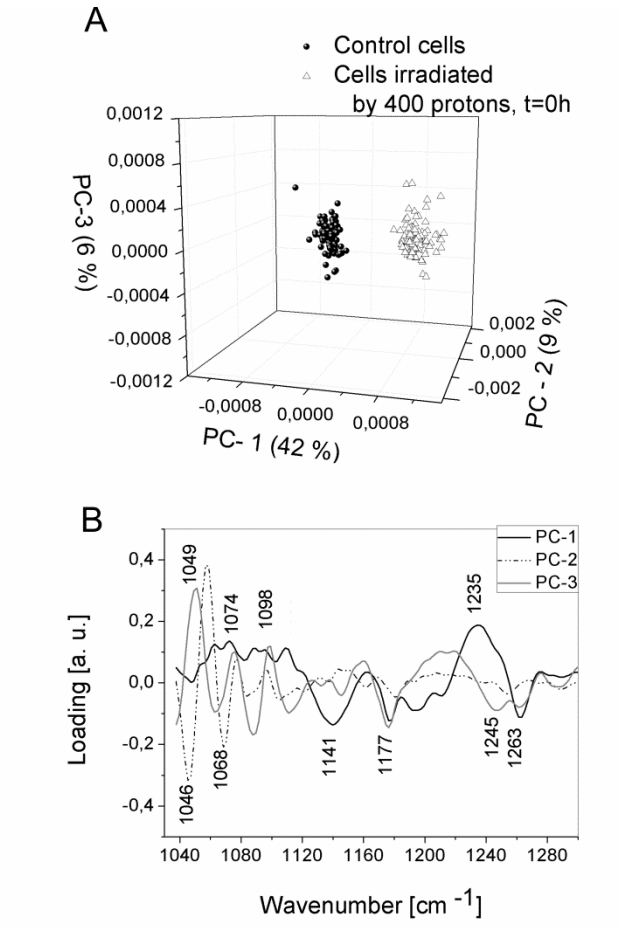

Figure 1 The results of PCA applied to 2 groups of spectra (control and irradiated by 400 of 2MeV protons) in the nucleic

acids spectral range showing a three dimensional Scores Plot (A) along with the corresponding Loadings Plot (B).

The results show a dose dependent shift of the O–P–O asymmetric stretching mode from 1235 cm^{-1} to 1245 cm^{-1}, consistent with local disorder in the B-DNA conformation along with a change in intensity of the O–P–O symmetric stretching band at 1098 cm^{-1} indicative of chromatin fragmentation - the natural consequence of a high number of DNA Double Strand Breaks (DSBs). 2D mapping collected at IRENI (Infrared Environmental Imaging) beamline of characteristic functional groups at the diffraction limit has showed evidence of lipid deposition and chromatin condensation in cells exposed to protons indicative of cell apoptosis following irradiation (Fig. 2).

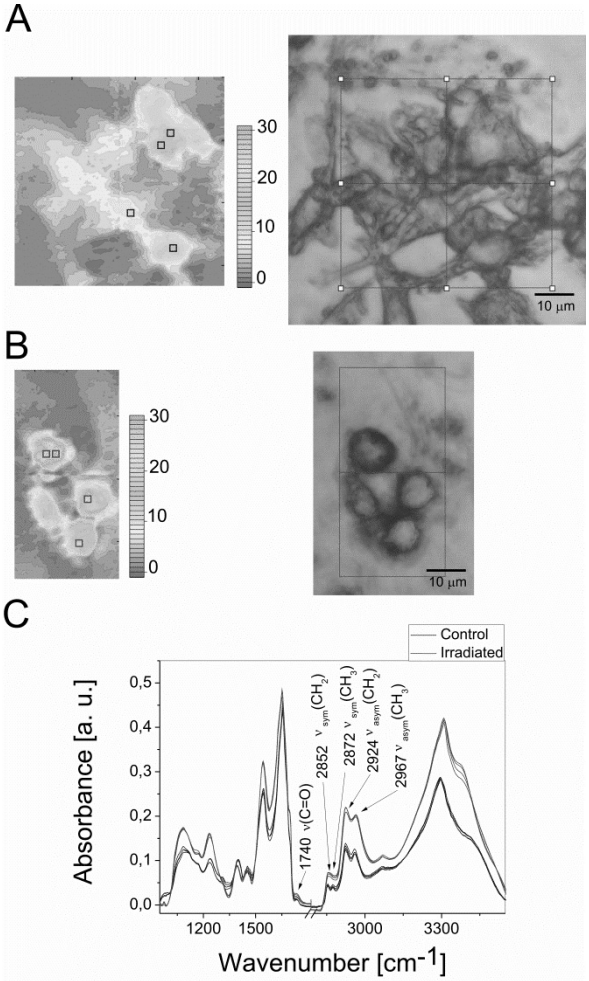

Figure 2 The distribution of CH_2, CH_3 stretching modes mainly from lipids bands (the integrated area of spectral range 3000 cm^{-1}-2800 cm^{-1}) together with corresponding microscopic images of control (A) and irradiated cells (B) and extracted averaged spectra from marked areas (C).

Bystander Effect

Synchrotron Radiation - Fourier Transform Infrared (SR-FTIR) microscopy coupled with multivariate data analysis was used as an independent modality to monitor the cellular bystander effect. Single, living prostate cancer PC3 cells were irradiated with various numbers of protons, ranging from 50-2000 with an energy of either 1 MeV or 2 MeV using a proton microprobe [5, 6, 7]. SR-FTIR spectra of cells fixed 24 h after exposure to protons and non-irradiated neighboring cells were recorded. Spectral differences were observed in both the directly targeted and non-irradiated neighboring cells (bystander cells) and included changes in the DNA backbone and nucleic bases along with changes in protein secondary structure. Principal Component Analysis (PCA) was applied to investigate the variance in the entire data set. Neighboring cells which spectra were clustered together with irradiated ones were considered as bystander cells. The percentage of bystander cells versus the applied number of protons with two different proton energies (1 MeV and 2 MeV) was calculated. It was found that out of all the applied doses, 400 protons at 2 MeV was the most effective in causing significant macromolecular perturbation in PC3 cells. [6]

"Sun light" influence on living cells

The response after laboratory "Sun light" exposure of COLO–679 cell line was successfully studied by SR–FTIR with subsequent multivariate data analysis. Living cells and isolated cellular nuclei after appropriate incubation time post irradiation, were investigated. The dose dependent intensity decrease of the C=O stretching mode at 1713 cm^{-1} is caused by base–pair damage such as purine, pyrimidine dimers formation or 6–4 lesions. The shift of O–P–O asymmetric stretching from 1230 cm^{-1} to 1240 cm^{-1} is associated with a partial conformation change from B–DNA to A–DNA. Additionally, an intensity increase in the Amide II band at 1549 cm^{-1} was observed following UV radiation exposure. This effect is possibly related to DNA repair, because the enzymes involved in DNA repair are mainly proteins and an increase in the amount of protein would result in an increase the intensity of Amide II band in the FTIR spectrum. This conclusion is confirmed by the observed intensity decrease of O–P–O symmetric and asymmetric stretching mode (1088 cm^{-1} and 1230 cm^{-1} – 1240 cm^{-1}) for cells irradiated for 4 minutes and 40 minutes, indicating that after radiation exposure the cells are stopped in G1 phase during the DNA repair stage. A nuclei isolation is recommended in study of the response to radiation using SR–FTIR. The spectral profiles of isolated nuclei and living cells are similar, however in nuclei spectra the DNA bands are more clearly defined and include the O–P–O stretching at 1088 cm^{-1}, 1170 cm^{-1}, 1230 cm^{-1} and C–O stretching at 970 cm^{-1} as well as base stacking mode: C=O stretching in purines and pyrimidines rings at 1713 cm^{-1}. [8]

The results presented herein enhance the knowledge about the interaction between radiation and living matter in a cell population, single cells, single extracted cellular nuclei, double stranded DNA and other radiobiologically relevant molecule levels, which has important implications in radiation effects protection and the treatment of tumors.

Acknowledgments: We acknowledge travel funding provided by the International Synchrotron Access Program (ISAP) managed by the Australian Synchrotron and funded by the Australian Government. BRW is supported by an Australian Research Council Future Fellowship (FT120100926). This

work was supported by the Multi-modal Australian ScienceS Imaging and Visualisation Environment (MASSIVE) (www.massive.org.au).

---

[1] E. Lipiec, R. Sekine, J. Bielecki, W. M. Kwiatek, B. R., Wood, *Angew. Chem.* **53** (2014) 169.
[2] W. H. L. Siu, J. Cao, R. W. Jack, R. S. S. Wu, B. J. Richardson, L. Xu, P. K. S. Lam, *Aquat. Toxicol.* **66** (2004) 381.
[3] L.J. Kuo, L.X. Yang, *In Vivo* **22** (2008) 305.
[4] E. Lipiec, K. R. Bambery , C. Hirschmugl, J. Lekki, W. M. Kwiatek, M. J. Tobin, C. Vogel, D. Whelan, B. R. Wood, *J. Mol. Str.* submitted.
[5] E. Lipiec, G. Birarda, J. Kowalska, J. Lekki, L. Vaccari, A. Wiecheć, B. R. Wood, W. M. Kwiatek, *Radiat. Phys. Chem.* **93** (2013) 135.
[6] E. Lipiec, K. R. Bambery, J. Lekki, M. J. Tobin, C. Vogel, D. Whelan, B. R. Wood, W. M. Kwiatek, *Radiat. Res.* submitted.
[7] E. W. Lipiec, J. Dulińska–Litewka, M. Kubica, J. Lekki, Z. Stachura, A. M. Wiecheć, J. Wiltowska–Zuber, W. M. Kwiatek, *Gen. Physiol. Biophys.* **31** (2012) 11.
[8] E. Lipiec, K. Bambery, P. Heraud, W. M. Kwiatek, M. Tobin, C. Vogel, B. R. Wood, Analyst, submitted

IO-09 **Wed. 18. 06., 15^{40}-16^{00}**

The chemical forms of sulfur in prostate cancer tissue analyzed by means of XAS

J. Czapla-Masztafiak[1]*, K. Okoń[2], M. Gałka[3], R. Steininger[4], J. Göttlicher[4], T. Huthwelker[5] and W. M. Kwiatek[1]

[1]*Institute of Nuclear Physics PAN, ul. Radzikowskiego 152, 31-342 Kraków, Poland*
[2] *Chair of Pathomorphology, Jagiellonian University Medical College, ul. Grzegórzecka 16, 31-531 Kraków, Poland*
[3] *Gabriel Narutowicz City Specialist Hospital, ul. Prądnicka 35-37, 31-202 Kraków, Poland*
[4]*Karlsruhe Institute of Technology, ANKA Synchrotron Radiation Facility, Hermann-von-Helmholtz-Platz 1, D-76344 Eggenstein-Leopoldshafen, Germany*
[5] *Swiss Light Source, Paul Scherrer Institute, 5232 Villigen PSI, Switzerland*

Keywords: sulfur, μXAS, prostate cancer

*e-mail: Joanna.Czapla@ifj.edu.pl

There is a increasing interest in the biochemistry of various elements in biosystems [1] and their role in human health and disease. The application of micro X-Ray Absorption Spectroscopy (μXAS) and the advantages of light produced by synchrotron radiation sources have made possible to determine chemical forms of different elements in complex structures such as cells and tissue. Knowledge about abnormalities of content and chemical forms of various elements is crucial in case of understanding the process of pathogenesis and molecular mechanisms underlying the etiology of many serious diseases e.g. cancer. XAS brings its own unique contribution to the list of experimental techniques used by structural biologists and starts to be complement to other spectroscopic structural methods.

Presented results were obtained during μXAS experiments performed at ANKA (Germany) and SLS (Switzerland) synchrotrons on the tissue originating from prostate cancer, one of the leading malignant disease with high risk of death among men. Prostate cancer is recognized as one of the major medical problems facing the male population and the factors that determine the risk of developing clinical symptoms are not well known [2]. Studies have shown that changes on the cellular and molecular level seems to be pathological basis of most diseases, resulting from the external factors or disrupted internal cellular processes [3]. Accurate knowledge of these mechanisms can create new opportunities to diagnose diseases at an early stage of their development and apply new, more effective therapies.

This work focused on determination of sulfur chemical species occurring in different parts of prostate cancer tissue. Sulfur was chosen as an element of interest as it plays an important role in human metabolic processes and the disruptions in homeostasis between its various forms may lead to serious pathological conditions. For instance changes in the ratio of oxidised and reduced sulfur forms may indicate changes in redox balance due to the oxidation stress, that is suspected to play significant role in carcinogenesis. Moreover, sulfur is found in one of the major low-molecular-mass thiol, essential for health - glutathione (GSH) - which has many physiological functions, including its involvement in the defence against reactive oxygen species. Therefore, changes in GSH homoeostasis are implicated in the aetiology and progression of a number of human diseases, including cancer, diseases of ageing and neurodegenerative diseases [4]. In addition, sulfenic, sulfinic and sulfonic derivatives are formed during severe oxidative stress as seen in prostate cancer and their presence in the tissue may indicate dysregulated redox balance [5].

In order to establish differences in content and distribution of various chemical form of sulfur in prostate cancer tissue two types of experiemnts were performed: 2D XAS imaging of selected areas of prostate cancer tissue and μ-XANES measurements on chosen points of interest. The prostate tissue was obtained during routine prostatectomies on patients suffering from prostate cancer. The excised gland was cut transversely with a sharp knife and a section were frozen to -20ºC, cut into 15 μm thick sections in a standard cryostat (Leica Microstystems, Germany). One section of each sample was placed on 1,5 μm thick Mylar foil (Goodfellow) and used for XAS analysis, while another adjacent section was used for histological examination. To all of the tissue sections Gleason score was assigned. The second group of sections were formalin-fixed, paraffin embedded by the routine histologic protocol.

2D XAS distribution maps were collected at the X07MB (PHOENIX I) beamline of the Swiss Light Source (Paul Scherrer Institut, Villigen, Switzerland) under high vacuum with a double crystal Si(111) monochromator to select the energy of the incoming beam. Focal spot size was about 10 μm x 10 μm on the sample. The X-ray fluorescence was detected by 4-element Si drift diode array (Vortex ME-4) placed at 90º to the incoming beam. Chosen region of the sample was scanned with the step of 10 μm and acquisition time of 0,4 s per point with four different energies corresponding to spectroscopic features in the near-edge XANES region. Chosen energies excited sulfur at different oxidation states. S K-edge μ-XANES measurements were also performed at the wiggler beamline SUL-X of the synchrotron radiation source ANKA (Karlsruhe Institute of Technology, Germany). A 7–element Si(Li) fluorescence detector (Gresham, now SGX Sensortech) was used. The dimension of the beam at sample position for this experiment was 100 μm x 100 μm. The energy was tuned with a double crystal monochromator (Si(111) crystal pair) in steps of 5 eV and 2 eV in the regions of -100 eV to -50 eV and -50 eV to -20 eV respectively before the edge and 0.2 eV in the edge region.

2D XAS distribution maps give opportunity to receive complete image of different species of the same element in the region of interest and correlate this information with histological stucture. In typical prostate tissue we can distinguish two main parts: prostatic glands and stroma composed from smooth muscle cells,

connective tissue and accompanying extracellular matrix. The example of 2D distribution of individual sulfur form fractions, calculated in accordance with the procedure proposed by Pickering et al. [6], together with the microscopic image obtained during experiment is presented in Fig. 1.

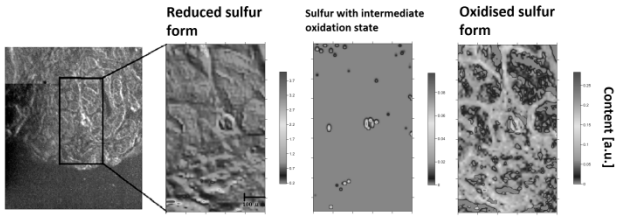

Figure 1. 2D maps of the distribution of individual chemical forms of sulfur in the selected areas of prostate cancer tissue samples together with microscopic image with marked area of scanning.

Presented sample was derived from patient diagnosed with Gleason score 6 prostate cancer. Based on the obtained results it is clearly visible that the most abundant sulfur species in examined area is the reduced form of sulfur that is present nearly homogeneously in all structures. Areas of elevated content of this S form are presented in nodular part of tissue. The sulfur with intermediate oxidation state is present in minute amounts in examined samples and it cannot be correlated with the specific histological structures. The highly oxidised forms of sulfur are minor components of glandular areas in studied prostate tissues, but their content in prostate stroma is significant [7].

In order to analyse differences in the content of chemical forms of sulfur in individual histological structures of prostate tissue, as well as in samples originating from prostate cancer with various Gleason grade, S K-edge μ-XANES measurements were performed. Point spectra were collected from samples with Gleason score 3, 4 and 5 and additionaly from samples of tissue diagnosed as benign prostatic hypeplasia (BPH). In cancerous tissue experimental points were chosen from areas of tumor cells and outside them. The representative S K-edge XANES spectra from all four sample types are presented in Fig. 2.

The shape of all spectra is similar to the one obtained for prostate cancer cell lines [8] with two strong features originatng from reduced and oxidised sulfur forms. It can be easily noticed that main differences between spectra are derived from different reduced/oxidised S forms ratio. Moreover, the structure of the second peak (around 2480 eV) indicates that it originates from the signal generated by S^{5+} and S^{6+} forms and that the content of these two forms also varies between individual samples. The detailed analysis of obtained spectra included the use of Principal Component Analysis (PCA) method to establish spectral differences and simmilarities between examined groups. Based on the evident differences in the content of oxidised sulfur species between individual samples the conclusion was drawn that the signifact role in case of prostate pathologies palys dyregulated redox balance.

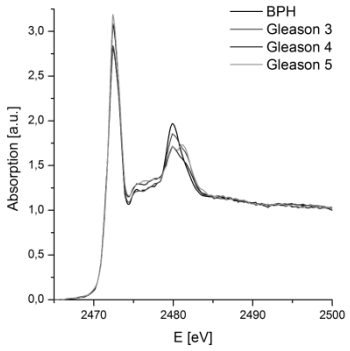

Figure 2. S K-edge μ-XANES spectra obtained on tissue samples originated from BPH and prostate cancer with various Gleson score.

The shape of all spectra is similar to the one obtained for prostate cancer cell lines [8] with two strong features originatng from reduced and oxidised sulfur forms. It can be easily noticed that main differences between spectra are derived from different reduced/oxidised S forms ratio. Moreover, the structure of the second peak (around 2480 eV) indicates that it originates from the signal generated by S^{5+} and S^{6+} forms and that the content of these two forms also varies between individual samples. The detailed analysis of obtained spectra included the use of Principal Component Analysis (PCA) method to establish spectral differences and simmilarities between examined groups. Based on the evident differences in the content of oxidised sulfur species between individual samples the conclusion was drawn that the signifact role in case of prostate pathologies palys dyregulated redox balance.

Acknowledgments: This work was supported by the Polish National Science Center (NCN) under the Grant No.: 2012/05/N/NZ5/00868. We acknowledge Swiss Light Source at Paul Scherrer Institute for granting the beamtime in the proposal 20120367 and 20121271. The research leading to these results has received funding from the European Community's Seventh Framework Programme (FP7/2007-2013) under grant agreement n.°312284 (CALIPSO). We acknowledge the Synchrotron Light Source ANKA for provision of instruments at their beamlines.

[1] R. W. Strange, M. C. Feiters, *Curr. Opin. Struct. Biol.* **18** (2008) 1.
[2] G. Aus, C. C. Abbou, M. Bolla *et al*., *Eur. Urol.* **48** (2005) 546.
[3] D. I. Quinn, S. M. Henshallb, R. L. Sutherland, *Eur. J. Cancer* **41** (2005) 858.
[4] N. Ballatori, S.M. Krance, S. Notenboom et. al., *Biol Chem*. **390 (**2009) 191.
[5] A. Paschos, R. Pandya, W. C. M. Duivenvoorden, J.H. Pinthus, *Prostate Cancer Prostatic Dis.* **16** (2013) 217.
[6] I. J. Pickering, E. Yu Sneeden, R.C. Prince, E. Block, H. H. Harris, G. Hirsch, G. N. George, *Biochemistry* **48** (2009) 6846.
[7] J. Czapla-Masztafiak, W. M. Kwiatek, K. Okoń, M. Gałka, T. Huthwelker, *Spectrochim. Acta Part B*, in review.
[8] J. Czapla, W. M. Kwiatek, J. Lekki, J. Dulinska-Litewka, R. Steininger, J. Gottlicher, *Rad. Phys. Chem.* **93** (2013) 154.

IO-10 **Wed. 18. 06., 15^{00}-15^{20}**

Relations between structural and magnetic properties in metallic ultrathin multilayers

A. Wawro[1]*, E. Milińska[1], A. Petruczik[1], P. Aleszkiewicz[1], J. Kanak[2], Z. Kurant[3], A. Maziewski[3], K. Ollefs[4] and A. Rogalev[4]

[1]*Institute of Physics Polish Academy of Sciences, Warsaw, Poland.*
[2]*Faculty of Physics University of Białystok, Białystok, Poland*
[3]*Faculty of Computer Science, Electronics and Telecommunications AGH University of Science and Technology, Kraków, Poland*
[4]*European Synchrotron Radiation Facility, Grenoble, France*

Keywords: magnetic multilayers, magnetic anisotropy, interlayer coupling, synchrotron radiation

*email: wawro@ifpan.edu.pl

Ultrathin magnetic multilayers attract scientific interest as excellent objects for studying nanomagnetism. They are of high technological relevance as potential materials for novel practical applications as well. Due to dimension confinement and substantial amount of atoms forming surfaces or interfaces such structures exhibit novel properties not encountered in bulk materials.

Investigations of structural features and manipulation at the atomic scale in correlation with observed magnetic properties allow on the one hand to understand physical phenomena and on the other hand to design and fabricate nanosystems with desired attributes. However, structural studies of ultrathin film are a challenge. Due weak signal from low amount of investigated material standard techniques cannot probe these properties reliably. Techniques exploiting X-ray (e.g. X-ray reflectivity, XRR) or synchrotron radiation are only methods enabling to gain an insight into atomic ordering (e.g. X-ray absorption near edge structure, XANES) and magnetic properties (e.g. X-ray magnetic circular dichroism, XMCD). Particularly, element sensitive synchrotron techniques are very powerful for investigations of low amounts of material.

In this work we focus attention mainly at the structural and magnetic properties of ultrathin Co/Mo multilayered system. Undertaken research has been inspired by the interface influence observed in our earlier studies of magnetic nanodots with perpendicular magnetization [1, 2] induced in ultrathin Co layer deposited on a patterned buffer in a form of Au islands self-assembled on the Mo buffer surface [3]. The Co/Mo system is particularly interested as the crystallographic difference of Co (hcp) and Mo (bcc) and lattice parameters allow for intentional modifications of magnetic layer structure and interfaces which substantially affect magnetic properties. It is worth also to mention that cobalt / nonmagnetic early transition metal systems in general have been studied to less extent, so far, and their properties are not recognized well, yet.

Investigated Co/Mo sandwiches, containing a single Co layer, or multilayers with higher repetition number of bilayers were grown on sapphire substrates in a molecular beam epitaxy (MBE) system. Dependently on measurements to be carried out thickness of the component layers was uniform or they were grown as wedges with use of a linear shutter moving during material deposition. The growth mode was monitored in-situ by reflection high electron energy diffraction (RHEED). This technique allows to determine a growth type (amorphous, polycrystalline or monocrystalline) and the symmetry of crystallographic structure and directions in monocrystalline layers. Moreover, it enables to estimate the strains induced by the lattice mismatch at the interfaces. Magnetic properties were measured exploiting magnetooptical Kerr effect (MOKE). Both polar (PMOKE) and longitudinal (LMOKE) configurations of the setup were used. Local probing of the magnetization is a very important advantage of this technique. In combination with wedge type structures it allows in an easy way to study magnetic properties in a function of a component layer thickness. Particularly, the sandwiches containing two wedge-like layer with orthogonally oriented thickness gradients enable to obtain two dimensional diagrams of magnetization processes and related parameters such as e.g. coercivity, effective anisotropy field or remnant magnetization. X-ray reflectivity was applied to study layered structure of sandwiches and quality of interfaces. Numerical fitting of obtained experimental spectra allows to confirm assumed thicknesses of the component layers and to determine roughness (or alloying extent) of the interfaces. Synchrotron radiation measurements were carried out in European Synchrotron Radiation Facility (ESRF) in Grenoble at the beamline ID12. Crystalline structure of grown Co ultrathin layers was inferred from XANES measurements at Co K edge. Magnetic moments induced at Mo atoms due to proximity with adjacent Co layers were determined from XMCD investigations performed at Mo $L_{2,3}$ edges in the magnetic field as high as 0.9 T.

Magnetization orientation in ultrathin films is governed by the effective magnetic anisotropy being an interplay of several components. Shape (dipolar) anisotropy results from the interaction of the magnetization with magnetic field generated by magnetic charges appearing in the perpendicularly magnetized films at the interfaces due to broken symmetry. This component always forces magnetization alignment in the sample plane. Remaining constituents may orient magnetization both in perpendicular direction to the sample plane or in the sample plane. Magnetocrystalline anisotropy is related to minimum energy of magnetization along low index crystallographic directions. Magnetoelastic anisotropy is associated with a lattice deformation. In thin film structures such deformation occurs mainly due to lattice misfit at the interfaces. Particularly, in the Co films with hexagonal (hcp) structure the anisotropy easy axis is parallel to c-axis. Under tensile strains magnetization rotates toward perpendicular direction to the strain axis. Thus for Co hcp layer with c-axis perpendicular to the film plane in-plane tensile strains enhance its perpendicular magnetic

anisotropy. A spin-orbit coupling is responsible for these two kinds of anisotropy. Finally, an interface anisotropy is another component that occurs in thin film structures. It originates from the broken symmetry in the surrounding atoms. The electronic structure of atoms forming the surfaces or interfaces may be modified due to non-saturated dangling bonds or electron hybridization with adjacent atoms of a different type, respectively.

As a result of anisotropy thickness dependence a spin reorientation transition (SRT) is a commonly observed phenomenon in the layered structures containing an ultrathin Co layer. Due to mentioned above effective anisotropy the magnetization of thin Co layer sandwiched between non-magnetic covers is oriented perpendicularly to the plane. At a critical thickness of the Co layer, d_{SRT}, it rotates towards in-plane alignment. The value of d_{SRT} depends on the covers type. One of the highest values are obtained for Au and Pt covers being equal to 1.8 and 2.2 nm, respectively [4, 5]. Such behavior is well described by a model of uniaxial anisotropy taking into consideration contributions from Zeeman energy and from effective anisotropy described by the coefficient K_{1eff}.

On the contrary to noble metal covers in Mo/Co/Mo sandwiches the SRT is not observed. It means that the Co layer is magnetized in the sample plane in the whole range of its thickness. The same magnetization alignment is found in the Co/Mo structures containing two or three Co layers. Additionally, from LMOKE investigations a strong magnetic anisotropy in the sample plane is inferred. The angular dependence of remnant magnetization, m_R and coercivity, H_C clearly prove a two-fold symmetry. This in-plane anisotropy is the common feature of structures consisting of one, two and three Co layers. The Co/Mo multilayers exhibit also very well distinguished antiparallel (antiferromagnetic) coupling of magnetization of the Co component layers. Such type of coupling is observed for the Mo spacer in the thickness range between 3 and 6 atomic layers (AL) and for the Co layer thickness of the order of several nanometers. The LMOKE magnetization curves consist of characteristic rectangular sub-loops of number corresponding to the number of Co layers in the studied sample. With farther increase of the Mo spacer thickness the interlayer coupling adopts a parallel order (ferromagnetic character). For that type of alignment the hysteresis loop exhibits a rectangular shape.

To explain magnetic behavior described above we studied structural properties of the multilayers in details.

Streak-like RHEED pattern proved the epitaxial character of Co/Mo multilayers at every stage of the growth process. However, non-uniform spotty structure of the streaks suggests roughness occurrence at the interfaces. To confirm assumed nominal structure of the studied multilayers the XRR measurements were carried out for uniform multilayers displaying mentioned interlayer magnetic couplings. The reflection spectra consist of expected Bragg peaks and Kiessig fringes. The parameters describing the structure were determined from the fitting procedure of calculated spectra to that obtained in the experimental way. Achieved thicknesses correspond well with assumed ones and were equal to 4 nm for Co layers and 0.8 and 1.8 nm for Mo spacers in the samples exhibiting antiparallel and parallel magnetic coupling, respectively. Interface roughness for those samples was equal to 0.3 and 0.5 nm. It correlates with spotty character of RHEED streaks.

In-plane magnetization alignment of the Co layers in the whole thickness range in Co/Mo multilayers indicates that sum of crystallinity, interface and strain contributions to magnetic anisotropy does not outweigh the shape influence. Thickness dependent crystalline structure of the Co layers was clearly inferred form XANES measurements. For this purpose we studied two Co/Mo multilayers with the same Mo spacer thickness, equal to 1.8 nm and different Co layer thicknesses of 0.9 nm and 4.1 nm. The absorption profiles at the Co K edge for these two samples differ substantially each other particularly in a shoulder shape around 7715 eV and the peaks appearing above 7720 eV. Comparison of experimentally achieved profiles from our samples with the profiles measured for intentionally grown fcc and hcp Co layers, simulated also numerically [6], evidently shows that the crystalline structure of the Co layer 0.9 nm thick is of fcc type whereas for thicker layer hcp stacking dominates. Thus one can draw a conclusion that for Mo buffer or spacer the Co layer grows in the initial stage in fcc structure. Such growth mode explains well magnetic properties of the Co layer deposited on Mo buffer. Magnetic anisotropy forcing perpendicular magnetization is much weaker for fcc structure. The structural evolution from fcc to hcp is also reflected well in the Co layer thickness dependence of effective anisotropy field H_{1eff} directly related to effective anisotropy characterized by the coefficient K_{1eff}.

A mechanism responsible for the observed interlayer coupling remains still undiscovered. Ruderman–Kittel–Kasuya–Yosida (RKKY) oscillating interaction mediated by conduction electrons is one of the candidates. A model of quantum well (QW) assuming spin-selective electron scattering at the interfaces can be also taken into account. In another approach the magnetic poles appearing at the interfaces due to their roughness may also couple the magnetic layers through magnetostatic interactions. To justify a nature of the interlayer coupling XMCD measurements probing magnetic moments at Mo atoms of the spacer were performed. The absorption was investigated at the Mo $L_{2,3}$ edge. Two studied multilayers differed in Mo spacer thicknesses equal to 0.8 nm and 1.8 whereas the Co layer thickness of ca. 4 nm was the same in both samples. Additionally, a reference film grown as a uniform alloy $Co_{96}Mo_4$ was also studied. In the alloyed film induced magnetic moment at Mo site was expected to be strongest. The measurements reveal this moment in the alloy sample as high as -0.21 μ_B. A moment weaker by almost an order of magnitude was found in the layered sample with thinner Mo spacer. In these two samples the induced moment was coupled antiparallel to the moment of adjacent Co atoms. The XMCD signal is below the detection limit for the layered sample with the thickest Mo spacer. One of possible interpretations of relatively large difference in detected induced moments at Mo site in alloy and the spacer is that the moments are aligned antiparallel in the

consecutive individual atomic layers of the Mo spacer. Such alignment of moments induced in W spacer has been found in Fe/W system [7]**.** For this purpose the measurements of X-ray resonant magnetic scattering (XRMS) measurements, i.e. a combination of X-ray circular magnetic dichroism (XMCD) with anomalous X-ray reflectivity (XRR) are planned in the next step of research.

Acknowledgments: This work is supported by the research funds from the National Science Centre in Poland under the projects: DEC-2011/03/N/ST3/02662 and DEC-2012/06/M/ST3/00475.

[1] A. Wawro, A. Petroutchik, L.T. Baczewski, Z. Kurant, A. Maziewski, *Europhys. Lett.* **89** (2010) 37003.

[2] A. Wawro, E. Sieczkowska, A. Petroutchik, L. T. Baczewski, Z. Kurant, and A. Maziewski, *Phys. Rev. B* **83** (2011) 092405.

[3] A. Wawro, M. Sobańska, A. Petroutchik, L. T. Baczewski, and P. Pankowski, *Nanotechnology* **21** (2010) 335606.

[4] M. Kisielewski, A. Maziewski, M. Tekielak, A. Wawro, and L. T. Baczewski, *Phys. Rev. Lett.* **89** (2002) 87203.

[5] J. Kisielewski, A. Maziewski, K. Postava, A. Stupakiewicz, A. Petroutchik, L.T. Baczewski, A. Wawro *J. Magn. Magn. Mater.* **322** (2010) 1475.

[6] Yu. A. Kozinkin, A. A. Novakovich, A. V. Kozinkin, R. V. Vedrinskii, Ya. V. Zubavichus, and A. A. Veligzhanin, *Phys. Solid State* **53** (2011) 1.

[7] N. Jaouen, G. van der Laan, T. K. Johal, F. Wilhelm, A. Rogalev, S. Mylonas, and L. Ortega, *Phys. Rev. B* **70** (2004) 094417.

IO-11 **Wed. 18. 06., 16^{20}-16^{40}**

XANES study of the $(H_3O)[Ni(cyclam)][Fe(CN)_6]\cdot 5H_2O$ dehydration process

W. Szmyt[1]*, T. Strączek[1], A. Czajka[1], K. Gąska[1], D. Zając[1], J. Zukrowski[1], Cz. Kapusta[1], M. Reczyński[2], B. Nowicka[2] and B. Sieklucka[2]

[1]*AGH University of Science and Technology, Faculty of Physics and Applied Computer Science, Department of Solid State Physics, al. A. Mickiewicza 30, 30-059 Kraków, Poland*
[2]*Faculty of Chemistry, Jagiellonian University, Ingardena 3, 30-060 Krakow, Poland*

Keywords: molecular magnet, XANES, Moessbauer, FEFF, XRD

*e-mail: Wojciech.Szmyt@fis.agh.edu.pl

Molecular magnets are a class of compounds which have recently attracted a great deal of interest owing to their potential usability in many fields of technology such as magnetoelectronics, spintronics or quantum information processing [1]. They can exhibit paramagnetic behaviour or, owing to spin-coupling, a long-range magnetic order at low temperatures can be achieved [2].

In this work we study a molecular magnet $(H_3O)[Ni(cyclam)][Fe(CN)_6]\cdot 5H_2O$, (cyclam = 1,4,8,11-tetraazacyclotetradecane) containing iron and nickel ions alternating in a chain sequence, which makes it a one-dimensional (1-D) structured material. The molecule unit is depicted in Figure 1.

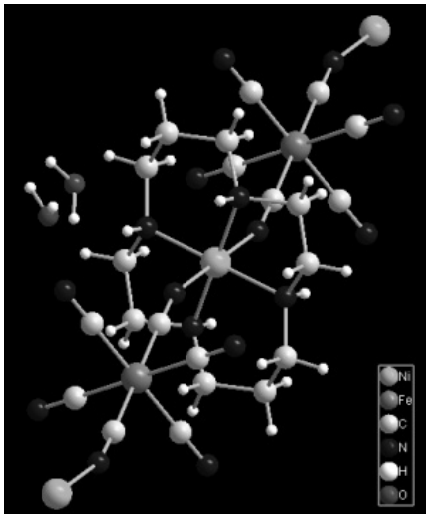

Figure 1. The illustration of the molecular structure – Fe-Ni molecular magnet with two H_2O molecules located. Structure investigated by XRD.

For the materials studies magnetic measurements have been carried out.

The temperature dependence of magnetic susceptibility shows that down to 100 K the hydrated compound is a paramagnet and the dehydration considerably changes the value of the effective magnetic moment. The measurements have also indicated that at low temperatures, below ~100 K, ferromagnetic correlations are possibly present, resulting in a significant increase in the magnetic susceptibility of the sample. The effect was much stronger in the case of dehydrated material and occured already at a higher temperature than for the hydrated material. Measurements of magnetisation versus magnetic field have shown a metamagnetic transition occuring for the dehydrated sample at a field of 6 kOe.

The material has also been examined by ^{57}Fe Moessbauer spectroscopy. An example of the spectrum measured at 4.2 K for the dehydrated sample is shown in Figure 2.

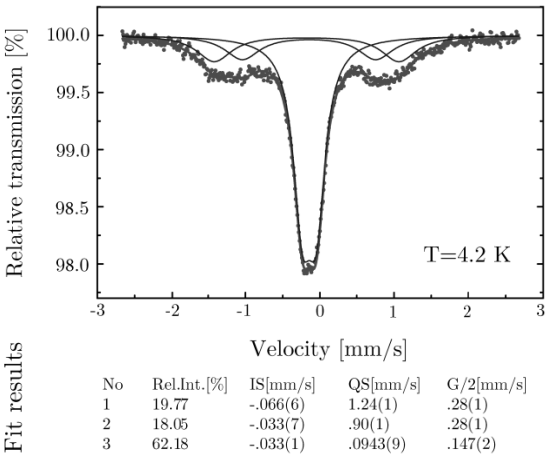

Fit results

No	Rel.Int.[%]	IS[mm/s]	QS[mm/s]	G/2[mm/s]
1	19.77	-.066(6)	1.24(1)	.28(1)
2	18.05	-.033(7)	.90(1)	.28(1)
3	62.18	-.033(1)	.0943(9)	.147(2)

Figure 2. ^{57}Fe Mossbauer spectrum of the dehydrated sample at the temperature 4.2 K together with a best fit result, green line. Three doublets fitted are marked as blue lines. Below the graph there are results of fitting, i.e. relative intensities of the doublets, their isomer shift, IS, quadrupole splitting, QS and the linewidth values shown.

No magnetic splitting is observed and the spectrum consists of three quadrupole doublets. For the hydrated sample just one doublet is observed corresponding to the most intense one with the smallest splitting observed for the dehydrated sample. The effect indicates that for the dehydrated sample two additional different states of Fe ion, corresponding to a higly nonspherical distribution of electronic charge appear.

X-ray Absorption Spectropy (XAS) study has been carried out in the XANES range of the Fe and Ni L_3 and L_2-edges. The measurements have been done in the Helmholtz-Zentrum Berlin at a bending magnet beamline of the synchrotron radiation storage ring BESSY II. The spectra were recorded in the total electron yield (TEY) and partial fluorescence yield (PFY) modes at room temperature. The TEY spectra are presented in Figure. 3. The L_2 and L_3 absorption edges correspond respectively to electronic transitions from the $2p_{1/2}$ and $2p_{3/2}$ core orbitals to the 3d states above the Fermi level.

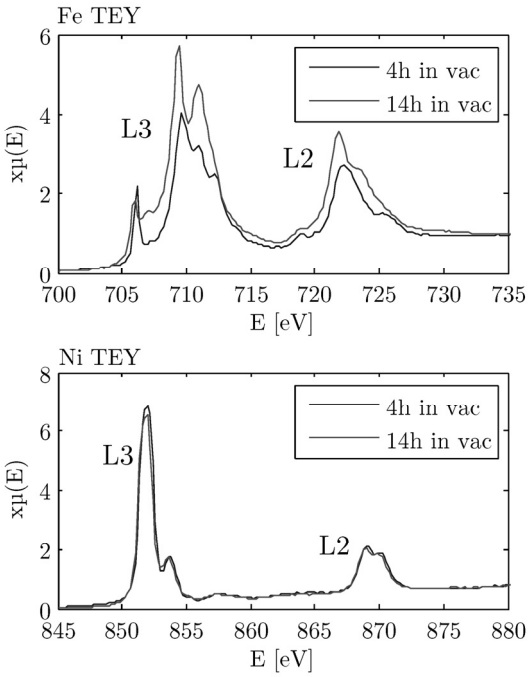

Figure 3. XANES spectra of the materials studied at the L_2 and L_3 edges of Fe and Ni in the TEY mode. Red line stands for dehydrated sample, blue line – for the hydrated one.

In the simulations of XANES spectra we have used the FEFF 8.4 XAS software and the IFEFFIT library-based software - ARTEMIS and ATHENA - to generate the sample and analyse the simulation results, respectively. Subsequent releasing of water molecules was realized by removing the two inequivalent molecules (**1** and **2**) in the unit cell. Four variants have been examined, i.e. both molecules present, molecule **1** present, molecule **2** present, none of them present. The resulting spectra are shown in Figure 4.

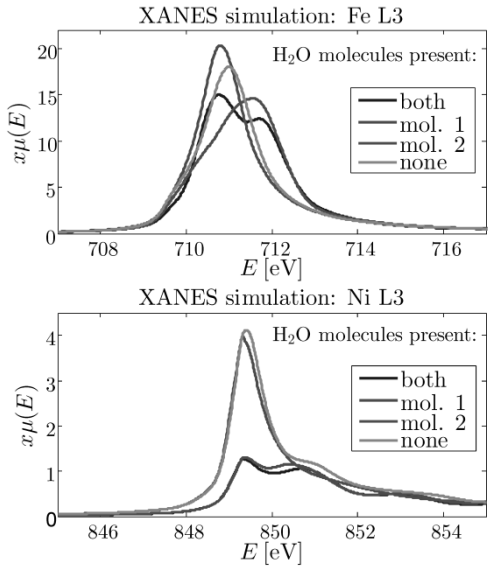

Figure 4. Simulated XANES spectra of $(H_3O)[Ni(cyclam)][Fe(CN)_6]\cdot 5H_2O$, at the L_3 edge of Fe and Ni.

A comparison of the experimental XANES spectra after 4 hrs in vacuum and 14 hrs in vacuum shows that the Ni spectrum does not change at all, whereas the Fe spectrum varies considerably. An inspection of the simulated spectra shows that the agreement with the experimental Ni spectrum can be obtained if the molecule **2** is released first and after 4 hrs in vacuum this process is completed within the probing depth of TEY detection, i.e. tens of nanometres. Release of the molecule 1 does not have further impact on the spectrum. This scenario is consistent with narrowing an shifting the center of gravity of the Fe L_3 edge to lower energies between 4 hrs and 14 hrs in vacuum, when possible, the process of releasing of the molecule 1 occurs.

Thus, we can conclude, that the process of dehydration of $(H_3O)[Ni(cyclam)][Fe(CN)_6]\cdot 5H_2O$ in vacuum occurs with a certain order of releasing particular inequivalent water molecules, which could be determined from a comparison of changes in the experimental simulated Fe and Ni L-edges XANES spectra.

[1] E.J.L.McInnes, R.E.P. Winpenny in *Comprehensive Inorganic Chemistry II (Second Edition)*, J. Reedijk, K. Poeppelmeier, Eds (Elsevier Amsterdam 2013) chap. 4.14.

[2] G. Christou, D. Gatteschi, D.N. Hendrickson R. Sessoli, *MRS Bulletin*, **25** (2000) 66.

IO-12 **Thu. 19. 06., 18^{10}-18^{30}**

Ultrafast pump-probe X-ray spectroscopy at SwissFEL

J. Szlachetko[1,2]*, C. Milne[1], R. Abela[1], B. Patterson[1], L. Patthey[1] and T. Penfold[1]

[1]*Paul Scherrer Institute, SwissFEL, Villigen, Switzerland*
[2]*Institute of Physics, Jan Kochanowski University, Kielce, Poland.*

Keywords: x-ray spectroscopy, x-ray free-electron laser

*e-mail: Jakub.szlachetko@psi.ch

With their unique combination of high per-pulse X-ray flux and femtosecond pulse durations, hard X-ray free electron lasers are an almost ideal source for time-resolved structural experiments. The SwissFEL, which is currently under construction at Paul Scherrer Institute, will be capable of generating femtosecond hard x-rays pulses in the photon energy range of 2-12 keV, with a planned emphasis on performing femtosecond pump-probe measurements. Experimental Station A (ESA) of the SwissFEL will focus on probing the ultrafast dynamics of systems in solution using a combination of X-ray spectroscopy and scattering. The primary goal of ESA will to enable users to perform X-ray absorption (XAS) and emission (XES/RIXS) spectroscopy pump-probe experiments with a focus on the 2-5 keV energy range with <50 fs time resolution (FWHM) using a range of excitation wavelengths (UV to IR). ESA will also be capable of using advanced methods for the injection of aerosol particles and sub-micron protein crystals. This presentation will provide an overview of the techniques we expect to have available at ESA and will present a prototypical 'ESA experiment' which uses a combination of femtosecond X-ray diffraction, scattering, and spectroscopy to investigate the electronic and structural dynamics. We will present recent results from an LCLS experiment devoted to study the interaction of intense femtosecond X-ray pulses with condensed matter. The electronic states of different forms of copper were probed on a shot-to-shot basis using a multi-crystal dispersive x-ray emission spectrometer. From these measurements we were able to establish the cross-sections of sequential-ionization and multi-photon absorption nonlinear processes.

IO-13 **Thu. 19. 06., 18^{30}-18^{50}**

Large amplitude spin dynamics driven by a THz pulse in resonance with an electromagnon

T. Kubacka[1]*, J.A. Johnson[2], M.C. Hoffmann[3], C. Vicario[4], S. de Jong[3], P. Beaud[2], S. Grübel[2], S-W. Huang[2], L. Huber[1], L. Patthey[4], Y-D. Chuang[5], J.J. Turner[3], G.L. Dakovski[3], W-S. Lee[3], M.P. Minitti[3], W. Schlotter[3], R.G. Moore[6], C.P. Hauri[4,7], S.M. Koohpayeh[8], V. Scagnoli[2], G. Ingold[2], S.L. Johnson[1], U. Staub[2]

[1]*ETH Zurich, Institute for Quantum Electronics, Wolfgang-Pauli-Strasse 16, 8093 Zurich, Switzerland*
[2]*Swiss Light Source, Paul Scherrer Institut, 5232 Villigen PSI, Switzerland*
[3]*Linac Coherent Light Source, SLAC National Accelerator Laboratory, Menlo Park, California 94025, USA*
[4]*SwissFEL, Paul Scherrer Institut, 5232 Villigen PSI, Switzerland*
[5]*Advanced Light Source, Lawrence Berkeley National Laboratory, Berkeley, California 94720, USA*
[6]*The Stanford Institute for Materials and Energy Sciences (SIMES), SLAC National Accelerator Laboratory, Menlo Park, California 94025, USA*
[7]*Ecole Polytechnique Federale de Lausanne, 1015 Lausanne, Switzerland*
[8]*Institute for Quantum Matter, Department of Physics and Astronomy, Johns Hopkins University, Baltimore, MD 21218, USA*

Keywords: free-electron laser, multiferroic, ultrafast dynamics, electromagnon, resonant magnetic diffraction, terahertz

*e-mail: tkubacka@phys.ethz.ch

Multiferroics are materials with more than one type of ferroic ordering. Recently they have attracted strong interest for potential applications where electric fields control magnetic order. The ultimate speed of control via magnetoelectric coupling, however, remains largely unexplored.

Recent developments in ultrafast pump-probe experiments have introduced new methods to selectively stimulate and observe the structural dynamics in strongly correlated electron systems. Their key element is the use of the extremely intense sources of short-pulse electromagnetic radiation over a broad frequency range from the far-infrared to x-rays. Pump-probe experiments exploiting these parts of spectrum offer unique ways to gain important information about the energy-transfer processes in crystals and thus insight into the microscopic mechanisms governing their behavior.

Here we report on an experiment [1] in which we use a pump-probe technique to study ultrafast spin dynamics in $TbMnO_3$, a model spin-cycloid multiferroic where the ferroelectric polarization arises directly from the frustrated magnetic order [2]. We excite coherent spin motion with an intense few-cycle terahertz (THz) light pulse tuned to resonance with an electromagnon, an electric-dipole active spin excitation associated with the magnetoelectric coupling [3]. To directly see the coherent response of the magnetic structure, we perform

femtosecond resonant x-ray diffraction measurement at the LCLS x-ray free electron laser. We determine the motion of the Mn spins during the excitation process by measuring the first harmonic magnetic diffraction peak. By comparison with a static x-ray diffraction experiment, we are able to determine that the THz pulse induces coherent rotation of the spin-cycloid plane with amplitude of 4°.

We prove that the pump-probe experiments employing ultrashort x-ray pulses can serve as a powerful spectroscopic tool which gives direct access to the spin dynamics and allows to visualize the spin motion associated with a particular excitation. Furthermore, we demonstrate that the magnetic structure of multiferroics can respond within a fraction of a picosecond after the excitation, what is far above the previously established limit of several milliseconds and suggests a way to achieve ultrafast heatless multiferroic domain switching.

Acknowledgments: This research was carried out on the SXR Instrument at the LCLS, a division of SLAC and an Office of Science user facility operated by Stanford University for the U.S. Department of Energy (DOE). The SXR Instrument is funded by a consortium including the LCLS, Stanford University through SIMES, LBNL, the University of Hamburg through the BMBF priority program FSP 301, and the Center for Free Electron Laser Science (CFEL). This research was supported by the NCCR MUST and NCCR MaNEP, funded by the Swiss National Science Foundation, and by the Swiss National Science Foundation (Grant No. 200021_144115). Our ultrafast activities are supported by the ETH Femtosecond and Attosecond Science and Technology (ETH-FAST) initiative as part of the NCCR MUST program. The Advanced Light Source is supported by DOE under contract No. DE-AC02-05CH11231. Crystal growth work at IQM was supported by DOE, Office of Basic Energy Sciences, Division of Materials Sciences and Engineering under Award DE-FG02-08ER46544. W.-S. L., Y.-D. C., and R. G. M. are supported by the Department of Energy, Office of Basic Energy Sciences, Materials Sciences and Engineering Division, under contract DE-AC02-76SF00515. S. L. J. and U. S. contributed equally to this work.

[1] T. Kubacka et al., *Science* **343** (2014) 1333.
[2] T. Kimura et al., *Nature* **426** (2003) 55.
[3] A. Pimenov et al., *Nat Phys* **2** (2006) 97.

IO-14 **Thu. 19. 06., 18^{50}-19^{10}**

Mainstream and alternative routes to photoinduced phase transitions

W. Kaszub, H. Cailleau, M. Cammarata,
M. Buron, M. Servol and E.Collet

Institute of Physics of Rennes UMR 6251 CNRS - University Rennes, France

The old adage, "seeing is believing", implies that our understanding of the working of nature is determined by our ability to capture a picture. A real time observation of temporally varying molecular structures during chemical reactions is a great challenge due to their ultrashort time scales. Ultrafast optical spectroscopies operating on the picosecond ($1ps=10^{-12}s$) and femtosecond ($1fs=10^{-15}s$) time scales have provided a wealth of information about the dynamics of chemical processes, such as bond breaking and bond formation, electron and proton transfer. Unfortunately the long wavelength of optical light precludes direct structural information at the atomic/molecular resolution. The early attempts in using monochromatic pulsed X-rays opened the doorway for visualizing photochemical dynamics in solution [1]. Technological innovations in synchrotron instrumentation [2,3,4,5], and the development of novel data analysis [6,7] have made it possible to track complex reactions by time-resolved X-ray diffraction to sub-100 ps temporal and sub-Angstrom spatial resolution. Several experiments at the cutting edge of the synchrotron and laser technologies have now provided essential insights into fields varying from the photoinduced phase transitions [8] to photochemistry [9,10] to protein crystallography [7]. The race for even better time resolution on high flux X-ray facilities has entered a new stage with the linear accelerator based X-ray Free-Electron Laser. Flux comparison with synchrotron sources show a 1000-fold increase of X-ray delivered per pulse in as short bursts as 100fs, or even shorter.

The general excitement born out of the ultrafast clock caused rush of new ideas, new materials, and new instruments. One feat in particular has been draining a lot of effort, namely the control of materials with an ultrashort laser pulse. There is ample evidence now that materials can be directed between different macroscopic states by using appropriate electronic, or structural, excitations. The switching with a laser pulse of such materials can severely change their macroscopic properties (electric conductivity, magnetism, colour, etc.), whereby emerging cooperativity and coherence of different degrees of freedom underpin the resulting phase transitions of various sorts [11]. However, the pertinent time scales for photo-switching processes in materials have been rather difficult to scrutinise. The pioneering investigations dealt mainly with the electron/phonon dynamics immediately following the femtosecond excitation, or the kinetics of recovery to the thermally stable states. Time-resolved X-ray diffraction and ultrafast VIS-IR spectroscopy reveal that the degrees of freedom triggered by a femtosecond laser pulse in a spin-crossover (SCO) material follow a sequence by which they appear during the out-of-equilibrium dynamics [12,13], characterised by elongation of covalent bondlengths between central Fe atom and its ligand. The time course of thermodynamic parameters, such as volume and temperature, shows evolution at later scale (100 ns, 1 μs), and eventually the return of the entire system to the equilibrium state. Those steps dissected in time, provided a mechanistic picture of a material transformation driven under different regimes (coherent or stochastic), [14]. The role of coherent optical phonons has been under intense scrutiny, whereas that of acoustic phonons and cell deformations, albeit looked upon, has not benefited from the same surge of effort. A likely explanation for this deficiency in providing global picture of transitions, is that crystal deformations occur on the periphery of ultrafast timescale. They involve propagation of a strain waves, essentially determined by sound velocity. This coherent process has the long coherence time of acoustic phonons and long range of elastic interactions. The coupling between the strain wave and the order parameter field raises a challenging question whether such coupling can lead to material transformation. SCO crystals composed of bistable molecules where the cooperativity is mainly governed by the change of molecular "volume" between the two states provide an excellent test bed for addressing this question.

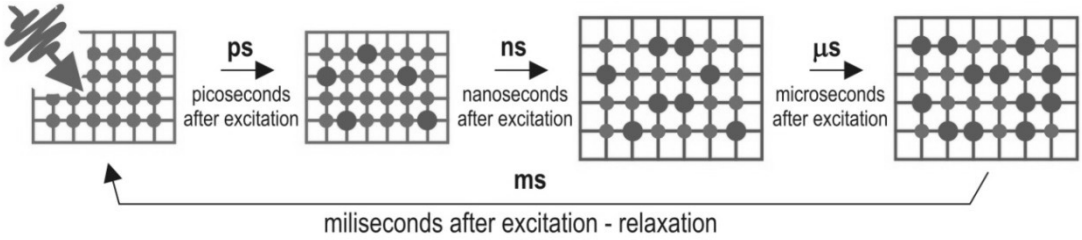

Figure 1. Schamtic drawing of the spin-state switching dynamics: HS molecules (red circles) generated within 1 ps by laser pulse in the cold (blue) lattice with mainly LS molecules (blue circles), warm (red) lattice expansion on 10s ns generating more HS molecules, thermal stabilisation of HS population within μs. Recovery to thermal equilibrium of the crystal with the environment (cryostat) on ms time scale.

We have investigated such materials over several time decades, and on samples of very different size, from nano- to macro-crystals [15,16]. These studies bring the photo-switching of materials into new perspective, notwithstanding its common perception, uniquely related to electronic or optical phonon dynamics.

Photo-switching on the ultrafast timescale still remains a fundamental problem in physics because of extremely fast inter-system crossing, which defies conventional understanding. Experiments carried out with 100 femtosecond resolution provide compelling evidence for a breakdown of Born-Oppenheimer approximation or Fermi Golden Rule [17]. Recent experiments carried out on X-FEL, operated conjunctly with the timing tools [18], corroborate recent theory [19] that the intersystem crossing results from the dephasing of the photoexcited state into the photoinduced phonon states, thus hindering the quantum recurrence, and instead favoring efficient damping in the excited state (submitted).

[1] R. Neutze *et al.*, *Phys. Rev. Lett.* **87** (2001) 195508.
[2] M. Wulff *et al.*, *J. Chem. Phys.* **124** (2006) 034501.
[3] M. Cammarata *et al.*, *Rev. Sci. Instrum.* **80** (2009) 015101.
[4] S. Nozawa *et al.*, *J. Synchrotron Rad.* **14** (2007) 313-319.
[5] T. Graber *et al.*, *J. Synchrotron Rad.* **18** (2011) 658-670.
[6] A. Plech *et al.*, *Phys. Rev. Lett.* **92** (2004) 125505.
[7] F. Schotte *et al.*, *Science* **300** (2003) 1944.
[8] E. Collet *et al., Science* **300** (2003) 612.
[9] H. Ihee *et al.*, *Science* **309** (2005) 1223.
[10] Ch. Bressler *et al.*, *Science* **323** (2009) 489.
[11] K. Nasu, Ed., *Photoinduced phase transitions* (Ed. World Scientist, Singapore, 2004)
[12] M. Lorenc *et al.*, *Phys. Rev. Lett*. **103** (2009) 028301.
[13] E. Collet *et al.*, *Chem. Eur. J.* **18** (2012) 2051.
[14] H. Cailleau *et al.*, *Acta Cryst.* **A66** (2010) 189.
[15] A. Bertoni *et al.*, *Angew. Chem. Int. Ed.* **51** (2012) 7485.
[16] M. Lorenc *et al.*, *Phys. Rev. B* **85** (2012) 054302.
[17] A. Marino *et al.*, *Angew. Chem. Int. Ed.* **53** (2014) 3863.
[18] M. Harmand *et al*., *Nat. Photonics* **7** (2013) 215.
[19] M. van Veenendaal *et al.*, *Phys. Rev. Lett.* **104** (2010) 067401.

O-01 **Mon. 16. 06., 11^{30}-11^{50}**

PhotoIonization and Velocity Map Imaging spectroscopy of atoms, molecules and clusters with synchrotron and Free Electron Laser Radiation at ELETTRA

M. Di Fraia[1]*, M. Coreno[2,3], K. C. Prince[3,4], R. Richter[3], C. Grazioli[3,4], M. de Simone[4], A. Kivimaki[4], P. O'Keeffe[2], P. Bolognesi[2], L. Avaldi[2], S. Stranges[4,7], M. Alagia[4], G. Cautero[3], R. Sergo[3], D. Giuressi[3], L. Stebel[3], O. Plekan[3], P. Finetti[2,3], A. La Forge[5], R. Katzy[5], V. Lyamayev[8], Y. Ovcharenko[5], M. Devetta[6], P. Piseri[6], T. Moeller[5], F. Stienkemeier[5] and C. Callegari[2,3]

[1]*Department of Physics, University of Trieste, 34127 Trieste, , Italy*
[2]*CNR-IMIP, UOS Area della Ricerca di Roma 1, 00010 Montelibretti, Italy*
[3]*ELETTRA-Sincrotrone Trieste S.C.p.A, Trieste, 34129 Trieste, Italy*
[4]*CNR-IOM, TASC Laboratory, in Area Science Park, Basovizza, 34149 Trieste, Italy*
[5]*Physikalisches Institut, Universität Freiburg, 79104 Freiburg, Germany*
[6]*Dipartimento di Fisica and CIMaINa, Università degli Studi di Milano, 20133 Milano, Italy*
[7]*Università degli Studi di Roma "La Sapienza", Dip. Chimica,00185 Rome, Italy*
[8]*European XFEL GmbH, 22761 Hamburg, Germany*

Keywords: synchrotron radiation, free-electron laser, Velocity Map Imaging, photo ionization, photoelectron spectroscopy

*e-mail: michele.difraia@phd.units.it

Advances in laser and synchrotron radiation instrumentation are continuously boosting fundamental research on the electronic structure of matter.

At ELETTRA the collaboration between several groups active in the field of atomic, molecular and cluster physics and the Instrumentation and Detector Laboratory has resulted in a set-up for Velocity Map Imaging (VMI) of charged particles [1,2]. It successfully tackles the challenges posed by the investigation of the electronic structure of isolated species in the gas phase by means of Synchrotron Radiation (SR) and Free Electron Laser (FEL) light.

The core of the setup scheme is the VMI system allowing the analysis of the kinetic energy and the angular distribution of the charged particles produced by photo ionization.

The unique combination here at ELETTRA of access to both SR and FEL sources, and of the realization of the setup described above allow to explore new frontiers in the study of matter, covering a wide spectrum of targets from energetic to dynamics. In fact our firs VMI setup was born for the SR application, but, by changing position sensitive detectors, tests with the FEL light source have been performed. Based on this successful preliminary tests a permanent setup has been realized also for FEL applications. I will present the two different setups for SR and FEL applications:

– In SR experiments, at the GasPhase beamline [3], a crossed delay line detector is used, coupled to a four-channel time-to-digital converter that reconstructs the position of the electrons. Simultaneously, a Time-of-Flight (TOF) mass spectrometer allows to acquire photoion spectra. In such a configuration Photo-Electron-PhotoIon-Coincidence detection (PEPICo) allows correlating the kinetic energy and exit angle of photo-emitted electrons with the mass of photo-ions, i.e., to the specific ionic state produced by photon absorption.
– In FEL experiments (notably differing from SR experiments in the much higher rate of events produced and detected, which forces one to forfeit coincidence detection), at the LDM beamline [4], a Micro Channel Plate (MCP) a phosphor screen and a CCD camera are used instead, allowing shot-by-shot collection of practically all events, albeit without time resolution. Femtosecond pump and probe experiments can also be performed to access the electron dynamics.

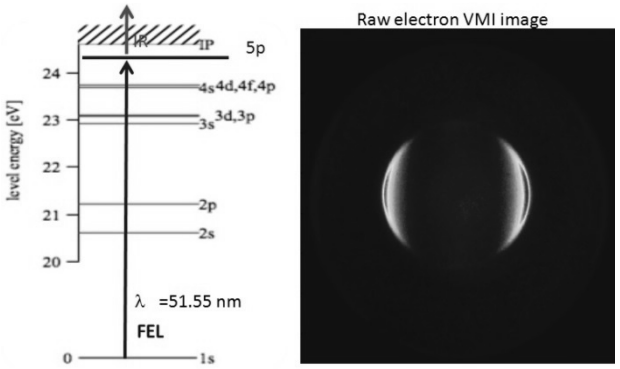

Figure 1: Two color experiments at the LDM beamline on atomic Helium photoemission, FEL at 24.05 eV and IR at 1.5 eV. On the right: a raw electron VMI image.

Recent results of experiments on rare-gas atoms and clusters performed at the GasPhase beamline of ELETTRA and at the LDM beamline (Low Density Matter, one recent result in fig.1) of the FEL FERMI [5,6] will be presented.

[1] P. O'Keeffe, *et al., Rev. Sci. Instrum.* **82** (2011) 033109.
[2] P. O'Keeffe, *et al., Nucl. Instr. Meth. B* **284** (2012) 69.
[3] K. C. Prince, *et al, J. of Synch. Radiation,* **53** (1998) 556-568.
[4] Viktor Lyamayev *et al, J. Phys. B: At. Mol. Opt. Phys.* **46** (2013) 164007
[5] E. Allaria*, et al, Nature Photonics* **6** (2012) 669-704.
[6] Fermi@Elettra website: http://www.elettra.trieste.it/FERMI/

O-02 **Mon. 16. 06., 12^{50}-13^{10}**

X-ray absorption fine structure study on electrochromic metallo-supramolecular polyelectrolytes

W. Szczerba*

BAM Federal Institute for Materials Research and Testing, Unter den Eichen 87, 12205 Berlin, Germany

Keywords: XAFS, electrochromism, structure, spin crossover, charge transfer

*e-mail: wojciech.szczerba@bam.de

Rigid rod type metallo-supramolecular coordination polyelectrolytes with divalent 3*d* metal centers (MEPE) exhibit remarkable electrochromic properties. The Fe-MEPE changes its color from blue to transparent, when an electric potential is applied to the material. In the case of Co-MEPE the change is from red to transparent. These materials are prospective candidates for application in so called smart windows that can be shaded on demand for e.g. privacy protection, large scale displays, and energy conservation in vehicles and buildings.

A comprehensive x-ray absorption fine structure (XAFS) study was made *in situ* and *in operando* on annealed MEPE powders and working electrochromic devices, respectively. It has been found that during annealing at temperatures above 100 °C a rearrangement of the ligands around the metallic center occurs without a redox reaction, but due to spin crossover only. The atomic positions and the alignment of the ligands with respect to the metallic center in the two states have been determined by use of first principle calculations.

The *in operando* experiments revealed that during the switching process from blue to transparent the metallic center changes its formal valence from 2+ to 3+. The charge transfer is not accompanied by any change in the local structure.

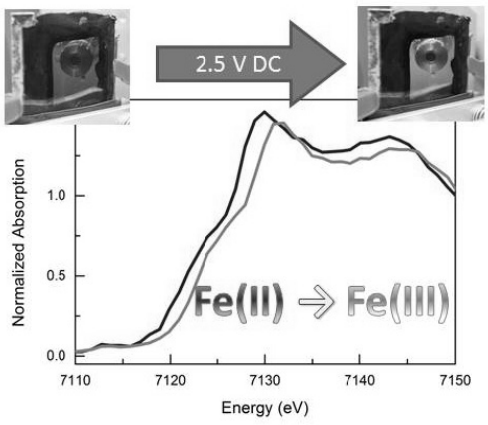

Figure 1. XANES of the *in operando* experiment on Fe-MEPE.

Acknowledgments: This work was supported by the German Federal Ministry of Education and Research (BMBF) within the BMBF Joint Project 'SmartWin MEPE', Grant No. 13N11285.

O-03 **Mon. 16. 06., 11^{30}-11^{50}**

Eu-XFEL upgrade

W. Grabowski[1], R. Nietubyć[1,2], J. Sekutowicz[3], M. Staszczak[1] and T. Wasiewicz[1]*

[1]*National Centre for Nuclear Research Świerk, Sołtana 7, 05-400 Otwock, Poland*
[2]*National Synchrotron Radiation Centre Solaris, Jagiellonian University, Gołebia 7/P.1.6, 30-387 Kraków*
[3]*Deutches Elektronen Synchrotron, Notkestrasse 85, 22607 Hamburg, Germany*

Keywords: FEL, Tesla, cavity, beam dynamics

*e-mail: tomasz.wasiewicz@ncbj.gov.pl

The talk presents beam properties calculation for the superconducting linear particle accelerator of free electron laser POLFEL [5] and possible XFEL [8] upgrade. Normalized slice emittance and bunch size are tracked for the 1.6-cell superconducting injector with solenoid followed by 2-structure cryomodules[3] of HZDR-type.

Main results are taken from ASTRA [2] 2D calculations. First the cavity and solenoid were tested in order to find the most suitable parameters. The criterion for optimization was normalized slice emittance. The key parameter is an inclination angle of the cavity rear wall to the longitudinal axis. During performed studies the 8 degree inclination angle was chosen as an optimal value for further test. Next the cryomodules were added and the beam size was honed due to its great focusing and reaching values near zero. We targeted the beam size instead of emittance, since computation results, after adding cryomodules, show almost no influence on emittance.

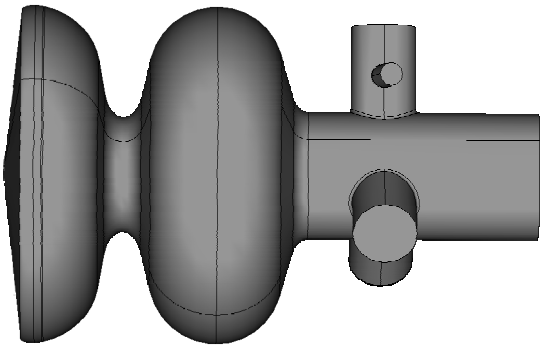

Figure 1. Tesla - type 1.6 cell cavity of electron gun.

Based on cavities shapes taken from FEM[6] program we made the 3D model of the accelerating structure using Microwave Studio [4] software. We tuned the model to match the calculations performed by Sekutowicz [7]. Then added the couplers. We do also have a model of Tesla - type 1.6 cell cavity of electron gun (Fig 1.). It was made using Cubit software [1] and exported to Microwave Studio. The goal is to build the same model as in ASTRA and to compare the emittance from both 2D and 3D modelling.

Acknowledgments: We want to express our gratitude to Dr. Klaus Floettmann for his assistance and helping us to run the ASTRA code.The work was supported by the EU and MSHE grant nr POIG.02.03.00-00-013/09.

[1] CUBIT, Sandia National Laboratories www.cubit.sandia.gov
[2] K. Floettmann, "ASTRA, A Space Charge Tracking Algorithm", v. 3.0, October 2011 www.desy.de/~mpyflo/Astra_dokumentation
[3] P. A. McIntosh et al, "*Realisation of a prototype superconducting CW cavity and Cryomodule for energy recovery*", SRF2007, Beijing, 864-868, (2007)
[4] Microwave Studio, CST www.cst.com/Content/Products/MWS/Overview.aspx
[5] POLFEL - Project Description polfel.pl/doc/polfel_booklet_en_2012_10_28-b.pdf
[6] J. Sekutowicz, "2D FEM code with third order approximation for RF cavity computation", Proc. Conf. Linear Acc., Tsukuba, 1994
[7] J. Sekutowicz, "Multi-Cell Superconducting Structures for High Energy e+ e- Colliders and Free Electron Laser Linacs; EuCARD Editorial Series on Accelerator Science and Technology, (J-P.Koutchouk, R.S.Romaniuk, Editors), Vol.01", EuCARD-BOO-2009-005
[8] XFEL – homepage: www.xfel.eu

O-04 **Mon. 16. 06., 12^{30}-12^{50}**

X-Ray diffraction study of stacking faults in silicoaluminophosphate SAPO-18/34

W. A. Sławiński[1]*, D. S. Wragg[1], D. Akporiaye[2] and H. Fjellvåg[1]

[1]*Centre for Materials Science and Nanotechnology, Department of Chemistry, University of Oslo, PO Box 1126, 0315 Oslo, Norway*
[2]*SINTEF Materials and Chemistry, Forskningsvn 1, 0314 Oslo, Norway*

Keywords: stacking faults, intergrowth, modelling, SAPO

*e-mail: w.a.slawinski@smn.uio.no

Silicoaluminophosphate framework structures have been widely studied because of their many technological applications. The most significant application of silicoaluminophosphate type framework catalysts is in the methanol-to-olefin (MTO) conversion process [1], catalysed by SAPO-34 (the silicoaluminophosphate form of the chabazite (CHA) zeolite framework with silicon substituted into its structure). The effectiveness of SAPO-34 in the MTO process is due to both the shape selective properties of the framework and the concentration and strengths of the acid sites created by silicon substitution [2]. Another aluminophosphate framework MTO catalyst is SAPO-18 (zeolite framework type (AEI)), which has a very closely related structure to SAPO-34 and can form intergrowths with it. It has been suggested that the level of intergrowth can affect the efficiency of the MTO process [3], however, assessment of the level of intergrowth has remained difficult.

We present a consistent model of the crystal structure of SAPO-18/34 family members which can accurately determine the level of intergrowth. The model utilises two types of stacking fault: Displacement and Growth which have significantly different effects on the diffraction pattern (see Fig. 1). A series of powder diffraction patterns is calculated using the Discus software package. Changes in the level of intergrowth and stacking fault type strongly affect the calculated pattern. A series of patterns has been calculated to illustrate this. The structure of an intergrown SAPO-34 sample with 4.8% Si content is modelled and refined using Displacement stacking faults. An example of "defect-free" AlPO-18 (0% Si content) is then presented. Refinement of the model shows that even this contains a small amount of stacking faults. Finally, a simple method for defect level estimation is proposed based on FWHM (Full Width at Half Maximum) ratios for selected Bragg reflections.

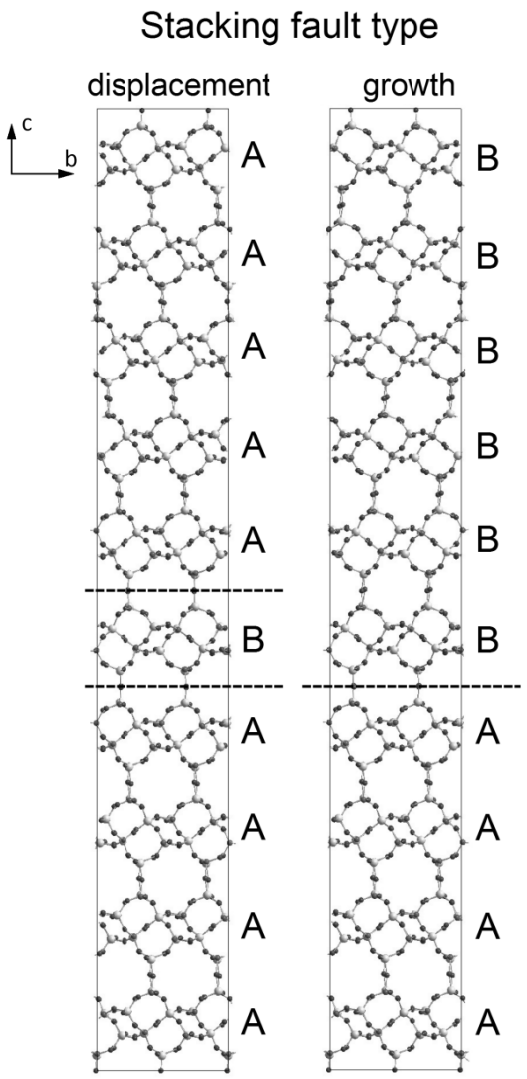

Figure 2. Displacement and Growth type of stacking faults in SAPO-18/34 structure

Acknowledgments: The work presented in this paper was part of the InterCat Project (Intergrowth Materials for Improved Methanol-To-Olefn Catalysts) funded by the GASSMAX program of the Research Council of Norway.

[1] D. Chen, K. Moljord, T. Fuglerud, A. Holmen, *Microporous and Mesoporous Materials* **29 (**1999) 191-203.
[2] F. Bleken, M. Bjrgen, L. Palumbo, S. Bordiga, S. Svelle, K. Lillerud, U. Olsbye, *Topics in Catalysis* **52** (2009) 218-228.
[3] M. Janssen, A. Verberckmoes, M. Mertens, A. Bons, W. Mortier, Exxon-Mobile Chemical Europe Inc. patent no. EP 1 365 992 B1 (2007).

O-05 **Mon. 16. 06., 12^{50}-13^{10}**

Attenuation and indirect excitation effects in x-ray fluorescence holography

D. T. Dul*, K. M. Dąbrowski and P. Korecki

Institute of Physics, Jagiellonian University, Reymonta 4, 30-059 Kraków, Poland

Keywords: x-ray fluorescence, atomic resolution holography, local structure imaging

*e-mail: dawid.tadeusz.dul@uj.edu.pl

Many physical properties of materials are determined by local atomic structure. A variety of imaging techniques have been developed over the years to gain local structure information. Among them is x-ray fluorescence holography (XFH) which gives direct access to the intensity and phase of the scattered radiation enabling full three dimensional imaging of atomic structure. The holographic pattern can be viewed as a small, direction dependent oscillatory part of the x-ray absorption coefficient and originates from the interference of an incident photon wave with waves scattered from atoms inside the sample. The holographic signal for a given element is probed by measuring characteristic fluorescence radiation. On the one hand the usage of x-rays and fluorescence allows studies of bulk materials, avoids strong multiple scattering and provides element sensitivity. On the other hand it might introduce parasitic effects such as indirect excitation (IE) and beam attenuation (BA).

In this work we discuss BA and IE effects in XFH and their influence on element sensitivity and local structure imaging. Beam attenuation simply refers to the decrease of the beam's intensity as it penetrates through the sample. Indirect excitation occurs when fluorescence from one kind of atoms can excite other types of atoms introducing secondary x-ray fluorescence. Both processes influence the number of measured fluorescence photons and therefore the measured holograms. Although IE can be avoided with an appropriate adjustment of the incident beam energy it limits the number of samples which can be analysed with XFH especially in the multi-energy variant of XFH.

We argue that in the presence of BA and IE the experimentally measured hologram should be regarded as a weighted sum of holograms from all the elements from which the sample is composed rather than as a single element hologram. In other words, that element sensitivity with respect to the central absorbing atom is reduced. As a consequence artifacts might arise in the reconstruction images. As an example, Figure 1 presents a multi-energy holographic reconstruction from simulated gallium holograms for GaAs. In the presence of BA and IE additional maxima appear apart from the ones which can be attributed to As atoms. These additional maxima cannot be attributed to remnants of twin images.

A model which takes BA and IE effects into account and which allows to correct for them is proposed [1]. The construction of the model is based on quantitative methods of x-ray spectrometry and holds for samples of arbitrary thickness. We consider both the monochromatic as well as the polychromatic case of XFH [2].

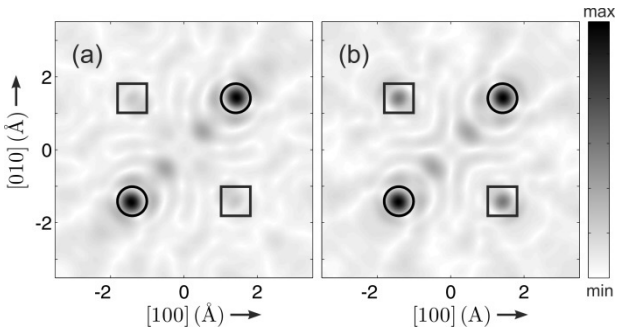

Figure 1. Multi-energy holographic reconstruction in the (004) plane from gallium holograms simulated for GaAs without (a) and with (b) BA and IE effects. Fifteen holograms have been used for the reconstruction with energies ranging from 12 keV to 19 keV with a step of 0.5 keV. The sample thickness was set to 30 μm. Black circles mark the expected positions of As atoms. Black squares mark positions where artefacts arise due to BA and IE.

Acknowledgments: This work was supported by the Polish National Science Center (grant. DEC-2013/09/N/ST3/04111) and in part by the KNOW Research Consortium through the Marian Smoluchowski fellowship.

[1] D. T. Dul, K. M. Dąbrowski, P. Korecki, *EPL (Europhysics Letters)* **104** (2013) 66001.
[2] K. M. Dąbrowski, D. T. Dul, T. P. Roszczynialski, P. Korecki, *Physical Review B* **87** (2013) 064111.

O-06 **Mon. 16. 06., 13^{10}-13^{30}**

Crystallographic studies on phase transition in copper based shape memory alloys

O. Adiguzel

Department of Physics, Firat University, 23169 Elazig, Turkey

Keywords: shape memory effect, martensitic transition, twinned and detwinned martensite,

e-mail: oadiguzel@firat.edu.tr

Abstract

Shape memory alloys take place in a class of smart materials by exhibiting a peculiar property called shape memory effect. This property is characterized by the recoverability of the desired shape on the material at different conditions. Shape memory effect is based on a solid state phase transition, martensitic transformation, and this transformation is characterized by a change in the crystal structure of the material. Martensitic transformations are first order diffusionless transitions and occur in thermal manner in the materials on cooling from high temperature. Thermal induced martensite occurs as multivariant martensite in self-accommodating manner on cooling from high temperature parent phase region, and this martensite is called self-accommodated martensite or multivariant martensite. Deformation of shape memory alloys in martensitic state proceeds through a martensite variant reorientation. Martensitic transformations occur with cooperative movement of atoms by means of lattice invariant shears on a {110} -type plane of austenite matrix which is basal plane of martensite. The lattice invariant shears occurs, in two opposite directions, <110>-type directions on the {110}-type basal plane. This kind of shear can be called as {110}<110>-type mode, and possible 24 martensite variants occur. Copper based alloys exhibit this property in metastable β–phase region, which has bcc-based structures at high temperature parent phase field and these structures martensiticaly turn into layered complex structures with lattice twinning following two ordered reactions on cooling. Copper based alloys exhibit this property in metastable β–phase region, which has bcc-based structures at high temperature parent phase field and these structures martensiticaly turn into layered complex structures with lattice twinning following two ordered reactions on cooling.

Introduction

Shape memory alloys take place in a class of functional materials exhibiting a peculiar property called shape memory effect. This property is characterized by the recoverability of desired shape on the material at different conditions. Shape memory phenomena are based on a solid state phase transformation, martensitic transition, which occurs on cooling from high temperatures. These alloys are plastically deformed in martensitic condition, and the material spontaneously returns to the original phase on heating over the austenite finish temperature. Shape memory effect is facilitated by martensitic transformation governed by changes in the crystalline structure of the material, and shape memory properties are intimately related to the microstructures of the alloy. Thermal induced martensite occurs as multivariant martensite in self-accommodating manner on cooling from high temperature parent phase region. Deformation of shape memory alloys in martensitic state proceeds through a martensite variant reorientation, and twinned martensite turns into the detwinned martensite. These processes are schematically illustrated in Figure 1 The first cycle proceeds as follow: cooling, deformation and heating. The oriented martensite turns into the ordered austenite structure through heating in both reversible and irreversible shape memory effect.[1]. The ordered parent phase structure turns into the twinned martensite on cooling after first cycle in irreversible case, and it turns into the oriented martensite in case of reversible shape memory effect [1,2].

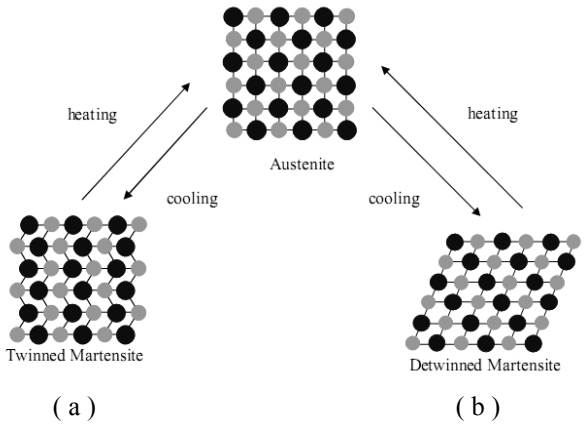

Figure 1. Schematic illustration of structural changes with phase transformation; (a) formation of twinned martensite structure on cooling, (b) formation of oriented martensite structure with deformation in low temperature martensitic state[1].

Martensitic transformations occur usually by two or more lattice invariant shears on a {110}-type plane of austenite matrix. Therefore, thermal induced martensites have 24 variants[3].

Copper based alloys exhibit this property in metastable β-phase field, and high temperature bcc-structures martensiticaly undergo non-conventional layered structures following two ordered reactions on cooling. The product phases have the unusual complex structures called long period layered structures such as 3R, 9R or 18R depending on the stacking sequences on the close-packed planes of the ordered lattice[3].

Experimental

In the present contribution, a CuZnAl alloy was selected for investigation: CuZnAl alloy with a nominal composition by weight of 26.1 %zinc, 4 % aluminium, and the balance copper. X-ray powder specimens were prepared by filling the alloy samples. Specimens for TEM examination were also prepared from 3 mm diameter discs and thinned down mechanically to 0.3 mm

thickness. These specimens were heated in evacuated quartz tubes in the β-phase field (15 minutes at 830°C for homogenization and quenched in iced-brine.

These specimens were also given different post-quench heat treatments and aged at room temperature.

TEM and X-ray diffraction studies carried out on these specimens. TEM specimens were examined in a JEOL 200CX electron microscope, and X-ray diffraction profiles were taken from the specimens using Cu-K_α radiation with wavelength 1.5418 Å.

Results and Discussion

An x-ray powder diffractogram taken from the aged CuZnAl alloy samples is shown in Figure 2. An electron diffraction pattern taken from CuZnAl alloy sample is also shown in Figure 3. X-ray powder diffractograms and electron diffraction patterns reveal that this alloy has an ordered structure in martensitic condition, and exhibit superlattice reflections. X-ray powder diffractograms and electron diffraction patterns were taken from the specimens in a large time interval and compared with each other. It has been observed that electron diffraction patterns exhibit similar characteristics, but some changes occur at the peak locations and intensities on the x-ray diffractograms with aging duration. These changes occur as rearrangement or redistribution of atoms in the material, and attribute to new transitions in diffusive manner [3]. The ordered structure or super lattice structure is essential for the shape memory quality of the material.

In the shape memory alloys, homogenization and releasing the external effect is obtained by ageing at β−phase field for adequate duration.

Crystallization is essential for shape memory quality, and crystallization and formation of the ordered structure is also obtained by the quenching process in the suitable media. The quenching rate is also important for the formation of homogenous ordered structures and shape memory optimization.

On the other hand, post-quench ageing and service processes in devices affect the shape memory quality, and give rise shape memory losses. These kinds of results lead to the martensite stabilization in the reordering or disordering manner [3, 4].

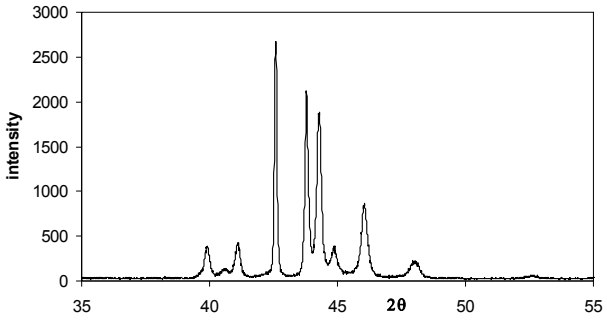

Figure 2. An x-ray diffractogram taken from the CuZnAl alloy sample.

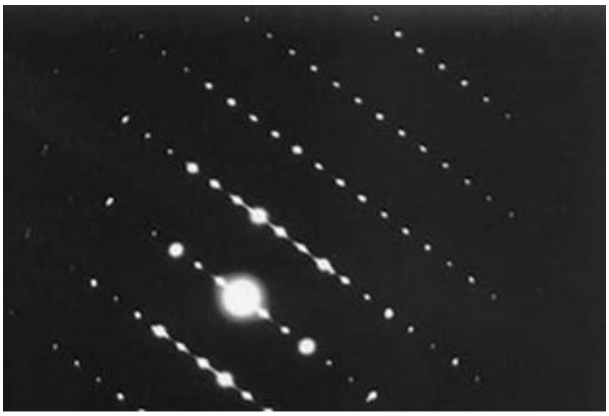

Figure 3. An electron diffraction patterns taken from CuZnAl alloy sample.

In order to make the material satisfactorily ordered and to delay the martensite stabilization, copper-based shape memory alloys are usually treated by step-quenching after homogenization.

Although martensitic transformation has displacive character, martensite stabilization is a diffusion controlled phenomena, and leads to redistribution of atoms on the lattices sites. Stabilization is important factor and causes to memory losses, and changes in main characteristics of the material; such as, transformation temperatures, and x-ray diffraction peak location and peak intensities.

It can be concluded from the above results that the copper-based shape memory alloys are very sensitive to the ageing treatments, and heat treatments can change the relative stability and the configurational order of crystal planes. This result attributes to a rearrangement of atoms.

[1] J. Ma, I. Karaman and R.D. Noebe, *International Materials Reviews* **55** (2010) 257.
[2] Y. Liu, Detwinning Process and Its Anisotropy in Shape Memory Alloys, *Smart Materials, Proceedings of SPIE* **4234** (2001) 82.
[3] O. Adiguzel, *Journal of Materials Processing Technology* **185** (2007) 120.
[4] J. Malarriaa, F.C. Lovey, M. Sade, *Materials Science and Engineering A* **517** (2009) 118.

O-07 **Mon. 16. 06., 18^{10}-18^{30}**

Advances in surface chemical state imaging and depth profiling using XPS

M. Szklarczyk[1], A.J. Roberts[2] and C. Moffitt[2]

[1] *Shim-Pol, ul. Lubomirskiego 5, 05-080 Izabelin*
[2] *Kratos Analytical Ltd, Wharfside, Trafford Wharf Road, Manchester, M17 1GP, UK.*

Keywords: angle resolved XPS, maximum entropy method

*e-mail: mareks@shim-pol.pl

As the critical dimensions of fabricated devices shrink and the explotation of novel nanotechnology effects, each material's surface properties begin to dominate, rather than the bulk properties. These dimensions are such that essentially the entire structure becomes composed of only surface material. Mechanisms to explore these surface properties become paramount to their understanding and characterization for technological development.

Elemental and chemical analysis using traditional x-ray, optical and electron techniques often does not differentiate subtle surface phenomena from bulk material as these techniques generally sample much deeper than the dimensions of many nanotechnology effects. In x-ray photoelectron spectroscopy (XPS), all of the signal comes from within 5-10 nm of the surface and this technique is sensitive to sub-monolayer differences in surface composition and even chemical state, wherein lies its power. XPS provides non-destructive chemical state analysis from the surface of insulating samples and is fundamentally directly quantitative, suffering no substantial matrix effects. This surface chemical signal can be obtained and processed in various ways to generate representative maps or images of the chemistry on a sample surface highlighting any sample inhomogeneities.

Although a counting technique generally beholden to Poisson statistics, similar to XRF, XPS has a distinct background effect, which can completely mask large differences in adjacent regions, if not properly addressed. Figure 1 shows how spectra from two adjacent regions of radically different composition would have nearly constant measured intensity, if no background correction were performed. Improved collection efficiency has limited sample damage, such that imaging of organic, polymeric and biological samples are done regularly, extending to recent work showing that XPS imaging characterization of DNA microarrays can be used as a complement to other surface analytical techniques in the exploration of surface chemistry effects [1].

Surface segregation of bulk materials, or enhancement of surface composition by external treatment is not easily addressed with bulk techniques at the heart of many industrial processes. A particular example exploring combinatorial screening of micro patterned co-polymer arrays for cell adhesion shows how imaging the sample array allows the mixtures with the suitable surface chemistry composition range to be quickly identified [2].

Angle resolved XPS (ARXPS) depth profiling might be an excellent technique for chemical state and molecular orientation determination. To realize these goals the high resolution spectrometer is required with proper and highly efficient charge neutralization and finally with the advanced software for background calculation. The developed advanced Maximum Entropy Method (MEM) software for ARXPS measurements may used to probe the chemical composition of the sample over the first few nm of the sample surface (Figure 2).

Furthermore, the hypothesised close packed surface arrangement with the molecular chains arranged perpendicular to the Si surface is confirmed.

Unlike electron excited techniques, which require conductive surfaces to avoid instantaneous deflection of the primary beam due to surface charging, XPS imaging of insulating surfaces is possible with modern charge neutralization schemes. The conductive coatings used in electron spectroscopy to analyze insulating surfaces would modify and fully obscure the chemistry of interest on a sample surface. Examples of thin surface enhancements on insulating samples will show that these can be immediately characterized as surface segregations, some of nearly monolayer thickness regions over large scales.

Multivariate methods are also finding foothold within the XPS community. As XPS is a spectroscopic technique at its heart, the high speed imaging afforded by modern systems allows stacks of data with both spatial and spectral information to be obtained. PCA processing of images will be seen to accentuates correlations while removing noise and cleaning up these images. The multivariate techniques can also be applied to the spectral components, fitting components to 64,000+ spectra generated at each pixel location from an image. These components are then used to generate a new image while removing noise, which is shown to improve the image quality.

[1] C. Y. Lee *et al.,J. Am. Chem. Soc.* **129** (2007) 9429-9438.
[2] D. G. Anderson *et al,Nature Biotechnology* **22 (7)** (2004) 863-866.

O-08 **Mon. 16. 06., 18^{30}-18^{50}**

Science Link: Cooperation between science and industry in the Baltic Sea Region

G. A. Appleby* and U. Sassenberg

Deutsches Elektronen-Synchrotron, Notkestr. 85, 22607 Hamburg, Germany

Keywords: synchrotron radiation, industrial measurements, regional development

*e-mail: graham.appleby@desy.de

Science Link is a European Union funded project which aims to support and encourage innovation and entrepreneurship in the Baltic Sea Region, to strengthen the region's competitiveness in a global context.

One way of encouraging innovation is by increasing the awareness about the existing research and scientific resources amongst industrial companies, as well as facilitating access to these valuable resources.

Science Link has created a network of synchrotron and neutron sources, physics research institutes and regional development agencies, involving 17 project partners from eight countries in the Baltic Sea Region. During the project period 2012 – 2014, three open calls have been made for companies to apply for an experimental measurement at a synchrotron source like DESY or MAX-Lab. From a total of 66 received applications, 48 have been accepted from diverse fields including construction, material science, life science and agriculture, while to date 36 of the measurements have been carried out.

This presentation will describe the Science Link project, its network and its results so far, with an overview of the industrial measurements already performed. Examples include the use of synchrotron x-ray diffraction analysis for new fertiliser materials, x-ray absorption spectroscopy on industrial catalysts for green chemistry, small angle x-ray scattering for understanding the behaviour of dispersants in paints, pigments and dyes, photoelectron emission microscopy for analysis of solar cell materials and synchrotron infrared spectroscopy to investigate the relationship between urinary sediments and kidney stone formation.

Acknowledgments: This work is part financed by the European Union (European Regional Development Fund – Baltic Sea Region 2007 – 2013).

O-09 **Mon. 16. 06., 18^{50}-19^{10}**

X-ray absorption spectroscopy for industry: examples from Science Link project

K. Lawniczak-Jablonska[1]*, J. Libera[1], A. Chruściel[2] and M. Krasowska[3]

[1]*Institute of Physics, Polish Academy of Sciences, Lotnikow Str 32/46, 02 668 Warsaw, Poland*
[2]*Scientific Consortium ADVANCE DMC, MEXEO, 47 225 Kędzierzyn-Koźle, Energetykow Str 9, Poland*
[3]*PPH Cerkamed, ul. Kwiatkowskiego 1, 37-450 Stalowa Wola*

Keywords: x-ray absorption spectroscopy, innovation in industry, polyaddition, catalysts

*e-mail: jablo@ifpan.edu.pl

The x-ray absorption spectroscopy (XAS) is a synchrotron base technique widely used in solving scientific problems and offering unique possibility. Few examples will be shown how this technique can be applied for innovation in the industry. This is an example of "smart specialization" – a cooperation between Research & Development in companies and basic research. The examples are based on the results of Science Link project, which is a network between leading research infrastructure of photon and neutron and their users. The project aims to support and encourage innovation and entrepreneurship in the Baltic Sea Region. The scientific cases from three Polish companies were chosen. Synchrotron base techniques need advanced analysis of the results to get out useful for industry information. Therefore, the involvement of scientists is a must particularly for small companies without R&D department.

XAS technique can be considered as a finger print of chemical bonding of element under consideration. Therefore, can be used to find the neighborhood of given element (number, distances and kind of surrounding atoms), the location of given element in the crystal structure, it's chemical bonding, and to estimate the proportion between few compounds of the same element in composite materials. This information can be of great importance in many technological problems.

One from investigated cases were the colored PVC materials used outdoor. In some of them, after two year exposure for the sunlight, the bleaching was observed. The PVC materials contain stabilizer with Zn element. The XANES and EXAFS measurements at the K-edge of Zn were performed and analyzed. The results indicated that the coordination of Zn atoms change after the exposure on light in the bleaching samples.

The other example are the pasts used in dental fillers. Products consist of amino and epoxy resin (filled with inorganic fillers), which react in the ratio of 1:1 in polyaddition process. The question was if the initial components remain in the final product. The K-edges of C, N and O were measured for each paste and compare with reference initial substances to decide if they can be distinguished in the paste after polyaddition process. The main conclusion was that no signs of any of the investigated initial materials could be clearly identified in the measured XANES spectra. New compound was formed in polyaddition process.

The next project was dedicated to the determination of structural characteristics of the non-stoichiometric composite transition metal complex salts, known as double metal cyanides (DMC), in order to correlate them with catalytic properties in the polyaddition of oxirane homologues used in manufacturing of important industrial polymeric materials (polyurethanes, surfactants etc.) as well as to compare synthesized catalyst with commercial reference one. The XANES and EXAFS spectra for Co and Zn elements were measured. It was shown that in all measured catalysts the neighborhood of Zn and Co centers were very similar and the atomic order around Co and Zn atoms was much closer to trygonal structure then cubic one.

Performed XAS measurements did not solve the technological problems reported by the companies but provide the suggestions where to look for the solution and usually were the beginning of scientific approach to the problem and need for further cooperation was clearly seen. They are a good examples how to initiate and maintain the useful cooperation between basic research and industry.

Acknowledgments: Research funded in part by the Projects BSR , Science Link and Innotech K2/IN2/21/181982/NCBR/ 12(K-DMC).

O-10 **Wed. 18. 06., 15^{00}-15^{20}**

Complex formation of pyrophosphatase with protein-partners investigated by small-angle X-ray scattering in solution

L.A. Dadinova[1,3]*, E.V. Rodina[2], N.N. Vorobieba[2] and E.V. Shtykova[1]

[1]*A.V.Shubnikov Institute of Crystallography, RAS, Leninsky pr., 59, Moscow, Russia*
[2]*Lomonosov Moscow State University, Chemistry Department, Leninskie gory, 1, Bldg. 3, Moscow, Russia*
[3]*Lomonosov Moscow State University, Physics Department, Leninskie gory, 1, Bldg. 2, Moscow, Russia*

Keywords: synchrotron radiation, small-angle X-ray scattering, proteins interaction

*e-mail: lubovmsu@mail.ru

Every living cell is a complicated adaptive system in which proteins and their molecular interactions are key factors. Taking into consideration the dynamic character of the system, it is important to understand how cells work in general, and to know functional relations between individual players participated in endless variations of responses to outer signals. For that it is necessary to study processes of cell metabolic regulation and interaction of different cellular components at functional level [1]. Inorganic pyrophosphatase (PPase) plays an important role in cell viability because its support of endergonic metabolic processes including biosynthesis of proteins and nucleic acids [2]. Therefore, PPase should be considered as a vital component of multiprotein complexes. Recently it has been shown [1] that PPase specifically interacts with such proteins expressed in E. coli as new type of fructose-1,6-bisphosphate aldolase (FbaB), cytoplasmic enzyme, which plays a crucial role in metabolic regulation [3]; 5-keto 4-deoxyuronate isomerase (KduI) involved in pectin degradation [4]; and glutamate decarboxylase (GadA) catalyzing the decarboxylation of glutamate to γ-aminobutyrate [5]. Study of interactions of these proteins could reveal new evidences on the PPase role in cell life cycle. In the present work for the first time PPase, its partner-proteins and their complexes in solutions at various concentrations were studied and characterized by small-angle X-ray scattering (SAXS) using synchrotron radiation on the P12 beamline at the PETRA III storage ring (DESY, Hamburg). On the basis of the experimental SAXS data, we calculated important structural parameters describing solution behavior of the specimens studied, and 3D models describing quaternary structure of the proteins and of their complexes in solution were offered. It was found that interactions took place in the presence of PPase, and complexes formed in solution comprised only some portion of the total amount of the proteins, being thus constantly in a dynamic equilibrium. A role of PPase in protein-protein interactions may consist in stabilization of its protein-partners preventing unfolding and consequent proteolytic degradation. Analysis of properties of the PPase partners shows that most of them are involved in stress response [1]. Thus, the results of our work provide new information on crucial role of PPase in metabolic regulation during processes like stress adaptation or “quorum sensing”.

[1] E.Rodina, N. Vorobieva, S. Kurilova, J. Mikulovich, J. Vainonen, E. M. Aro, T. Nazarova, *Biochimie* **93** (2011) 1576-1583.
[2] J. K. Heinonen, *Biological Role of Inorganic Pyrophosphate. Kluwer Academic Publishers, Boston,* 2001.
[3] E. Lorentzen, E. Pohl, P. Zwart, A. Stark, R. B. Russell, T. Knura, R. Hensel, B. Siebers, *J Biol Chem.* **278** (2003) 47253-47260.
[4] G. Condemine, J. Robert-Baudouy, *Mol. Microbiol.* **5** (1991) 2191-2202.
[5] G. Capitani, D. De Biase, C. Aurizi, H. Gut, F. Bossa, M. G. Grütter, *Embo J.* **22** (2003) 4027-4037.

O-11 **Wed. 18. 06., 16^{00}-16^{20}**

Speciation and distribution of phosphorus in environmental samples using the ID21 beamline, at the ESRF

C. Rivard[1]*, B. Lanson[2], C. Giguet-Covex[3], B. Kim[4], T. Jilbert[5] and M. Cotte[1,6]

[1]*European Synchrotron Radiation Facility, CS 40220, 38043 Grenoble Cedex 9, France*
[2]*Institut des Sciences de la Terre, Univ. Grenoble Alpes – CNRS, 38041 Grenoble, France*
[3]*EDYTEM, Univ. Savoie, CNRS Pole Montagne, 73376 Le Bourget du Lac, France*
[4]*INSA of Lyon, Univ. Lyon. LGCIE, 69621 Villeurbanne Cedex, France*
[5]*Faculty of Geosciences, Utrecht University, P.O Box 80.021, 3508 TA Utrecht, The Netherlands*
[6]*Laboratoire d'archéologie moléculaire et structurale, UMR 8220, CNRS, 75005 Paris, France*

Keywords: phosphorus, X-ray fluorescence, X-ray absorption spectroscopy

*e-mail: camille.rivard@esrf.fr

Phosphorus (P) is an essential nutrient for life, phosphates being elementary blocks of DNA, ATP and phospholipids. P is thus one of the main fertilizer inputs for agricultural soils. Excessive P inputs are nevertheless damaging for the environment as leaching of extra P directly increases the amount of P in natural aquatic systems, potential destabilizing the ecosystems. In this way, anthropogenic P present in domestic wastewaters or at a larger scale accumulated in coastal marine environments, has received increasing attention in recent years [1], [2].

P is present in many environments and also under numerous forms (dissolved, in the structure of minerals, organic, bound or adsorbed to mineral or organic substrates). Despite growing interest, the geochemical cycle of P is only partially understood.

ID21 (ESRF) [3] is a beamline dedicated to micro-X-ray fluorescence (μ-XRF) and micro-X-ray absorption spectroscopy (μ-XANES) in the tender X-ray domain (2-9.2 keV). The X-ray beam can be focused using KB mirrors to achieve a beam spot of about 0.4 x 0.6 (H x V) μm^2 with a flux of $4.5x10^9$ph/s at P K-edge (2.15 keV).

μ-XRF provides spatial P-distribution and elemental co-localization with a micron resolution. The shape of the P XANES spectra is characteristic of species or at least groups of species. In particular, inorganic-P, organic-P and adsorbed-P are easily distinguished from each other and minerals with structural P present unique P XANES features. The identification of P-bearing species is based on a comparison with XANES spectra recorded on references and the relative abundance of P-species in a mixture can be determined using linear combination fitting (Fig. 1).

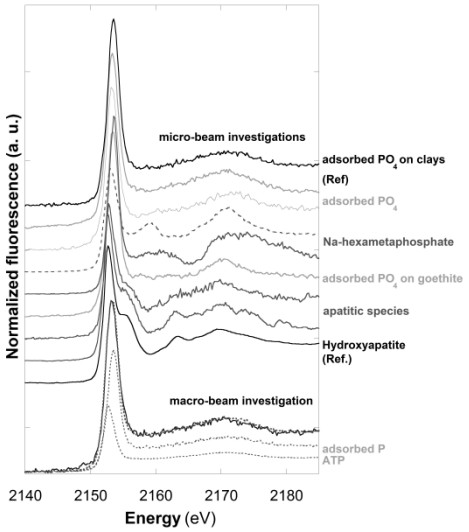

Figure 1. Phosphorus K-edge XANES spectra on soil samples. Bottom: Linear combination fit of a macro-beam spectrum. Top: μ-beam XANES spectra and comparison with references.

Here, the advantages, and the limits of μ-XANES for P speciation and distribution investigations will be discussed using a variety of examples from different aspects of the P geochemical cycle. A first example concerns soil genesis after the glacial retreat in mountain ecosystems, in which evidence is provided for an increase in P species diversity with time, due to pedogenetic processes [4]. The second example is related to agricultural soil samples and action of fertilizers. Analyses on undisturbed agricultural soil samples showed the predominance of adsorbed-P on organic matter together with the concentration of P in small hot spots (0.5-10 μm large), related to the presence of minor P species like apatite, polyphosphates or phosphates adsorbed on iron oxides (Fig. 1). A third set of experiments, conducted on sludges precipitated in sewage water treatment after $FeCl_3$ injection, aims at better understanding P removal mechanism through the determination of the P-bearing phases formed at different stages of the process. In the last example, P is investigated in Baltic Sea sediments to better understand marine burial of P. XRF maps evidenced the accumulation of P in biogenic stuctures and its association with Mn.

The use of complementary techniques like solid state NMR or XANES at the Fe, Mn or Ca edge can be applied to obtain a global view of the P species in a sample. μ-XANES is a useful tool in the field of Earth and Environmental Sciences, providing P spatial distribution and speciation and highlighting both major and minor phases.

[1] B. Kim *et al. Water Science and Technology* **68** (2013) 2257.
[1] T. Jilbert *et al. Biogeosciences* **8** (2011) 1699.
[2] M. Salomé *et al. J. Phys.: Conf. Ser.* **425** (2013) 182004.
[3] C. Giguet-Covex *et al. Geochim. Cosmochim. Acta* **118** (2013) 129.

O-12 **Wed. 18. 06., 16^{20}-16^{40}**

Laboratory laser-produced plasma source of soft X-rays for radiobiology studies

Daniel Adjei[1]*, Mesfin Getachew Ayele[1], Przemyslaw Wachulak[1], Andrzej Bartnik[1], Henryk Fiedorowicz[1], Inam Ul Ahad[1], Lukasz Wegrzynski[1], Anna Wiechecka[2], Janusz Lekki[2] and Wojciech M. Kwiatek[2]

[1]*Institute of Optoelectronics, Military University of Technology, 00-908 Warsaw, Poland*
[2]*Institute of Nuclear Physics PAN, Krakow, Poland*

Keywords: laser produced plasma, soft X-rays, radiobiology experiments

*e-mail: dadjei@wat.edu.pl

Various sources are used to investigate the effects of ionizing radiation on biological cells and tissue, including γ sources, heavy-ion accelerators, synchrotrons and laboratory scale X-ray sources [1, 2, 3]. It was demonstrated that micro-focus X-ray tubes delivering broadband radiation at energies up to 15 keV, or quasi-monochromatic radiation at 284 eV, 1.5 keV, 4.5 keV or 5.4 keV are highly useful for radiobiology studies [4, 5, 6]. However, this radiation is delivered to the sample at a low dose rate, and thus a relatively long irradiation time is needed to induce measurable biological effects. Higher dose rates can be achieved with laser-produced plasma light sources emitting high-intensity pulses of X-ray radiation. Application of a single-shot laser plasma X-ray source driven by a large scale laser facility in radiobiology studies has been demonstrated [7]. A laser plasma X-ray source driven with a femtosecond laser has been also used for this purpose [8].

In this paper a compact, desk-top laser plasma soft X-ray source developed for radiobiology research is presented. The source is based on a double-stream gas puff target irradiated with a commercial Nd:YAG laser generating laser pulses of 4 ns time duration and energy up to 800 mJ at 10 Hz operation rate (EKSPLA) [9]. The source has been optimized for maximum emission in the "water window" wavelength range from 2.3 nm to 4.4 nm by using proper gas (argon and argon/krypton mixture). Results of the source characterization measurements and dosimetry of the produced soft X-ray radiation are shown and discussed. It is expected that the source would have a unique capability for irradiation of cells with high pulse dose and dose rates without much robust X-ray optics. Investigations on irradiation of biological cells with the use of the source are planned.

Acknowledgements: The authors acknowledge the financial support from the EU FP7 Erasmus Mundus Joint Doctorate Programme EXTATIC under framework partnership agreement FPA-2012-0033.

[1] A. Facoetti, F. Ballarini, R.. Cherubini, S. Gerardi, R. Nano, A. Ottolenghi, K. M. Prise, K. R. Trott, C. Zilio, *Radiat. Prot. Dosim.* **122** (2006) 271.
[2] N. Usami, M. Maeda, K. Eguchi-Kasai, H. Maezawa, K. Kobayashi, *Radiat. Prot. Dosim.* **122** (2006) 307.
[3] M. Folkard, B. Vojnovic, S. Gilchrist, K.M. Prise, B. D. Michael, *Nucl. Inst. Met.s in Phys. Res. B* **210** (2003) 302.
[4] G. Schettino, M. Folkard, B. D. Michael, K. M. Prise, *Radiat.Res.* **163** (2005) 332.
[5] Y. Tanno, K. Kobayashi, M. Tatsuka, E. Gotoh, K. Takakra, *Radiat. Prot. Dosim.* **122** (2006) 301.
[6] M. Folkard, G. Schettino, B. Vojnovic, S. Gilchrist, A. G. Michette, S. J. Pfauntsch, K. M. Prise, B. D. Michael, *Radiat. Res.*, **156** (2001) 796.
[7] M. Davídková, L. Juha, M. Bittner, S. Koptyaev, V. Hájková, J. Krása, M. Pfeifer, V. Štísová, A. Bartnik, H. Fiedorowicz, J. Mikolajczyk, L. Ryc, L. Pína, M. Horváth, D. Babánková, J. Cihelka, S. Civiš, *Radiat. Res.* **168** (2007) 382.
[8] M. Nishikino, K. Sato, N. Hasegawa, M. Ishino, S. Ohshima, Y. Okano, T. Kawachi, H. Numasaki, T. Teshima, H. Nishimura, *The Review of Scientific Instruments*, **81** (2010) 026107.
[9] P. W. Wachulak, A. Bartnik, H. Fiedorowicz, P. Rudawski, R. Jarocki, J. Kostecki, M. Szczurek, *Nucl. Inst. Meth. Phys. Res. B* **268** (2010) 1692.

O-14 **Wed. 18. 06., 15^{20}-15^{40}**

Modification of magnetic properties of Pt/Co/Pt trilayer under nanosecond EUV irradiation

I.Sveklo[1]*, A.Bartnik[3], R.Sobierajski[2], E.Dynowska[2], J.Pelka[2], P.Dłużewski[2], A.Rogalev[4], A.Wawro[2], L.T.Baczewski[2], J.Kisielewski[1], P.Mazalski[1], Z.Kurant[1] and A.Maziewski[1]

[1]*University of Bialystok, Lipowa 41, Bialystok 15-424, Poland*
[2]*Institute of Physics, Polish Academy of Sciences, 02-668 Warszawa, Poland*
[3]*Institute of Optoelectronics, WAT, 00-908 Warszawa, Poland*
[4]*European Synchrotron Radiation Facility, Grenoble, France*

Keywords: EUV irradiation, perpendicular magnetic anisotropy

*e-mail: jo@uwb.edu.pl

Ion bombardment driven transition from perpendicular to in-plane magnetization state was investigated since fifteen years, see e.g. [1]. It has been lately shown [2,3] that 30 keV Ga+ ion irradiation can induce transitions from in-plane to out-of-plane state (PMA) of magnetic anisotropy in Pt/Co/Pt thin trilayers. Similar behavior has been very recently reported for femtosecond pulse laser irradiation in [4]. PMA creation we have also found by using extreme ultraviolet EUV pulses. The purpose of the current work is a study of relation between structural and magnetic changes in Pt/Co/Pt under EUV light irradiation and understand a mechanics of observed transitions.

Trilayers with a structure of (substrate-Al2O3(00.1))/(Pt(111) 5 nm)/(Co(00.1) 3 nm)/(Pt(111) 5 nm) were epitaxially grown with MBE technique in UHV conditions. As grown samples have smooth surface and in-plane magnetic anisotropy.

A laser-plasma extreme ultraviolet (EUV) source is based on a double-stream gas puff target created in a vacuum chamber synchronously with the pumping laser pulse [5]. The target is formed by pulsed injection of a Kr Xe gas mixture into a hollow stream of helium. The gas puff target is irradiated with 3ns Nd:YAG (λ=1.06 μm) laser pulses with energy of 0.8J and repetition rate of 10 Hz. The EUV radiation is focused using a grazing incidence gold-plated ellipsoidal collector. Spectrum of the reflected radiation consists of a narrow feature with intensity maximum at 10–11 nm wavelength and a long-wavelength spectral tail up to 70 nm. As a result this EUV source was capable to irradiate in vacuum a sample with single/multiple pulses with energy density up to 100 mJ/cm^2 and duration about 3 ns. Radial distribution of energy density σ(x) is shown in Figure 1.

After irradiation in vacuum with single EUV pulse we observed the appearance of spot with out-of-plane magnetization visible in remanence polar magneto-optical Kerr (PMOKE) images (Figure 2).

Bright black ring corresponds to PMA region, but inside spot magnetization is in-plane. Using calibration curve from Figure 1 we obtain that PMA state corresponds to irradiation energy density from 60 to 75 mJ/cm^2, but above this value magnetization returns to in-plane state.

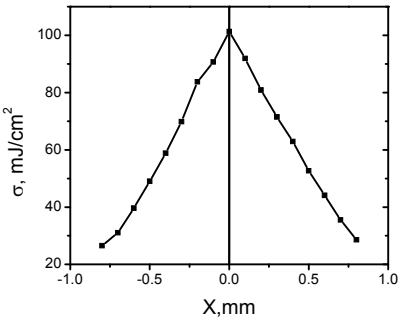

Figure 1. . Radial distribution of energy density for EUV source measured with pin-hole detector.

Detailed atomic force microscopy (AFM) imaging of the center of the irradiated stop revealed the appearance of micrometer range holes (Figure 3). These holes penetrate entire metallic trilayer down to substrate. The appearance of the holes in the metallic films under nanosecond laser pulses is explained with beginning of the film dewetting [6], i.e. transition of film to liquid state.

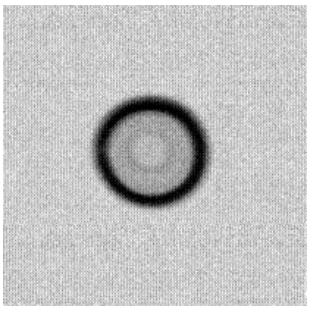

Figure 2. PMOKE remanence image of irradiated spot. Image size 2x2 mm^2.

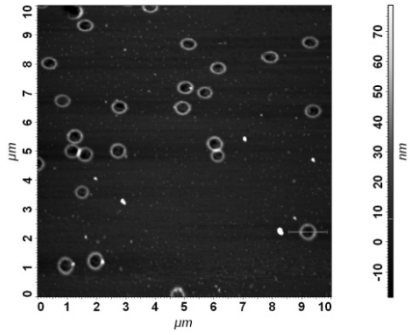

Figure 3. AFM image of the black interior inside irradiated spot.

Magnetic force microscopy (MFM) reveals tiny domain structure in irradiated spots. In Figure 4 we see MFM image at the boundary between in-plane central circle (left) and PMA ring (right). In PMA region the sizes of magnetic domain are about 2 μm and quickly reduced to zero for in-plane region. The transition is very sharp (order of 2 μm) while at outer boundary it is more then ten times blurred.

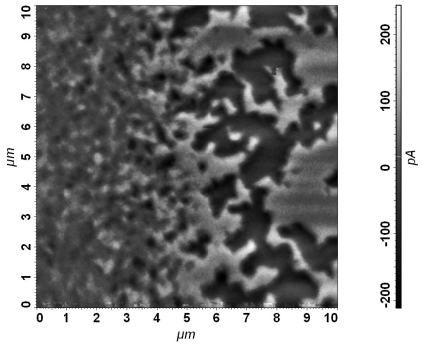

Figure 4. MFM image at the boundary of central black interior (left) and white ring (right).

Using PMOKE image processing techniques we have measured the dependence of magnetic parameters (maximal Kerr rotation, remanence, coercivity) as a functions of distance from the spot center. As an example, the dependence of Kerr rotation remanence $\theta_{REM}(r)$ is shown in Figure 5. The difference in sharpness of transition for internal boundary between MFM (Figure 4) can be attributing to the dithering of irradiation energy density on azimuth angle and averaging of PMOKE results for entire ring of constant radius.

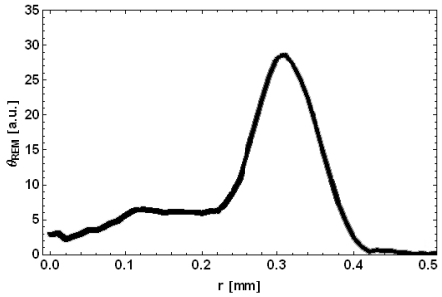

Figure 5. Radial dependence of Kerr rotation remanence θ_{REM}.

For structural XRD measurements we have prepared big sample (5x5 mm^2) with quasi-uniform (stop-by-spot) irradiation with a energy density corresponding to the PMA region. The appearance after irradiation of the strong diffraction peak can be considered as $Co_{0.5}Pt_{0.5}$ alloy formation. This alloy is chemically disordered because peaks of ordered alloy $L1_0$, $L1_2$ and etc. are not detected. High resolution transmission electron microscopy (HR-TEM) images of cross-section of irradiated trilayer reveal mixing Co/Pt (lack of mass contrast between Co and Pt layers) but atomic layer structure is still posses. So in such way created oriented cobalt platelets can induce PMA in similar way as it was observed in [6].

Summarizing, the increase of irradiation energy firstly lead to formation of Co-Pt alloy without lattice destruction. Such alloy has PMA due to the presence cobalt platelets which conserve initial orientation. With an increase of incident power above 75 mJ/cm^2 the Pt/Co/Pt trilayer begins to melt and after recrystallization it loses initial crystal lattice structure which is observed as rotation of magnetic anisotropy to in-plane state.

Acknowledgments: This work was supported by: NCN project HARMONIA Nr 2012/06/M/ST3/00475 and SYMPHONY project (Polish Science Team Programme, European Regional Development Fund, OPIE 2007–2013.

[1] H. Bernas editor, *Material Science with Ion Beams,Topics in Applied Physics*, Vol. 116 (Springer-Verlag, Berlin, 2010).
[2] J. Jaworowicz *et al., APL* **95** 022502 (2009).
[3] A. Maziewski *et al., Phys. Rev. B* **85** (2012) 054427.
[4] J. Kisielewski *et al., JAP* **115** 053906 (2014)
[5] A. Bartnik *et.al, Nuclear Instruments and Methods in Physics Research A* **647** (2011) 125.
[6] J. Bischof *et al. PRL* **77** (1996) 1536.
[7] J. O. Cross et al., *J. Phys.: Condens. Matter* **22** (2010) 146002.

O-15 **Wed. 18. 06., 15^{40}-16^{00}**

Spin state and satellite structures in Co and Fe based absorber materials and catalyst

D.Schmeißer[1]*, J.Haeberle[1], P.Brazda[2], M.Tallarida[1] and M.Richter[1]

[1]*BTU Cottbus-Senftenberg, Applied Physics and Sensors, Konrad-Wachsmann-Allee 17, 03046 Cottbus, Germany*
[2]*Inorganic Chemistry, Charles University in Prague, Czech Republic*

Keywords: synchrotron radiation, resonant photoelectron spectroscopy

*e-mail: dsch@tu-cottbus.de

We use resonant photoelectron spectroscopy at the Fe2p and the Co2p absorption edges to report on spectroscopic investigation of Co-oxides and Fe-oxides prepared by sol-gel, ALD, and as naoparticles (NP) [1]. α-Fe_2O_3 is commonly used as photocathode for water splitting for the hydrogen production [2]. On the other hand ε-Fe_2O_3 is of interest because of its magnetic properties [3]. Co-oxide as prepared as Co-Pi is a catalyst for the OER reaction [6, 7].

For both well-defined oxidic systems we analyze the electronic structure and determine the partial density of states for the valence and conduction bands. From these data we can derive a band scheme and compare it with recent band structure calculations [4] of the corresponding bulk phases.

The resPES data at the Fe2p and Co2p absorption edge spectra are analyzed to give evidence about the involved spin states in both phases. We find that for the ε-Fe_2O_3 the majority is due to $Fe3d^5$ HS state. Contributions of the corresponding LS state are small and are found to be higher for the α-Fe_2O_3 phase. In α-Fe_2O_3 prepared by ALD we identify in addition a LS $3d^6L$ state [5]. In Co-Pi we find a transition from Co^{2+} to Co^{3+} species depending on the catalysts film thickness. In addition we identify a $Co3d^7L$ CT state right at the Fermi energy. We attribute such an electronic constellation being favorable for a multiple charge transfer reaction.

[1] P. Brázda, D. Nižňanský, J.-L. Rehspringer, and J. P. Vejpravová, J Sol-Gel Sci Technol,51(1), **8** (2009).
[2] K. Sivula, F. Le Formal and M. Grätzel, ChemSusChem 2011, **4**, 432 .
[3] Gich M, Frontera C, Roig A, Taboada E, Molins E, Rechenberg HR, Ardisson JD, MacedoWAA, Ritter C, Hardy V, Sort J, Skumryev V, Nogues J (2006) Chem Mater 18:3889.
[4] Timo Jakob, private communication.
[5] K. Kukli, M. Chandra Dimri, A. Tamm, M. Kemell, T. Käämbre, M. Vehkamäki, M. Puttaswamy, R. Stern, I. Kuusik, A. Kikas, M. Tallarida, D. Schmeißer, M. Ritala, and M. Leskelä, ECS JSST 2 N45-N54 (2013).
[6] M.Richter, D.Schmeißer, ECS Transactions **50** (2013) 113.
[7] M.Richter, D.Schmeißer, *Applied Physics Letters* **102** (2013) 253904.

O-16 **Wed. 18. 06., 16^{00}-16^{20}**

Spectroscopic insights into nitrogenase structure

J. Kowalska[1]*, R. Bjornsson[1], F. A. Lima[1;2], T. Weyhermüller[1], O. Einsle[3], F. Neese[1] and S. DeBeer[1,4]

[1]*Max Planck Institute for Chemical Energy Conversion, Stiftstrasse 34-36, 45 470 Muelheim an der Ruhr, Germany*
[2]*Centro Nacional de Pesquisa em Energia e Materiais, Brazilian Synchrotron Light Laboratory, CP 6192, 13084 971 Campinas/SP, Brazil*
[3]*Albert-Ludwigs-Universität Freiburg, Albertstrasse 21, 79 104 Freiburg, Germany*
[4]*Cornell University, Ithaca, New York 14853, USA*

Keywords: nitrogenase, FeMoco, dinitrogen reduction, HERFD XAS, XMCD

*e-mail: Joanna.Kowalska@cec.mpg.de

The fundamental processes behind the making and breaking of chemical bonds are essential to nearly every facet of human lives. Inert dinitrogen from the atmosphere must be converted into a bioavailable form for incorporation into amino acids or/and DNA. The process of reducing dinitrogen to ammonia is also essential for producing fertilizers that feed the world's growing population. [1]

In nature, the conversion of dinitrogen (N_2) into ammonia (NH_3) is realized by the enzyme known as Mo-nitrogenase. Nitrogenase is a large protein containing an active multimetallic site (so called FeMoco) consisting of 1 molybdenum atom, 7 iron atoms, 9 sulphur atoms and a carbide in the middle (Figure 1). The central carbon was recently revealed by X-ray emission spectroscopy, X-ray crystallography and ESEEM. [2,3]

While the atomic composition of FeMoco is now complete, the left questions towards understanding the mechanism of dinitrogen reduction remain in the lacking of electronic structure like oxidation states and total charge of the cluster.

Recently, we have utilized high energy resolution fluorescence detected X-ray absorption spectroscopy (HERFD XAS) to evaluate the oxidation state of the Mo atom in this cluster. Based on this determination [4,5] and the proposed main oxidation state assignments we took similar approach to investigate Fe oxidation states in FeMoco. Although HERFD XAS allow spectra to be obtained at resolutions below the core hole lifetime broadening of the Fe 1s electron, the presence of 7 iron atoms and the lack magnetic information in such spectra, limits the information that can be deduced from such spectra. To overcome these limitations, we have applied X-ray Magnetic Circular Dichroism spectroscopy on series of Fe-Mo-S model complexes of FeMoco, allowing quantitative assessment of the obtained data.

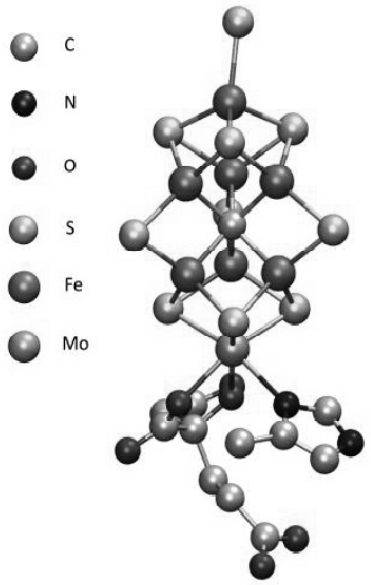

Figure 1. FeMoco cluster of nitrogenase [4].

Fe HERFD XAS and XMCD data on series of Fe-S and Mo-Fe-S model complexes ane FeMo cofactor will be presented. Based on both experimental data and theoretical calculations possible scenarios will be presented, as well as future directions towards understanding the structure and mechanism of nitrogenase.

Acknowledgments: This work was supported by Max Planck Society, European Synchrotron Radiation Facility (ESRF) and ERC Consolidator Grant.

[4] B. E. Smith, *Science* **297** (2002) 1654.
[1] K. M. Lancaster, M. Roemelt, P. Ettenhuber, Y. L. Hu. M. W. Ribbe, F. Nesse, U. Bergmann, O. Einsle, S. DeBeer, *Science* **334** (2011) 974.
[2] T. Spatzal, M. Aksoyoglu, L. Zhang, S. L. Andrade, E. Schleicher, S. Weber, D. C. Rees, O. Einsle, *Science* **334** (2011) 940.
[3] R. Bjornsson, F. A. Lima, T.Weyhermüller, P. Glatzel, T. Spatzal, O. Einsle, E. Bill, F. Neese, S. DeBeer, *Chem. Science* (2014) doi: 10.1039/C4SC00337C.
[4] F. A. Lima, R. Bjornsson, T. Weyhermüller, P. Chandrasekaran, P. Glatzel, F. Neese, S. DeBeer, *Phys. Chem. Chem. Phys.* **15** *(*2013) 20911.

O-17 **Wed. 18. 06., 16^{40}-17^{00}**

Energy converting interfaces studied by synchrotron radiation

C. Pettenkofer*

Helmholtz-Zentrum-Berlin
Albert-Einstein Str.15, 12489 Berlin, Germany

Keywords: synchrotron radiation

*e-mail: pettenkofer@helmholtz-berlin.de

The electronic and electrical properties of semiconductor hetero contacts depend crucially on the morphology of the contact plane. In particular thin film solar cells are dependent on well designed interfaces to allow for a favorable band alignment and a low density of defect states in the interface minimizing recombination losses. Chalcopyrite thin film cells had recently overcome the 20% efficiency barrier. Here we report on our attempts to model the junction in chalcopyrite thin films by well defined interfaces to clarify the influence of grain boundaries, lateral inhomogenities and chemical variations across and aside the contact plane. Chalcopyrites of the Type $CuInX_2$ (X = S, Se) were grown by MBE as single crystalline samples in various orientations and were studied by surface analytical tools like XPS, UPS, LEED, STM and XPEEM in situ. Especially the application of synchrotron radiation in photo emission experiments is an extremely powerful tool to gain insight into the morphology and structure of hetero contacts. In a deposition experiment the band alignment, band bending, chemical reacted interfaces and their crystalline structure are determined with high accuracy. By following the development of the contact phase to ZnO, ZnSe, ZnS step by step in an UHV environment, all properties of the interface are determined on an atomic scale with high resolution. Beside the formation of an ordered vacancy compound of the absorber the existence of various interfacial layers are detected and their influence on the parameters of a cell is discussed. By careful analysis of the obtained data new strategies to overcome i.e. the wet chemical processing of the absorber in CIGSE cells will be discussed.

For $CuInSe_2$ the appearance of a Cu poor interface layer is observed by SRXPS during the formation of the interface to ZnSe buffer layers. The development of Cu-poor surface phases was discussed by Zunger et al. and is here detected unambiguously.

To determine the band alignment valence band spectra have to be recorded to obtain the valence band onset. Here we will show that the correct value can only be obtained by using synchrotron radiation as the position of the valence band in k-space has to be determined at the Γ-point.

Further details on interface properties will be given by presenting XPEEM results on energy converting interfaces.

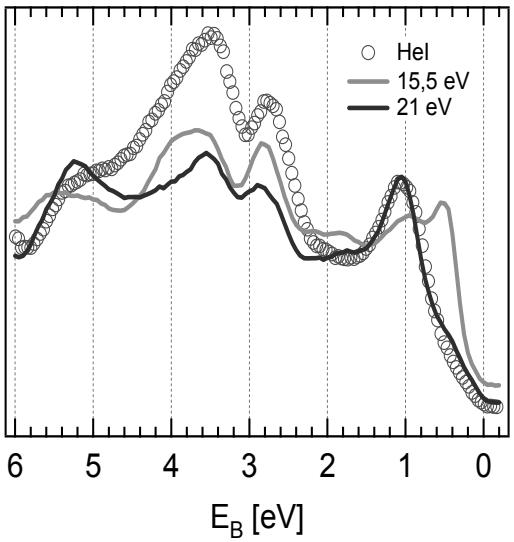

Figure 1. Valence band for $CuInSe_2$ (112) for different photon energies.

O-18 **Fri. 20. 06., 9^{40}-10^{00}**

First bending magnet beamline at Solaris

M. Zając[1]*, A. Bianco[2], C.J. Bocchetta[1], E. Busetto[2], P. Goryl[1], J. Korecki[3,4], M. Sikora[3,5], M.J. Stankiewicz[1], M. Ślęzak[3], A.I. Wawrzyniak[1] and Ł. Żytniak[1]

[1]*National Synchrotron Radiation Centre SOLARIS at Jagiellonian University, ul. Gołębia 24, 31-007 Kraków, Poland*
[2]*Synchrotron ELETTRA, Strada Statale 14, 34149 Basovizza, Trieste, Italy*
[3]*Faculty of Physics and Applied Computer Science, AGH University of Science and Technology, Al. Mickiewicza 30, 30-059 Kraków, Poland*
[4]*Jerzy Haber Institute of Catalysis and Surface Chemistry, Polish Academy of Sciences, ul. Niezapominajek 8, 30-239 Kraków, Poland*
[5]*Academic Centre of Materials and Nanotechnology, AGH University of Science and Technology, Al. Mickiewicza 30, 30-059 Kraków, Poland*

Keywords: synchrotron radiation, beamline, energy resolution.

*e-mail: mar.zajac@uj.edu.pl

The first bending magnet beamline built in the National Synchrotron Radiation Centre Solaris is optimized for the soft X-ray photon energy range 200-2000 eV. The calculated energy resolving power (E/ΔE) is of the order of 4000 or higher. The chosen optical design based on plane grating monochromator working in the collimated light has been studied by the Elettra group. The results of the final optical configuration ray-tracing and energy resolution calculations are presented. Additionally, detailed explanation of the purpose of each optical element is reported. The dimensions of the focalized beam at the end station, which will host a Photoemission Electron Microscope (PEEM), are 100μm (H) x 50μm (V). In the future additional refocusing device can be installed to increase the photon flux density on the sample for more demanding experiments. The actual time schedule and final design for the beamline component will be presented and discussed.

Within the framework between Jagiellonian University and Jerzy Haber Institute of Catalysis and Surface Chemistry PAS, the Photoemission Electron Microscope will be main end station of the first beamline. The PEEM was successfully tested at the Pollux beamline in the Swiss Light Source. Exchangeable with microscope we foresee to use separate chamber for X-ray absorption spectroscopy measurements. It will be dedicated to experiments in the field of biology, chemistry, catalysis, material science and physics. In the future, the spectroscopy chamber could be adapted to the other techniques like X-ray magnetic circular dichroism or scanning transmission X-ray microscope chamber.

Acknowledgments: Work supported by the European Regional Development Fund within the frame of the Innovative Economy Operational Program:
POIG.02.01.00-12-213/09.

O-19 **Fri. 20. 06., 10^{00}-10^{20}**

Single yoke double bend achromat of the MAX IV 1.5 GeV and Solaris storage rings

R. Nietubyć[1,2]* and M.A.G Johansson[3]

[1]*National Synchrotron Radiation Centre Solaris, Jagiellonian University, Czerwone Maki 98, 30-348 Kraków, Poland*
[2]*National Centre for Nuclear Research Świerk, Sołtana 7, 05-400 Otwock, Poland*
[3]*MAX IV Laboratory, Ole Römers väg 1, 223 63, Lund, Sweden*

Keywords: accelerator magnets, Max IV, Solaris

*e-mail: robert.nietubyc@maxlab.lu.se

The MAX IV and Solaris synchrotron radiation facilities being constructed in Lund, Sweden and in Krakow, Poland respectively benefit from cutting edge integrated magnet technology [1,2]. The rings, 96 m in circumference, are composed of 12 magnet blocks, that function as double bend achromats (DBA) and will permit storing a 1.5 GeV electron beam with 10^{-9} m·rad horisontal emittance [3]. The ring is an outstandingly gainful optimization between size and emittance, which satisfies demanding experimental requirements while saving space and costs.

Each of the 12 DBA units consists of 25 magnetic elements. One of two constituent bending dipoles will provide soft x-ray photons for experimental stations.

The integration of so many magnets into a single yoke structure, where they are aligned with a precision ranging down to 20 μm represents a challenging engineering task for the designers.

The current status of integrated magnets technology implementation in MAX IV 1.5 GeV and Solaris storage rings will be presented.

Acknowledgments: Work supported by the European Regional Development Fund within the frame of the Innovative Economy Operational Program: POIG.02.01.00-12-213/09. Authors would like to thank MAXIV team for all the support and know-how shared during the project.

[1] E.S. Reich, *Nature* **501** (2013)148-149.

[2] M. Johansson, "*Design of The MAX IV/Solaris 1.5 GeV Storage Ring Magnets*, WEPO016, Proc. IPAC2011, San Sebastian, Spain, pp. 2430 – 2432

[3] M.R. Bartosik et al.,"Solaris—National Synchrotron Radiation Centre, project progress, May2012", *Radiat. Phys. Chem.* **93** (2013) 4-8.

O-20 **Fri. 20. 06., 10^{20}-10^{40}**

Prospects of X-ray Photoemission Electron Microscopy at the first beamline of Polish synchrotron SOLARIS

M. Ślęzak[1]*, T. Giela[2], D. Wilgocka-Ślęzak[2], N. Spiridis[2], T. Ślęzak[1], A. Kozioł-Rachwał[1], M. Zając[3], M. Stankiewicz[3], N. Pilet[4], J. Raabe[4], C. Quitmann[4] and J. Korecki[1,2]

[1]*Faculty of Physics and Applied Computer Science, AGH, Kraków, Poland*
[2]*Jerzy Haber Institute of Catalysis and Surface Chemistry, PAN, Kraków, Poland*
[3]*National Synchrotron Radiation Centre SOLARIS, Jagiellonian University, Kraków, Poland*
[4]*Swiss Light Source, Paul Scherrer Institut, Switzerland*

Keywords: synchrotron facility Solaris, soft X-ray micro-spectroscopy beamline, electron microscopy, XPEEM

*e-mail: mislezak@agh.edu.pl

The first Polish synchrotron radiation facility "Solaris" is currently being built in Krakow [1]. The first experimental beamline at "Solaris" will use bending magnet radiation and two exchangeable end-stations: a spectroscopic X-ray photoemission electron microscope (SPE-XPEEM) and a soft X-ray absorption spectroscopy (XAS) chamber. In this contribution we present the beamline specification and exemplary results obtained with our end-station microscope, which (in the status nascendi of "Solaris") has been operated at the NanoXAS beamline in Swiss Light Source (SLS). The end-stations should be available for broad users community at "Solaris" in 2015/2016.

The SPE-XPEEM instrument, equipped with the energy analyzer, can also work in the Low Energy Electron Microscopy (LEEM) mode, which expands its application field also to structural surface studies. A preparation chamber is attached to the microscope, which enables in situ MBE growth and characterization of metal and oxide surfaces, films and nanostructures. Most of the X-PEEM [2] capabilities including imaging with chemical and magnetic [3] sensitivity given by XAS, X-ray photoemission spectroscopy and magnetic dichroism (XMCD and XMLD) could be tested and verified. The full-field spectro-microscopy and micro-spectroscopy including broad range of elements and their chemical as well as magnetic states will be demonstrated for in situ and ex situ prepared surface nanostructures.

The best spatial resolution of approximately 15 nm is demonstrated in Fig.1 where secondary electrons XPEEM image of self-organised Fe stripes prepared on a W(110) single crystal is shown.

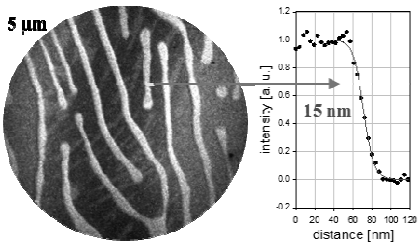

Figure 1. XPEEM images of Fe stripes on a W(110) single crystal at the Fe L3 edge. The intensity profile across an Fe stripe demonstrates the spatial resolution of 15 nm.

The XPEEM micro-spectroscopic capabilities can be best exploited for multicomponent or structured samples, such as multilayers and wedge-shaped samples used for thickness dependent studies. An example of such a sample is an epitaxial Fe/Au/Co structure grown on W(110). The base 200 Å Fe(110) layer is followed by a (111)-oriented 7 Å Au film. Using a shutter in front of the tungsten crystal, a part of the sample was covered with 20 Å of cobalt. In this manner, at the border between the Fe/Au bilayer and the exchange coupled Fe/Au/Co trilayer, a Co microwedge was formed with a thickness ranging from 0 to 10 ML, as determined by the quartz microbalance. In Fig. 2a, an image of the Co microwedge area is presented, which was obtained as a difference between two images: the first one taken at the L3 edge of Co and the second one at the pre-edge energy (i.e., 10 eV below). The intensity changes across the image, from the dark area, without cobalt, to the bright area, where the Co thickness saturates at 10 ML, can be quantitatively examined by analysing the local XAS spectra. The XAS spectra for the Fe/Au and Fe/Au/Co areas are presented in Fig. 2b as A and B, respectively.

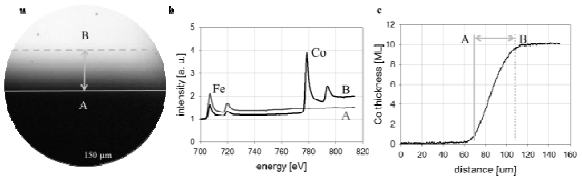

Figure 2. (a) Differential image of Co distribution in a microwedge and the surrounding area of the sandwiched Fe/Au/Co sample described in the text. The FOV was 150 µm. (b) XAS spectra taken at positions A and B. (c) The L3 Co intensity profile across the Co microwedge. The vertical lines refer to the corresponding lines in (a). The Co thickness scale is derived within the linear thickness – intensity relation.

The intensity profile (Fig. 2c) demonstrates that the thickness of the Co layer can be precisely determined at a given position on the sample.

Another exemplary result is shown in Fig.3, where both chemical an magnetic sensitivity is exploited to image the magnetic domain structure in Fe/Au/Co trilayers grown in situ on W(110).

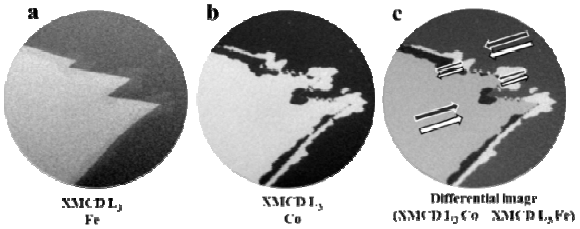

Figure 3. Magnetic domains structures in Fe/Au/Co trilayers grown on W(110) as seen by XMCD-PEEM. Arrows indicate relative magnetization alignment of Fe and Co layers.

Magnetic domain structures were imaged for both magnetic sublayers by tuning the L3 absorption edges of Fe (Fig. 3a) and Co (Fig. 3b). Inside the domains, the magnetisation direction of Fe is reflected in the Co layer – the Fe and Co layers are ferromagnetically coupled. At the domain borders, a secondary domain structure is observed with antiparallel Co and Fe magnetisation alignment, as shown schematically by arrows in the Fig. 3c. This secondary structure can be better visualised based on the image obtained as a difference between the Fe and Co XMCD images (Fig. 3c).

The set of images presented in Fig. 4 shows the evolution of the magnetic structure during the thickness-induced in-plane spin reorientation transition (SRT) in Fe/W(110) [3]. All the XPEEM images presented in

Fig. 4 are the single frames from a movie recorded during the growth of the Fe film at the Fe L_3 edge for the circularly polarised photons.

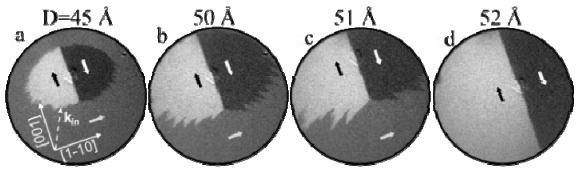

Figure 4. In-plane thickness-induced SRT in Fe/W(110) observed using XPEEM with circularly polarised X-rays at the Fe L3 edge. The FOV was 150 μm.

For all images (frames) in Fig. 4 the exposure time was only 0.2 s. It demonstrates the usefulness of the XPEEM technique for studying slowly varying physical processes in real time.

Acknowledgments: This work was supported by EU European Regional Development Fund and by the Scientific Exchange Programme NMS-CH (SCIEX) project.

[1] M. R. Bartosik *et al., Radiat. Phys. Chem.* **93** (2013) 4-8.
[2] A. Locatelli, E. Bauer, *J. Phys.: Condens. Matter* **20** (2008) 093002.
[3] M. Ślęzak et al., Journal of Magnetism and Magnetic Materials **348** (2013) 101.

O-21 **Fri. 20. 06., 11^{10}-11^{30}**

Synchrogrid: IT services for Polish Synchrotron operators and users

T. Szymocha[1]*, M. Stankiewicz[2], A. Wawrzyniak[2], P. Goryl[2], M. Zając[2], M. Nowak[2], Ł. Żytniak[2] and F. Melka[2]

[1]*AGH University of Science and Technology, ACC CYFRONET AGH, Nawojki 11, 30-950 Kraków, Poland*
[2]*National Synchrotron Radiation Center Solaris, Gronostajowa 7, P. 1-6, Kraków, Poland*

Keywords: synchrotron, IT services

*e-mail: tadeusz.szymocha@cyfronet.pl

Building and bringing into operations the National Synchrotron Radiation Centre „Solaris" is a engineering and organizational challenge. Apart from support of construction work, support for its operations is needed. The operations require not only qualified personnel, but also appropriate IT solutions for its support.

High Performance Computing centers in Poland founded consortium, which main aim is to support polish science with IT solutions in close collaboration with users. The consortium built IT infrastructure, that provides scientists computing and storage. The next step is building services dedicated to scientific domains services. One of identified groups are the synchrotron radiation users.

As the Solaris is in installation phase and will start commissioning soon, services developed so far only indirectly support end users of synchrotron radiation [1]. These services are facilitating everyday operations of Synchrotron by supporting beam scientists and operators with virtual model of the synchrotron for testing synchrotron control software on the computing model [2]

The main need of synchrotron operators and users in first phase of production operation was identified to be storage and management of the data. The PL-Grid infrastructure user will be allowed to store the data from experiment and execute analysis software placed in user area. Additionally, user can use number of scientific applications like Matlab that are available on infrastructure [3].

Acknowledgments: This research was supported in part by PL-Grid Infrastructure.

[1] T. Szymocha et all., *Services for Synchrotron Deployment and Operation* In: Bubak, M., Kitowski, J., Wiatr, K. (eds.) eScience on Distributed Computing Infrastructure, Achievements of PLGrid Plus. LNCS, vol. 8500, Springer (accepted)

[2] P. Goryl, et al; "An implementation of the virtual accelerator in the Tango control system"; MOSB3; Proceedings of the ICAP2012, Rostock-Warnemünde, Germany (2012)

[3] PL-Grid infrastructure webpage: http://www.plgrid.pl/oferta

P-01

UARPES -Angle Resolved Photoelectron Spectroscopy beamline at National Synchrotron Radiation Centre SOLARIS

J.J. Kolodziej[1,2]* and K. Szamota-Leandersson[2]

[1]*Faculty of Physics, Astronomy and Applied Computer Science, Jagiellonian University, Kraków, Poland*
[2]*National Synchrotron Radiation Centre SOLARIS, Krakow, Poland*

Keywords: angle resolved photoelectron spectroscopy, synchrotron radiation, synchrotron facilities

*e-mail: jj.kolodziej@uj.edu.pl

The Angle Resolved Photoelectron Spectroscopy (ARPES) allows for measurements of fundamental quantities describing the electron state in space, i.e. the energy (E) and the momentum (k). Additionally, if the spin selector is used, a complete set of quantum numbers for electron in space may be obtained. Within a so called sudden approximation the electron energy, momentum and spin measured over the sample surface may be related, to binding energy, quasimomentum, and spin, that the electron had in the solid before the photoelectric event took place. Thus a complete image of the electronic band structure of the studied solid is obtained experimentally. Beside this simple picture ARPES gives also detailed insights into complex electron – electron and electron – lattice interactions in the solid.

Nowadays there are hopes that advanced techologies, conserving natural resources (e.g. for energy production and supply) may be developed based on new materials and devices. The key for advances here will be likely found in the knowledge about the electronic structure of complex systems. This point of view is well illustrated by recent developments of knowledge with reference to collossal magnetoresistance, high temperature superconductivity, topological insulators as well as to many other interesting phenomena [1-13]. A lot of these developments have been enabled by ARPES studies.

The importance of ARPES technique for contemporary science and technology is widely recognized. Dedicated ARPES beamlines exist at almost all synchrotron radiation centers worldwide. Typically, for these beamlines, the demanded beamtime many times surpasses the offered one. Based on these considerations it is predicted that the high demand for ARPES studies will continue in future.

To meet this expected demand a beamline dedicated for Angle Resolved Photoelectron Spectroscopy will be constructed as one of the first at SOLARIS synchrotron facility. We have proposed the acronym UARPES (Ultra ARPES) as the name for this research installation.

The UARPES beamline is being designed to have the following performance:
energy range of 8-100 eV,
resolving power ≥ 20 000 over the full energy range,
ph. flux on the sample≥5x10^{11} photons/s @20000 RP,
available polarizations: linear: vertical, horizontal, inclined; circular; elliptical,
higher harmonics at the sample position < 1%,
excited spot size on the sample < 500 x 500 μm^2

Elliptically polarizing, APPLE-II type undulator is chosen as a light source. The undulator will have quasi-periodic geometry for suppression of unwanted harmonics in its radiation spectrum. It will be capable of both parallel and antiparallel modes of operation ensuring the full control over the light polarization.

The monochromator will be combining normal (NIM) and grazing incidence (PGM) optics, similarly to recent implementation at SLS [14]. The NIM mode is helpful for additional harmonics rejection, where they are particularly abundant, i.e. at the lowest photon energies. Thus the NIM mode will be used in the energy range 8 – 30 eV while the PGM mode will be used in the energy range 25 – 100 eV.

The experimental endstation will be composed of several ultrahigh vacuum chambers designed for sample processing and analysis, as well as for storage and transfer. Cryogenic, 5-axes manipulator will be capable of stabilizing the sample temperature in the range 10 – 500 K, as well as of precise positioning of the sample surface for experiments. State-of-the-art electron energy spectrometer, having energetic resolution down to 1 meV, will be capable of massively parallell recording of angle-resolved data. Advanced automation will make possible remote ARPES experimentation. Low energy electron diffractometer, with MCP image amplifier, will be available for surface structure studies. Sample processing devices will allow for typical in situ preparation techniques such as sputter cleaning, thermal annealing, thin film growth, sample cleaving, surface reactions in the gas phase.

[1] A. Damascelli, *et al., Rev. Mod. Phys.* **75** (2003) 473.
[2] J. C. Campuzano *et al., Phys. of Supercond.* **2** (2003) 167.
[3] M. A. Hossain *et al., Nature* **425** (2008) 527.
[4] V. B. Zabolotnyy *et al., Phys. Rev. B* **76** (2007) 064519.
[5] T. Nakagawa, *et al., Phys. Rev. Lett.* **86** (2001) 854.
[6] F. Schiller, *et al., Phys. Rev. Lett*. **93** (2004).
[7] Y. Kamihara, *et al., J. Am. Chem. Soc*. 130 (2008) 3296.
[8] G. Grüner, "*Density Waves in Solids*", Addison-Wesley, Reading, MA, USA, 1994.
[9] T. Aruga, *J. Phys. Cond. Mat*. **14** (2002) 8393; *Surf. Sci. Rep.* **61** (2006) 283; F. Gebhard, "*The Mott metal-insulator transition*" (Springer, 1997)
[10] T. Giamarchi, *Chem. Rev.* **104** (2004) 5037.
[11] V. I. Anisimov *et al. J. Phys. Cond. Mat*. **9** (1997) 7359; A. Yamasaki *et al.* Phys. *Rev. Lett*. **96** (2006) 166401.
[12] K. Haule *et al. Phys. Rev. Lett*. **94** (2005) 036401; S. Y. Savrasov *et al. Nature* **410** (2001) 703.
[13] Oshima *et al., International Journal of Modern Physics B* **16** (2002) 1681-1690.
[14] U. Flechsig, *et al., Nucl. Instr. Meth. A* **467** (2001) 479.

P-02

Shape reconstruction of nanoparticles in clusters using SAXS data

D. I. Chekrygina*, V. V. Volkov and E. V. Shtykova

A.V.Shubnikov Institute of Crystallography, RAS, Leninsky pr., 59, 119333, Moscow, Russia

Keywords: small-angle x-ray scattering; shape determination, structure modeling

*e-mail: denizamsu@gmail.com

The level of structural information that can be obtained from small angle X-ray scattering (SAXS) data generally is determined by the nature of the scattering objects. For monodisperse systems of identical particles SAXS intensity is directly related to the structure and provides the unique opportunity to determine their shape and size, and in some cases, the internal structure with resolution of about 1 nm. However, in practice, the samples may contain some amount of aggregates or clusters, which cannot be removed from the specimens by conventional methods of purification due to association effects which are essential features and functional properties of some biomacromolecules. Thus, to reveal a structure of individual scattering objects in the associates and to determine their mutual packing within the clusters is of great practical interest. In the present work a large series of computer simulations was made to reconstruct structures of clusters composed of geometrical bodies ("monomers") different in size, shape and mutual arrangement. The task was complicated by certain polydispersity of the associates. *Ab initio* low resolution shape restoration of the "monomers" and of the clusters was performed by a program DAMMIN based on the simulated annealing minimization procedure [1]. Shape of the "monomers" was chosen using information about actual problems arising in structural studies of proteins due to their properties of inherent self-assembly. As a result of the modeling conclusions on the certain limitations and applicability of the shape restoration of macromolecules within clusters were made.

[1] D. I. Svergun, *Biophys. J.* **76** (1999) 2879-2886.

P-03

Interaction of selected gemini surfactants with two model proteins: BSA and HEWL

W. Gospodarczyk* and M. Kozak

Department of Macromolecular Physics, Faculty of Physics, Adam Mickiewicz University, Umultowska 85, 61-614 Poznań, Poland

Keywords: protein-surfactant interaction, gemini surfactants

*e-mail: 1kamien@amu.edu.pl

The protein-surfactant interactions has been examined over a few past decades, as this problem is vitally important due to its prospective applications of surfactants in medicine, biotechnology, food industry and many others. Proteins bind various substances, giving complexes. The research on protein-surfactant interactions can help to understand the influence of surfactants on processes of denaturation, solubilization and renaturation of proteins. Another fundamental process set under researchers scrutiny is protein aggregation, underlying numerous severe human neurodegenerative diseases and being often considered as undesired effect in biotechnology.

Gemini surfactants is a group of novel and very interesting surfactants. The gemini molecules consist of two polar heads interconnected via a spacer group and bound to two hydrophobic chains. They exhibit very low critical micellization concentrations (cmc), a diversity of forms, making their properties easily adjustable, and they can assemble into micelle-like structures similar to biological membranes.

Bovine serum albumin (BSA) is an important transport protein binding various ligands, including fatty acids and metals. Hen egg white lysozyme (HEWL), on the other hand, is a well-known model protein for studies of aggregation phenomena.

The investigation of interaction of BSA and HEWL with gemini surfactants has been carried out with use of three different techniques: small angle X-ray scattering (SAXS), circular dichroism (CD) and nuclear magnetic resonance diffusiometry (NMRD). Its results will be presented at the conference.

Acknowledgments: The research was supported by research grant (UMO-2011/01/B/ST5/00846) from National Science Centre (Poland).

P-04

The SAXS studies of complexation dicationic gemini surfactants with low molecular nucleic acids DNA and siRNA

W. Andrzejewska*, M. Skupin and M. Kozak

Department of Macromolecular Physics, Faculty of Physics, A. Mickiewicz University, ul.Umultowska 85, 61-614 Poznań, Poland

Keywords: gemini surfactants, DNA, siRNA, gene therapy

*email: andrzejewskaw@gmail.com

Specific physico-chemical properties of dicationic (gemini) surfactants are the reason for a broad their use in studies as delivery systems of therapeutic molecules (i.e. nucleic acids) into cells. To support the cell transfection process, the carrier molecules must connect with a therapeutic molecules and form stable complexes [1,2]. Due to the self-assembly process, in solution complexes between nucleic acids and gemini surfactants are organized in different structural forms, such as for example: lamellaes, micells or hexagonal phase.

Very promising method to study of such systems is small angle scattering of synchrotron radiation (SAXS). This method is able to demonstrate structural changes occur within the studied delivery systems [3,4].

The presented here experimental results concern the structural analysis (SR-SAXS) of mixtures of bis(1-dodecyl imidazole) derivatives with low molecular DNA and RNA. The presence of characteristic diffraction peaks (see Figure 1) indicates probable formation of cubic and hexagonal phases in the studied solutions.

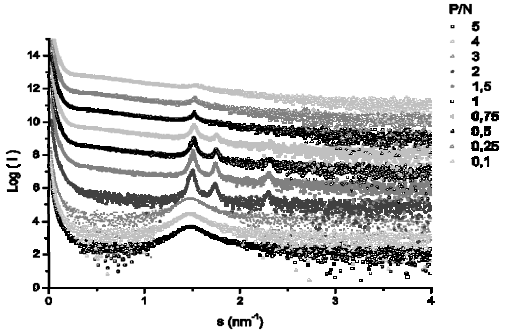

Figure 1.

Acknowledgments: *The research was supported by research grant (UMO-2011/01/B/ST5/00846) from National Science Centre (Poland).*

[1] S. Szala (red.), Gene therapy, *PWN*, 2003, Warszawa.
[2] R. Zieliński, *Surfactants. sructure, properties, applications* (WUP, 2009, Poznań)
[3] Z. Pietralik, R. Krzysztoń, W. Kida, W. Andrzejewska and M. Kozak, *Int. J. Mol. Sci.* **14 (**2013) 7642-7659.
[4] Ch. Wang, X. Li, D. Wettig, I. Badea, M. Foldvarid, R. E. Verrall, *Phys. Chem. Chem. Phys.* **9** (2007) 1616-1628.

P-05

SAXS studies of zwitterionic lipoplexes – nanosystem based on phospholipids and surfactants as innovative delivery systems for gene therapy

P. Egierska, M. Skupin*, B. Urban*, J. Wolak, W. Andrzejewska, Z. Pietralik and M. Kozak

Departament of Molecular Physics, Faculty of Physics, Adam Mickiewicz University, 85b, Umultowska, 61-614 Poznań, Poland

Keywords: small angle scattering of synchrotron radiation, gene therapy, sulfobetaine derivatives

*misiaskupin@gmail.com ;*barbaraurban2@gmail.com

In the recent years there has been a number of technological breakthroughs that have allowed clinical trials in gene therapy [1]. Progress in molecular medicine, especially discovering new routes and methods for gene delivery has provided promising means of treatment of genetic disorders and cancers. Development of effective gene carriers which can increase specificity of targeting and decrease harmfulness to adjacent healthy tissues is very important. Suitable for this purpose are thought to be delivery nanosystems based on lipid-surfactant mixtures [2]. The aim of this study was to determine the possibility to use amphoteric surfactants (zwitterionic alkyl derivatives of sulfobetaine [3]) as complexing agents for nucleic acids, with potential applications for gene delivery [4]. A series of the small angle scattering of synchrotron radiation (SR-SAXS) measurements was performed on selected lipoplexes based on short DNA duplex (21 bp) and zwitterionic surfactants.

The poster presents the structural analysis of these DNA/zwitterionic surfactant systems on the basis of scattering data. The SAXS data for selected DNA/zwitterionic surfactant systems were collected P12 beam line of EMBL Hamburg Outstation on PETRA III storage ring at DESY. The measurements were performed on solutions in 10 mM sodium phosphate pH 7.5 with different DNA/surfactant molar ratio.

Acknowledgments: The study was supported by research grant „GENERACJA PRZYSZŁOŚCI" from Ministry of Science and Higher Education (Poland) – decision: 12/POIG/GP/2013.

[1] S. Mali, *Indian J. Hum. Genet.* **19(1)** (2013) 3-8.
[2] N. L. Slack, A. Ahmad, H. M. Evans, A. J. Lin, C. E. Samuel, C.R. Safinya, *Curr. Med. Chem.* **11** (2004) 133.
[3] M. Kozak, K. Szpotkowski, A. Kozak, R. Zieliński, D. Wieczorek, M. J. Gajda, *Rad. Phys. Chem.* **78** (2009) S112.
[4] N. Dan, *Biophys. J.* **73** (1997) 1842.

P-06

Low resolution solution structure of the HSP90:SGT1 complex from the Small-Angle X-ray Scattering

M. Taube[1]*, A. Jarmołowski[2] and M. Kozak[1]

[1]*Adam Mickiewicz University, Faculty of Physics, Department of Macromolecular Physics, Umultowska 85, 61-614 Poznań, Poland*
[2]*Adam Mickiewicz University, Faculty of Biology, Department of Gene Expression, Umultowska 89, 61-614 Poznań, Poland*

Keywords: synchrotron radiation, small angle X-ray scattering, molecular chaperons

*e-mail: mtaube@amu.edu.pl

Heat Shock Protein 90 kDa (HSP90) is a molecular chaperon that is involved in protein folding and maturation [1,2]. It is conserved across species and in higher organisms exist in multiple isoforms that are differentially regulated or have distinct cellular localization. HSP90 plays important role during heat shock and other stress conditions but is also engaged in maintaining protein homeostasis during normal growth of the cell. In contrast to other heat shock proteins HSP90 binds to the partially folded client proteins and interacts with many co-chaperones that modulate HSP90 cycle through inhibition/activation of its ATPase activity. Moreover some co-chaperones are specific for one class of client proteins like for example kinases or innate immunity receptors. Briefly, co-chaperone cycle of Hsp90 is as follows [2]: partially folded protein is transported to the HSP90 from the HSP40/HSP70 protein complex by the binding to the HOP protein. At the same time HSP90 dimer binds two ATP molecules. Subsequently Peptidyl-Proly Isomerase (PPIase) binds to the HSP90/HOP/ATP/client protein complex and next AHA1 protein displaces HOP from HSP90 complex and stimulates formation of closed N-terminal dimerized conformation of HSP90. After N-terminal dimerisation, p23 binds and displaces from the complex AHA1 and stabilizes the closed conformation. After ATP hydrolysis PPIase, p23 and mature client protein is released.

HSP90 is composed of three structural domains: N-terminal domain (NTD) responsible for nucleotide binding and its hydrolysis, middle domain (MD) that plays role in ATP hydrolysis and is involved in the protein substrate binding and C-terminal domain (CTD) which is responsible for constitutive dimer formation. In solution HSP90 exists in equilibrium between open "apo-like" conformation and closed "nucleotide bound-like" conformations in the absence and in complex with ATP [3]. In addition in electron microscopy experiments, distinct, ADP bound compact conformation could be observed. Conformational equilibrium can be changed by the increased concentration of osmolites and pH. Equilibrium is also species dependent. In bacteria HSP90 homolog exists as a mixture of open and closed states as opposed to the human homolog which exists mainly in open conformation and closed state could be observed in electron microscopy after cross-linking.

Suppressor of G2 allele of SKP1 (SGT1) protein is HSP90 co-chaperone and its also conserved across species. SGT1 protein plays important role in innate immunity in both plants and animals. It is required for proper function and stability of nucleotide binding leucine-rich repeats (NB-LRR) class of cytosolic receptors that recognizes pathogenic molecules inside the cell and triggers immune response [4,5]. Sgt1 consists of three domains N-terminal TPR domain required for dimerisation, middle CS domain that interacts with HSP90 and RAR1, SGS domain required for association with R proteins.

In this study we investigated complex formation between truncated SGT1 protein (without SGS domain) from barley and HSP90 protein from wheat in the presence of ADP. Using MCR-ALS method and series of SAXS experimental data for the SGT1-TPR-CS, HSP90 and complex at various stoichiometries we extracted pure scattering curve for the complex. Unexpectedly, comparison of molecular weight obtained from SAXS revealed presence of putative 2:1 HSP90:SGT1 complex. Our results are unexpected because each HSP90 monomer possesses one binding site for CS domain of SGT1. Moreover HSP90 in complex with SGT1 exists in open conformation so there is no interaction between HSP90 monomers that could disrupt SGT1 binding.

Acknowledgments: This work was supported in part by grant 2012/05/N/ST3/03087 from the Polish Ministry of Science and Higher Education.

[1] M. Taipale, D.F. Jarosz, S.Lindquist S. *Nat Rev Mol Cell Biol.* **11** (2010) 515-528.
[2] A. Röhl, J. Rohrberg, J. Buchner. *Trends Biochem Sci.* **38** (2013) 253-262.
[3] [3] K.A. Krukenberg, T.O. Street, L.A. Lavery, D. A. Agard, *Q Rev Biophys.* **44** (2011) 229-255.
[4] Y.Kadota, K. Shirasu. *Biochim Biophys Acta.* **1823** (2012) 689-697.
[5] Y. Kadota, K. Shirasu, R. Guerois. *Trends Biochem Sci.* **35** (2010) 199-207.

P-07

Gemini surfactant as effective agents for delivery of nucleic acids

Ż. Kołodziejska*[1], Z. Pietralik*[1], M. Weiss[2] and M. Kozak[1]

[1]*Department of Macromolecular Physics, Faculty of Physics, Adam Mickiewicz University, Umultowska 85, 61-614 Poznań, Poland*
[2] *Solid State Spectroscopy Division, Faculty of Technical Physics, Poznań University of Technology, Nieszawska 13a, 60-965 Poznań, Poland*

Keywords: gene therapy, gemini surfactant, lipoplex, SAXS, CD, AFM

*e-mail: zan.ka@amu.edu.pl, zuzannap@amu.edu.pl

To be considered for medical applications, the drug delivery systems should be effective and nontoxic. Conventionally, such systems are comprised of therapeutic substances (drug molecules, proteins, genes) encapsulated within a carrier. When dealing with genes, many macromolecules like viruses, polymers and lipids have already been tested as potential carriers, but recently, due to their advantages like increased surface activity or reduced toxicity, a diverse group of gemini surfactants turned up to be a promising type of carriers for nonviral gene delivery systems [1-3].

This study was performed on mixed systems, composed of DNA and gemini surfactants, namely alcoxyderivatives of bis-imidazolium quaternary salts with different length of hydrophobic side-chains. Their ability to bind nucleic acids was tested on three types of DNA with different sizes, i.e. 21 bp, 200 bp and 20 kbp.

The synchrotron radiation small angle X-ray scattering (SAXS) measurements were performed in DESY, Beam Line X33 (EMBL Outstation Hamburg, Germany) [4]. To gain additional structural information, the atomic force microscopy and circular dichroism spectroscopy were also applied.

Results of structural studies have allowed us to assess the connection between the geometry of gemini surfactant, composition of binary systems and formed nanostructures.

Acknowledgments: This work was supported by research grant (UMO-2011/01/B/ST5/00846) from National Science Centre (Poland).

[1] V. D. Sharma, M. A. Ilies. *Med Res Rev.*, **20** (2012) 1-44.
[2] L. Wasungu, M. C. Stuart, M. Scarzello, J. B. Engberts, D. Hoekstra. *Biochim Biophys Acta.* **1758** (2006) 1677-1684.
[3] L. Karlsson, M. C. van Eijk, O. Soderman. *J. Colloid Interface Sci.* **252** (2002) 290-296.
[4] M.W. Roessle, R. Klaering, U. Ristau, B. Robrahn, D. Jahn, T. Gehrmann, P. Konarev, A. Round, S. Fiedler, C. Hermes, D. Svergun. *J. Appl. Crystallogr.* **40** (2007) 190-194.

P-08

Novel nanocomposites created by $Cu(hfa)_2$ and $Co_2(CO)_8$ via Focused-Electron-Beam-Induced-Deposition

A. Szkudlarek[1]*, W. Szmyt[2], Cz. Kapusta[2] and I. Utke[3]

[1]*AGH University of Science and Technology Academic Centre for Materials and Nanotechnology al. A. Mickiewicza 3030-059 Krakow, Poland*
[2]*AGH University of Science and Technology, Faculty of Physics and Applied Computer Science, Department of Solid State Physics, al. Mickiewicza 30, 30-059 Krakow, Poland*
[3]*Laboratory for Mechanics of Materials and Nanostructures, Empa, Feuerwerkerstrasse 39, 3602 Thun, Switzerland*

Keywords: nanocomposites, electron beam deposition

*e-mail: aleszkud@agh.edu.pl

The new type of materials containing nanocrystals of Co and Cu have been fabricated via Focused-Electron-Beam-Induced-Deposition (FEBID). In this method the precursor gas molecules are introduced into the electron microscope chamber by Gas Injection System, where being physisorbed onto the substrate surface, they are dissociated upon the interaction with electron beam. This nanolithography technique allows to fabricate 3D structures in one single step with a regular resolution of 10nm [1]. The composition of such materials depends on the beam settings, e.g. beam size, electron flux and the scanning parameters, e.g. dwell time, pitch point, etc. [2].

In this work two precursor gases: $Cu(hfa)_2$ and $Co_2(CO)_8$ were simultaneously co-injected into the electron microscope chamber (see Figure 1). A series of squared deposits (3um x 3um) with different dwell times: 1us, 10us, 100us, 1ms, but constant dose, have been obtained.

The fabricated structures s have been preliminary analyzed with TEM, EDX, AFM techniques. The results showed that composition and deposit height depend on the chosen dwell time. Further analysis of local structure and magnetic properties by means of X-ray micro-spectroscopy techniques is planned. Assessment of the results expected, based on theoretical modeling of XAS and XMCD spectra, will be discussed.

[1] I. Utke, A. Gölzhäuser, *Angew. Chem. Int. Ed.* **49** (2010) doi: 10.1002/anie.201002677
[2] L. Bernau, M. Gabureac, R. Erni, I. Utke, *Angew. Chem. Int. Ed.* **49** (2010) doi:10.1002/anie.201004220

P-09

Structural and electronic properties of Bi_2Te_3/Eu/Bi_2Te_3 films

K. Balin*, A. Sowa, R. Rapacz and J. Szade

A. Chełkowski Institute of Physics, University of Silesia, 40-007 Katowice, Poland

Keywords: electronic structure, topological insulator, Bi_2Te_3, europium valency

*e-mail: katarzyna.balin@us.edu.pl

Bi_2Te_3 - one of the known topological insulators is considered as a promising material for multiple applications in next generation electronic or spintronic devices [1]. The crystal of Bi_2Te_3 is a semiconductor with the bulk energy bandgap of 0.3 eV. Its bandgap contains gapless, topologically protected surface states responsible for its exceptional magnetoelectric properties [2]. The time-reversal symmetry, responsible for linear dispersion of the surface states, can be broken to open a gap by different factors (e.g. Coulomb, magnetic and disorder perturbations).

Here we focused on the response of a Bi_2Te_3 surface to the disorder introduced by a layer of europium placed between the Bi_2Te_3 layers. Europium was selected due to its magnetic properties, directly related to its valency state; Eu^{3+} is non-magnetic (J = 0) while the Eu^{2+} has a large pure spin moment (J = 7/2) [3]. The applicability of the same element which may exhibit in in two different valency states (of which one is magnetically ordered and second is not) was crucial indicator of europium selection.

The growth of the multilayer structure of the Bi_2Te_3 and europium was realized in the MBE chamber. The films were grown on mica substrate with the following order of layer stack; 15nm thick Bi_2Te_3 layer, 0.5 or 2nm thick europium liner layer, 2nm thick Bi_2Te_3 top layer.

The structural characterization of grown layers was realized using the RHEED and LEED techniques. Crystalized in hexagonal phase 15nm thick Bi_2Te_3 is covered by partially textured polycrystalline europium liner, whereas the 2nm thick Bi_2Te_3 top layer shows a polycrystalline arrangement.

The electronic structure studies were conducted at each step of the growth procedure using the X-ray Photoelectron Spectrometer (XPS). Angle dependent measurements were conducted in order to observe in detail the Eu-Bi_2Te_3 interfaces. The chemical states of bismuth and tellurium were obtained from the detailed analysis of the Bi*4*f and Te*3*d multiplets. The chemical state and the valency state of europium were investigated by the analysis of Eu3*d* and Eu4*d* multiplets.

The analysis of the chemical shifts of the core levels as well as the relative changes in photoemission lines area ratio, allowed to conclude that
(1) within the examined system the layers are inter-mixing at room temperature,
(2) europium remains in divalent state,
(3) the exchange splitting of the Eu $4d_{5/2}$ core level is clearly resolved with a splitting of 0.9 eV,
(4) partial oxidation and/or reaction with Bi_2Te_3 layers leads to europium valency transition $Eu^{2+} \leftrightarrow Eu^{3+}$,
(5) the valency transition of europium entails shifting of the Te3*d* satellites.

Acknowledgments: This work was supported by the FORSZT PhD fellowship.

[1] M. Zebarjadi *et al. Energy Environ. Sci.* **5** (2012) 5147.
[2] Y. L. Chen *et al. Science,* **325** (2009) 178.
[3] A. R. Miedema, *J. Less-Common Met.* **46** (1976) 167.

P-10

Raman spectroscopy of graphene - based composite

L. Jarosinski[1]*, Cz. Kapusta[1] and A. Rybak[2]

[1]*AGH University of Science and Technology, Faculty of Physics and Applied Computer Science, Department of Solid State Physics*
[2]*ABB Corporate Research Center, Krakow, Poland*

Keywords: Raman spectroscopy, graphene, epoxy composite

*e-mail: lukasz.jarosinski@yahoo.pl

Graphene is a 2-dimensional crystalline allotrope of carbon with honeycomb lattice of sp2-bonded carbon atoms [1]. Its composites have recently attracted considerable attention owing to their unusual properties.

Raman spectroscopy is a powerful, non-invasive method widely used for characterisation of interatomic bonds. It is very effective in distinguishing details of bonding and local atomic environments in carbon containing structures. In particular, the information on disorder, surface, grain boundaries, doping and strain can be learnt from the Raman spectrum of graphene and its behaviour under varying physical condition [2]. However, much less research on graphene materials such as graphene-based composites can be found [3].

In this work results of Raman spectroscopic/spectromicroscopic studies of graphene filler - epoxy resin matrix composites are reported. They are discussed in terms of a relation to thermal and electrical transport properties as well as of possible mutual graphene - epoxy resin effects.

[1] A, K. Geim, K. S. Novoselov, *Nature Mater.* **6** (2007) 183-191.
[2] I. Childres, L. A. Jauregui, W. Park, H. Cao, Y. P. Chen, *Raman spectroscopy of graphene and related materials,* J.I. Jang (Ed.)*, Developments in photon and materials research,* 978-1-62618-384-1, Nova Science Publishers (2013).
[3] S. Stankovich, D. A. Dikin, G. Dommett, K. A. Kohlhaas, E. J. Zimney, E. A. Stach, R. D. Piner, S. T. Nguyen, R. S. Ruoff, *Nature* **442** (2006) 282-286.

P-11

Extreme ultraviolet irradiation effects on PVDF polymer surface

B. Korczyc[1]*, T.J. Kałdoński[2], I. U. Ahad[1], P. Wachulak[1], J. Kostecki[1], A. Bartnik[1], and H. Fiedorowicz[1]

[1]*Institute of of Optoelectronics Military University of Technology, 2, Kaliskiego Str, 00-908 Warsaw, Poland*
[2]*Faculty of Mechanical Engineering, Military University of Technology, 2, Kaliskiego Str, 00-908 Warsaw, Poland*

Keywords: extreme ultraviolet radiation, laser-plasma source, polymer surface modification

*e-mail: bkorczyc@wat.edu.pl

Extreme ultraviolet (EUV) light, due to its special qualities, can be exploited in various novel biomedical applications. Recent research priorities are to use EUV radiation as a highly efficient surface modification method [1].

In this work EUV irradiation effects in polyvinylidene fluoride (PVDF) thin foil were investigated. PVDF is fluoropolymer with excellent mechanical strength and durability making it suitable for tissue engineering and vascular prostheses applications. It is noteworthy that efficient micromachining of PVDF by direct photo-etching with EUV has been demonstrated for the first time by scientists at MUT [2]. In case of polymers, the penetration depth of EUV photons is limited to a very thin surface layer, while leaving the bulk material properties intact. Penetration depth in PVDF is about 100nm. Taking advantage of this fact fluoropolymer samples were irradiated using a laser-plasma EUV source, based on a gas-puff target excited with the 3-ns/0.8J/10Hz Nd:YAG laser [3]. The spectrum of focused extreme ultraviolet radiation used for samples treatment was in the wavelength range from 5 to 70 nm with relatively narrow peak, centred at about 10 nm wavelength.

The wettability of PVDF has been efficiently tuned as a consequence of a proper combination of surface topography and chemistry, achieved through EUV irradiation. Wettability studies were performed by measuring water contact angle. Significant difference in the angle between pristine and EUV modified PVDF samples, approximately 50 degrees, was obtained. The surface layer morphology was investigated using high resolution scanning electron microscopy.

Acknowledgments: The research was supported by LASERLAB-EUROPE III (grant agreement n° 284464, EC's Seventh Framework Programme) and EXTATIC

[1] I. U. Ahad et al., *J Biomed Mater Res Part A*, article in press (2013), DOI: 10.1002/jbm.a.34958.
[2] A. Bartnik et al., *Appl Phys A* **106** (2012) 551.
[3] A. Bartnik et al., *Appl Phys A* **647** (2011) 125.

P-12

Simulations of von Hamos X-ray spectrometer based on segmented-type diffraction crystal

P. Jagodziński[1]*, J. Szlachetko[2,3], D. Banaś[2]
A. Kubala-Kukuś[2] and M. Pajek[2]

[1]*Department of Physics, Kielce University of Technology, Tysiąclecia PP 7, 25-314 Kielce, Poland*
[2]*Institute of Physics, Jan Kochanowski University, Świętokrzyska 15, 25-406 Kielce, Poland*
[3]*SwissFEL, Paul Scherrer Institute (PSI), 5232 Villigen, Switzerland*

Keywords: Monte-Carlo simulations, ray-tracing, von Hamos spectrometer, segmented-type diffraction crystal

*e-mail: jagodzin@tu.kielce.pl

Wavelength-dispersive spectrometers use the diffraction of X-rays on a crystal to spread out the incident radiation with respect of its wavelength. The dispersed X-rays, detected by a position sensitive detector, give thus precise information on their wavelengths, which is the main concept of a high-resolution diffraction X-ray spectroscopy. The wavelength-dispersive spectrometers can be equipped with flat [1], bent [2,3,4] or bent/ground [5] crystals. The bending of the crystal results the improvement of the spectrometer efficiency, but causes also worsening the energy resolution because of the deformation and waviness of the curved crystal. To avoid deformations caused by crystal bending, the diced or segmented-type crystal can be use, which is easy to implement for any spectrometer geometry.

An example of a device with diced crystal is the developed von Hamos spectrometer based on a segmented-type diffraction crystal and CCD detector [6] installed on SuperXAS beamline at Swiss Ligth Source laboratory in Villigen. It is dedicated to X-ray emission spectroscopy, in particular resonant inelastic X-ray scattering (RIXS) studies for X-ray energies about 10 keV. The design and performance of this spectrometer was preceded by a computer simulation of its properties. The calculations were compared with experimental results of X-ray elastic scattering for photon beam energies in the range 8-10 keV [6]. In this spectrometer a continuously bent crystal is replaced by a segmented crystal consisting of flat segments, which are tangent in the focusing plane to the bending circle of a crystal in a standard von Hamos geometry. This arrangement leads to quasi-focusing of X-rays and enlargement of observed distribution in focusing plane on the detector, but in the dispersion plane, the X-ray are diffracted always on a flat-crystal segment.

In the present work the main properties (resolution, efficiency) of a von Hamos spectrometer with a segmented-type crystal were studied for low energy X-rays of about 3 keV. Such spectrometer is planned to be used the EBIS facility at the Institute of Physics of Jan Kochanowski University [7] to study with a high-resolution the X-rays emitted from highly charged ions. In order to determine the spectrometer properties, the Monte-Carlo ray-tracing simulations, which combine the laws of optics with dynamical theory of crystal reflectivity and X-ray diffraction, were developed [8].

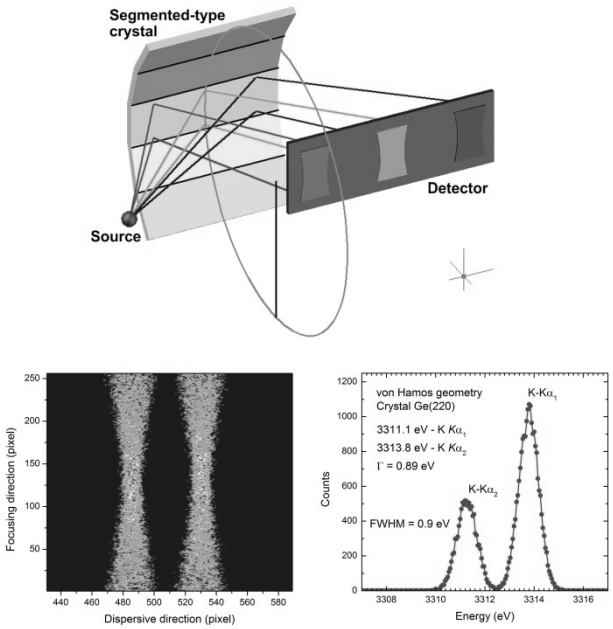

Figure 1. (*Top*) Scheme of the von Hamos geometry with a segmented-type diffraction crystal. (*Left*) 2D-distribution of photon hits in a plane of CCD detector, simulated for a potassium $K\alpha_1$ and $K\alpha_2$ X-ray. (*Right*) Simulated profile of X-rays obtained by projecting the 2D-distribution on a dispersive direction in a plane of a detector.

Using ray-tracing simulation technique the influence of various spectrometer parameters, as crystal/segment size, bending radius defining arrangement of crystal segments, X-ray source size, spatial resolution of the detector, on the spectrometer resolution was studied in details. Some examples are shown in Fig.1. Systematic results of the simulations will be presented and discussed.

[1] J. Szlachetko et al., *J. Synchrotron Rad.***17** (2010) 400-408.
[2] L. von Hamos, *Annalen der Physik* **409** (1933) 716-724.
[3] L. von Hamos, *Annalen der Physik* **411** (1934) 252-260.
[4] H. H. Johann, *Zeitschrift für Physik* **69** (1931) 185-206.
[5] T. Johansson, *Zeitschrift für Physik* **82** (1933) 507-528.
[6] J. Szlachetko et al., *Rev. Sci. Instrum.* **83** (2012) 103105.
[7] D. Banaś et al., *J. Instrum*, **5** (2010) C09005.
[8] P. Jagodziński et al.. *Nucl. Instrum. Methods A* (2014).

P-13

Influence of imperfections in a wedged multilayer Laue lens for the focusing of X-rays investigated by beam propagation method

A. Andrejczuk[1]*, J. Krzywiński[2] and S. Bajt[3]

[1]*Faculty of Physics, University of Bialystok, Lipowa 41 Str. 15-424 Bialystok, Poland*
[2]*SLAC National Accelerator Laboratory, 2575 Sand Hill Road MS 29, Menlo Park, CA 94025, USA*
[3]*DESY, Notkestr. 85, 22607 Hamburg, Germany*

Keywords: synchrotron radiation, multilayer Laue lens

*e-mail: andra@alpha.uwb.edu.pl

The Multilayer Laue Lens (MLL) is a new X-ray diffraction element, which connects features of Fresnel Zone Plate (FZP) and a multilayer mirror [1]. It is made by the thin layer deposition technique with layers thicknesses corresponding to the FZP zone radius equation. If the deposition is done in such a way that every layer thickness varies linearly along the beam propagation direction then the efficiency of the focusing substantially increases. Such a lens is called a wedged MLL [1].

In this work we investigated the performance of a wedged MLL focusing 20 keV x-rays in one dimension. The lens had a focal length of 1.25 mm and it consisted of 5500 layers made of less and more absorbing materials. We applied 1D Beam Propagation Method (BPM) [2] to calculate the intensity in the focus plane and at the far screen. According to the simulations a perfect lens will focus the beam to 5 nm FWHM with the intensity increase exceeding $2 \cdot 10^3$ as compared to the intensity of the primary beam. The effect of various random and systematic errors in layer' thickness and their placement was studied in detail. The influence of the scaling of these imperfections on the intensity distributions in the focal plane and in the far field will be discussed.

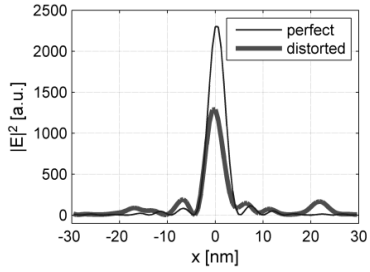

Figure 1. The intensity distribution at focal plane for a perfect lens (thin line) and the lens with random errors of layers thicknesses with standard deviation of 0.07 nm (thick line).

[1] H. Yan et. al., *X-Ray Optics and Instrumentation* (2010) 401854.
[2] O. K. Ersoy, *Diffraction, Fourier Optics and Imaging* New Jersey, John Wiley and Sons (2007).

P-14

Investigation of the thin films properties using X-ray reflectometry and grazing incident X-ray diffraction methods

D. Banaś[1,2], A. Markowska[1], M. Sobisz[1]*, I. Stabrawa[2], A. Kubala-Kukuś[1,2], J. Braziewicz[1;2], K. Dworecki[1], E. Tomal[3], U. Majewska[1,2], M. Pajek[1], J. Wudarczyk-Mońko[2] and S.Góźdź[2,4]

[1]*Institute of Physics, Jan Kochanowski University, Świętokrzyska 15, 25-406 Kielce, Poland*
[2]*Holycross Cancer Center, Artwińskiego 3, 25-734 Kielce, Poland*
[3]*Institute of Biology, Jan Kochanowski University, Świętokrzyska 15, 25-406 Kielce, Poland*
[4]*Institute of Public Health, Jan Kochanowski University, IX Wieków Kielc 19, 25-317 Kielce, Poland*

Keywords: XRR, GIXD, biointerfaces

*e-mail: milenasobisz@interia.pl

The X-ray reflectometry (XRR) [1], which uses the effect of total external reflection of X-rays, is surface sensitive analytical technique for investigation of the near surface regions of different sample systems including single crystalline, polycrystalline and amorphous samples, polymers, organic samples and fluids. Reflectometry pattern obtained for the reflection angles from 0 to about 5 degrees allows the measurement of thin film thicknesses of single and multilayer systems, density profiles of near surface regions and roughness (from 0.1 nm to 5 nm) of the surfaces and interfaces.

The method of grazing incident X-ray diffraction (GIXD) is a modification of standard X-ray diffraction technique, which due to low incident angle of the X-ray beam maximizes signal from the surface and as a result allows for phase analysis on very thin layers and depth profiling of the phase composition of layered samples.

In this work the XRR and GIXD techniques were applied to analysis and characterization of thin gold layers used further for studies of interactions between lipopolysaccharides (LPSs) and gold surfaces. Understanding of interaction of complex biomolecules and different material surfaces (biointerfaces) is important in many research area of biology, biotechnology, diagnostics and medicine. Determination of properties of such biointerfaces is not possible or very difficult without earlier precise characterization of the material surface. The gold layers studied in this work were prepared on a glass slide support covered by evaporation with 2 nm of chromium, which improved the adhesion of the gold film to the glass substrate.

In this work the motivation of the experiment, physical basis of the methods used, experimental setups, results of optimization of the measurement procedure and results of the measurements for gold surfaces of different thicknesses will be presented.

[1] L. G. Parratt, *Phys. Rev,* **95** (1954) 359-369.
[2] H. Kiessig, *Ann. d. Phys*. **10** (1931) 769.

P-15

Determination of the lead and lead oxides concentration in human biological and environmental samples using X-ray spectrometry techniques

A. Kubala-Kukuś[1,2], E. Kopeć[1]*, W. Kurtek[1], D. Banaś[1,2], J. Braziewicz[1,2], U. Majewska[1,2], M. Pajek[1], J. Wudarczyk-Moćko[2], I. Stabrawa[2] and S. Góźdź[2,3]

[1]*Institute of Physics, Jan Kochanowski University, Świętokrzyska 15, 25-406 Kielce, Poland*
[2]*Holycross Cancer Center, Artwińskiego 3, 25-734 Kielce, Poland*
[3]*Institute of Public Health, Jan Kochanowski University, IX Wieków Kielc 19, 25-317 Kielce, Poland*

Keywords: XRPD, TXRF, WDXRF, lead concentration, human biological material samples, environmental samples

*e-mail: eva010@interia.pl

Elemental analysis of the human biological material (serum, urine, hair) carries the essential information about the state of the organism. Determination of the lead concentration, which is present in all tissues of the human body, is an example of a such analysis. The lead concentration is mostly a function of its content in the environment and the time of impact on human body. Lead inserted into the body goes almost entirely into the blood. Part of it is deposited in bone, soft tissue, hair, and the rest is eliminated. The lead content in the blood is a sensitive indicator of risk of the organism [1].

In the presented studies, the concentration of lead in the samples of the human biological material was determined by total reflection X-ray fluorescence analysis (TXRF) technique using the PICOFOX spectrometer (Bruker). Due to expected concentration of lead close to the detection limit of the TXRF method (ppb range) optimization of the measuring procedure (sample preparation, internal standard selection, measurement time, quantitative calibration of the spectrometer) is necessary. In this work the physical basis of TXRF method, an experimental setup, sample preparation procedure of human biological material and spectrometer calibration will be discussed.

Parallel, the lead concentration and content of lead oxides will be determined in environmental samples (water, soil, minerals, sediments) using X-ray spectrometry and diffraction techniques (TXRF, WDXR, XRPD). The main motivation of the studies is optimization measurement procedure and determination the detection limit of lead and lead oxides for each analysed samples and used analytical techniques.

Acknowledgments: The equipment was purchased thanks to the financial support of the European Regional Development Fund in the frame work of the Polish Innovative Economy Operational Program (Contract no.WNPPOIG.02.02.00-26-023/08).

[1] A. Kabata-Pendias, A. B. Mukherjee, *Trace Elements from Soil to Human* (Springer, 2007).

P-16

Application of the X-ray spectrometry methods in analysis of the diet supplements

A. Kubala-Kukuś[1,2], D. Maniak[1]*, D. Banaś[1,2], J. Braziewicz[1,2], U. Majewska[1,2], M. Pajek[1,2], J. Wudarczyk-Moćko[1,2], I. Stabrawa[2], S. Góźdź[2,3] and A. Kowalska[2]

[1]*Institute of Physics, Jan Kochanowski University, Świętokrzyska 15, 25-406 Kielce, Poland*
[2]*Holycross Cancer Center, Artwińskiego 3, 25-734 Kielce, Poland*
[3]*Institute of Public Health, Jan Kochanowski University, IX Wieków Kielc 19, 25-317 Kielce, Poland*

Keywords: XRPD, TXRF, WDXRF, diet supplements

*e-mail: maniak.dominika@gmail.com

The registration and marketing of medicative products and medicinal devices are directly related to their quality, safety and therapeutic efficacy. The analysis of the drugs concentrates on bioavailability and bioequivalence studies, on their elemental and chemical composition and possible impurities.

The topic of this report is the application of the X-ray spectrometry methods in analysis of the pharmaceutical samples. In presented studies different commercially available diet supplements containing trace elements essential for the proper functioning of the human body, namely: Mg, Cr, Se and Zn [1], will be analysed using WDXRF, TXRF and XRPD techniques. The studies concentrate on elemental and chemical composition analysis. Firstly, the sample preparation requirements for applied techniques will be optimized (needed amount of sample, necessity for sample digestion, matrix effects, quantitative calibration). For TXRF metod the choice of internal standard will be also discussed. Next, the conditions of the measurements will be optimized and discussed in context of sensitivity of the methods for different elements and compounds. As a result, the elemental (respectively Mg, Cr, Se and Zn) and chemical composition of the diet supplements will be obtained. The analysis of pharmaceutical samples will include also identification of the samples impurities and estimation of the detection limit. The composition of studied different diet supplements will be compared and interpreted using the statistical method BIPLOT.

The presented studies can be next applied in topic of the detection of the medicament in human biological material. As an example from our laboratory, monitoring of selenium concentration in the serum of patients with thyroid diseases treated with selenium will be discussed.

Acknowledgments: The equipment was purchased thanks to the financial support of the European Regional Development Fund in the frame work of the Polish Innovative Economy Operational Program (Contract no.WNPPOIG.02.02.00-26-023/08).

[1] A. Kabata-Pendias, A. B. Mukherjee, *Trace Elements from Soil to Human* (Springer, 2007).

P-17

Crystal structure and defect structure of selected $Ca_9RE(VO_4)_7$ single crystals: A high-resolution diffraction, white beam topography and powder diffraction study

A. Behrooz[1]*, W. Paszkowicz[1], P. Romanowski[1], B. Nazarenko[2], A. Shekhovtsov[2], W. Wierzchowski[3], K. Wieteska[4] and C. Paulmann[5]

[1]*Institute of Physics, Polish Academy of Sciences, al. Lotnikow 32/46, PL-02668 Warsaw, Poland,*
[2]*Institute for Single Crystals, NAS of Ukraine, Lenin Ave. 60, 61001, Kharkov, Ukraine*
[3]*Institute of Electronic Materials Technology (ITME), Wólczyńska 133, Warszawa 01-919, Poland*
[4]*National Centre for Nuclear Research, Radioisotope Centre POLATOM (NCNR), Andrzeja Soltana 7, Otwock-Świerk 05-400, Poland*
[5]*HASYLAB at DESY, 85, Notkestr., Hamburg 22607, Germany*

Keywords: calcium rare earth vanadate, structure refinement

*e-mail: behrooz@ifpan.edu.pl

Compounds of $Ca_9RE(VO_4)_7$ formula (RE = a rare earth) are structurally closely related to whitlockite mineral, $Ca_9(MgFe)(PO_4)_6PO_3OH$. Such materials are considered for applications in optoelectronics, e.g., in white-light emitting diodes, as discussed in Refs. [1, 2]. Compounds of $Ca_9RE(VO_4)_7$ structure (space group $R3c$) accommodate the RE atoms in Ca sites by assigning a partial occupancy of Ca and RE atoms [3, 4]. The current survey, extracts some basic information on structure and quality of $Ca_9RE(VO_4)_7$ (R = La, Nd, Gd) single crystals with the use of high-resolution diffraction, white beam topography and powder diffraction.

$Ca_9RE(VO_4)_7$ single crystals were grown by the Czochralski method. Phase analysis has shown that the crystals are pure $Ca_9RE(VO_4)_7$ phases. The results of Rietveld refinements are compared with literature data for polycrystalline samples prepared by solid state reaction [3, 4]. Small discrepancies in lattice parameter values are attributed to minor excess from stoichiometry of the single crystal studied. X-ray rocking curves and reciprocal space maps were established using a laboratory high-resolution diffractometer. Topographs have been obtained in reflection geometry using white beam at a synchrotron beamline. A comparison among the results of all applied approaches shows that the studied crystals reveal specific similarities and differences in the defect structure. The rocking curves as well as the reciprocal space maps of symmetrical 0 0 30 and asymmetrical 1 0 16 reflections prove that the crystals are generally of good quality and display the defects characteristic for the given crystal, such as dislocations, point defects and mosaics. The analysis of the topographs clarifies the existence of dislocations and/or small inclusions in the $Ca_9La(VO_4)_7$ and $Ca_9Nd(VO_4)_7$ single crystals and the incoherent inclusions in the $Ca_9Gd(VO_4)_7$ single crystal.

[1] X. Wu, Y. Huang, H.J. Seo, *Ceramics Int.* **37** (2011) 2323.
[2] L. Liu, R.-J. Xie, N. Hirosaki, Y. Li, *J. Spectrosc. Dyn*. **3**, (2013) 1.
[3] A. A. Belik, V. A. Morozov, R. N. Kotov, S. S. Khasanov, B.I. Lazoryak, *Crystallogr. Rep*. **42** (1997) 751.
[4] A. A. Belik, V. A. Morozov, S. V. Grechkin, S. S. Khasanov, B. I. Lazoryak, *Crystallogr. Rep*. **45** (2000) 798.

P-18

X-ray spectrometry and microtomography techniques in geological applications

A. Kubala-Kukuś[1,2], M. Mazurek[1]*, D. Banaś[1,2], J. Braziewicz[1,2], U. Majewska[1,2], M. Pajek[1], J. Wudarczyk-Mońko[2], I. Stabrawa[2] and S. Góźdź[2,3]

[1]*Institute of Physics, Jan Kochanowski University, Świętokrzyska 15, 25-406 Kielce, Poland*
[2]*Holycross Cancer Center, Artwińskiego 3, 25-734 Kielce, Poland*
[3]*Institute of Public Health, Jan Kochanowski University, IX Wieków Kielc 19, 25-317 Kielce, Poland*

Keywords: XRPD, TXRF, WDXRF, microtomography, geological samples

*e-mail: marta10mazurek@wp.pl

The well known X-ray spectrometry and diffraction techniques: WDXRF, TXRF, XRPD and X-ray microtomography, allow the study of materials in broad range of research interest [1-4]. A particular issue is the application of these techniques in studies of the multielemental sample composition in a wide range of concentrations (samples with different matrices) and characterized with different grain size. Typical examples of these kind of samples are soil or geological samples (soil, till, sand, sediment, mineral). The elemental and chemical analysis of soil and geological samples is in the interest of many fields of science as for example agriculture, biology or geography. Analysis of these samples is however difficult due to the matrix effects and grain size effect [1].

The aim of the study is analysis of the samples with soil and geological matrix using WDXRF, TXRF, XRPD and X-ray microtomography techniques. The samples will be characterized additionally by different grain sizes and different kind of material packing. The main motivation of undertaken this research topic is the improvement of the qualitative and quantitative analysis of the materials with a particular kind of matter, namely, the soil and geological matrix materials. The WDXRF and TXRF measurements give information about elemental concentration of the samples. The XRPD technique gives information about the chemical sample composition and allows study mineralogical effects i.e. the influence of the mineral type in which the analysed element occurs on the intensity of its characteristic X-ray. In the case of TXRF measurements choice of internal standard needs optimization in such a way that its presence in a sample does not make difficulty in measurement of characteristic radiation of the element analysed in the sample. The result of the study will be also development of the calibration curves for TXRF spectrometer for samples with soil and geological matrices. More complex interpretation of the elemental and chemical composition analysis of the samples will be possible using X-ray microtomography. Morphology of each sample can be in this way characterized in micrometers scale especially in the context of the information about grains size. The obtained results of analysis of the samples with soil and geological matrices will be interpreted using the statistical method BIPLOT, which is practical tools for the compositional data analysis [5].

Acknowledgments: The equipment was purchased thanks to the financial support of the European Regional Development Fund in the frame work of the Polish Innovative Economy Operational Program (Contract no.WNPPOIG.02.02.00-26-023/08).

[1] J. P. Willis, A. R. Duncan, *Understanding XRF Spectrometry* (PANalytical B.V., Almelo, 2008)
[2] R. Klockenkämper, *Total-Reflection X-Ray Fluorescence Analysis* (Wiley Interscience, John Wiley & Sons, New York, 1997)
[3] V. K. Pecharsky, P. Y. Zavalij, *Fundamentals of Powder Diffraction and Structural Characterization of Materials* (Springer, New York, 2009)
[4] R. Cierniak, *X-ray computed tomography in biomedical engineering* (Springer, London, 2011)
[5] K. R. Gabriel, *Biometrika* **58** (1971) 453.

P-19

Equation of state of monazite-type lanthanum orthovanadate: *in situ* high-pressure powder diffraction and *ab initio* calculations

O. Ermakova[1,2]*, J. López-Solano[3,4], R. Minikayev[1], S. Carlson[5], A. Kamińska[1], M. Glowacki[1], M. Berkowski[1], and W. Paszkowicz[1]

[1] *Polish Academy of Sciences, Institute of Physics, al. Lotników 32/46, 02-668 Warsaw, Poland*
[2] *Russian Academy of Sciences, Ural Branch, Institute of Solid State Chemistry (ISSC), Pervomayskaya 91, 620219 Ekaterinburg, Russian Federation*
[3] *Departamento de Física Fundamental II, MALTA Consolider Team, and Instituto de Materiales y Nanotecnología, Universidad de La Laguna, 38205 Tenerife, Spain*
[4] *Izaña Atmospheric Research Center, Agencia Estatal de Meteorología (AEMET), 38071 Tenerife, Spain*
[5] *MAXlab, Lund University, SE-22100 Lund, Sweden*

Keywords: synchrotron radiation, high-pressure, powder diffraction, DFT calculation

*e-mail: Olga.N.Ermakova@gmail.com

Lanthanum orthovanadate ($LaVO_4$) is one of a few of the RVO_4 compounds which can crystallize in the monazite-type structure. In the present study, equation of state of the monazite-type of $LaVO_4$ is studied using *in situ* high-pressure powder diffraction at room temperature, and *ab initio* calculations within the framework of the density functional theory.

A polycrystalline $LaVO_4$ sample was prepared by solid state reaction between dried La_2O_3 (Auer-Remy 4N) and V_2O_5 (Alfa Aesar 4N5) oxides mixed at equimolar ratio. Mixed and ground oxides were compressed into pellets and sintered in air at 1300°C during 6 hours. After the sintering process, the sample was re-ground, pressed into pellets and sintered at 1300°C for 6 h again**.**

In situ high-pressure powder diffraction experiment was performed in a diamond anvil cell at the I711 beamline of the MAX IV synchrotron (Lund, Sweden). A preindented steel gasket of 100 μm thickness with a 200 μm hole was used for the encapsulation between the diamond anvils of the studied sample using the ethanol-methanol-water pressure-transmitting medium. The experiment was performed in hydrostatic conditions up to pressure of 9.1 GPa. Applied pressure was calibrated by the laser-excited ruby fluorescence peak position. To perform the Rietveld analysis with the Fullprof.2k 5.30 package, the 2D data were converted to 1D patterns with the Fit2D program. The calculated dependence of the unit cell volume on pressure was used in the fitting of a third-order Birch-Murnaghan equation of state with EOSfit52 program.

The fitted parameters of a third-order Birch-Murnaghan equation of state are found to be in good agreement with theoretical ones.

P-20

Mechanochemical synthesis of the scheelite-type $PrVO_4$ and $HoVO_4$

O. Ermakova[1,2], W. Paszkowicz[1]*, D. Oleszak[3], M. Berkowski[1], M. Czech[1] and M. Glowacki[1]

[1] *Instytute of Physics of Polish Academy of Sciences, al. Lotnikow 32/46, 02-668 Warsaw, Poland*
[2] *Institute of Solid State Chemistry, Russian Academy of Sciences, Ekaterinburg, Russian Federation*
[3] *Division of Structural and Functional Materials, Warsaw University of Technology, Wołoska 141, 02-507 Warsaw, Poland*

Keywords: ball milling, orthovanadate phase transition

*e-mail: paszk@ifpan.edu.pl

At ambient conditions, rare-earth orthovanadates adopt zircon-type structure (space group $I4_1/amd$) except $LaVO_4$ which typically crystallizes in monazite-type structure. Zircon-type RVO_4 can be prepared in single crystal form using several crystal growth techniques or in powder form e.g. as a product of solid state reaction between rare-earth and vanadium It is known, that at high-pressure conditions (5-10 GPa) RVO_4 materials with zircon structure undergo a transformation to the scheelite-type structure (space group $I4_1/a$). Tojo *et al*. [1] have shown, for selected RVO_4 (R = Y, Nd, Sm, Gd, Dy and Er) crystals that the scheelite-type phase can be obtained via mechanochemical reaction between R_2O_3 and V_2O_5 oxides.

In the present work, we desctibe successful attempts to obtain scheelite-type $PrVO_4$ and $HoVO_4$ by means of ball milling of zircon-type samples. Experiments were performed using a ball grinder. The primary sample of $HoVO_4$ was grown in single crystal form by Czochralski method, the $PrVO_4$ sample was prepared by solid state reaction between Pr_6O_{11} and V_2O_5 oxides. Both samples were ground for 1, 2, 4, 8 and 16 hours of milling. All specimens were studied using a laboratory X-ray powder diffractometer. The diffraction patterns demonstrate that the scheelite-type structure appears after 1 hour of milling and that its content in the specimen grows with increasing duration of mechanochemical reaction. After 16 hours of milling the scheelite-type phase dominates in both, $HoVO_4$ and $PrVO_4$, samples, as shows the exaple for $HoVO_4$ (Fig. 1): after 16 h only two reflections of the zircon-type polymorph remain.

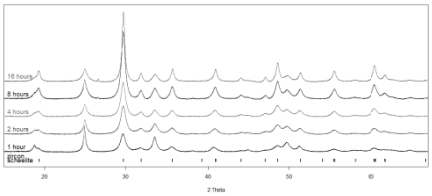

Figure. 1. Variation of phase composition for ball miling of zircon-type $HoVo_4$ sample. Small vertical bars at the bottom part mark the diffraction peaks of the scheelite type phase.

[1] T. Tojo, Q. Zhang, F. Saito, *J. Alloys Compds* **427** (2007) 219.

P-21

Structure of AlN films deposited by magnetron sputtering method

K. Nowakowska-Langier[1]*, R. Chodun[2], K. Zdunek[2,1], R. Minikayev[3] and R. Nietubyć[1]

[1]*In Material Physics Department, National Centre for Nuclear Research (NCBJ) , Andrzeja Soltana 7, 05-400 Otwock-Swierk, Poland*
[2]*Faculty of Materials Science and Engineering, Warsaw University of Technology, Woloska 141, 02-507 Warsaw, Poland*
[3]*Institute of Physics, Polish Academy of Sciences, Al.Lotników 32/46, 02-668, Warsaw, Poland*

Keywords: AlN films, magnetron sputtering method, crystalline /amorphous structure

*e-mail: k.nowakowska-langier@ncbj.gov.pl

The AlN films on the Si substrate were synthesized by the magnetron sputtering method. The dual magnetron system [1] operating in AC mode was used in the experiment. Processes of synthesis were carried out in the atmosphere of a mixture of argon (as the source of ions sputtered the material of cathode) and nitrogen. Morphology and phase structure of the AlN films were investigated as a function of pressure of Ar/N_2 and the deposition time. Structural characterizations were performed by means of SEM and X-ray diffraction method carried out at W1.1 beamline (Hasylab/DESY). Our results show that the use of magnetron sputtering method in the dual magnetron sputtering system is an effective way to produce a thin, transparent AlN layers which are characterized by a good adhesion to the silicon substrate. The morphology of the films is strongly depend on the Ar/N_2 gas mixture pressure. Increase of the mixture pressure is accompanied by columnar growth of the layers. The films obtained at the pressure below 1 Pa are characterized by more fine and compacted structure. The thick films are characterized by hexagonal AlN structure, while the AlN thin films with the thickness less than 100 nm exhibits amorphous structure. Obtained results allow us to assume a possible mechanism of the AlN layers formation.

[1] K. Zdunek, K. Nowakowska-Langier, J. Dora, R. Chodun, *Surface and Coatings Technology* **228** (2013) S367.

P-22

XANES lattice location of cobalt implanted into monocrystalline ZnO and plasma pulse annealed

Z. Werner[1]*, R. Nietubyć[1, 2], C. Pochrybniak[1], M. Barlak[1] and R Ratajczak[1]

[1]*National Centre for Nuclear Research (NCBJ), Sołtana 7, 05-400 Otwock, Poland*
[2]*National Synchrotron Radiation Centre Solaris, Jagiellonian University, Czerwone Maki 98, 30-348 Kraków, Poland*

Keywords: plasma annealing, implantation, XAFS

* e-mail: z.werner@ncbj.gov.pl

Energy pulse annealing associated with transient melting and crystallization of implanted surface layer is considered as an effective method of implantation damage removal and impurity solubility enhancement[1]. To examine applicability of this method to manufacture of diluted magnetic semiconductors (DMS) we implanted monocrystalline ZnO with cobalt to a dose of 10^{16} ions/cm^2. Next the samples were either thermally annealed at 800°C in argon or treated with high energy plasma pulses of an energy density in the range of 1 – 1.5 J/cm^2. The location of cobalt atoms in the lattice was studied by X-ray absorption near edge spectroscopy (XANES) using ELETTRA synchrotron radiation. An analyses of the obtained XANES spectra reveals absence of Co precipitates and an important difference between the Co spectrum obtained after 1.5 J/cm^2 treatment and the remaining spectra . The results are analyzed in terms of Co atoms positioned substitutionally in ZnO after pulse melting and crystallization.

[1] E. Fogarassy, R. Stuck, J. J. Grob, A. Grob, P. Siffert, *J. de Physique* **41** (1980) C4.

P-23

XAFS investigations of local structural changes in (Ga,Mn)As thin layers at low temperature postgrowth annealing

I. N. Demchenko[1]*, M. Chernyshova[2], P. Konstantynov[1], J. Domagala[1], Y. Melikhov[1] and J. Sadowski[3]

[1]*Institute of Physics, Polish Academy of Sciences, Al Lotnikow 32/46, PL-02-668 Warsaw, Poland*
[2]*Institute of Plasma Physics and Laser Microfusion, 23 Hery Street, PL-01-497 Warsaw, Poland*
[3]*MAX IV Laboratoriet, Box 118, 221 00 Lund, Sweden*

Keywords: synchrotron radiation, XAFS, XRD, EDX

*e-mail: demch@ifpan.edu.pl

One of the most pressing problems of spintronics is to find new materials with properties combining both ferromagnets and semiconductors. Such magnetic semiconductors can be produced by deliberate doping of a given semiconductor with atoms of a magnetic material, such as Mn. The most studied material among these dilute magnetic semiconductors (DMS) is (Ga, Mn) As, and with the optimized MBE growth and post-growth annealing procedures nowadays (Ga, Mn) As layers have T_C as high as about 200 K. This is remarkably high as for DMS, but still too low in view of potential application in spintronics devices. Theoretically, up to now there is no universal model which adequately describes in details the processes of ferromagnetic ordering in the DMS. The most common theory is Ruderman-Kittel-Kasuya-Yosida (RKKY) model, in which the ferromagnetic ordering of the localized spins occurs through the exchange interaction with the gas of free carriers (valence-band holes in the case of (Ga, Mn) As), has its own limitations predicting not always experimentally observed increase of the Curie temperature (T_C) with increasing concentration of impurities. Further studies **not only** of the influence of microstructure and its inhomogeneities upon material's properties **but also** of *dynamical processes* (as well as formation and migration of point defects) taken place in microstructure evolution of (Ga, Mn) As during growth and postgrowth annealing should lead to an improved understanding of the whole picture and could potentially lead to further progress in T_C increasing of (Ga, Mn) As.

The project's goal was to check the effectiveness of EXAFS (extended x-ray absorption fine structure) as a probe of *local dynamics* and thermally activated decomposition of DMS, namely, (Ga, Mn) As after post growth annealing (up to about 600 ^{o}C). In order to determine the local atomic structure around Mn atoms we analyzed the XAFS (X-ray absorption fine structure) spectra at the K-edges of Mn for investigated samples. The samples devoted for the XAFS measurements were grown at MAXLab MBE system, by Dr Janusz Sadowski. After growth the samples were subsequently annealed at the temperatures 200, 300, 400, 500 and 600°C, respectively. The measurements were done at the I811 beamline of MaxLab II. The x-ray beam was monochromatized by two parallel silicon crystals with flat reflecting (111) faces, detuned to reduce the harmonics influence. The beam intensity was measured before the sample by argon-filled ionization chamber. Total fluorescence signal from the sample was gathered by Vortex silicon-drift detector. The measurements were done at liquid nitrogen (LN) to reduce thermal vibration of atoms.

Obtained X-ray absorption fine structure (XAFS) data along with X-ray diffraction (XRD) and Energy-dispersive X-ray spectroscopy (EDX) results will be presented and discussed in details.

[1] J.Sadowski and J. Z. Domagala, chapter 2 in *Advanced Functional Materials: A perspective from theory to experiment.* Edited by B. Sanyal and O. Eriksson. (Elsevier, 2012)

P-24

Structural investigation of ultrathin Pt/Co/Pt trilayer films with perpendicular magnetic anisotropy induced by extreme ultraviolet light irradiation

E. Dynowska[1]*, J. B. Pelka[1], D. Klinger[1], R. Minikayev[1], A. Petruczik[1], A. Wawro[1], R. Sobierajski[1], P. Dluzewski[1], J. Sveklo[2], A. Maziewski[2], A. Bartnik[3] and O.H. Seeck[4]

[1]*Institute of Physics, Polish Academy of Sciences, al. Lotnikow 32/46, PL-02-668 Warsaw, Poland*
[2] *Faculty of Physics, University of Białystok, 41 Lipo str, 15-424 Białystok, Poland*
[3]*Institute of Optoelectronics, Military University of Technology, ul. S. Kaliskiego 2, 00-908 Warsaw, Poland*
[4]*DESY, Nottke Str. 85, 22607 Hamburg, Germany*

Keywords: synchrotron radiation, Pt/Co/Pt films, structural characterization, magnetic properties

*e-mail: dynow@ifpan.edu.pl

The ultrathin Pt/Co/Pt trilayer films with tunable magnetization direction are of particular importance for spintronics. It was previously evidenced that the out-of-plane to in-plane magnetization reorientation can be induced in this system by light irradiation. Femtosecond laser pulses (in visual range) driven transition from in-plane into out-of-plan magnetization state has been recently reported [1]. Similar effect induced by extreme ultraviolet (EUV) light pulses also exists in Pt/Co/Pt. Structural study of EUV modified nanostructures is the goal of this presentation.

Investigations were performed on the MBE fabricated layered system containing ultrathin (3 nm) cobalt layer grown on 5 nm thick Pt buffer layer and covered by 3 nm thick second layer of Pt. Nanostructures were irradiated with EUV pulses (about 3ns duration and 11nm light length) from plasma source operating with gas target Kr/Xe/He excited with an optical laser. The structural characterization has been done by X-ray diffraction (XRD) methods with use of the synchrotron radiation at the P-08 beamline of Petra III at DESY as well as the laboratory diffractometer X'Pert PRO MPD Panalytical configured for Bragg-Brentano diffraction geometry, equipped with a strip detector and an incident-beam Johansson monochromator.

The diffraction patterns of the as grown samples show only thickness fringes related to the total thickness of the multilayers (~10 nm). Direct observation of the diffraction peaks from the individual layers were not possible due to their very small thickness. The detailed analysis of the patterns allows to estimate the position of the 111 diffraction peak from the Pt layers (total thickness ~8 nm) and to calculate the value of the lattice spacing d_{111}, which is very close to that characteristic for Pt. Unfortunately, the diffraction signal from the Co layer (~3 nm) is not visible.

The thickness fringes from the irradiated places of the samples show pronounced changes in the films structure. More detailed insight suggests creation of substitutional alloy $Pt_{1-x}Co_x$ with the interplanar distance d_{111} of the layer system significantly smaller than that for as grown samples.

The grazing-incidence diffraction recorded at an angle of incidence of 0.5° has shown a polycrystalline phase component in platinum film, both in as grown and irradiated places.

After the X-ray measurements the morphology of the samples was examined by transmission electron microscopy methods (TEM) using the FEI Titan CUBED 80-300 microscope. It was confirmed that irradiation leads to complete intermixing of the cobalt film with the platinum covers resulting in substitutional $Pt_{1-x}Co_x$ alloy.

From the experiment at P-08, it has been found that outside of EUV irradiated spot the X-ray beam footprints on the surface of the samples, visible as a slightly darker areas. We performed special tests explaining the beam influence on the formation of these features. Our observations suggest that the effect of "discoloration" may appear due oxidation of the sample induced by ozon generated by high energy density of photons flux. As a result outside of EUV irradiated spot sample losts his ferromagnetic properties. Comparison of measurements with synchrotron radiation and with laboratory diffractometer, where this discoloration does not appear, showed that the general features of the diffraction patterns at intermediate 2θ angles, with thickness fringes, stays unaffected.

Acknowledgments: This work was partially supported by the Polish National Science Center (Grant No. 2012/06/M/ST3/00475) The research leading to these results has received funding from the European Community's Seventh Framework Programme (FP712007-2013) under grant agreement n° 312284 (CALIPSO).

[1] J. Kisielewski *et al., J. Appl. Phys.* **115** (2014) 053906.

P-25

Data processing for soft X-ray diagnostics based on GEM detector measurements for fusion plasma imaging

T. Czarski[1]*, M. Chernyshova[1], S. Jabłoński[1], G. Kasprowicz[2], K. T. Poźniak[2], A. Byszuk[2], B. Juszczyk[2], J. Wojeński[2] and P. Zienkiewicz[2]

[1]*Institute of Plasma Physics and Laser Microfusion, 23, Hery Str, 01-497 Warsaw, Poland*
[2]*Institute of Electronic Systems, Warsaw University of Technology, 15/19, Nowowiejska Str, 00-665 Warszawa, Poland*

Keywords: GEM detector, FPGA, fusion plasma

*e-mail: tomasz.czarski@ipplm.pl

The measurement system based on GEM - Gas Electron Multiplier detector [1] is developed for X-ray diagnostics of magnetic confinement tokamak plasma. The current signal generated by the detector carries information about the energy and position of X-rays. The multi-channel data acquisition system [2] is designed for estimation of the energy and position of an X-ray source. Cluster charge value distribution corresponds directly to the energy spectral lines of X-ray source. Cluster charge position distribution corresponds to the energy for Bragg diffraction precise spectroscopy. The FPGA based system performs the basic functions of data processing: the identification of charge clusters and charge value and position histogramming [3]. Selected data series are transferred to a PC in order to obtain detailed analysis and visualization of results. The system interface, based on MATLAB package, accomplishes control, communication, data processing and imaging results. This allows one to study properties of the detector, measuring system diagnostics, optimization of working conditions and system development. Series of the procedures: multi-channel calibration, energy range control and scaling, have been developed for optimization of the measurement condition, to improve quality of the acquired data and for the efficient presentation of the results.

[1] F. Sauli, *Nuclear Instruments and Methods in Physics Research Section A* **386** (1997) 531-534.
[2] J. Rzadkiewicz *at al*., *Nuclear Instruments and Methods in Physics Research A* **720** (2013) 36-38.
[3] K.T. Pozniak, *at al*., *Proc. of SPIE*, 0277-786X, **8903**, index: 2F, Wilga (2013).

P-26

Crystallochemical reason for degradation of the Baltic amber (succinite) nugget

P. Piszora[1]*, J. Czebreszuk[2], K. Kwiatkowska[3] and D. Baralkiewicz[4]

[1]*Department of Materials Chemistry, Faculty of Chemistry, Adam Mickiewicz University, Grunwaldzka 6, 60-780 Poznań, Poland*
[2]*Adam Mickiewicz University, Department of Prehistory of Poland, Institute of Prehistory, ul. Św Marcin 78, 61-809 Poznań, Poland*
[3]*Museum of the Earth, Polish Academy of Sciences, 20/26 Aleja na Skarpie, 00-488 Warszawa, Poland*
[4]*Department of Trace Element Analysis by Spectroscopy Method, Faculty of Chemistry, Adam Mickiewicz University, Umultowska 89b, 61-614 Poznań, Poland*

Keywords: X-ray diffraction, crystallochemistry

*e-mail: pawel@amu.edu.pl

Baltic amber is a fossil resin with ambiguous paleobotanical origin [1]. The X-ray diffraction pattern of pure amber specimen exhibits amorphous character. However, it is possible to observe a crystalline inclusion in the amber matrix [2,3]. We examined with XRD the amber specimens selected from a large collection of the Museum of the Earth of Polish Academy of Sciences in Warsaw. Rietveld refinement reveals that the crystalline content of cracks is indeed different than the depositional environment. Specimens on display can be subjected to changes in humidity and temperature for a long time. Based on the XRD results a crystallochemical transformation pathway is proposed. Thus, the results of our work may provide practical guidance how to prevent disintegration of the amber nuggets.

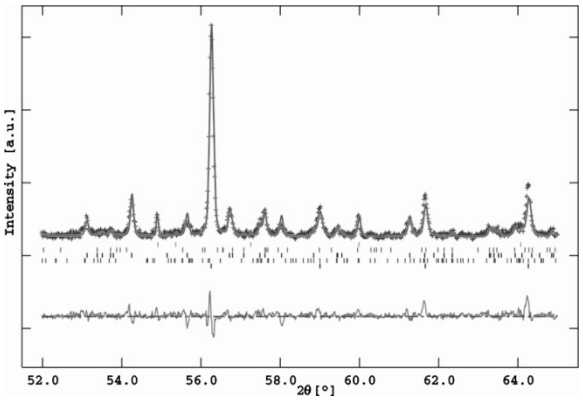

Figure 1. Results of Rietveld refinement of the crystalline content of cracks in amber nuggets.

[1] A. P. Wolfe, R. Tappert, K. Muehlenbachs, M. Boudreau, R. C. McKellar, J. F. Basinger, A. Garrett, *P. Roy. Soc. B: Biol. Sci.,* **276** (2009) 3403-3412.
[2] I. Pakutinskiene, J. Kiuberisa, P. Bezdicka, J. Senvaitiene, A. Kareiva *Can. J. Anal. Sci. Spect.,* **52** (2007) 287-294.
[3] B. Kosmowska-Ceranowicz, C. Kulicki, M. Kuzniarski *Prace Muzeum Ziemi* **49** (2008) 109.

P-27

Local electronic and crystal structure of $CuCr_2Se_4$ doped with Ge

P. Zajdel[1]*, E. Maciążek[2], J. Goraus[1], I. Jendrzejewska[2], A. Bujak[1] and M. Telko[1]

[1]*Institute of Physics, University of Silesia, ul. Uniwersytecka 4 , 40-007 Katowice, Poland*
[2]*Institute of Chemistry, University of Silesia, ul. Szkolna 9 , 40-006 Katowice, Poland*

Keywords: spinel, germanium, selenides, XAFS

*e-mail: pawel.zajdel@us.edu.pl

Chromium based chalcogenide spinels (ACr_2X_4 where A=Zn, Cd, Hg, Cu, X=S, Se, Te) have been researched since 1960's due to their potential applications arising from significant Seebeck coefficient or colossal magnetoresistance [1,2]. Subsequently they were replaced by other compounds but are still promising for further development due to their relative ease of synthesis and great flexibility of the starting matrix.

Current research aims at the enhancement of their response to the magnetic field by increasing bond frustration present in the system through doping of the ferromagnetic metal $CuCr_2Se_4$ (Tc = 405 K) with germanium.

In the spinel structure, there are two possible sites for cation doping: tetrahedral (A) and octahedral (trigonal antiprismatic) (B). The nominal compositions of the germanium doped materials $CuCr_{1.80}Ge_{0.15}Se_4$, $CuCr_{1.80}Ge_{0.3}Se_4$ and $CuCr_{1.90}Ge_{0.15}Se_4$ aimed at locating them on the B site. The Ge occupancy refined from XRD was in all cases found to be under 0.15.

Therefore XANES and EXAFS studies were carried out on the CEMO beamline of the DORIS III storage ring in order to elucidate the local electronic and crystal structure around the dopant as well as its influence on the matrix.

The Ge K edges for the germanium doped spinels, presented in Figure 1, are located between spectra for GeSe (nominaly Ge^{2+}) and $GeSe_2$ (Ge^{4+}), which suggests that the formal oxidation state of germanium is forced by the matrix to be close to +3. Additionally, a systematic shift of edge (see inset in Fig. 1) is observed, indicating that Ge adopts to the charge imbalance caused by the different nominal chromium content.

In order to analyze the electronic structure of the solid solution a DFT based coherent potential approximation (CPA) calculations [3] of a hypothetical $CuCr_{1.80}Ge_{0.2}Se_4$ have been performed and will be compared to the experimental data.

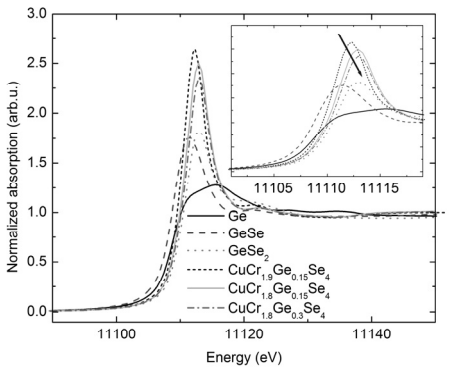

Figure 1. Ge K edges of the studied selenides. Inset shows increasing chemical shift of the Ge K absorption edge from GeSe towards $GeSe_2$.

Acknowledgments: The funding for the experiment EC20110679 was provided by the European Community's 7th Framework Programme (FP7/2007-2013) under grant agreement n° 312284 (CALYPSO).

[1] D.R. Parker, M. A. Green, S. T. Bramwell, A. S. Wills, J. S. Gardner, D. A. Neumann, *J. Am. Chem. Soc*. **126** (2004) 2710.

[2] P. Zajdel, A. Kisiel, J. Warczewski, J. Konior, LI Koroleva, J. Krok-Kowalski, P. Gusin, E. Burattini, G. Cinque, A. Grilli, R. Demin, *J. of Alloys and Comp.* **401** (2005) 145.

[3] K.Koepernik and H.Eschrig, *Phys. Rev. B* **59**, 1743 (1999), K. Koepernik, B. Velicky, R. Hayn, H. Eschrig, *Phys. Rev. B* **55** (1997) 5717.

P-28

X-ray fluorescence holography studies for an ordered and disordered Cu_3Au crystal

K. M. Dąbrowski*, D. T. Dul and P. Korecki

Institute of Physics, Jagiellonian University, Reymonta 4, 30-059 Kraków, Poland

Keywords: x-ray fluorescence holography; atomic structure determination; polycapillary optics

*e-mail: karol.dabrowski@uj.edu.pl

X-ray fluorescence holography (XFH) is a three-dimensional method of atomic structure imaging. The fine structure in directional dependence of fluorescence yield originates from an interference of the beam incident on the sample with waves scattered at the atomic sites [1]. Element sensitivity for multi-component crystals is feasible by measuring distinct fluorescence from particular kind of atoms. However, recently it was demonstrated that matrix effects, such as beam attenuation and indirect excitation result in losing chemical resolution, therefore a numerical correction for these effects is required [2].

In this work we demonstrate the XFH analysis performed for a Cu_3Au (001) single crystal sample in ordered and disordered phase. In the ordered $L1_2$ phase Cu atoms occupy three non-equivalent positions, therefore the measured signal is the sum of the three different local structure. The disordered fcc phase poses the same position of atoms as the ordered one but differ in the average occupancy of the atomic sites. This makes Cu_3Au an ideal test sample to demonstrate sensitivity of XFH to the change of site occupancy.

In the experiments we used a tabletop setup equipped with a low-power 50 watt Mo tube combined with collimating polycapillary optics and HOPG monochromator [3]. Cu K and Au L fluorescence spectra were collected using an energy resolved silicon drift detector. The transition from the ordered to the disordered phase was carried out through annealing and quenching the ordered sample. An x-ray fluorescence and a ToF-SIMS analysis showed that during this procedure polycrystalline thin Cu_2O layer precipitated on the sample. We show that the matrix effects correction restores chemical resolution in the XFH maps as well as it is able to remove the influence of the top layer.

Figures 1(a) and 1(b) show XFH maps recorded for Cu_3Au sample. Because of the similarity between $L1_2$ and fcc structures, the difference between the XFH maps recorded for different phases is small [figure 1(a)]. However, subtraction of Au and Cu maps [figure.1 (b)], clearly demonstrates the differences in the experimental data.

Figures 1(c) and 1(d) present electron density maps reconstructed from XFH data. The plots demonstrate full three-dimensional reconstruction of atomic positions. Moreover, the intensities of maxima agree with the theoretical electron density at the given atomic sites. This indicates the possibility of direct and precise determination of atomic sites occupancy using XFH.

The possibility of performing XFH experiments using a low power laboratory x-ray source reveal the possibility of future x-ray holographic experiments at SOLARIS [4].

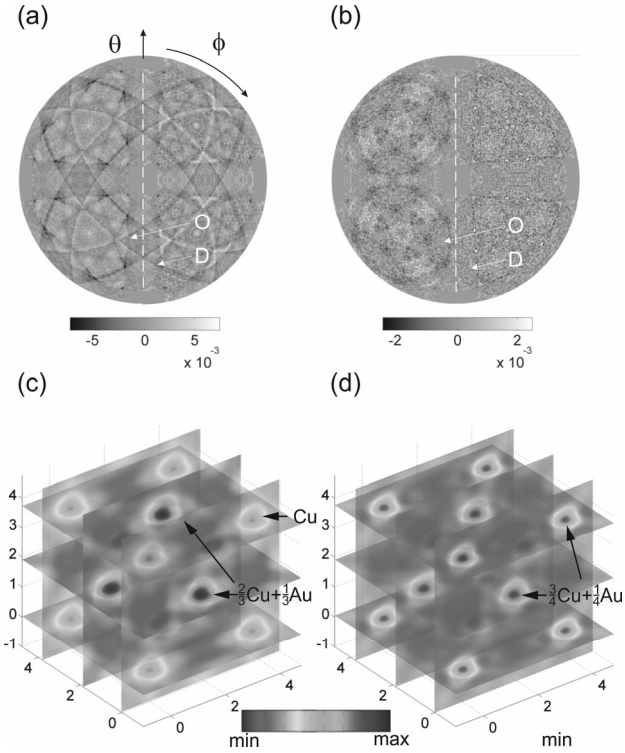

Figure 1. (a) XRF hologram recorded by measuring Cu fluorescence. (b) Holographic data obtained by subtraction of XRF holograms recorded for Cu and Au. (O, D) denotes ordered and disordered phase, respectively. (c,d) Three-dimensional linear regression reconstruction of the electron density from XFH maps recorded for Cu fluorescence from ordered (c) and disordered sample (d). Labels describe the theoretical average occupancies of atomic sites.

Acknowledgments: This work was supported by Polish National Science Center (DEC-2013/09/N/ST3/02309), and in the part by the KNOW Research Consortium through the Marian Smoluchowski fellowship.

[1] G. Faigel, G. Bortel, C. S. Fadley, A. S. Siminovici and M. Tegze, *X-Ray Spectrom.* **36** (2007) 3.
[2] D. T. Dul, K. M. Dabrowski and P. Korecki, *EPL (Europhysics Letters)* **104** (2013) 66001.
[3] K. M. Dabrowski and P. Korecki, *Nucl. Instrum. Methods Phys. Res. Sect.* B **285** (2012) 94.
[4] M. R. Bartosik et. al., *Rad. Phys. and Chem.* **93** (2013) 4-8.

P-29

High harmonic generation from a multi-jet gas puff target for FEL seeding

T. Fok [1]*, Ł. Węgrzyński[1], M. Kozlova[2], J. Nejdl[2], P.W. Wachulak[1], R. Jarocki[1], A. Bartnik[1] and H. Fiedorowicz[1]

[1]*Institute of Optoelectronics, Military University of Technology, Kaliskiego 2, 00-908 Warsaw,*
[2]*Institute of Physics, The Academy of Sciences of the Czech Republic, Na Slovance 2, 182 21 Prague*

Keywords: high harmonics generation, free-electron laser, seeding

*e-mail: tfok@wat.edu.pl

As a result of interaction of ultra-short, high power laser pulses with gases high-order harmonics generation (HHG) occurs. It is the most promising methods to obtain coherent radiation in the soft X-ray (SXR) and extreme ultraviolet (EUV) regions [1, 2]. This radiation is highly attractive for applications in various areas, including seeding of a free electron laser (FEL) [3].

Seeding of FEL with an external source will improve the temporal coherence, ensure high shot-to-shot stability and high peak power, and will decrease the saturation length. This method was presented e.g. on Spring-8 Compact SASE Source (Japan) [4] and FLASH FEL (Germany) [5].

In this paper we present the recent results of HHG experiments with the use of a multi-jet gas puff target, developed at the Institute of Optoelectronics, MUT [6]. The results should be useful for the development of an efficient, quasimonochromatic source of coherent EUV radiation [7], with potential application to FEL seeding.

Acknowledgments: The research was supported by LASERLAB-EUROPE III (grant agreement No. 284464, EC's Seventh Framework Programme), Ministry of Education of the Czech Republic (project Nos. CZ.1.07/2.3.00/30.0057 and ELI Beamlines CZ.1.05/ 1.1.00/02.0061).

[1] P. Jaegle, Coherent Sources of XUV Radiation, Springer 2006 (and references herein),
[2] J.G. Eden, *Progress in Quantum Electronics* **28** (2004) 197-246.
[3] G. Lambert, *et al.*, *Nature Physics* 4 (2008) 296.
[4] Belle Dumé, Free-electron laser benefits from 'seed' light, Physics World, Mar 12, 2008
[5] Photon Science 2013, Highlights and Annual Report, Light Source, 93
[6] P.W. Wachulak, *et al.*, *Nucl. Instr. and Meth. in Phys. Res. B* (2012),
[7] T. Fok, *et al.*, *PLP*, Vol. **6** (2014) 14-16.

P-30

Extreme ultraviolet surface modification of fluoropolymers for biocompatibility control

I. U. Ahad[1,2], M. Ayele[1]*, B. Butruk[3], B. Korczyc[1], B. Budner[1], D. Adjei[1], A. Bartnik[1] , H. Fiedorowicz[1], T. Ciach[3] and D. Brabazon[2]

[1]*Institute of Optoelectronics, Military University of Technology, 00-908 Warsaw, Poland*
[2]*Advanced Processing Technology Research Centre Dublin City University, Dublin 9, Ireland*
[3]*Department of Biotechnology and Bioprocess Engineering, Warsaw University of Technology, 00-645 Warsaw, Poland*

Keywords: polymer surface modification, biocompatibility control, extreme ultraviolet (EUV)

*e-mail: mgayele@wat.edu.pl

Recent advancements in organic materials as “Green Alternatives” in various applications dramatically increased the requirement of efficient surface modification technique which would be able to tune the surface properties without altering mechanical properties of bulk materials[1][2]. The thickness of such materials (e.g biosensors, bio-mimetic artificial implants, artificial muscles, organic electrodes for biomedical engineering applications, and many more) will be limited to few millimeters or up to few hundred microns in particular applications. The conventional ultraviolet (UV) and plasma based techniques produce undesirable effects such as alteration of bulk material properties. This problem limit their applicability in biomedical engineering applications. Extreme ultraviolet (EUV) photons with energies from 30 eV up to 250 eV (corresponding to wavelengths in vacuum from 40 nm to 5 nm respectively) have limited penetration depths (up to 100 nm) in to the polymer surface[3]. Therefore the modification of physical and chemical properties will be limited to upper layer surface and the bulk properties will remain intact. EUV photons can be produced by synchrotron radiation (SR) sources or laser-plasma sources. The limited number and accessibility to large scale SR facilities encouraged the development of compact laboratory EUV sources. Such sources are currently being used by a few groups to investigate new applications of EUV technology in various fields.

This study demonstrates the use of EUV surface modification technique in biomedical engineering applications. Micro and nano-patterned surfaces, functionalized with special reactive groups are often desirable for improved biocompatibility of various polymers in vascular prosthesis and tissue engineering applications. A number of polymers such as PC, PET, PTFE and PVF have been irradiated with a laser-plasma EUV source based on a double-stream gas-puff target, irradiated with the 3 ns/0.8J Nd:YAG laser pulse at 10Hz [4]. The EUV irradiated samples were characterized through SEM, AFM, XPS and water contact angle measurements. The irradiation of EUV photons on

polymer surfaces resulted in the formation of nano- and micro-patterning. It has been demonstrated that tuning of physical and chemical properties is possible by EUV surface modification. Increased surface roughness up to many folds, controlled wettability (increased hydrophilicity or hydrophobicity as per requirements) and improved biocompatibility levels (improved cell attachment and cell adhesion) have been observed. Fig. 1 demonstrates improved cell attachment of L929 fibroblasts on EUV irradiated PTFE surface (b) as compared to pristine control sample (a).

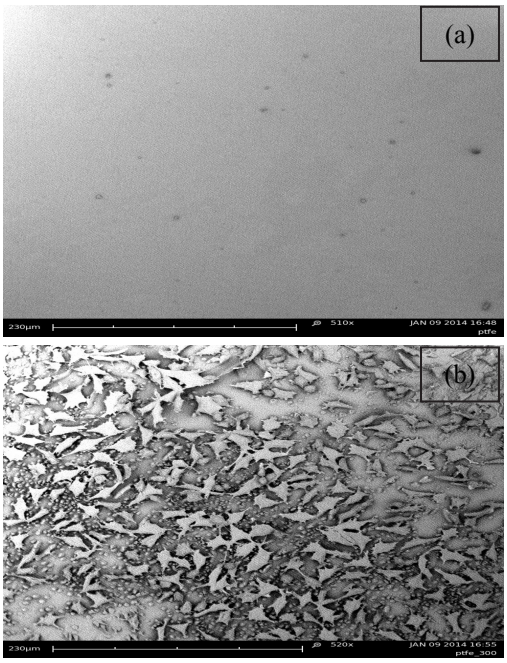

Fig. 1 SEM images of washed PTFE surfaces after incubated with L929 fibroblasts for 24 hours (a) pure sample, (b) irradiated with 300 EUV shots.

Acknowledgments: The authors acknowledge financial support from the EU FP7 Erasmus Mundus Joint Doctorate Program EXTATIC under framework partnership agreement FPA-2012-0033. Laserlab Europe project (No. 284464).

[1] Y. Kanbur, M. Irimia-Vladu, E. D. Głowacki, G. Voss, M. Baumgartner, G. Schwabegger, L. Leonat, M. Ullah, H. Sarica, S. Erten-Ela, R. Schwödiauer, H. Sitter, Z. Küçükyavuz, S. Bauer, and N. S. Sariciftci, *Org. Electron*. **13** (2012) 919-924.

[2] M. Irimia-Vladu, E. D. Głowacki, G. Voss, S. Bauer, and N. S. Sariciftci, *Mater. Today* **15** (2012) 340–346.

[3] I. U. Ahad, A. Bartnik, H. Fiedorowicz, J. Kostecki, B. Korczyc, T. Ciach, and D. Brabazon, *J. Biomed. Mater. Res. Part A* (2013) [DOI: 10.1002/jbm.a.34958]

[4] A. Bartnik, H. Fiedorowicz, R. Jarocki, J. Kostecki, M. Szczurek, and P. W. Wachulak, *Nucl. Instruments Methods Phys. Res. Sect. A* **647** (2011) 125-131.

P-31

X-Ray Absorption and Resonant Photoemission studies of Fe doped $SrTiO_3$ films for different parameters of PLD deposition

J. Kubacki[1]*, D. Kajewski[1], A. Koehl[2] and J. Szade[1]

[1]*Silesian Centre of Research and Education, Institute of Physics, University of Silesia, 75 Pulku Piechoty 1, 141-500 Chorzow, Poland*
[2]*Peter Gruenberg Institute and JARA-FIT, FZ Juelich, D-52425 Juelich, Germany*

Keywords: synchrotron radiation, thin films, X-ray absorption, photoelectron spectroscopy

*e-mail: jerzy.kubacki@us.edu.pl

The $SrTiO_3$ is an insulator with the energy gap of 3.2 eV, for which the nature of the resistive switching process was described in the filamentary model [1]. The STO thin film has promising properties of the resistive switching for future RRAM application [2]. Doping by acceptor and donor allow tuning of the electrical properties for this material. The doping is crucial for the electronic structure, especially in the energy gap. Last time the most of studies of Nb, Mn and Fe doping STO films were performed from the resistive switching process point of view [3-5]. In our work we focused on Fe doping and its contribution to the valence band. Three samples with different amount of defects were prepared by changing the PLD parameters, i.e. oxygen pressure and energy of laser. In order to describe the contribution of the Fe and main components to the electronic structure, the X-Ray Absorption Spectroscopy and Resonant Photoemission Studies were performed.

The epitaxial Fe doped STO films with thickness of about 20 nm were obtained by PLD (Pulsed Laser Deposition) method on the Nb doped $SrTiO_3$ single crystal substrate. Three samples 2% Fe doped $SrTiO_3$ were studied for three various parameters of PLD deposition. The samples were annealed in UHV conditions prior to study at 150ºC, 300 ºC and 630 ºC.

The Ti $L_{2,3}$, Fe $L_{2,3}$ and O K XAS spectra were obtained with used to of the two methods – total electron yield (TEY) measured by the drain current and Auger electron yield (AEY). The methods have different surface sensitivity.

The XAS spectra showed that Fe presents in the sample in two oxidation states 2+ and 3+. The relative content of these states is dependent on the deposition parameters.

The different parameters of the film deposition led to changes in the structure of the valence band, especially in partial density of states (PDOS) for broad Fe^{2+} structure and intensity of the top valence band Fe^{3+} components.

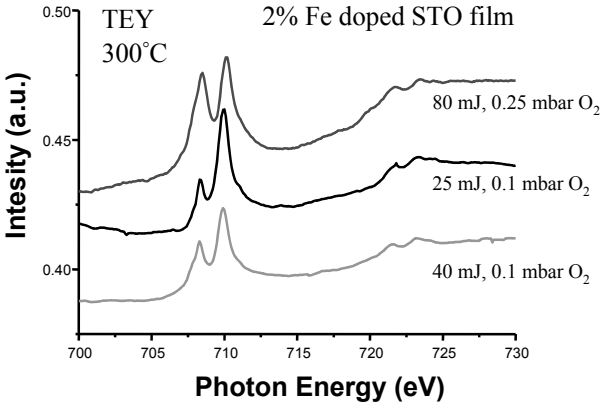

Figure 1. XAS spectra of the 2% Fe doped $SrTiO_3$ film obtained in TEY mode for various parameters deposition of the films after annealed at 300ºC.

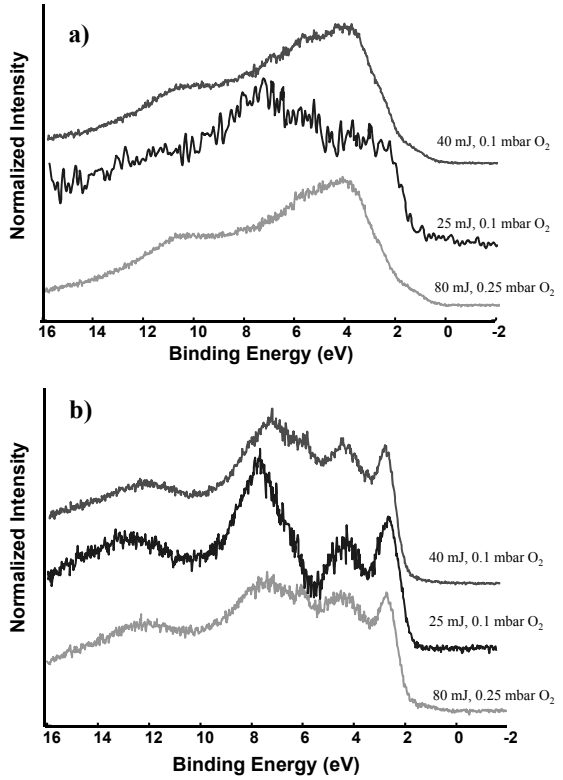

Figure 2. Partial density of Fe 3d states (PDOS) obtained as the difference between the valence band at: a) 708.3, b) 710 eV (on resonance) and 700 eV (off resonance), recorded from the various types 2% Fe doped $SrTiO_3$ films, annealed at 300ºC.

[1] K. Szot, W. Speier, G. Bihlmayer, R. Waser, *Nature Materials* **5** (2006) 312.

[2] K. Szot, R. Dittmann, W. Speier, R. Waser, *Physica Status Solidi –Rapid Research Letters* **1** (2007) R86.

[3] R. Münstermann, R. Dittmann, K. Szot, S. Mi, C. L. Jia, P. Meuffels, R. Waser *Applied Physics Letters* **93**, (2008) 023110.

[4] J. Kubacki, D. Kajewski, A. Koehl, M. Wojtyniak, R. Dittmann, J. Szade *Radiation Physics and Chemistry* **93** (2013) 123-128.

[5] A. Koehl, D. Kajewski, J. Kubacki, C. Lenser, R. Dittmann, P. Meuffels, K. Szot, R. Waser, J. Szade, *Phys.Chem. Chem. Phys.* **15** (2013) 8311-8317.

P-32

Raman scattering as a tool to study structural changes induced in silicon wafers by Intense Femtosecond X-ray Free-Electron Laser pulses

W. Szuszkiewicz[1]*, K. Gas[1], R. Sobierajski[1], D. Klinger[1], J. B. Pełka[1], M. Klepka[1], P. Dłużewski[1], P. Jarocki[1], A. Kamińska[2], T. Balcer[3], J. Chalupský[3], J. Gaudin[3], V. Hájková[3], T. Burian[3], A. J. Gleeson[4], L. Juha[3], H. Sinn[5], K. Tiedtke[6], S. Toleikis[6] and L. Vyšin[3]

[1]*Institute of Physics PAS, Al. Lotników 32/46, 02-668 Warszawa, Pola*nd
[2]*Institute of Physical Chemistry PAS, ul. Kasprzaka 44/52, 01-224, Warszawa, Poland*
[3]*Institute of Physics, Academy of Sciences of the Czech Republic, Na Slovance 2, 182 21 Prague 8, Czech Republic*
[4]*CCRLC Daresbury Laboratory, Warrington, Cheshire WA4 4AD, United Kingdom*
[5]*European XFEL, DESY, Notkestr. 85, D-22607 Hamburg, Germany*
[6]*Hasylab, DESY, Notkestr. 85, D-22607 Hamburg, Germany*

Keywords: raman scattering, free-electron laser

*e-mail: szusz@ifpan.edu.pl

The irradiation of solid materials with femtosecond extreme ultraviolet (XUV) pulses extensively studied in recent years offers a number of advantages. First of all it permits a high degree of electronic excitation but with a strongly reduced influence of optical nonlinearities i.e., multiphoton absorption and free-carrier absorption. Moreover, for frequencies range between the plasma frequency and the frequency of the innershell absorption edge, the absorption length for solids varies over orders of magnitude. Therefore, ultrashort XUV pulses allow the preparation of rather well-defined excitation conditions for a variety of excitation depths and optical laser ablation has important practical implications, for example in data storage technology.

The recent development of short wavelength (XUV and X-ray) free-electron lasers, also known as fourth-generation X-ray light sources, enables the study of interaction of ultrashort, femtosecond, intense X-ray pulses with matter. We report on the results of experiments performed at FLASH free-electron laser facility on the interaction of ultrashort high intensity 1012 - 1014 W/cm^2 XUV (λ = 13.5 nm) pulses with solid silicon surfaces at the grazing angle below the critical angle. Silicon is a suitable material for comparisons, broadly studied with femtosecond optical lasers and picoseconds XUV lasers. Moreover it is a standard substrate material for the optical coatings in XUV optics where radiation damage is a key issue. Samples were irradiated by single shots of FLASH radiation. An analysis of possible mechanisms of different, intensity dependent stages of the surface damage requires a knowledge about the spatial distribution of polymorphic crystal structures (amorphous Si, selected pressure-induced phases) introduced by the irradiation. It is demonstrated that Raman scattering technique is an efficient, non-destructive method to detect various Si crystal phases and to estimate the thickness of amorphous layer with an accuracy high enough to make possible further modeling of physical phenomena.

Acknowledgments: We would finally thank the FLASH team at DESY for their continuous support, and we gratefully acknowledge the support for access to FLASH by the European Community under contract RII3-CT-2004-506008 (IA-SFS). This work was partially supported by the Polish National Science Center (Grant No. DEC-2011/03/B/ST3/02453), and by the European Regional Development Fund within the Innovative Economy Operational Programme 2007-2013 No POIG.01.01.02-00-008/08 and No POIG.02.01-00-14-032/08.

P-33

SR diffraction studies of the structural inhomogeneities of $CaCu_3Ti_4O_{12}$

W.A. Sławiński[1(a)], R. Przeniosło[1]*, D. Wardecki[1], I. Sosnowska[1], A. Hill[2(b)], A.N. Fitch[2] and M. Bieringer[3]

[1]*Institute of Experimental Physics, University of Warsaw, Hoża 69, 00-681 Warsaw, Poland*
[2]*European Synchrotron Radiation Facility, BP220, F38042, Grenoble, France*
[3]*Department of Chemistry, University of Manitoba, Winnipeg, R3T 2N2,Canada*

Keywords: colossal dielectric constant, perovskite, oxides

*e-mail: radek@fuw.edu.pl

$CaCu_3Ti_4O_{12}$ is a material which shows colossal dielectric constants ~10^4 over a wide range of temperatures and frequencies [1-3]. A dielectric anomaly is observed in $CaCu_3Ti_4O_{12}$: between 100 K and 200 K [1-3] the dielectric constant, ε, jumps up to values about 10^6 between 200K and 600K. At higher temperatures there are pronounced maxima of ε in the 650K – 1050 K region [4,5]. No structural phase transitions were reported from X-ray and neutron diffraction studies of $CaCu_3Ti_4O_{12}$ up to 1270K [3,6].

The crystal structure of $CaCu_3Ti_4O_{12}$ has been studied by using the high resolution synchrotron radiation based X-ray powder diffraction [7]. The observed X-ray diffraction patterns show pronounced Bragg peak asymmetries which should not be present assuming the commonly accepted cubic crystal structure of $CaCu_3Ti_4O_{12}$ described by the space group *Im*-3. Several structural models are discussed. The first model assumes a coexistence of two phases with the cubic symmetry (both space group *Im*-3) and different lattice constants. Next models are based on subgroups of the cubic space group *Im*-3. The best agreement is obtained with the two-phase cubic model [7]. The single cubic phase model gives worse agreement as compared with the two-phase cubic one. None of the models based on the subgroups *C*2/*m, Immm* or *P*2/*c* gives better agreement than the two-phase cubic model.. An inspection of the peak shape shows that for some peaks, see e.g. (4,4,4) in Fig. 1e,f, the two-phase cubic model gives a better agreement.

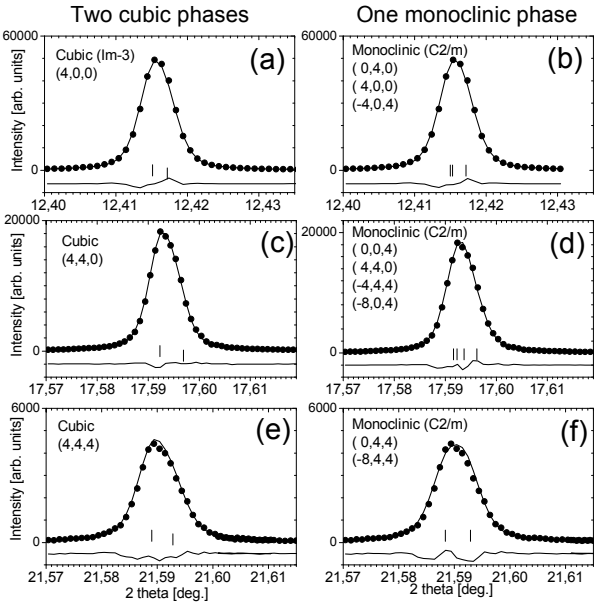

Figure 1. (from [7]) Parts of SR diffraction patterns of $CaCu_3Ti_4O_{12}$ (experimental data = solid symbols). The measurements were performed with $\lambda = 0.39996$ Å at RT. Panels a,c,e present the refinement with the two-phase cubic model, space group Im-3 (solid line). Panels b,d,f present the refinement with the monoclinic model, space group *C*2/*m* (solid line). Ticks indicate the positions of the Bragg peaks due to both cubic phases (a,c,e) and the monoclinic phase (b,d,f). The bottom solid lines are difference curves. The corresponding (hkl) are listed.

Acknowledgments: Thanks are due to the Ministry of Science and Higher Education (Poland) for funding the project No. 2011/01/B/ST3/02401 and funding access to the ESRF facilities. MB acknowledges support from NSERC.

[(a)]W. Sławiński present address:
Centre for Materials Science and Nanotechnology, Department of Chemistry, University of Oslo, PO Box 1126, 0315 Oslo, Norway
[(b)]A. Hill present address: Johnson Matthey Technology Centre, Savannah, GA, USA.

[1] M. A. Subramanian, D. Li, N. Duan, B.A. Reisner, A. W. Sleight *J. Solid State Chem.* **151** (2000) 323.
[2] C. C. Homes, T. Vogt, S. M. Shapiro, S. Wakimoto, A. P. Ramirez *Science,* **293** (2001) 673.
[3] A. P. Ramirez, M. A. Subramanian, M. Gardel, G. Blumberg, D. Li,T. Vogt, S. M. Shapiro, *Solid State Comm*, **115** (2000) 217.
[4] M. N. Zhang, K. B. Xu, G. J. Wang, C. C. Wang, *Chinese Science Bulletin*, 58 (2000) 713.
[5] A. Onodera *, et al. Japanese J. of Appl. Phys.*, **47** (2008) 7753.
[6] A. Bochu, M. N. Deschiseaux, J. C. Joubert. A. Collomb, J. Chenavas, M. Marezio, *J. Solid State Chem.*, **29** (1979) 291.
[7] W. A. Sławiński, R. Przenioslo, D. Wardecki, I. Sosnowska, A. Hill, A. N. Fitch, M. Bieringer, *Materials Research Express*, **1** (2014) 016306.

P-34

$SrRuO_3$ Valence Band study by means of Resonant Photoelectron Spectroscopy

S. Grebinskij*, S. Mickevičius, V. Lisauskas and M. Senulis

Semiconductor Physics Institute of Center for Physical Science and Technology, A. Goštauto St. 11, LT-01108 Vilnius, Lithuania.

Keywords: synchrotron radiation, photoelectron spectroscopy, partial density of states

*e-mail: segre@pfi.lt

Thin epitaxial $SrRuO_3$ films were studied by means of resonant photoelectron spectroscopy using UV synchrotron radiation in the energy range 37 – 81 eV. Obtained spectra show evident Fano behavior [1,2], however cannot be successfully fitted with only one Fano resonance in whole binding energy (BE) range. According to the resonance energy E_R, width w and asymmetry parameter q valence band may be divided into two BE regions with actually constant, but strongly different two parameters sets: $E_R = 51.8 \pm 0.7$ eV, $w = 10.1 \pm 0.4$ eV, $q = 1.14 \pm 0.16$ and $E_R = 5.0 \pm 0.4$ eV, $w = 4.5 \pm 0.6$ eV, $q = 0 \pm 0.05$ for Ru 4d [-0.4..2.3] eV and O 2p [5.0..8.0] eV regions respectively. Figure. 1 illustrate the partial density of states (DOS) from different type of Ru 4d states obtained by fitting measured constant initial state spectra with two Fano resonances and parameters listed above.

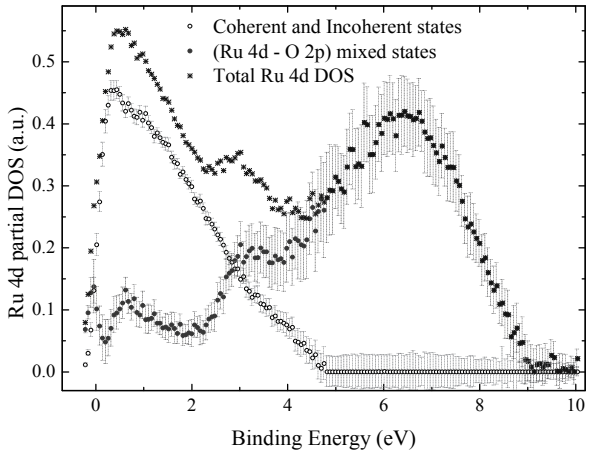

Figure 1. Ru 4d partial DOS. Error bars corresponds to the standard error of fitting.

DOS dominating in Ru 4d region may be attributed to coherent and incoherent states of ruthenium, while dominating in O 2p region to (Ru 4d – O 2p) Ru states in an agreement with theoretical calculations [2,3].

Acknowledgments: This work was partially supported by DESY and the European Commission under Grant Agreement ELISA 226716, IA-SFS Project No. DESY-D-I-20100305 EC.

[1] S. Grebinskij *at al*., *Rad. Phys. Chem.* **B80** (2011) 1140.
[2] S. Grebinskij *at al*., *Phys. Rev.* **B87** (2013) 035106.
[3] E.B. Guedes *at al*., *Phys. Rev.* **86** (2012) 235127.

P-35

Au covered ZnO layers irradiated by femtosecond laser pulses

D. Klinger[1]*, R. Minikayev[1], I. Yatsyna[1], E. Lusakowska[1], E. Guziewicz[1], A. Reszka[1], W. Caliebe[2], V. Hajkova[3], T. Burian[3], L. Juha[3], M. Nagasono [4], M. Yabashi [4] and R. Sobierajski[1]

[1]*Institute of Physics, Polish Academy of Sciences, Warsaw, Poland*
[2] *Hasylab at DESY, Hamburg, Germany*
[3]*Institute of Physics of the ASCR, Prague, Czech Republic*
[4]*RIKEN/SPring-8 Kouto 1-1-1, Sayo, Hyogo, 679-5148, Japan*

Keywords: synchrotron radiation, free electron laser, ZnO, surface morphology, crystal structure

*e-mail: Dorota.Klinger@ifpan.edu.pl

We report on the results of structural modifications induced in ZnO by single-shot irradiations with intense femtosecond VUV pulses. The radiation was generated by a free electron laser [1] operating in the wavelength range of 51-60 nm. The studied samples were thin ZnO layers on Si substrate, with and without Au overlay.

The samples were treated according to the irradiation procedure described in [2]. As a result, the sample surface was irradiated in hundreds of spots arranged in rows. The distance between spots was typically approx. 300 μm to avoid possible overlapping of defects induced in neighboring areas [3]. The spot area, depending on fluency, material properties and irradiation geometry, changed from few up to few tens μm^2.

After irradiation, the samples were examined by means of the atomic force microscopy, interference-polarizing microscopy and **c**athodoluminescence. Further structural characterization was done with synchrotron radiation at the DORIS W1.1 beamline in Hasylab with the monochromatic X-ray beam of wavelength 1.54056 Å. The measurements were recorded in a 2θ scan mode in the grazing incidence geometry. The ω-2θ scans were also recorded in order to find the structural changes in the near-surface layers affected by the irradiation.

Acknowledgments: The research leading to these results has received funding from the European Community's Seventh Framework Programme (FP7/2007-2013) under grant agreement no 226716 and the Polish National Science Center, Grant No. DEC-2011/03/B/ST3/02453.

[1] T. Shintake, et al., *Nature Photon.* **2** (2008) 555–559.
[2] R. Sobierajski,et al., *J. Instrumen.* **8** (2013) 02010.
[3] W. Wierzchowski, et al., *Radiat. Phys. Chem.* **80** (2011) 1036-1040.

P-36

Deposition and processing of thin-layer lead cathodes for hybrid niobium superconducting RF photoinjector

J. Lorkiewicz[1]*, R. Nietubyć[1], M. Barlak[1], J. Sekutowicz[2], R. Mirowski[1] and J. Witkowski[1]

[1]*National Centre for Nuclear Research, 7,A. Soltana Str, 05-400 Otwock-Swierk, Poland*
[2]*Deutsches Elektronen Synchrotron 85, Notkestrasse, 22-607 Hamburg, Germany*

Keywords: superconducting RF injector, thin layer lead cathode, UHV arc deposition, heat treatment

*e-mail: jerzy.lorkiewicz@ncbj.gov.pl

The idea of a Nb/Pb hybrid superconducting electron injector was proposed within the last decade [1]. Thin-layer lead cathode was coated onto the rear wall of a 1.6 cell RF electron photoinjector built in TESLA technology. It is destined for superconducting linacs of free electron lasers (FELs) which provide up to 1 mA of mean current in 10^5 Hz repeated, 1 nC bunches to a FEL undulator. Though the usefulness of this solution was proved in a single proof-of-principle experiment [2] the quantum efficiency (QA) of different photoinjectors was not reproducible and depended on the cathode preparation. The tests indicated that reaching a high layer smoothness at its sufficient thickness (1-2 μm) is necessary to operate such injector. Though UHV arc lead coating on niobium substrate assured the highest QA values reached so far [1] the biggest disadvantage of this method is the presence of surface extrusions formed by lead droplets detached from the cathodes of arc devices. To overcome this problem two approaches were proposed at NCBJ within last year: 1. fast coating in a short planar arc device followed by Pb layer melting and recrystallization in a pulsed plasma ion beam in a rod plasma injector and 2. lead deposition in arc device equipped with angular magnetic filter to remove microdroplets from lead plasma stream. The first procedure was effective in smoothing only the lead surface extrusions with lateral size up to ca.25 μm using Ar^+ ion pulses of 1.5 J/cm^2 fluency. Further increasing of the fluency led to discontinuities of a 2 μm thick layer. Works on improving the niobium surface wettability with molten lead are underway. Deposition with droplets filter led to droplets density reduction in a surface layer to below 10/mm^2, their size to ca 10 μm and to satisfactory cleanliness of the film. The obtained Pb layers will be checked as photocathodes for QA and dark current in the RF injector at Helmholz-Zentrum Dresden-Rossendorf.

Acknowledgments: Studies were supported with European Coordination in Accelerator Research, a part of FP7.

[1] J. Smedley, T. Rao, J. Sekutowicz, *Physical Review Special Topics – Accelerators and Beams* **11** (2008) 013502.
[2] J. Lorkiewicz, R. Nietubyć, M. Barlak, R. Mirowski, A. Bartnik, J.Kostecki, J. Sekutowicz, P. Kneisel, A. Malinowska and J. Witkowski., *Physica Scripta T* (2014), in press.

P-37

Threshold fluence of ultra-short VUV laser pulse for structure modification of gallium arsenide

D. Klinger[1], E. Lusakowska[1], J. B. Pelka[1], D. Żymierska[1]*, W. Wierzchowski [2], K. Wieteska [3], J. Chalupský[4], V. Hájková[4], T. Burian[4], L. Juha[4], K. Tiedtke[5], S. Toleikis[5], H. Wabnitz[5], M. Nagasono[6], M. Yabashi[6] and R. Sobierajski[1]

[1]*Institute of Physics, PAS,32/46, Al. Lotników Str, 02-668 Warsaw, Poland*
[2]*Institute of Atomic Energy POLATOM, 05-400 Świerk-Otwock, Poland*
[3]*Institute of Electronic Materials Technology, 133, Wólczyńska Str, 01-919 Warsaw, Poland*
[4]*Institute of Physics, Academy of Sciences of the Czech Republic, Na Slovance 2, 182 21 Prague 8,Czech Republic*
[5]*HASYLAB/DESY, Notkestr., 85 D-22607 Hamburg, Germany*
[6]*RIKEN/SPring-8 Kouto 1-1-1, Sayo, Hyogo, 679-5148, Japan*

Keywords: synchrotron radiation, free electron laser, gallium arsenide, surface morphology, crystal structure

*e-mail: Danuta.Zymierska@ifpan.edu.pl

Damage processes induced by laser pulses lead to the formation of specific morphological structures of sizes in micrometer and nanometer scales [1,2]. In the current work we present the investigations of gallium arsenide modified by femtosecond laser pulse [3]. The irradiations sources were free electron lasers [4,5] operating in the wavelength range of 32-51 nm.

The samples were examined by the interference-polarizing microscopy and atomic force microscopy to determine threshold values of laser beam fluence for creation of different morphological structures.

The X-ray diffraction was used to examine the structural changes in the near-surface layer in irradiated region. The structural characterization was done with synchrotron radiation at the DORIS W1.1 beamline in Hasylab with the monochromatic beam of wavelength 1.54056 Å. The measurements were recorded in a 2θ scan mode in the grazing incidence geometry. The ω-2θ scans were also recorded in order to find the structural changes in the near-surface layers affected by the irradiation.

The deformation stress was studied in back-reflection geometry by means of white beam projection topography at the F1 experimental station of DORIS in Hasylab.

[1] Pelka J.B, *Rad. Phys Chem.* **78** (2009) S46-S52.
[2] R. Sobierajski *et al., Proc. SPIE* **7361** (2009) 736107.
[3] R. Sobierajski *et al., J. Instrumen.* **8** (2013) 02010
[4] T. Shintake *et al., Nature Photon.* **2** (2008) 555–559
[5] V. Ayvazyan *et al. Phys. Rev. Lett.* **88** (2002) 104802.

P-38

Low temperature structure transformation of Ni doped $La_{2-x}Sr_xCuO_4$

R. Minikayev[1]*, A. Malinowski[1], W. Szuszkiewicz[1], V. Bezusyy[1] E. Dynowska[1] and A. T. Bell[2]

[1]*Institute of Physics PAS, Al. Lotników 32/46, 02-668 Warszawa, Poland*
[2]*Hasylab, DESY, Notke str. 85, D-22607 Hamburg, Germany*

Keywords: synchrotron radiation, phase transition, structures of high-temperature superconductors.

*e-mail: minik@ifpan.edu.pl

For more than two decades, the $La_{2-x}Sr_xCuO_4$ (LSCO) high temperature superconductors with the K_2NiF_4 (SG *I*4/*mmm*) structure are a subject of research [1, 2]. Doping the LSCO with magnetic elements such as Fe, Co, Ni destroys the superconductivity. For more thorough understanding the structure changes, determination of the temperature- dependent structure evolution in different LSCOs comprising a transition metal may be helpful. In this work, we focus on Ni-doped LSCO. Previous studies [3, 4] show mainly the low temperature structure transformation of $La_{2-x}Sr_xCuO_{4+\delta}$ whereas the information about Ni doped materials is still missing. The aim of present study is to fill the gap in this knowledge. The polycrystalline samples of tetragonal $La_{1.85}Sr_{0.15}Cu_{1-x}Ni_xO_4$ (Ni – 2% and 19%) were synthesized by means of a conventional solid-state reaction method. The XPD measurements were carried out at B2 beamline (Hasylab/DESY), using the Debye–Scherrer experimental geometry. The applied temperature range was from 10 K to 300 K. Crystallographic characterisation and structure refinement was done with help of Fullprof.2k (v. 2.70) program [5]. The temperature lattice parameters, free atomic position evolution and phase transition temperature are determined. The present results are discussed on the basis of earlier data.

[1] J. W. Halley *Theories of high temperature superconductivity* (Addison-Wesley, Reading, MA, 1988)
[2] B. Brodsky, R. C. Dynes, K. Kitazawa, H. L. Tuller *High-temperature superconductors* (Materials Research Society, Pittsburgh, 1988)
[3] K. Yamada, C. H. Lee, K. Kurahashi, J. Wada, S. Wakimoto, S. Ueki, H. Kimura, Y. Endoh, S. Hosoya, G. Shirane, R. J. Birgeneau, M. Greven, M. A. Kastner, and Y. J. Kim, *Phys. Rev. B* **57**(10) (1998) 6165.
[4] R. Moret, J. P. Pouget and G. Colli *Europhys. Lett.* **4** (1987) 365.
[5] J. Rodriguez-Carvajal, *Newslett. IUCr Commission Powd. Diffr*., **26** (2001) 12.

P-39

Intense synchrotron radiation sources in probing the biostructures and life processes

J. B. Pełka*

Institute of Physics, Polish Academy of Sciences, Al. Lotników 32/46, 02-668 Warsaw, Poland

Keywords: synchrotron radiation, free-electron laser, biostructures, life science

*e-mail: pelkay@ifpan.edu.pl

Unique properties of 3rd generation synchrotron radiation (SR) sources have opened-up, about 30 years ago, new opportunities of probing the structures and processes of life. Intense and stable SR beams, together with countless improvements both in the experimental and computational techniques, contributed to a substantial progress in understanding molecular foundations of many biological phenomena. Well known examples are here the rapid development of macromolecular crystallography with atomic resolution as well as studies of biochemical reactions dynamics in the picosecond time domain.

The history repeats itself over the last decade, due to a rapid development of the 4th generation sources of synchrotron radiation, the short-wavelength (SASE) FEL lasers.

SASE-FELs can produce tunable monochromatic radiation in ultrafast femtosecond pulses with a peak power up to several GW, in the wide range of wavelength including hard X-rays. With new methods emerging to fully exploit unique emission properties of the FELs, new qualities in probing the secrets of life with unprecedented temporal and spatial resolution are expected.

Some of the key experimental techniques have already been implemented and their invaluable potential confirmed. Included are, among other, new techniques of structure determination without the need of conventional crystallization, applicable both to large biomolecules and molecular complexes, a possibility of obtaining the precise structural information by collecting diffraction patterns of a large number of small nanocrystals (known as serial nanocrystallography) and imaging of small objects with a spatial resolution close to diffraction limit. Underway are also developments of new techniques dedicated to ultrafast dynamic study of biochemical processes with the femtosecond resolution.

This poster presentation is focused on chosen examples of some newly emerging experimental techniques exploiting intense SR x-ray beams for biology-related research.

P-40

Energy transport by hot electrons in c-Si irradiated with 5.5 and 12 keV photons

R. Sobierajski[1], A. Aquila[2], D. Klinger[1], I. Yatsyna[1], T. Burian[3], J. Chalupský[3], P. Dłużewski[1], V. Hájková[3], Y. Inubushi[4], M. Klepka[1], T. Koyama[5], H. Ohashi[4,5], C. Özkan[2], K. Tonoe[5], M. Yabashi[4] and J. Gaudin[2,6]

[1]*Institute of Physics, PAS Al. Lotników 32/46, Warsaw, PL-02-668, Poland*
[2]*European XFEL GmbH, Albert-Einstein-Ring 19, Hamburg, D-22671, Germany*
[3]*Institute of Physics, ASCR, Na Slovance 2, Prague 8, 182 21, Czech Republic*
[4]*RIKEN/SPring-8 Kouto 1-1-1, Sayo, Hyogo, 679-5148 Japan,*
[5]*Japan Synchrotron Radiation Research Institute (Japan)*
[6]*Univ. Bordeaux, CEA, CNRS, CELIA (Centre Lasers Intenses et Applications) UMR5107, F-33405 Talence, France*

Keywords: free-electron laser, energy transport, phase transitions in solids

The rapid development of a new generation of X-ray radiation sources providing ultrashort (from atto- to femtoseconds) pulses creates unique possibilities for generating high energy density states of matter. Instruments, like free-electron lasers (FELs) produce pulses of very high intensity and allow to extend the optical studies of radiation induced phase transitions of solids. The excitation of solid materials with x-ray femtosecond pulses offers a number of advantages over irradiation with femtosecond optical lasers. First of all the energy deposition process is not influenced by optical nonlinearities i.e. multiphoton absorption and free carrier absorption. Moreover the absorption depth can be varied over many orders of magnitude. E.g. for silicon it changes from a few nanometres up to hundreds of microns. Therefore, ultrashort X-ray pulses allow the preparation of well-defined excitation conditions in variable sample volumes and thus to study the energy transport processes.

Single shot irradiations of the Si flat mirror were performed at SACLA FEL facility at 5.5 and 12 keV photon energies, at grazing angles below and above critical angle. Similar morphology of the exposed spots was observed for all irradiation conditions. TEM images of the cross-section show that the radiation induced structural modification of materials is related to melting of Si and its resolidification. The observed structural modifications have threshold nature. The experimental damage thresholds in case of the irradiations above the critical angle [1] are close to the energy density required for melting of Si (approx. 0.9 eV/atom). The energy transport by hot electrons does not significantly influence the energy density distribution over the sample depth due to relatively high excited volume.

The experimental damage thresholds are the highest in case of the irradiations below the critical angles. In these cases the energy density of the radiation absorbed at the sample's surface can reach above a melting threshold without any structural modification. This may be explained by the transport of the energy out of the excitation volume (limited to the absorption skin depth) by hot electrons on the time scales shorter than the one typical for the electron-phonon coupling (~2 ps for Si). Modelling of the energy transport by ballistic electrons has been performed by means of the PENELOPE simulation code.

Acknowledgments: The authors wish to thank the staff of SACLA, Japan for all the help during experimental beam time. This work was partly supported by the Polish National Science Center (Grant No. DEC-2011/03/B/ST3/02453)

[1] T. Koyama et al., *Optics Express* **21** (2013) 15382.

P-41

2D and 3D calculations in modified Tesla-like cavities

W. Grabowski[1], R. Nietubyć[1,2], J. Sekutowicz[3], M. Staszczak[1]* and T. Wasiewicz[1]

[1]*National Centre for Nuclear Research Świerk, Sołtana 7, 05-400 Otwock, Poland*
[2]*National Synchrotron Radiation Centre Solaris, Jagiellonian University, Gołebia 7/P.1.6, 30-387 Kraków*
[3]*Deutches Elektronen Synchrotron, Notkestrasse 85, 22607 Hamburg, Germany*

Keywords: FEL, Tesla, cavity, beam dynamics

*e-mail: marcin.staszczak@ncbj.gov.pl

The poster presents beam properties calculation for the superconducting linear particle accelerator of free electron laser POLFEL[4]. Normalized slice emittance and bunch size are tracked for the 1.6-cell superconducting injector with solenoid followed by 2-structure cryomodules[2] of HZDR-type.

Main results are taken from ASTRA[1] 2D calculations. First the cavity and solenoid were investigated in order to find optimal parameters. The criterion for optimization was normalized slice emittance. After that stage the cryomodules were added and both the beam size and slice emittance were studied.

At this moment 3D calculations are performed for the model using Microwave Studio[3]. We are trying to build a full 3D model of the gun and crymodules with couplers in order to compare emittance from both 2D and 3D modelling.

Acknowledgments: We want to express our gratitude to Dr. Klaus Floettmann for his assistance and helping us to run the ASTRA code. The work was supported by the EU and MSHE grant nr POIG.02.03.00-00-013/09.

[1] K. Floettmann, "ASTRA, A Space Charge Tracking Algorithm", v. 3.0, October 2011 www.desy.de/~mpyflo/Astra_dokumentation
[2] P. A. McIntosh et al, "Realisation of a prototype superconducting CW cavity and Cryomodule for energy recovery", SRF2007, Beijing, 864-868, (2007)
[3] Microwave Studio, CST www.cst.com/Content/Products/MWS/Overview.aspx
[4] POLFEL - Project Description polfel.pl/doc/polfel_booklet_en_2012_10_28-b.pdf

P-42

Time-resolved SAXS studies of morphological changes in a blend of linear polyethylene with homogeneous ethylene-1-octene copolymer

Cz. Ślusarczyk*

Institute of Textile Engineering and Polymer Materials, University of Bielsko-Biała, Willowa 2, 43-309 Bielsko-Biała, Poland

Keywords: synchrotron radiation, isothermal crystallization, polyethylene blend, nanostructure evolution

*e-mail: cslusarczyk@ath.bielsko.pl

The understanding of the phase behavior of polyethylene (PE) blends is of great commercial importance because in the polyethylene industry, different types of polyethylenes are often blended together to meet various kinds requirements of processing and final products. It is common to blend a high density PE (HDPE) with zero or very low short-chain branch concentration and poly(ethylene-α-olefin) copolymers with high short-chain branch concentration and highly regular (homogeneous) distribution of these branches. The homogeneous copolymer increases the toughness and impact strength of the blend, while HDPE enables the blend to maintain good tensile properties.

It is well established that the mechanical properties of semi-crystalline polymers are closely related to their crystalline morphology. Despite more than a decade of studies of the morphologies of polyethylene blends, a little is known about the crystallization characteristics of the HDPE and poly(ethylene-α-olefin) blends. Hence, in the present paper isothermal melt crystallization in the blend of HDPE and a homogeneous copolymer of ethene-1-octene was studied by time-resolved synchrotron small-angle X-ray scattering (SAXS). The SAXS profile was analyzed both by correlation, $\gamma(r)$, and interface distribution, IDF, functions. These functions allow for determination the values of the long period (LP), the crystalline and amorphous layer thickness (L_C and L_A respectively) and the local volume fraction crystallinity (Φ_L). The chosen isothermal crystallization temperatures covered a wide range of temperature, during which a different mechanisms of crystallization have been observed.

P-43

Influence of the crystalline microstructure on the magnetic ordering of nanocrystalline chromium

D. Wardecki[1]*, R. Przeniosło[1], M. Bukowski[2], R. Hempelmann[2], A. N. Fitch[3] and P. Convert[4]

[1]*Faculty of Physics, University of Warsaw, Hoża 69, 00-681 Warsaw, Poland*
[2]*Institute of Physical Chemistry, University of Saarbrücken, D66123, Saarbrücken, Germany*
[3]*European Synchrotron Radiation Facility, BP 220 F-38043, Grenoble Cedex, France*
[4]*Institute Laue Langevin, BoîtePostal 220 F-38043, Grenoble Cedex, France*

Keywords: nanocrystalline chromium, magnetic ordering, neutron diffraction, synchrotron radiation diffraction

*e-mail: dward@fuw.edu.pl

The combination of two powder diffraction techniques: neutron diffraction as well as synchrotron radiation (SR) diffraction was used in order to study the influence of the microstructure of nanocrystalline chromium (n-Cr) on its magnetic ordering.

The characterization of the n-Cr microstructure was performed by using the Warren-Averbach method [1] with SR data. It was shown that the average crystalline size D for the studied samples of n-Cr varies in the range from 29 nm up to 65 nm, whereas the related microstrain fluctuations Δd/d are in the range of 0.39 – 0.13%, respectively [2]. The parameters of the log-normal distributions of the crystallite sizes were calculated as well (see Figure 1a).

The analysis of the magnetic Bragg peaks intensities in the studied n-Cr samples allowed to determine the type of magnetic ordering in each n-Cr sample as well as the contribution of the particular magnetic phases.

In our model we assumed that the smallest crystallites have only the antiferromagnetic phase (AF_0). The question which arises form this approach is: what is the critical size of the crystallites that have only the AF_0 phase? As it is shown in Figure 1b the values of the cumulative distribution function G(V) can be related to the contribution of the antiferromagnetic phase m_{AF0}. From this comparison it is possible to determine the critical size which is similar for all studied samples of n-Cr and its average values is D_C = 18±2 nm [3].

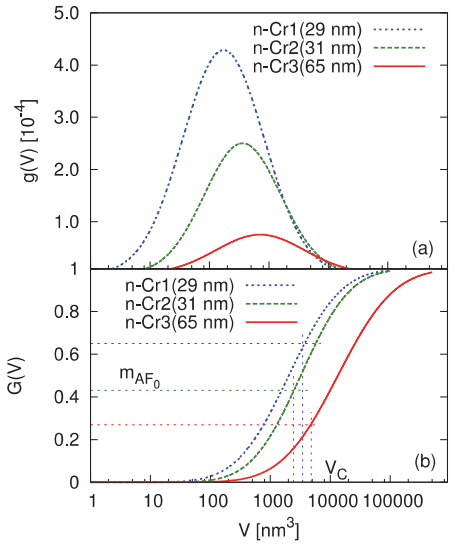

Figure 1. Log-normal distribution function g(V) (a) and the cumulative distribution function G(V) (b) for three n-Cr samples.

Acknowledgments: This work has been supported by the Ministry of Science and Higher Education (Poland) under Projects No. 458/1/N-ILL/2010/0 and No. 155/ESR/2006/03, respectively.

[1] B. Warren, B. Averbach, *J. App. Phys.* **21** (1950) 595.
[2] D. Wardecki, R Przeniosło, A Fitch, M Bukowski and R. Hempelmann, *Journal of Nanoparticle Research* **13** (2011) 1151.
[3] D. Wardecki, R. Przeniosło, M. Bukowski, R. Hempelmann, A. Fitch, P. Convert, *Phys. Rev. B* **86** (2012) 064410.

P-44

Synchrotron topographic evaluation of strain around craters generated by irradiation with x-ray pulses from free electron laser with different intensities

W. Wierzchowski[1]*, K. Wieteska[2], R. Sobierajski[3], D. Klinger[3], J. Pełka[3], D. Żymierska[3] and C. Paulmann[5]

[1]*Institute of Electronic Materials Technology, Wólczyńska 133, Warsaw 01-919, Poland*
[2]*National Centre for Nuclear Research, Soltana 7, Otwock-Świerk 05-400, Poland*
[3]*Polish Academy of Sciences, Institute of Physics, al. Lotników 32/46, Warsaw 02-668, Poland*
[4]*DESY HASYLAB, Notkestrasse 85, D-22607 Hamburg, Germany*

Keywords: synchrotron diffraction topography, free-electron laser

*e-mail: wojciech.wierzchowski@itme.edu.pl

The important question associated with the use of new 4th generation of radiation sources, the free electron lasers (FELs), refers to the interaction of the extremely intense beam with solids.

In our previous experiments exploring X-ray topography it was possible to reveal many important features of the strain fields connected with the craters generated by the FUV pulses from FLASH at HASYLAB. It also was possible to evaluate the depth extension of the damaged area by means of the synchrotron transmission section white beam topography [1]. The completion of the section topographs was the simulation of contrast obtained using the approximation of damaged area connected with the craters by "droplet-like" inclusion.

In the present case we studied the silicon sample irradiated at the Linac Coherent Light Source (LCLS) with X-ray pulses of three different wavelength corresponding respectively to 830 eV, 1855 eV and 2000 eV and different impact energy of pulses differing from 1 to 17 μJ. It was established that the pulses were non Gaussian fluency distribution [2], and much of them caused melting of the irradiated silicon. The important goal of the experiment was evaluation and comparison of the strain field connected with generated craters.

The topographic investigation has been performed at DORIS III at HASYLAB. The most important experiments were realized using monochromatic beam topography but they were also completed with both projection and section white beam reflection topography. The topographs revealed many characteristic features of the damages related with the craters, which usually significantly exceeded the beam size, and the real diameter increased with the energy of the pulse. It was in particular indicated that the relative lattice parameter change in the inner, most probably melted region of the craters was on the level up to 5×10^{-5}. The interference fringes connected with the craters were also observed in the white beam section topography.

Acknowledgment: The synchrotron investigations were supported by the HASYLAB project I-20110423 EC. This work was also supported by the Polish National Science Centre (Grant no. DEC-2011/03/B/ST3/02453)

[1] W. Wierzchowski *et al. Radiation Physics and Chemistry* **93** (2013) 99.
[2] J. Gaudin *et al. Physical Review B* **86** (2012) 024103.

P-45

Method for characterization of gas-puff targets for high energy laser matter interactions

L. Węgrzyński*, P.W. Wachulak, A. Bartnik, T. Fok and H. Fiedorowicz

Institute of Optoelectronics, Military University of Technology, Kaliskiego 2 Str., 00-908 Warsaw, Poland

Keywords: synchrotron radiation, free-electron laser,

*e-mail: lwegrzynski@wat.edu.pl

In order to use gas-puff targets in high power laser matter interaction experiments the characterization measurement of the targets are require. One possible method is an extreme ultraviolet (EUV) pulsed radiography (shadowgraphy) [1,3]. The shadowgrams are formed by EUV light, illuminating the gas-puff target. From the shadowgrams it is possible to obtain the density of the target using numerical method. The result of experiments is 2-D density map of the targets. Using pulsed radiography method, possible is to get fully 3-D reconstruction of measured object (ex. gas-puff targets). 3-D representation of pulsed gaseous target has been obtained using special software [2] by combining 2-D shadowgram images, recorded at various rotation angles.

In this paper we present some results of characterization of gas-puff target, developed at the Institute of Optoelectronics, MUT. This method of characterization should be useful for developing a new EUV or X-ray sources based on interaction of gas-puff targets with high power lasers. For that purpose we demonstrated a desktop backlighting system based on a laser-plasma gas puff target EUV source. The tomographic method allows for more complete characterization of objects, e.g. some additional information regarding the complicated density structure of the target [3].

Acknowledgments: The research was supported by LASERLAB-EUROPE III (grant agreement No. 284464, EC's Seventh Framework Programme), COST Action MP0601 and MP1203) European Economic Area (EEA) grants.

[1] P.W. Wachulak, A. Bartnik, J. Kostecki, Ł. Wegrzynski, T. Fok, R. Jarocki, M. Szczurek, H. Fiedorowicz, (2013) *Photonics Letters of Poland*
[2] available from *http://www.volumegraphics.com*
[3] P.W. Wachulak, Ł. Węgrzyński, Z. Zápražný, A. Bartnik, T. Fok, R. Jarocki, J. Kostecki, M. Szczurek, D. Korytár and H. Fiedorowicz, *Applied Physics B* DOI 10.1007/s00340-014-5829-7

P-46

Structural studies of Au layers irradiated by intense EUV nanosecond pulses

D. Klinger[1], I. Yatsyna[1]*, R. Minikayev[1], J.B. Pełka[1], A. Bartnik[2], W. Caliebe[3] and R. Sobierajski[1]

[1]*Institute of Physics, Polish Academy of Sciences, Al. Lotników 32/46 02-668 Warsaw, Poland*
[2]*Military University of Technology, 2 Kaliskiego Street, 00-908 Warsaw, Poland*
[3]*Hasylab at DESY, Notkestr. 85, D-22603 Hamburg, Germany*

Keywords: synchrotron radiation, plasma source, Au thin film, surface morphology

*e-mail: Ivanna.Yatsyna@ifpan.edu.pl

Present results refer to the samples irradiated in single-shot mode with the laser plasma source with a spectrum containing an intensity maximum at 10–11nm wavelength [1]. The experiments were carried out for the thin Au layers with different thickness. The fluence of EUV beam has been regulated by moving the sample in and out of focus. The radiation modified area depending on fluency and irradiation geometry was around 0,8 mm^2.

After irradiation, the samples were examined by the atomic force microscopy, interference-polarizing microscopy and the X-ray diffraction. The structural characterization was done with synchrotron radiation at the DORIS W1.1 beamline in Hasylab with the monochromatic beam of wavelength $\lambda = 1.54056$ Å. The measurements were recorded in a 2θ scan mode in the grazing incidence geometry. The ω-2θ scans were also recorded in order to find the structural changes in the near-surface layers affected by the irradiation.

Acknowledgments: The research leading to these results has received funding from the European Community's Seventh Framework Programme (FP7/2007-2013) under grant agreement no 226716 and the Polish National Science Center, Grant No. DEC-2011/03/B/ST3/02453.

[1] A. Bartnik, H.Fiedorowicz, R.Jarocki, J.Kostecki, M.Szczurek, P.W.Wachulak, *Nucl. Instr. Meth. Phys. Res.* **A647** (2011) 125.

P-47

Application of synchrotron radiation for study Fano type Mn (3p-3d) photoemission resonances

E. Guziewicz*, B. A. Orlowski, B. J. Kowalski and K. Kopalko

Institute of Physics, Polish Academy of Sciences, Warsaw, Poland

Keywords: synchrotron radiation, photoemission spectroscopy, zinc selenide, zinc oxide

*e-mail: guzel@ifpan.edu.pl

The synchrotron radiation beam in the continuous energy range from 40 to 160 eV was used to obtain EDC photoemission spectra of the valence band and the resonant photoemission Fano type resonance for the Mn (3p-3d) transition. The wide bandgap II-VI semiconductors containing ions of the 3d Transition Metals (TM) are promising materials for short wavelength magneto-optical applications.

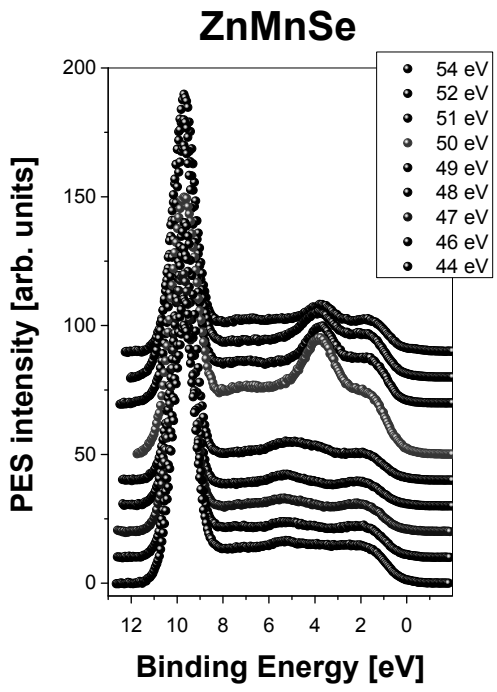

Fig.1. Photoemission EDC spectra of ZnMnSe ternary alloy measured in the region of the Fano resonance corresponding to the Mn3p-3d photoionization threshold.

The electronic valence band structure and especially the contribution of localized and delocalized Mn3d states in respect to the valence band edge and the Fermi level is of great importance for most of these applications.

In the experiment presented here we investigated the Mn3d contribution to the valence band of ZnMnSe and ZnMnO semiconductors. The resonant photoemission Energy Distriution Curves (EDCs) have been measured in the binding energy range from the valence band edge to 14 eV below. We explored the photon energy range across the Mn3p-3d photoionization threshold (44 eV – 54 eV).

The resonant photoemission study shows the fingerprints of the Mn3d states in the valence band region within 9 eV below the Fermi edge. One can distinguish three Mn3d related structures: a structure around the Fermi edge (1-3 eV below EF), the main peak between 3.8 and 4.5 eV, and a broad satellite located between 5.5 and 9 eV below the Fermi edge. The branching ratio of the satellite/main structure is related to the Vpd hybridization parameter [1] and it decreases with increase of hybridization. The branching ratio was measured as 0.43 for ZnMnO and 0.9 for ZnMnSe. It indicates a high degree of hybridization between manganese's and ligand's electron states. The branching ratio obtained for ZnMnO and ZnMnSe alloys follow the trend towards higher hybridization as we move up in the Periodic Table, which was observed in ZnY compounds (Y=S, Se, Te) [1, 2].

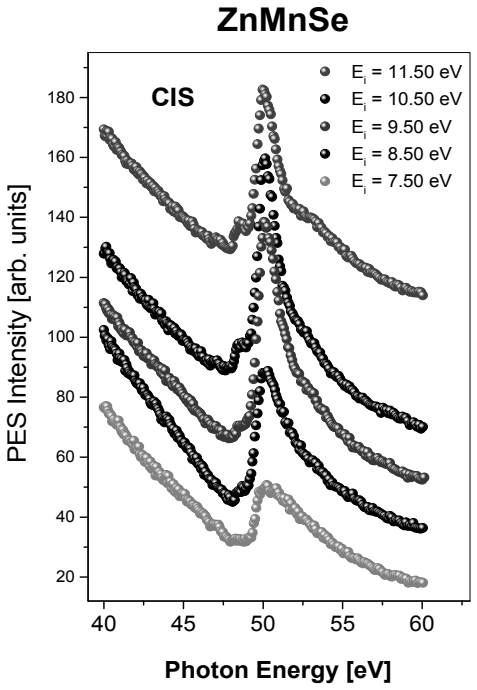

Fig.2. Photoemission Constatnt Initial State (CIS) spectra of ZnMnSe showing the Fano resonance curves of ZnMnSe measured across of the Mn3p-3d photoionization threshold.

Acknowledgement: The work was partially supported by the Polish NCN project DEC-2012/07/B/ST3/03567.

[1] R. Weidemann *et al., Phys. Rev. B* **45** (1992) 1172.
[2] E. Guziewicz *et al., Physica Scripta* **T115** (2005) 541.

P-48

Surface states on topological crystalline insulator $Pb_{1-x}Sn_xSe$ – an ARPES study

B. J. Kowalski[1]*, P. Dziawa[1], C. M. Polley[2], J. Adell[2], T. Balasubramanian[2], M. H. Berntsen[3], B. M. Wojek[3], O. Tjernberg[3], A. Szczerbakow[1], A. Reszka[1], R. Minikayev[1], J. Z. Domagala[1], S. Safaei[1], P. Kacman[1], R. Buczko[1] and T. Story[1]

[1]*Institute of Physics, Polish Academy of Sciences, 02-668 Warsaw, Poland*
[2]*MAX IV Laboratory, Lund University, 221 00 Lund, Sweden*
[3]*KTH Royal Institute of Technology, ICT Materials Physics, Electrum 229, 164 40 Kista, Sweden*

Keywords: topological crystalline insulators, photoelectron spectroscopy

*e-mail: kowab@ifpan.edu.pl

It was recently realized that the concept of topological protection can be extended to other symmetries beyond that of time reversal (crucial for topological insulators). For the case of point-group symmetries, this gives rise to the new class of "topological crystalline insulators" (TCI) in which specific crystalline symmetries warrant the topological protection of metallic surface states [1,2]. A group of IV-VI semiconductors, in particular SnTe, was indicated as possible examples of TCIs [2].

We report on the angle-resolved photoelectron spectroscopy (ARPES) and spin-resolved photoelectron spectroscopy experiments, supported by band structure calculations which have proven existence of topologically protected surface states with the Dirac-like dispersion on the (100) and (111) surfaces of $Pb_{1-x}Sn_xSe$ and have showed that this narrow-gap semiconducting solid solution belongs to the class of topological crystalline insulators (TCI) [3-5].

$Pb_{1-x}Sn_xSe$ offers advantageous conditions for search for surface states of the TCI phase. The increasing Sn content leads to closing the energy gap at some specific crystal composition. For higher Sn contents, the gap opens again but the parity of electronic states at band edges is reversed. Since this transition can also be induced by temperature for properly chosen Sn contents, in these crystals it is possible to study both the open-gap topologically trivial case and open-inverted-gap with topologically nontrivial properties.

The ARPES experiments were performed on the I3 and I4 beam lines at the MAX-III synchrotron facility in Lund (Sweden). The (100) surfaces were obtained by *in situ* cleavage of $Pb_{1-x}Sn_xSe$ crystals grown by self-selecting vapour growth method. $Pb_{1-x}Sn_xSe$ films with (111) surfaces were grown *in situ* on BaF_2 (111) substrates using an open hot wall epitaxy method.

In the ARPES studies for $Pb_{0.77}Sn_{0.23}Se$, the band inversion at T_C=150 K was achieved. Below the inversion temperature we observed the formation of topological states with Dirac-like energy dispersion and the Dirac cones centered in the vicinity of the $\bar{X}$ point of the surface Brillouin zone [3]. Our spin-resolved ARPES experiments enabled us to prove also the existence of spin polarization around the $\bar{X}$ point in the surface Brillouin zone in the TCI phase of $Pb_{0.73}Sn_{0.27}Se$ [5]. In contrast to the (100) face, the Dirac-like surface states on (111) are well separated and noninteracting, located at the time reversal invariant momenta $\bar{\Gamma}$ and $\bar{M}$ in the surface Brillouin zone. Our observations are consistent with the results of tight binding band structure calculations studying surface states on surfaces of topological crystalline insulators.

Acknowledgments: This work was made possible through support from the European Commission Network SemiSpinNet (PITN-GA-2008-215368), the European Regional Development Fund through the Innovative Economy Grant (No. POIG.01.01.02-00-108/09), the Polish National Science Centre (NCN) Grant No. 2011/03/B/ST3/02659, and the Knut and Alice Wallenberg Foundation, the Swedish Research Council. P.D. and B.J.K. acknowledge support from the Baltic Science Link project coordinated by the Swedish Research Council, VR.

[1] L. Fu, *Phys. Rev. Lett*. **106** (2011) 106802.
[2] T. H. Hsieh, H. Lin, J. Liu, W. Duan, A. Bansil, L. Fu, *Nat. Commun*. **3** (2012) 982.
[3] P. Dziawa, P. Dziawa, B.J. Kowalski, K. Dybko, R. Buczko, A. Szczerbakow, M. Szot, E. Lusakowska, T. Balasubramanian, B.M. Wojek, M.H. Berntsen, O. Tjernberg, T. Story, *Nat. Mater*. **11** (2012) 1023.
[4] C. M. Polley, P. Dziawa, A. Reszka, A. Szczerbakow, R. Minikayev, J. Z. Domagala, S. Safaei, P. Kacman, R. Buczko, J. Adell, M. H. Berntsen, B. M. Wojek, O. Tjernberg, B. J. Kowalski, T. Story, T. Balasubramanian, *Phys. Rev. B* **89** (2014) 075317.
[5] B. M. Wojek, R. Buczko, S. Safaei, P. Dziawa, B.J. Kowalski, M. H. Berntsen, T. Balasubramanian, M. Leandersson, A. Szczerbakow, P. Kacman, T. Story, O. Tjernberg, *Phys. Rev. B* **87** (2013) 115106.

P-49

Simulation of the emitter existence conditions during cathode arc deposition of refractory materials

V.D. Alimov[1], A.V. Nedolya[1]* and I.N. Titov[2]

[1]*Zaporizhzhya National University, Applied Physics Department, 66 Zhukovsky Str., 69600 Zaporizhzhya, Ukraine*
[2]*STC PAS NAS Ukraine, 1 Chubanova Str., 69600 Zaporizhzhya, Ukraine*

Keywords: refractory, vacuum-arc, ecton, warm-up time.

*e-mail: nedolya@znu.edu.ua

The vacuum cathode arc deposition technology offer an excellent approach to production pure metal, alloy and compound at very high rates and with excellent adhesion and density. This allows efficient use of the method for applying coatings to accelerator technology [1]. However, there are problems with the choice of process parameters which will form a uniform film without dropping faction [2]. Therefore, the use of modeling processes of the formation of the plasma is an urgent problem.

Significantly upgrading one-dimensional mathematical model [3], which took into account the dependence of the heat capacity and thermal conductivity on temperature [4], the finite element method calculated the temperature distribution along the height of the emitter at different values in vacuum-arc deposition of zirconium, titanium and titanium nitride on the substrate.

Calculated minimum temperature explosion ecton and his warm-up time before the explosion at the characteristic of the current density ($1{,}2 \cdot 10^{12}$ A/m^2), which makes up for titanium nitride t = 9.86 ns at T = 6136 K, for titanium t = 9.48 ns at T = 7002 K, for zirconium t = 9.04 ns at T = 8336 K (fig. 1).

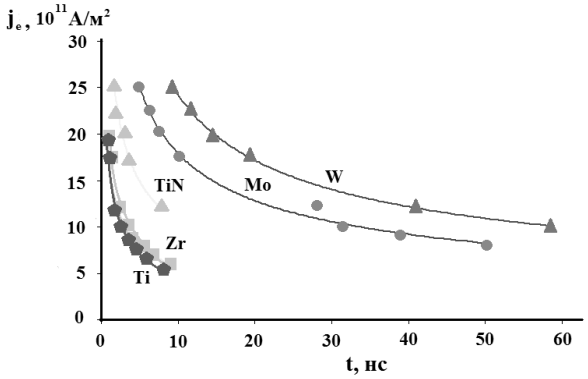

Fig. 1. Change the emitter heating time for different values of the emission current density.

The calculation in the model will improve the effectiveness of materials deposition by pre-determining the main technological parameters of sedimentation: current density, pulse discharge time, frequency UVH generation.

[1] P. Strzyzewski, M. J. Sadowski, R. Nietubyc *et al.*, *Mater. Sci. Poland.* **26** (2008) 213-220.
[2] Anders, *Handbook of Plasma Immersion Ion Implantation and Deposition* (John Wiley & Sons, New York 2000).
[3] E.A. Litvinov, G. A. Mesyats and D.I. Proskurovsky, *Physics-Uspekhi (Advances in Physical Sciences),* **139** (1983) 265-302.
[4] A.V. Nedolya, E.I. Pivaev, I.N. Titov. *J. PSE (Physical surface engineering),* **7** (2009) 330-334.

P-50

Synchrotron radiation photoemission study of $Pb_{1-x}Cd_xTe$ crystal with local structure

B. A. Orlowski[1]*, K. Gas[1], A. Szczerbakow[1], A. Reszka[1], B. J. Kowalski[1], S. Thiess[2] and W. Drube[2]

[1]*Institute of Physics, Polish Academy of Sciences, Al. Lotników 32/46, 02-668 Warsaw,Poland*
[2]*Hamburger Synchrotronstrahlungslabor HASYLAB am DESY, Notkestr. 85, D-22603 Hamburg, Germany*

Keywords: synchrotron radiation, free-electron laser

*e-mail: orbro@ifpan.edu.pl

The high energy photoemission experiment was performed using the Tunable High Energy X-ray Photoemission Spectrometer (THE-XPS) at wiggler beam line station BW2 of the HASYLAB, Hamburg, Doris III synchrotron storage ring**.** Double crystal monochromator with crystal Si(111) works in energy range from 2,4 to 10keV with photon flux of about $5x10^{12}$ photons/s of monochromatic beam and with total energy resolution power of 0,5 eV for radiation energy around 3000 eV. The photoemission studies were performed at room temperature.

The crystals PbTe and CdTe are of different crystalline structure and their relative solubility is remarkably low. The PbTe belongs to the group o IV-VI narrow gap (0.23eV) semiconductor compounds and crystallizes in the six fold coordinated lattice of rock salt (lattice constant 6,462Å) while the CdTe belongs to the group of II – VI middle gap (1.45eV) semiconductor compounds and crystallizes in four fold coordinated zinc blend lattice (lattice constant 6.480 Å). The remarkable low relative solubility of PbTe and CdTe leads to the unexpected effects in a case of attempting to grow MBE layers of ternary alloy of these two crystals. In the case, nanostructures with a quantum dots of PbTe surrounded by CdTe or quantum dots of CdTe surrounded by PbTe were grown .

The paper presents comparison of high energy photoemission spectra of two kind of semiconductor samples. The one is ternary crystal of $Pb_{0.94}Cd_{0.06}Te$ [1, 2] with the frozen rock salt structure. In these crystal the crystalline local structure is expected to be created due to the differences of the radiuses size of Pb^{2+} (1.2 Å) and Cd^{2+} (0.97 Å) cation. The second one sample is the layer nanostructure CdTe(6nm)/PbTe(6nm)/CdTe(40nm)/ GaAs(0.5mm) grown in thermal equilibrium by Molecular Beam Epitaxy (MBE) method [2 - 4] were crystalline local structure is not expected to be created. The high energy photoemission spectra showed that for crystalline sample with local structure the electron binding energies of cations are higher (about +0.2eV) while for anion they are lower (about -0.01eV) than for layer. Obtained shifts of binding energies are of opposite sign for electrons of anions than of cation. The model of the created crystalline local structure collapse is proposed.

As a conclusion we can say that obtained electron binding energy differences are caused by the crystalline local structure in the crystal of $Pb_{0.94}Cd_{0.06}Te$.

Acknowledgments: The authors acknowledge support by MSHE of Poland research Projects DESY/68/2007 and by the European Community via "Integrating Activity on Synchrotron and Free Electron Laser Science") at DESY. Partially supported by European Union through an Innovative Economy grant (POIG.01.01.02-00-108/09) and (POIG.01.01.02-00-008/08).

[1] Szczerbakow, K. Durose, *Prog. Cyst. Growth Charac. Mater*. **51** (2005) 81.
[2] M. Szot, K. Dybko, P. Dziawa, et al. *Cryst. Growth Des*. **11** (2011) 4794.
[3] B.A. Orlowski, A. Szczerbakow, B.J. Kowalski, *et al. J. Elec. Spec. Rel. Phen*. **184** (2011) 199.
[4] B. A. Orlowski, S. P. Dziawa, K. Gas, et al. *Acta. Phys. Pol. A* **120** (2011) 960.

P-51

XPS characterization of functionalized materials for photo-voltaic industry

D. A. Zatsepin[1,2]*, E. Z. Kurmaev[2], I. S. Zhidkov[2,3], S. O.Cholakh[3] and D. W. Boukhvalov[4]

[1]*Institute of Physics PAS, PL-02-668 Warsaw, Al. Lotników 32/46, Poland*
[2]*RAS Ural Division – Institute of Metal Physics, 620990 Yekaterinburg, 18 Kovalevskoj Str., Russia*
[3]*Ural Federal University, 620002 Yekaterinburg, 19 Mira Str., Russia*
[4]*KIAS, Seoul 130-722, Hoegiro 87, Korea*

Keywords: ion-implantation, x-ray-photoelectron spectroscopy

*e-mail: zatsepin@ifpan.edu.pl

The modification of the electronic structure in semiconducting materials is the most actual task for the photo-voltaic Power Industry, because none of the undoped semiconductors is directly suitable to be the prototype of the photo-voltaic functionalized material [1]. The requirements for the "ideal" photo-catalyst allow to consider ZnO-Me (Me = Fe, Co, Mn) as a perspective, because the partial isovalent substitution of Zn-atoms in ZnO-host with 3*d*-metal atoms will results in E_g effective value reduction due to electron exchange-interaction [2]. This can be achieved using the pulsed ion-beam implantation (mono- and dual-type-ion) as a versatile tool for atomic structure engineering [3].

The electronic structure re-arrangement of the ZnO:Me (Me = Fe, Co, Mn) were found due to XPS characterization, which results in the appearance of the mid-gap-states in the valence band with the most dramatic VB structure transformations for dual-implanted ZnO:[Co-Mn]. As for the single ion-implanted ZnO-host, the ZnO:Fe system can be potentially assumed as promising photovoltaic substrate because, as it was established, Fe-doping also strongly reduces the band gap, and in this regime, the high level of doping used in the samples herein is appropriate.

Acknowledgments: This work was partially supported by Ural Division of Russian Academy of Sciences (Project 12-I-2-2040), Russian Foundation for Basic Research (Project 13-08-00059) and European Union 7.FP under grant REGPOT-CT-2013-316014-EAgLE

[1] Kumar, J. B. M. Krishna, D. Das, S. Keshri, *Applied Surface Sci.* **258** (2012) 2237.
[2] S. Rehman, R. Ullah, A. M. Butt, N. D. Gohar, J. Hazard, *Mater.* **179** (2009) 560.
[3] J. A. McLeod, D. W. Boukhwalov, D. A. Zatsepin, R. J. Green, B. Leedahl, L. Cui, E. Z. Kurmaev *et al*., *J. Phys. Chem. C* **118** (2014) 5336.
[4] S. Tougard, *Solid State Communs.* **61** (1987) 547.

P-52

Nanosystem based on phospholipids and surfactants as innovative delivery system for gene therapy- circular dichroism and Fourier transform infrared spectroscopy studies

P. Egierska*, M. Skupin, B. Urban, J. Wolak*, Z. Pietralik and M. Kozak

Department of Macromolecular Physics, Faculty of Physics, Adam Mickiewicz University, 85b, Umultowska, 61-614 Poznań, Poland

Keywords: gene therapy, circular dichroism, Fourier transform infrared spectroscopy, sulfobetaine derivatives

*paulina.egierska@gmail.com
*joannaw14@gmail.com

The medical applications of gene therapy started in the end of XX century and now it's one of the most promising methods for treating a wide range of genetic diseases as well as neurodegenerative disorders or cancer. The main idea of this method is exchanging the defective gene with its proper copy or to block biosynthesis of improper proteins. Corrected genes are introduced to cells by special vectors (delivery systems). Perfectly suitable for this purpose are non-viral vectors - delivery system based on lipid/surfactant mixtures [1].

The aim of this study was to determinate the possible use of amphoteric surfactants (zwitterionic akyl derivates of sulfobetaine [2]) as agents forming complexes with nucleic acids. These complexes have potential applications for gene delivery [3].

A series of measurement of DNA conformation of DNA/zwitterionic surfactant lipoplexes were performed using the circular dichroism (CD) spectroscopy. CD spectra were recorded in the range 350 – 200 nm using J - 815 spectrometr (Jasco). The CD spectrum of pure DNA solution exhibits a positive band with maximum near 277 nm, the negative band with minimum near 245 nm and cross point near 260 nm. These parameters clearly indicate the B-DNA form (fully-hydrated). The increased surfactant concentration slightly shifts the bands towards higher wavelength.

Fourier transform infrared spectroscopy (FTIR) was used to analyse the structure and organization of lipoplexes. FTIR spectra of lipoplexes were collected using BRUKER Tensor 27 spectrometer (spectral range was 4000 - 400 cm^{-1} and temperature 275-313 K). The FTIR data proved the existence of stable lipoplexes.

Acknowledgments: This study was carried out with financial support from the Ministry of Science and Higher Education (Poland) - programme "Generacja Przyszłości" (decision number: 12/POIG/GP/2013).

[1] N.L. Slack, A. Ahmad, H.M. Evans, A.J. Lin, C.E. Samuel, C.R. Safinya, *Curr. Med. Chem.* **11** (2004) 133.
[2] M. Kozak, K. Szpotkowski, A. Kozak, R. Zieliński, D. Wieczorek, M.J. Gajda, *Rad. Phys. Chem.* **78** (2009) S112.
[3] N. Dan, *Biophys. J.* **73** (1997) 1842

P-53

Nano-structured Pt embedded in the acidic salts of heteropolymolybdate matrices: MS XAFS study

A. Witkowska[1]*, S. Dsoke[2], R. Marassi[2] and A. Di Cicco[3]

[1]*Department of Solid State Physics, Gdansk University of Technology, Narutowicza 11/12, 80-233 Gdansk, Poland*
[2]*Chemistry Department, University of Camerino, I-62032 Camerino (MC), Italy*
[3]*School of Science and Technology, Physics Division, University of Camerino , I-62032 Camerino (MC), Italy*

Keywords: Pt nanoparticles, catalysts, PEM FC, MS EXAFS

*e-mail: agnieszka@mif.pg.gda.pl

In the contribution, X-ray absorption spectroscopy (XAS) study combined with TEM and XRD analysis of a novel Pt-based catalyst operating at low temperature fuel cells (FCs) is presented. Low temperature fuel cells generally utilize solid polymer electrolytes and they are a promising class of compact devices representing a future alternative to fossil fuels based engines. Up to now one of the most challenging goals in development of these type of FCs is to accelerate too slow oxygen reduction reaction (ORR) and limit the requested amount of Pt in the catalyst [1,2]. A significant decrease of the Pt loading during the last two decades accompanied by tangible improvements of power density has been achieved [3]. The result has been obtained mainly by diminishing the metal grain size to the nanometric scale and by improving homogeneity of the nanocatalysts dispersion on a support.

Innovation in the case of the considered catalyst resides in the use of a porous inorganic matrix of acidic heteropolymolybdate salts of composition $X_{2.5}H_{0.5}YMo_{12}O_{40}$, where X = Cs, Rb and Y = P, Si as a catalyst support [4,5]. The meso-microporous matrix is characterized by good stability, insolubility in water, and exhibits high acidity (proton availability and mobility). To prepare electrocatalysts, the platinum ions were introduced using electrochemical method to the heteropolyacid salts and then were reduced using an H_2/Argon stream at 300ºC. Most of the Pt metallic nanoparticles created during the reduction process were embedded into a support pores which size can be controlled by the kind and content of cation used. Thus, the desired/optimal Pt nanoparticle size can be precisely defined by the proper heteropolyacid salt composition.

Presented results show the relation between the matrix composition and the size of the obtained metallic Pt nanoparticles determined mainly by mean of multiple-scattering extended X-ray absorption fine structure (MS EXAFS) analysis [6] (using two- and three-body configurations degeneracies as shown in Figure 1 and relation between the first shell mean distance and coordination number introduced in [7]). TEM and XRD-extracted nanoparticle diameters are also presented and compared with XAFS results. Accuracy and sensibility of the applied techniques and approaches in micro- and nanoscopic structural analysis of these novel low-Pt content catalysts are discussed.

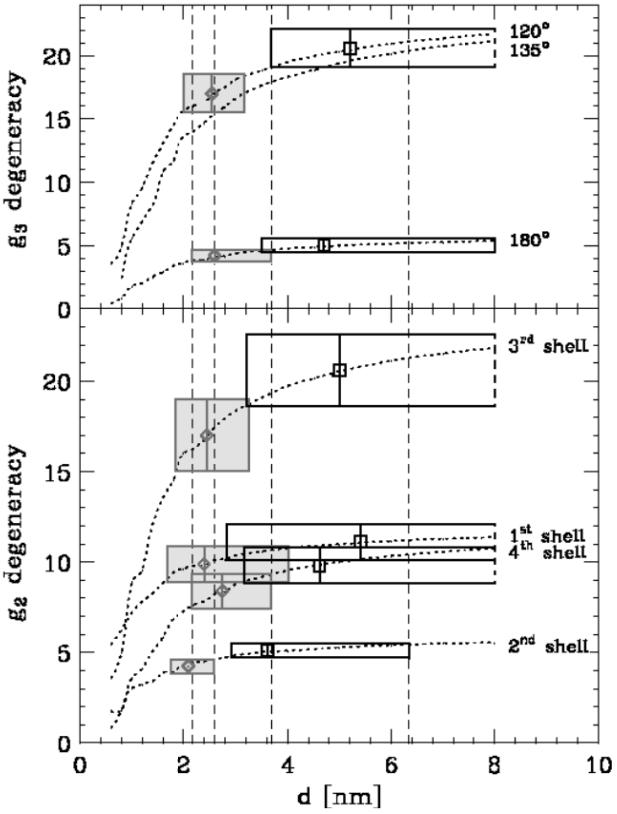

Figure 1. Pt nanoparticles size determination performed on the base of model calculations (doted lines) and MS EXAFS analysis for: $5\%Pt^{IV}$-$Cs_{2.5}H_{0.5}PMo_{12}O_{40}$ catalyst (d_{ave}= 2.4(2)nm) – diamond and gray uncertainty box; $5\%Pt^{IV}$-$Rb_{2.5}H_{0.5}PMo_{12}O_{40}$ catalyst (d_{ave} = 5.0(1.3)nm) – square and white uncertainty box.

Acknowledgments: We gratefully acknowledge the support of the European Synchrotron Radiation Facility (Grenoble, France) in providing synchrotron radiation facilities for the ch-2446 experiment carried out at BM29 station.
This research has been carried out within the NUME Project "Development of composite proton membranes and of innovative electrode configurations for polymer electrolyte fuel cells" (MIUR, FISR 2003).

[1] V. R. Stamenkovic, B. Fowler, B. S. Mun, G. Wang, P. N. Ross, C. A. Lucas, N. M. Markovic, *Science* **315** (2007) 493.
[2] S. Chen, W. Sheng, N. Yabuuchi, P. J. Ferreira, L. F. Allard, Y.Shao-Horn, *J. Phys. Chem. C* **113** (2009) 1109.
[3] H. A.Gasteiger, S. S. Kocha, B. Sompalli, F. T. Wagner, *Appl. Cat. B* **56** (2005) 9.
[4] R. Wlodarczyk, M. Chojak, K. Miecznikowski, A. Kolary, P. J. Kulesza, R. Marassi, *J. Power Sources* **159** (2006) 802.
[5] R. Wlodarczyk, A. Kolary, R. Marassi, M. Chojak, P. J. Kulesza, *Electochimica Acta* **52** (2007) 3958.
[6] A. Witkowska, A. Di Cicco, E. Principi, *Phys. Rev. B* **76** (2007) 104110.
[7] S. Calvin, C. J. Riedel, E. E. Carpenter, S. A. Morrison, R. M. Stroud, V. G. Harris, *Phys. Scr.* **T 115** (2005) 7.

P-54

Generation of X-ray radiation with a femtosecond laser system

Ł. Węgrzyński[1]*, T. Fok[1], P. Wnuk[2], Y. Stepanenko[2]
P.W. Wachulak[1], A. Bartnik[1], C. Radzewicz[3],
H. Fiedorowicz[1] and K. Lawniczak - Jablonska[4]

[1]*Institute of Optoelectronics, Military University of Technology, Kaliskiego 2, 00-908 Warsaw, Poland*
[2]*Institute of Physical Chemistry, Polish Academy of Science, Kasprzaka 44/52, 01-224 Warsaw, Poland*
[3]*Institute of Experimental Physics, University of Warsaw Hoża 69, 00-681 Warsaw, Poland*
[4]*Institute of Physics, Polish Academy of Sciences Al. Lotników 32/46, 02-668 Warsaw, Poland*

Keywords: X-rays, femtosecond lasers, laser plasma X-ray sources

*e-mail: lwegrzynski@wat.edu.pl

Generation of X-ray radiation from a plasma produced as a result of interaction of femtosecond laser pulses with a solid target is presented. The laser pulses of 16fs time-duration and energy about 50mJ were created at 10Hz repetition rate with a femtosecond high-power (10TW) laser system developed recently at the Institute of Physical Chemistry PAS [1]. The laser system is based on the Noncollinear Optical Parametric Chirped Pulse Amplifier (NOPCPA) approach [2].

The laser pulses have been focused with a spherical lens (f = 50mm) on a solid target in a form of a metal plate. The lens and the target were mounted inside a vacuum chamber using translation and rotation stages. The translation stage made possible to change position of the target in respect to the laser focus and the rotation stage allowed irradiating previously undamaged surface of the target.

X-ray emission has been detected for the first time using a scintillator (P43) combined with a CCD camera. The preliminary spectral measurements performed for different target materials (Cu, Al) using the absorption filters technique confirmed that X-ray pulses were produced as a result of femtosecond K_α X-ray generation process [3, 4]. Intensity of X-rays strongly depended on the polarization of laser radiation. The new source can be used in fast X-ray diffraction studies and pulsed micro-radiography.

Acknowledgments: The research has been done under the research and development project funded by the National Center for Research and Development (NCBiR) Nr 02-0019-10/2011 and was supported by the 7th Framework Programme Laserlab-Europe Project No. 284464.

[1] Y.Stepanenko *JOSAB* 28 (2011) 2337, Y. Stepanenko *et al.* (in preparation)
[2] Dubietis et al., *Opt. Commun*. **88** (1992) 437.
[3] Rischel et al., *Nature* **390** (1997) 490.
[4] Salzmann et al., *Phys.Rev.E* **65** (2002) 03640.

P-55

Status and solutions for the Solaris control system

P. P. Goryl[1*], C. J. Bocchetta[1], V. Hardion[2], A. Kisiel[3],
K. Kopeć[1], P. Kurdziel[1], J. Lidon-Simon[2], F. Melka[1],
M. Ostoja-Gajewski[1], D. Spruce[2], M. J. Stankiewicz[1],
J. Szota[1], T. Szymocha[3], A. I. Wawrzyniak[1],
K. Wawrzyniak[1], M. Zając[1] and Ł. Żytniak[1]

[1]*National Synchrotron Radiation Centre 'Solaris', Jagiellonian University, ul. Czerwone Maki 98, 30-392 Kraków, Poland*
[2]*MAX IV Laboratories, Lund, Sweden*
[1]*AGH University of Science and Technology, ACC CYFRONET AGH, Nawojki 11, 30-950 Kraków, Poland*

Keywords: synchrotron radiation, IT, control system

*e-mail: piotr.goryl@uj.edu.pl

The Solaris control system has been designed and is in the implementation phase, now. Final development in the field of IT and control systems for the light source is now ongoing.

Control system implementation is based on several collaborations with other institutes supporting Solaris with both technological solutions and work. Among them, there are the MAX IV, the Elettra and the project PLGrid Plus. Some of implementation tasks are outsourced to companies having related experience. The main one are for PLC systems fabrication and for control system software and hardware integration.

The key choices are the TANGO CS for hardware integration, the Sardana software for experiments' control and the IcePAP system for motorization. Timing system will be built using hardware provided by Micro Research Finland, so called MRF system.

Implementation strategy and status along with technological choices and their impact for future facility operation will be presented.

Acknowledgments: Work supported by the European Regional Development Fund within the frame of the Innovative Economy Operational Program:
POIG.02.01.00-12-213/09

P-56

Laboratory laser-produced plasma source of soft X-rays for radiobiology studies

D. Adjei[1]*, M. G. Ayele[1], P. Wachulak[1], A. Bartnik[1], H. Fiedorowicz[1], I. U. Ahad[1], L. Wegrzynski[1], A. Wiechecka[2], J. Lekki[2] and W. M. Kwiatek[2]

[1]*Institute of Optoelectronics, Military University of Technology, 00-908 Warsaw, Poland*
[2]*Institute of Nuclear Physics PAN, Krakow, Poland*

Keywords: laser produced plasma, soft X-rays, radiobiology experiments

*e-mail: dadjei@wat.edu.pl

Various sources are used to investigate the effects of ionizing radiation on biological cells and tissue, including γ sources, heavy-ion accelerators, synchrotrons and laboratory scale X-ray sources [1, 2, 3]. It was demonstrated that micro-focus X-ray tubes delivering broadband radiation at energies up to 15 keV, or quasi-monochromatic radiation at 284 eV, 1.5 keV, 4.5 keV or 5.4 keV are highly useful for radiobiology studies [4, 5, 6]. However, this radiation is delivered to the sample at a low dose rate, and thus a relatively long irradiation time is needed to induce measurable biological effects. Higher dose rates can be achieved with laser-produced plasma light sources emitting high-intensity pulses of X-ray radiation. Application of a single-shot laser plasma X-ray source driven by a large scale laser facility in radiobiology studies has been demonstrated [7]. A laser plasma X-ray source driven with a femtosecond laser has been also used for this purpose [8].

In this paper a compact, desk-top laser plasma soft X-ray source developed for radiobiology research is presented. The source is based on a double-stream gas puff target irradiated with a commercial Nd:YAG laser generating laser pulses of 4 ns time duration and energy up to 800 mJ at 10 Hz operation rate (EKSPLA) [9]. The source has been optimized for maximum emission in the "water window" wavelength range from 2.3 nm to 4.4 nm by using proper gas (argon and argon/krypton mixture). Results of the source characterization measurements and dosimetry of the produced soft X-ray radiation are shown and discussed. It is expected that the source would have a unique capability for irradiation of cells with high pulse dose and dose rates without much robust X-ray optics. Investigations on irradiation of biological cells with the use of the source are planned.

Acknowledgements: The authors acknowledge the financial support from the EU FP7 Erasmus Mundus Joint Doctorate Programme EXTATIC under framework partnership agreement FPA-2012-0033.

[1] A. Facoetti, F. Ballarini, R.. Cherubini, S. Gerardi, R. Nano, A. Ottolenghi, K. M. Prise, K. R. Trott, C. Zilio, *Radiat. Prot. Dosim.* **122** (2006) 271.
[2] N. Usami, M. Maeda, K. Eguchi-Kasai, H. Maezawa, K. Kobayashi, *Radiat. Prot. Dosim.* **122** (2006) 307.
[3] M. Folkard, B. Vojnovic, S. Gilchrist, K.M. Prise, B. D. Michael, *Nucl. Inst. Met.s in Phys. Res. B* **210** (2003) 302.
[4] G. Schettino, M. Folkard, B. D. Michael, K. M. Prise, *Radiat.Res.* **163** (2005) 332.
[5] Y. Tanno, K. Kobayashi, M. Tatsuka, E. Gotoh, K. Takakra, *Radiat. Prot. Dosim.* **122** (2006) 301.
[6] M. Folkard, G. Schettino, B. Vojnovic, S. Gilchrist, A. G. Michette, S. J. Pfauntsch, K. M. Prise, B. D. Michael, *Radiat. Res.*, **156** (2001) 796.
[7] M. Davídková, L. Juha, M. Bittner, S. Koptyaev, V. Hájková, J. Krása, M. Pfeifer, V. Štísová, A. Bartnik, H. Fiedorowicz, J. Mikolajczyk, L. Ryc, L. Pína, M. Horváth, D. Babánková, J. Cihelka, S. Civiš, *Radiat. Res.* **168** (2007) 382.
[8] M. Nishikino, K. Sato, N. Hasegawa, M. Ishino, S. Ohshima, Y. Okano, T. Kawachi, H. Numasaki, T. Teshima, H. Nishimura, *The Review of Scientific Instruments*, **81** (2010) 026107.
[9] P. W. Wachulak, A. Bartnik, H. Fiedorowicz, P. Rudawski, R. Jarocki, J. Kostecki, M. Szczurek, *Nucl. Inst. Meth. Phys. Res. B* **268** (2010) 1692.

P-57

Trans-Reflection SR-FTIR technique applied to biomedical coatings study

C. Paluszkiewicz[1*], W. M. Kwiatek[1], E. Długoń[2] and M. Cestelli Guidi[3]

[1]*Institute of Nuclear Physics, PAN, ul. Radzikowskiego 152, 31-342 Kraków, Poland*

[2]*AGH - University of Science and Technology, Faculty of Materials Science and Ceramics, al. Mickiewicza 30, 30059 Kraków, Poland*

[3]*INFN - Laboratori Nazionali di Frascati, via E. Fermi 40, 00040 Frascati (RM)), Italy*

Keywords: synchrotron radiation, biomedical coatings, FTIR

*e-mail: czeslawa.paluszkiewicz@ifj.edu.pl

It is known that coating titanium and related films with ceramics such as hydroxyapatite has been studied for use as body implants. Chemical bonding between the implant and host tissue takes place through the phosphate layer, which is created on the bioactive materials surface when in contact with the body fluids environment.

Synchrotron Radiation Fourier Transform Infrared (SR-FTIR) spectroscopy can yield micro-structural information on the segment level complementary to the morphological information acquired from X-ray scattering and optical as well as electron microscopy.

SR-FTIR method is applied to thin films study on the different substrates. Moreover SR-FTIR microscopy allows to obtain surface and cross section maps in reflection and transmission mode. This leads to visualization of chemical imaging between substrates and films.

More than a few modification have been engaged to coat metal including electrodeposits system (EPD). In our work the films with different addition of nano-hydroxyapatite and nano-silicate were deposited by EPD method on titanium and/or steel.

Analysis of received biomaterials were determined by FTIR trans-reflection technique based on focal plane array (FPA) detection system at Dafne beam line in Frascati. SR-FTIR spectra were collected using Bruker spectrometer with microscope (Hyperion-3000) equipped with MCT and FPA (64x64 pixel) detectors.

The spectra were recorded in the mid IR-range by averaging 256 scans with 4cm^{-1} of resolution. The aperture of 25 x 25 μm was used with MCT detector experiments and in the case of FPA detector the area 170 μm x 170 μm was measured. The spectral data were baseline corrected and calculations the area of the Si-O as well as P-O bands and in the region from 1200 cm^{-1} to 900 cm^{-1} were done which allow us to show chemical imaging of the samples.

Furthermore a scanning electron microscopy (SEM) with X-ray microanalysis was applied to determine morphology and structure of the samples.

Acknowledgments: "The research leading to these results has received funding from the European Community's Seventh Framework Programme (FP7/2007-2013) under grant agreement n.°226716."

[1] C. Paluszkiewicz, J. Czechowska, A. Slósarczyk, Z. Paszkiewicz *Journal of Molecular Structure* **1034** (2013) 295.

[2] C. Paluszkiewicz, E. Dlugoń, W. Kwiatek, *Acta Physica Polonica A,* **121** (2012) 551-554.

[3] C. Paluszkiewicz, A. Ślósarczyk, D. Pijocha, M. Sitarz, M.Bućko, A. Zima, A. Chróścicka, M. Lewandowska-Szumieł, *Journal of Molecular Structure* **976** (2010) 301.

[4] C. Paluszkiewicz, W.M. Kwiatek, E. Długoń, A. Wesełucha-Birczyńska, M. Piccinini, *Acta Physica Polonica A* **115** (2009) 533.

P-58

Electron and photon beam parameters for SOLARIS synchrotron light source

A.I. Wawrzyniak[1,2*], C.J. Bocchetta[1], R. Nietubyć[1,3], M.J. Stankiewicz[1,2] and M. Zając[1]

[1]*National Synchrotron Radiation Centre SOLARIS, Jagiellonian University, Kraków, 98, Czerwone Maki, 30387 Kraków, Poland*
[2]*Institute of Physics, Jagiellonian University, Kraków, 4, Reymonta,30059 Kraków, Poland*
[3]*National Centre for Nuclear Studies, Świerk, 7, Andrzej Sołtan, 05400 Otwock, Poland*

Keywords: storage ring, electron beam, emittance, energy spread, photon beam

*e-mail: adriana.wawrzyniak@uj.edu.pl

The Solaris synchrotron light source is composed of a 60 m long 600 MeV linear accelerator with a thermionic electron RF gun and a vertical transfer line as well as the 1.5 GeV storage ring with a circumference of 96 m, which is a replica of the MAXIV 1.5 GeV storage ring [1-3]. Since the injection energy is 600 MeV, an energy ramp in the storage ring to the final operating energy is required [4]. This compact 3rd generation light source has been designed to have an emittance of 6 nmrad and to operate with 500 mA stored current for IR, VUV and soft X-ray production. The compact magnet design allows twelve 3.5 m long straight sections. Three of these sections are occupied by injection components, diagnostics and RF cavities, whereas the rest are available for long insertion devices. The electron beam parameters are presented in Table 1.

Table 1. The electron beam parameters in Solaris storage ring

Electron energy	0.6 - 1.5 GeV
Design current	500 mA
Bunch charge	5 nC
Number of circulating bunches	32
Natural bunch length σ_z	14.2 mm
Natural bunch length with Landau Cavity	60 mm
Natural emittance (bare lattice @1.5GeV)	5.982 nmrad
Coupling constant	0.01
Energy spread (bare lattice @1.5 GeV)	0.000745
Beam size in the straight section center (h/v)	184/13 μm

For X-ray production up to 2 superconducting wigglers can be installed, while undulators will be used for variable polarised light production [5, 6].

Up to now two beamlines have been funded. The Photoemission Electron Microscope (PEEM) beamline utilizes light from a bending magnet in the energy range from 200 up to 2000 eV [7] whereas the Ultra Angle Resolved Photoelectron Spectroscopy (UARPES) beamline will use an elliptical polarized undulator (EPU) with 120 mm period length as a light source [8]. The synchrotron radiation spectrum from the bending magnet is presented in Fig. 1. The critical energy of photon spectrum is 1959.88 eV, whereas the total synchrotron radiation power is 58.62 kW. Within this presentation the photon beam parameters for various insertion devices will be given.

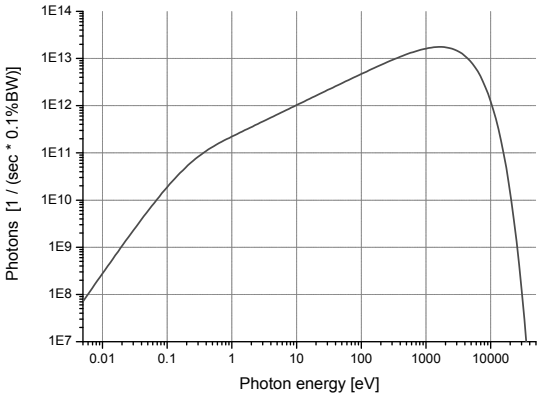

Fig. 1 The photon spectrum from the Solaris storage ring bending magnet centre

Acknowledgments: Work supported by the European Regional Development Fund within the frame of the Innovative Economy Operational Program: POIG.02.01.00-12-213/09. Authors would like to thank MAXIV team for all the support and know-how shared during the project.

[1] M. R. Bartosik et al., Solaris—National Synchrotron Radiation Centre, project progress, May2012, *Radiat. Phys. Chem.*,**93** (2013) 4-8. http://dx.doi.org/10.1016/j.radphyschem.2013.03.036

[2] C. J. Bocchetta et al., *Solaris Project Progress*, MOPEA046, Proc. IPAC2013, Shanghai, China, (2013) 181-183. http://accelconf.web.cern.ch/AccelConf/IPAC2013/papers/mopea046.pdf

[3] MAXIV Detailed Design Report; https://www.maxlab.lu.se/node/1136

[4] A. I. Wawrzyniak, R. Nietubyć, C.J. Bocchetta, D. Einfeld, *Ramping of the Solaris Storage Ring Achro*mats, MOPEA047, Proc. IPAC'13, Shanghai, China, ,pp. 184-186, (2013); http://accelconf.web.cern.ch/AccelConf/IPAC2013/papers/mopea047.pdf

[5] A. I. Wawrzyniak , C.J. Bocchetta, S. C. Leemann, M. Ericksson, *Solaris Storage Ring Lattice Optimisation with Strong Insertion Devices*, TUPPC025, Proc. IPAC'12, New Orleans, USA, (2012) 1218-1220. http://accelconf.web.cern.ch/AccelConf/IPAC2012/papers/tuppc025.pdf

[6] E. Wallén, *Elliptically Polarizing Undulators for the ARPES beamline at the Solaris Light Source*, Internal Report, 20. 12. 2012

[7] M. Zając, A. Bianco, C. J. Bocchetta, et al., *First bending magnet beamline at Solaris*, these proceedings.

[8] J. J. Kolodziej, K. Szamota-Leandersson, *UARPES -Angle Resolved Photoelectron Spectroscopy beamline at National Synchrotron Radiation Centre SOLARIS*, these proceedings.

P-59

SRF performance of Tesla 1.6-cell cavity with plug photocathode

D. Kostin[1], W. Grabowski*[2] and J. Sekutowicz[1]

[1] *Deutsches Elektronen Synchrotron (DESY), Notkestrasse 85, 22607 Hamburg, Germany*
[2] *National Centre for Nuclear Research (NCBJ), Sołtana 7, 05-400 Otwock, Poland*

Keywords: FEL, Tesla, cavity, superconducting, photocathode, plug

* e-mail: wojciech.grabowski@ncbj.gov.pl

We present results of measurements of superconducting 1.6-cell gun with photocathode placed on removable plug [1]. This photoinjector is designed for the superconducting linear particle accelerator of free electron laser POLFEL [2] and for for future modification of free electron laser European XFEL.

We present measurements of quality factor performed at DESY, in comparison with baseline test performed in Jefferson Laboratory. We also indicate differences between those tests. At the end we show modification of superconducting photocathode plug designed for increasing its performance.

---

[1] J. Sekutowicz et al., "*Cryogenic Test of the Nb-Pb SRF Photoinjector Cavities*", Proceedings of PAC09, Vancouver, 2010

[2] POLFEL – Project Description http://polfel.pl/doc/polfel_booklet_en_2012_10_28-b.pdf

FUTURE CONFERENCES AND WORKSHOPS

conference	web address	date
International Conference on Surface X-Ray and Neutron Scattering (Hamburg, Germany)	http://www.sxns13.de/	2014-07-07 - 2014-07-11
11th International Conference on the Structure of Surfaces (Coventry, UK)	https://www.eventsforce.net/iop/frontend/reg/thome.csp?pageID=106741&eventID=264&eventID=264	2014-07-21 - 2014-07-25
Denver X-ray Conference (Big Sky, USA)	http://www.dxcicdd.com/	2014-07-28 - 2014-08-01
International IUCr Congress (Montreal, Canada)	http://www.iucr2014.org/	2014-08-05 - 2014-08-12
ECM29 / 29th Meeting of the European Crystallographic Association (Rovinj)	http://ecm29.ecanews.org/	2014-08-23 - 2014-08-28
FEL2014 (Basel, Switzerland)	http://www.fel2014.ch/	2014-08-25 - 2014-08-29
ECOSS 30: European Conference on Surface Science (Antalya)	http://www.ecoss30.org	2014-08-31 - 2014-09-05
Coherence 2014: The International Workshop on Phase Retrieval and Coherent Scattering (Evanston / Northwestern University)	https://www.regonline.com/coherence2014	2014-09-02 - 2014-09-05
SR2A 2014: Conference on Synchrotron Radiation in Art and Archaeology (Paris)	http://ipanema.cnrs.fr/spip/scientific-events/synchrotron-radiation-in-art-and/article/synchrotron-radiation-in-art-and	2014-09-10 - 2014-09-12
EMRS-Fall Meeting including *Crystallography in materials science: Novel methods for novel materials (Symposium N),* (Warsaw, Poland)	http://www.emrs-strasbourg.com/	2014-09-15 - 2014-09-19
Science@FELs 2014 (Viligen, Switzerland)	https://indico.psi.ch/conferenceDisplay.py?confId=2910	2014-09-15 - 2014-09-17
57. Zjazd Polskiego Towarzystwa Chemicznego oraz Stowarzyszenia Inżynierów i Techników Przemysłu Chemicznego (Częstochowa, Polska)	http://ptchem2014.czest.pl/	2014-09-14 - 2014-09-18
XTOP: 12th Biennial Conference on High Resolution X-Ray Diffraction and Imaging (Villard de Lans)	http://xtop2014.org	2014-09-14 - 2014-09-19
German Conference for Research with Synchrotron Radiation, Neutrons and Ion Beams at Large Facilities 2014 (Bonn, Germany)	https://www.sni-portal.de/sni2014/index-engl.php	2014-09-21 - 2014-09-23
SNI2014: Deutsche Tagung für Forschung mit Synchrotronstrahlung, Neutronen, und Ionenstrahlen an Großgeräten (Bonn)	http://sni-portal.uni-kiel.de/sni2014/	2014-09-21 - 2014-09-23
MEDSI 2014: 8th International Conference on Mechanical Engineering Design of Synchrotron Radiation Equipment and Instrumentation (Melbourne)	http://www.medsi2014.org/	2014-10-20 - 2014-10-24
XRM2014, 12th International Conference on X-Ray Microscopy (Melbourne)	http://www.xrm2014.com/	2014-10-26 - 2014-10-31
ICMFS: 22nd International Colloquium on Magnetic Films and Surfaces (Cracow)	http://icmfs2015.agh.edu.pl/	2015.07.12 – 2015.07.17

Crystallography in materials science: Novel methods for novel materials (EMRS-Fall Meeting Symposium N, Warsaw, Poland, Sept. 15-19 2014)

http://www.emrs-strasbourg.com/

Crystal structure is one of principal factors determining the material properties. X-ray, neutron and electron diffraction methods of crystal and defect structure investigation are continuously developing, leading to new opportunities in materials investigation. Diffraction methods have been developing rapidly during last decades. They can be used for solving a variety of problems including crystal structure solution, defect structure determination, understanding of thin film structure and quality. structure variation mapping, structure dynamic changes, chemical reactions. The symposium will be a forum of presentation of such methods and their applications.

Hot topics to be covered by the symposium:

structure solution: methods and applications, structure refinement: methods and applications, defect structure of single crystals and thin films: methods and applications, use of specular reflectivity for film analysis, new instruments, use of X-ray, neutron and electron diffraction, including a combined use, use of classical and synchrotron beams, study of phase diagrams by diffraction methods, chemical reactions on very short time scale, in-situ studies at extreme conditions, nanocrystals, polycrystals, bulk single crystals, materials of various dimensionality including quantum dots, thin films, heterostructures, semiconductors, superconductors, ferroelectrics etc., energy related materials, biological materials.

Invited speakers:

Andre Authier (Paris, France) - Early days of X-ray crystallography - first applications to materials science

Izabela Sosnowska (Warsaw, Poland) - Fifty years of Time-of-Flight (TOF) neutron diffraction at pulsed neutron sources

Krzysztof Woźniak (Warsaw, Poland & Cambridge, UK) - X-ray structural analysis century after the Braggs - success or failure?

Wladek Minor (Charlottesville, USA) - Structural Biology - Next 100 Years of X-rays

Angela Altomare (Bari, Italy) - Recent advances in crystal structure solution

Bill David (Didcot, UK) - To be confirmed

Matteo Leoni (Trento, Italy) - Progress in microstructure analysis by diffraction

Louisa Meshi (Beer Sheva, Israel) - Strategies for solution of atomic structure of aluminides using Precession Electron Diffraction

Sven Lidin (Lund, Sweden) - A periodic materials: Why and how

Walter Steurer (Zürich, Switzerland) - Quasicrystal structure analysis - goals and limits

Manfred Burghammer (Grenoble, France) - Reciprocal space meets real space - looking at the structure of matter with scanning diffraction

Jung Ho Je (Pohang, South Korea) - Diffraction and phase contrast imaging of defects in crystals

Dénes L. Nagy (Budapest, Hungary) - Synchrotron Mössbauer reflectometry: A tool for magnetic thin film analysis

Marek Stankiewicz (Kraków, Poland) - SOLARIS synchrotron facility in Kraków – a state-of-the-art tool for materials scientists and solid state physicists and chemists

Alex Hannon (Didcot, UK) - Title to be announced

Jarek Majewski (Los Alamos, USA) - X-ray and neutron scattering studies of bio-relevant structures: from model lipid membranes to living cell cultures under flow stress

Zuzanna Liliental-Weber (Berkeley, USA) - Determination of growth polarity by Convergent Beam Electron Diffraction in III-V semiconductors

Pierre Ruterana (Caen, France) - The combined topological analysis, atomistic modelling and HRTEM of grain boundaries in wurtzite materials

Daniel Errandonea (Valencia-Burjassot, Spain) - Exploring the properties of materials using high-pressure x-ray diffraction: Recent advances and future challenges

Andrzej Katrusiak (Poznań, Poland) - Paving the way to unexplored Universe and gaining profits from high-pressure conditions

David Rafaja (Freiberg, Germany) - Crystallography of nanomaterials

Kenny Stahl (Lyngby, Denmark) - Zeolitic materials

Janez Dolinsek (Ljubljana, Slovenia) - Physical properties of complex metallic alloys in relation to crystal structures

Wiesław Łasocha (Kraków, Poland) - New hybrid organic-inorganic materials: Synthesis, structure, applications

Laura Leon-Reina (Málaga, Spain) - Quantitative XRD analysis, a tool for the quality control of clinker and cements

Yuri Grin (Dresden, Germany) - Crystallographic features and chemical bonding in thermoelectric materials

Magali Morales (Caen, France) - Combined refinement of GIXRF, XRR and XRD data in a global approach: analysis of textured ITO/Ag/ITO/Si architectures and III-V based heterostructures

Michael Knapp (Karlsruhe, Germany) - In-situ synchrotron studies on Li-battery cathode materials

Matteo Bianchini (Grenoble, France) - In-situ and ex-situ neutron diffraction experiments on electrode materials for Li-ion batteries

SCIENTIFIC COMMITTEE: A. Balagurov, Dubna, Russian Federation, **D. Billing**, Johannesburg, South Africa, **R. Cernik**, Manchester, UK, **F. Fauth**, Barcelona, Spain, **M. Gdaniec**, Poznań, Poland, **C. Giacovazzo**, Bari, Italy, **P. Gille, Munich**, Germany, **F. Gozzo**, Villigen, Switzerland, **Yu. Grin**, Dresden, Germany, **A.C. Hannon**, Didcot, UK, **J. Härtwig**. Grenoble, France, **J.Z. Jiang**, Hangzhou, P.R. China, **J.H. Je**, Pohang, South Korea, **G. Kimmel**, Beer Sheva, Israel, **M. Kozak**, Poznań, Poland, **K.J. Kurzydlowski**, Warsaw, Poland, **R. Kužel**, Prague, Czech Republic, **M. Leszczyński**, Warsaw, Poland, **Z. Liliental-Weber**, Berkeley, CA, USA, **J. Lipkowski**, Warsaw, Poland, **J. Majewski**, Los Alamos, NM, USA, **A. Meden**, Ljubljana, Slovenia, **W. Minor**, Charlottesville, VA, USA, **P. Ruterana**, Caen, France, **H. Schenk**, Amsterdam, The Netherlands, **J. Schneider**, Hamburg, Germany, **E. Talik**, Katowice, Poland, **E. Tillmanns**, Vienna, Austria, **L. Vasylechko**, Lvov, Ukraine, **E.V. Zharikov**, Moscow, Russian Federation,

Sponsors:

International Union of Crystallography will sponsor a limited number of young participants.

Polish Academy of Sciences

Symposium organizers:

Wojciech Paszkowicz (Institute of Physics, PAS Warsaw, Poland, **CONTACT: paszk@ifpan.edu.pl, +48 221163301)**, Radovan Cerny (Univ. Genève, Switzerland), Irene Margiolaki (Univ. Patras, Greece), Hartmut Fuess (Univ. Technology, Darmstadt, Germany), René Guinebretiere (ENSCI, Limoges France)

INFORMATION on EAgLE Project

(EU-FP7 grant no. REGPOT-CT-2013-316014-EAgLE)

The EAgLE project aims at establishing at the Institute of Physics, Polish Academy of Sciences (IF PAN) a leading multiprofile research Centre for designing and fabricating new materials, their characterization and testing under extreme experimental conditions. The Centre will identify and select novel materials, structures, phenomena, and computational protocols for functional new-concept nanodevices.

☆

The Centre benefits from twinning with 16 partnering institutions having the sound expertise in the field of materials fabrication (e.g. MBE, chemical synthesis, lithography, FIB), characterization (e.g. XPS, TEM, EELS, synchrotron – diffraction and spectroscopy, NMR), nanodevice design and testing (e.g. semi- and superconducting electronics, cryogenics, computer simulations). The research potential will be enhanced through employment of both experienced and young researchers in the relevant fields.

☆

Within the project an X-Ray Photoelectron Spectrometer (XPS) will be acquired, making it possible to perform element specific and chemical sensitive characterization of materials with 3D resolution. A cryogen-free dilution refrigerator will be another essential purchase opening new opportunities to follow properties of the materials and devices down to a few miliKelvins.

☆

An important goal of the Centre is exploration and standardization of user-friendly computational methods for materials design and for modeling of functional properties and nanodevices, including code validation and benchmarking, available also to external users.

☆

The awareness of issues related to the field of intellectual property, licensing, and patenting will be raised among the staff members via a series of dedicated workshops, in order to improve the transfer of innovations to new spin-offs, SMEs, and industry.

☆

The EAgLE project has been supported also scientific workshops and international conferences. Among others are the “Antiferromagnetic spintronics: materials, characterization, functionalities” symposium within the E-MRS Fall Meeting 2014, the International School and Symposium on Synchrotron Radiation in Natural Science, ISSRNS 2014, and Topical Session “Materials in Spintronics during the ICGE-17 Conference in 2013.

☆

The International Steering Committee chaired by prof. Tomasz Dietl (Institute of Physics, PAS, Poland) is an advisable body to the EAgLE project. ISC consists of 15 internationally renowned experts representing research sector as well as regional authorities and industry.

☆

More information about the EAgLE project you will find at the internet pages:

http://www.eagle-regpot.eu/

Presenting Authors' Index